INTERACTIONS OF NS5 THAT DRIVE ITS FUNCTION IN DENGUE PATHOGENESIS

MOON TAY YUE FENG
B.Science (Hons), NTU

A THESIS SUBMITTED

FOR THE DEGREE OF DOCTOR PHILOSOPHY
DUKE-NUS GRADUATE MEDICAL SCHOOL

2015

DECLARATION

I hereby declare that the thesis is my original work and it has been written by me in its entirety. I have duly acknowledged all the sources of information which have been used in the thesis.

This thesis has also not been submitted for any degree in any university previously.

Tay Yue Feng

6th March 2015

Interactions of NS5 that drive its function in Dengue pathogenesis

by

TAY Yue Feng

PhD Program in Integrated Biology and Medicine
Duke-NUS Graduate Medical School

Date: 6th March 2015

Approved:

Subhash Vasudevan, Thesis Advisor

Ooi Eng Eong

Manoj Krishnan

Patrick Casey

David Jans

Dissertation submitted in partial fulfillment of
the requirements for the degree of
Doctor of Philosophy
Duke-NUS Graduate Medical School
National University of Singapore
March 2015

ABSTRACT

Dengue virus nonstructural protein 5 (NS5), containing both methyltransferase and RNA-dependent-RNA-polymerase (RdRP) activities, is responsible for plus- and minus-strand viral RNA synthesis and can be found in both cytoplasm and nucleus of infected cells. Cytoplasmic NS5 interacts with NS3 (protease/helicase) in the perinuclear region to synthesize the viral RNA genome whereas nuclear NS5 interacts with importin-α/β1 in the cytoplasm and is translocated to the nucleus to mediate in cellular events that are not fully understood. In recent years, NS3-NS5 and NS5-importin-α/β1 interaction sites have been proposed to be attractive targets for antiviral drug design but molecular interaction details are lacking. This study has found that subcellular localization of NS5 varies in a serotype dependent manner and identified amino acids NS3 ^{570}N, and NS5 ^{887}KR and ^{890}RR to be important in NS3-NS5 and NS5-importin-α/β1 interaction, respectively. Mutational analysis with an infectious cDNA clone of DENV2 showed that the identified residues are critical for viral replication. Moreover, the study found that NS3-NS5 interaction has an important role in the balanced synthesis of plus- and minus-strand RNA for robust viral replication. Importantly, the functional studies in this work reveal an unexpected convergence of these critical interactions to the thumb subdomain of NS5. Employing co-immunoprecipitation coupled to mass spectrometry in this study addressed the differential subcellular localization pattern of NS5 from the different serotypes and is currently validating several potentially critical hits.

Interactions of NS5 that drive its function in Dengue pathogenesis

by

TAY Yue Feng

PhD Program in Integrated Biology and Medicine
Duke-NUS Graduate Medical School

Date: 6th March 2015

Approved:

Subhash Vasudevan, Thesis Advisor

Ooi Eng Eong

Manoj Krishnan

Patrick Casey

David Jans

An abstract of a dissertation submitted in partial
fulfillment of the requirements for the degree
of Doctor of Philosophy
Duke-NUS Graduate Medical School
National University Singapore
March 2015

Abstract

Dengue virus (DENV), the causative agent of "breakbone fever", is the most important mosquito-borne human pathogen that put more than half of the world's population to be at risk of infection. As of now, the treatment is mainly supportive and there is no licensed vaccine or antiviral drug to limit the infection. The interplay between viral and host factors dictates the severity of disease and a good understanding of this interplay will help to clarify the roles of these factors in severe dengue pathogenesis.

The aim of my thesis is to characterize the interaction of nonstructural protein 5 (NS5) with its viral replication partner, NS3 and its host nuclear-trafficking partner, importin-α/β1. NS5, the largest and most conserved viral protein, has both methyltransferase and RNA-dependent RNA polymerase (RdRP) activities that are required for RNA type 1 cap formation and viral RNA replication, respectively. Although DENV replicates in the cytoplasm, most of the NS5 is found in the nucleus. In the cytoplasm, NS5 interacts with NS3, a protease/helicase viral protein to work in concert to synthesize viral genomic RNA. Disruption of this interaction is known to be lethal to virus. This study fine mapped the interaction region between NS3 and NS5 and investigated its impact on virus replication. The interaction site was identified to reside within residues 566-585 of NS3 and residues 320-341 of NS5. Further sequence interrogation led to the discovery of a conserved residue in NS3, N570 to be crucial for NS3-NS5 interaction. Alanine mutagenesis study of NS3:N570 within DENV2 cDNA infectious clone, in conjunction with a previously characterized NS3-NS5 interaction defective mutant NS5:K330A, led to surprising finding. In

agreement with previous study, mutation that disrupts NS3-NS5 interaction is lethal. However, with thorough characterization, NS3:N570A behaved slightly differently; unlike NS5:K330A, it could undergo low, yet unsustainable viral RNA replication. With careful quantification using RT-PCR, we observed an accumulation of negative-sense RNA synthesis with NS3:N570A mutant. This suggests that optimum protein interaction affinity between NS3 and NS5 may be required for long term coordinated synthesis of negative- and positive-sense RNA. Hence, this study demonstrates for the first time that NS3-NS5 interaction may play an important role in the balanced synthesis of positive- and negative-strand RNA for robust viral replication.

For NS5 to traffic into the nucleus, NS5 has to interact with host nuclear import transporter, importin-α/β1 via its basic residues of nuclear localization signal (NLS) and this has only been demonstrated for NS5 of DENV serotype 2. Therefore, in the second part of my PhD study, we investigated the nuclear targeting ability of NS5 from DENV serotypes 1, 3 and 4 and for the first time, we could show in both infected and transfected cells that DENV2 and 3 NS5 were predominately nuclear, whereas DENV1 and 4 NS5 were more cytoplasmic. Based on this finding, we explored further by focusing on DENV1 and 2 NS5 to determine the region on DENV1 NS5 that is responsible for its cytoplasmic retention, despite its ability to bind to importin-α/β1. This, however, has led to a discovery of a novel dominant NLS that resides at the C-terminal end of DENV2 NS5 via extensive swapping of DENV1 and 2 NS5 gene fragments. Through alanine mutagenesis analysis of NLS sequence, we could disrupt the nuclear targeting ability of DENV2 NS5 by mutating ^{887}KR, ^{890}RR, ^{887}KR+^{890}RR, and when the same mutations were engineered into DENV2 cDNA infectious clone, ^{887}KR and ^{887}KR+^{890}RR mutations were found to be lethal to

virus. Hence, in this study, we have identified a novel C-terminal NLS in DENV2 NS5 that is important for NS5 nuclear trafficking and virus replication.

Overall, our findings have unexpectedly converged both NS3-NS5 and NS5-importin-α/β1 interaction sites on thumb subdomain of NS5 RdRP, which collectively suggests that the thumb subdomain may play a role in mediating NS5 subcellular localization.

Acknowledgments

Foremost, I would like to express my deep and sincere gratitude to my mentor, Professor Subhash Vasudevan, for his constant encouragement, patient guidance, valuable suggestions and insightful comments throughout the PhD study.

I am deeply grateful to my thesis advisory committee, Professor David Jans, Professor Patrick Casey, Associate Professor Ooi Eng Eong and Assistant Professor Manoj Krishnan for their great help and advices for this study.

I gratefully thank my collaborators Professor Gerhard Grüber, Associate Professor Julien Lescar, Associate Professor Jade Forwood, Assistant Professor Luo Dahai, Dr Johanna Fraser and Saw Wuan Geok for their contribution to my study.

I wish to express my warm and sincere thanks to my laboratory colleagues Dr Satoru Watanabe, Dr Nancy Brown, Dr Chandrakala Basavannacharya, Dr Abhay Rathore, Zhao Yong Qian, Kitti Chan Wing Ki, Lee Chin Chin and Daljit Singh for providing technical assistance and support in my study.

Lastly, I am deeply indebted to my family members, Tay Peng Nguan, Ang Mary, Tay Yue Xiang, Tay Lai Wen and Tay Yue Ting and my fiancé, Xu Zhen Xiang for their love and understanding throughout the whole process.

Contents

List of Figures

List of Tables

List of abbreviations

ADE	Antibody dependent enhancement
BCA	Bicinchoninic acid
BHK-21	Baby hamster kidney
BSA	Bovine serum albumin
C	Capsid
cDNA	Complementary DNA
CFI	Cell-based flavivirus immunodetection
CK2	Casein kinase 2
Co-IP	Protein-complex immunoprecipitation
CRM1	Chromosome region maintenance 1; also referred to as exportin 1
CRS	Cytoplasmic retention signal
D1	Dengue virus serotype 1
D2	Dengue virus serotype 2
DAXX	Death domain-associated protein 6
DENV	Dengue virus
DF	Dengue fever
DHF	Dengue hemorrhagic fever
DNA	Deoxyribonucleic acid
dsRNA	Double-stranded RNA
DSS	Dengue shock syndrome
E	Envelope
E. coli	Escherichia coli
EC_{50}	Half-maximal effective concentration
EDEN	Early Dengue infection and outcome
EDTA	Ethylenediaminetetraacetic acid
ELISA	Enzyme-linked immunosorbent assay
ER	Endoplasmic reticulum
Fn/c	Nuclear to cytoplasmic fluorescence ratio
Fab	Fragment antigen-binding
FBS	Fetal bovine serum
FP	Forward primer

GFP	Green fluorescent protein
GO	Gene ontology
GPI	Glycosylphosphatidylinositol
GST	Glutathione S-transferase
GTase	Guanylyltransferase
IC_{50}	Half-maximal inhibitory concentration
IFA	Immunofluorescence assay
IgG	Immunoglobulin G
IP	Immunoprecipitation
IRES	Internal ribosome entry site
JEV	Japanese encephalitis virus
HIV	Human immunodeficiency virus
HRP	Horseradish peroxidase
Huh-7	Human hepatoma cell
LB	Luria Broth
LC-MS/MS	Liquid chromatography tandem mass spectrometry
LD	Loading dye
LMB	Leptomycin B
PCR	Polymerase chain reaction
M	Membrane
MOI	Multiplicity of infection
MTase	Methyltransferase
NEAA	Non-essential amino acids
NEB	New England Biolabs
NLS	Nuclear localization signal
NS	Nonstructural
NSD	Normalized spatial discrepancy
NP	Nucleoprotein
P/S	Penicillin-streptomycin
PAGE	Polyacrylamide gel electrophoresis
PBS	Phosphate buffered saline pH 7.2
PBST	PBS with 0.1% Tween 20
PBST-M	PBST with 5% (w/v) skim milk powder

PCR	Polymerase chain reaction
pfu	Plaque forming units
PKG	Protein kinase G
ppm	Parts per million
prM	Pre-membrane
RdRP	RNA-dependent RNA-polymerase
RNA	Ribonucleic acid
RP	Reverse primer
rpm	Rounds per minute
RT	Reverse transcription
RT	Room temperature
RTPase	RNA 5'-triphosphatase
SAM	S-adenosyl-L-methionine
SAXS	Small angle X-ray scattering
SD	Standard deviation
SDM	Site-directed mutagenesis
SDS	Sodium dodecyl sulfate
SEM	Standard error of the mean
SPR	Surface plasma resonance
STAT1	Signal transducers and activators of transcription 1
SV	Simian virus
TGN	Trans-Golgi network
TM	Transmembrane
TMB	3,3′,5,5′-tetramethylbenzidine
WHO	World Health Organization
w/v	Weight/volume
WNV	West Nile virus
WT	Wildtype
v/v	Volume/volume
YFV	Yellow fever
RT-PCR	Reverse transcription-PCR
UTR	Untranslated region

List of publications

1. **Tay, M. Y.**, Saw, W. G., Zhao, Y., Chan, K. W., Singh, D., Chong, Y., Forwood, J. K., Ooi, E. E., Gruber, G., Lescar, J., Luo, D. & Vasudevan, S. G. (2014b). The C-terminal 50 amino acid residues of Dengue NS3 protein are important for NS3-NS5 interaction and viral replication. J Biol Chem 290, 2379-2394.
2. **Tay, M. Y.**, Lee, C. C., Vasudevan, S. G. & Moreland, N. J. (2014a). Identification of dengue-specific human antibody fragments using phage display. Methods Mol Biol 1138, 161-173.
3. Zhao, Y., Moreland, N. J., Tay, **M. Y.**, Lee, C. C., Swaminathan, K. & Vasudevan, S. G. (2014). Identification and molecular characterization of human antibody fragments specific for dengue NS5 protein. Virus Res 179, 225-230.
4. **Tay, M. Y.**, Fraser, J. E., Chan, W. K., Moreland, N. J., Rathore, A. P., Wang, C., Vasudevan, S. G. & Jans, D. A. (2013). Nuclear localization of dengue virus (DENV) 1-4 non-structural protein 5; protection against all 4 DENV serotypes by the inhibitor Ivermectin. Antiviral Res 99, 301-306.
5. Moreland, N. J., **Tay, M. Y.**, Lim, E., Rathore, A. P., Lim, A. P., Hanson, B. J. & Vasudevan, S. G. (2012). Monoclonal antibodies against dengue NS2B and NS3 proteins for the study of protein interactions in the flaviviral replication complex. J Virol Methods 179, 97-103.

Manuscript in preparation

1. **Tay, M. Y.**, Chan, K. W., Jans, D. A. & Vasudevan, S. G. The discovery of a novel C-terminal nuclear localization signal in Dengue virus 2 NS5.

List of conference posters

1. **Tay, M. Y.**, Saw, W. G., Zhao, Y., Chan, K. W., Singh, D., Chong, Y., Forwood, J. K., Ooi, E. E., Gruber, G., Lescar, J., Luo, D. & Vasudevan, S. G. (2014b). The C-terminal 50 amino acid residues of Dengue NS3 protein are important for NS3-NS5 interaction and viral replication. 40th Lorne Conference on Protein Structure and Function (Lorne, Australia).
2. **M.Y.F. Tay**, J.E. Fraser, M. Pezzullo, W.K.K. Chan, S. Watanabe, M. Milani, D.A. Jans, S.G. Vasudevan. Serotype-Dependent Differential Localization of Dengue NS5 Protein: Implications for Antiviral Activity of Putative Nuclear Transport Inhibitor Ivermectin. 3rd International Conference on Dengue and Dengue Haemorrhagic Fever (Bangkok, Thailand)

Chapter 1: Introduction

1.1 Dengue epidemiology

Globally, dengue is the most prevalent and important mosquito-borne viral disease and it is endemic in more than 100 tropical and subtropical countries (Figure 1-1). It is estimated that 3.6 billion people (>50% of the world's population) are at risk of infection and it is estimated to be causing >390 million human infections that results in ~100 million symptomatic dengue cases (Bhatt *et al.*, 2013; Gubler, 2012).

Dengue infection in humans results in a wide-spectrum of clinical symptoms, ranging from fully asymptomatic to self-limiting dengue fever (DF) and life-threatening severe dengue (dengue hemorrhagic fever (DHF)/dengue shock syndrome (DSS)), which can be caused by any one of the four distinct, but closely related serotypes (DENV1-4) (Halstead, 1988). In the last five decades, the global incidence of dengue has increased significantly (Figure 1-2) but the main factors that are responsible for the increased transmission of dengue may be multifactorial and remains poorly understood. However, there seems to be a close correlation between the increased global prevalence of dengue cases and unregulated urbanization together with overcrowding (Gubler, 1998).

In Singapore, dengue is endemic and all four serotypes co-circulate continuously - a situation that is termed as “hyperendemicity”, with DENV1 and DENV2 being the most common serotypes in causing dengue infection (Lee *et al.*, 2010b; NEA, 2014). Despite effective vector control program since late 1960s (Ng & Ho, 2013) (Ler *et al.*,

2011), we had still two dengue outbreaks that were caused by DENV1 and one that was caused by DENV2 in the last decade. The 2005 epidemic has been suggested to be due to the sudden switch of the predominant viral serotype, from DENV2 to DENV1 that occurred in 2004; this led to dengue epidemic, with 14,006 cases being reported and a total of 27 local deaths were observed (Lee *et al.*, 2010b). Again in 2007, Singapore experienced a DENV2 outbreak, due to a serotype switch from DENV1 to a new strain of DENV2 and this resulted in 8,826 cases and 24 fatalities being reported (Ler *et al.*, 2011). Lastly, in 2013, the dengue epidemic was driven by a new strain of DENV1, which became dominant in March 2013 and was responsible for 85% of all diagnosed cases; a total of 22,318 cases were reported (~55% more than 2005 outbreak) and fewer deaths were observed (seven local deaths) when compared to 2005 outbreak (NEA, 2014). Taken together, it appears that the interplay between the viral and host factors is important in shaping the disease outcome, serotype dominance and case fatality rates.

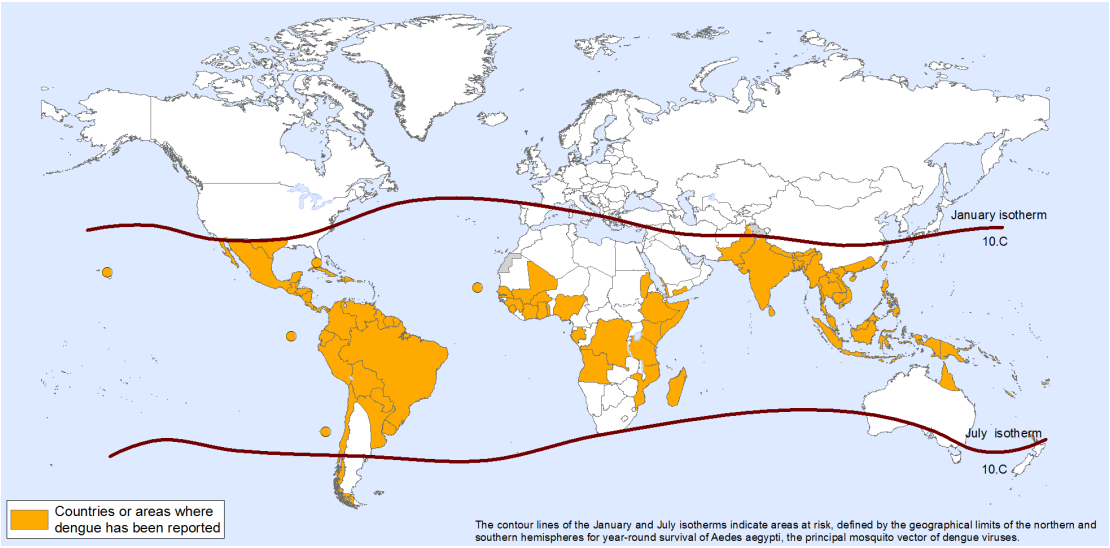

Figure 1-1: Global representation of countries or areas where dengue was reported in 2013 by WHO. Figure is adopted from (WHO, 2014).

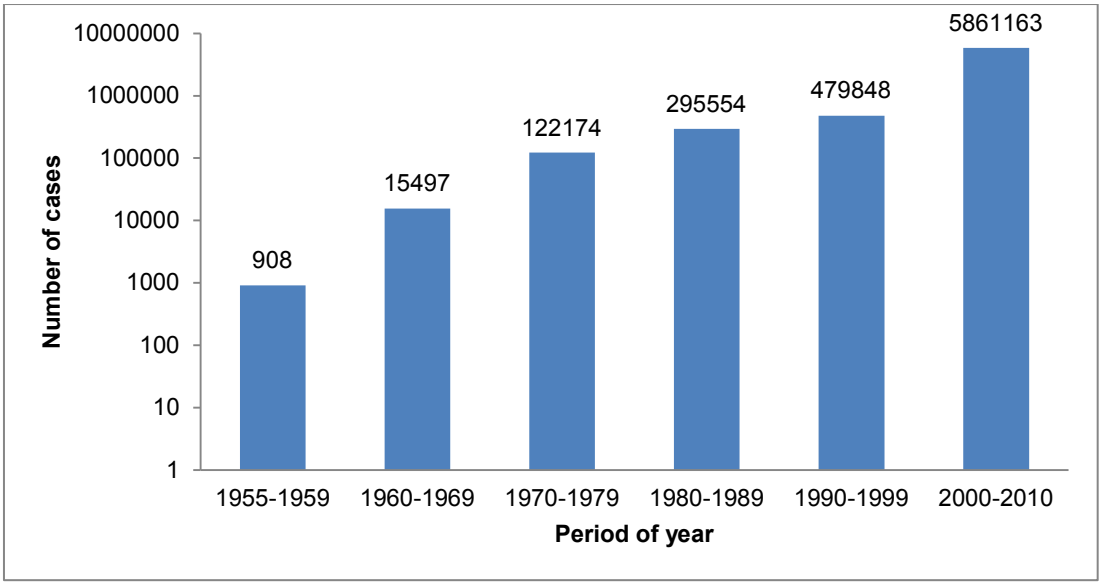

Figure 1-2: Average number of total dengue cases reported to WHO from 1955-2010. The y-axis denotes the number of cases in $\log_{10}$ scale whereas the x-axis denotes the year when the cases was reported. Figure is adapted from (WHO, 2012).

1.2 Transmission cycle of DENV

DENV is transmitted to humans through the bite of infected female *Aedes* mosquito - *Aedes aegypti* or *Aedes albopictus*. *Aedes aegypti* is the principal vector for DENV transmission in urban centers (Gubler, 1998). Once a person is bitten by an infected mosquito, the virus undergoes an average incubation period of 4 - 7 days, after which the person may experience acute onset of fever, which typically last for 3 - 7 days (Figure 1-3) and is accompanied by a variety of non-specific signs and symptoms (also see section 1.3, Figure 1-4). During the acute febrile period, virus can be detected in the peripheral blood and naïve-mosquito can acquire the virus while feeding on the blood of infected individual and transmit to others after 8 - 12 days of incubation within the mosquito (intrinsic cycle) (Gubler, 1998).

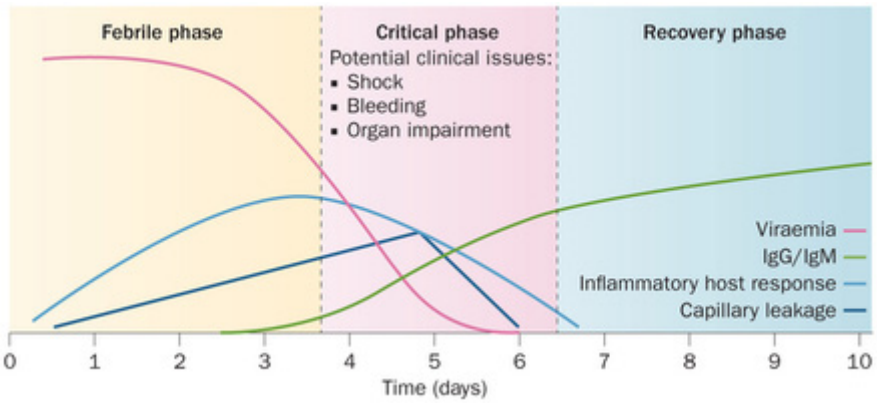

Figure 1-3: Disease progression of dengue. Following the incubation period, the disease undergoes three phases - febrile, critical and recovery. For DF patients, they usually only experience the febrile phase for 3-7 days and after which, enters the recovery phase. For DF patients that progress to severe dengue, they are placed under strict observation for timely medical intervention if needed. Figure is adopted from (Yacoub *et al.*, 2014).

1.3 Clinical manifestations

As mentioned, most DENV infections are usually asymptomatic and symptomatic cases make up 10-50% of total dengue infections (the ratio of asymptomatic/symptomatic cases is age-dependent (Guzman & Kouri, 2002)). The most commonly reported disease manifestation is DF (Kyle & Harris, 2008), which is characterized by sudden onset of self-limiting fever and a variety of nonspecific signs and symptoms, including headache, retro-orbital pain, aches/pains, nausea/vomiting, weakness, rash and/or any warning signs (Figure 1-4) (Halstead, 2007; WHO, 2009). However, in some DF cases, the disease may progress to severe dengue disease (DHF/DSS) at late febrile phase around the time of defervescence, when signs of thrombocytopenia (platelet count $\leq$ 100,000/mm^3), common haemorrhagic phenomena (eg. petechiae, bleeding gums, gastrointestinal bleeding and etc.) and increased vascular permeability with intravascular fluid leakage suddenly develop (Figure 1-4) (Halstead, 2007; WHO, 2009) and that can be fatal if not correctly managed as there is no antiviral therapy available.

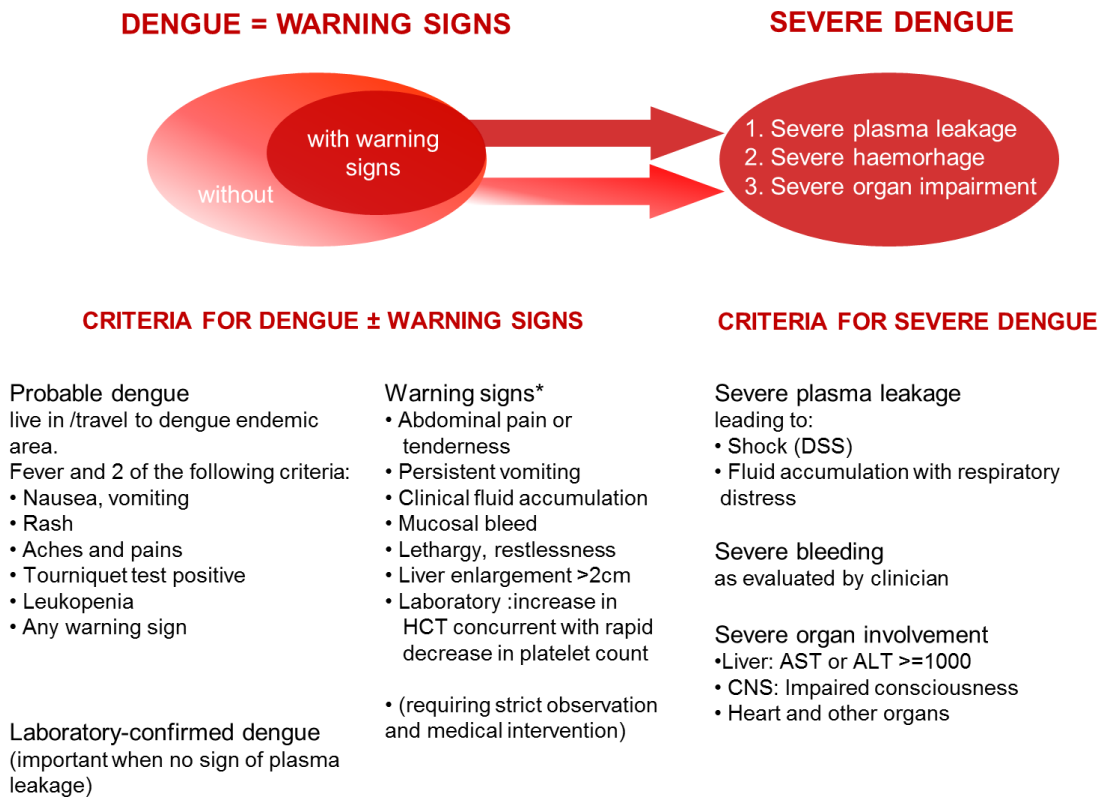

Figure 1-4: Classification of dengue and severe dengue. Since 2009, the WHO has simplified dengue classification to ease the identification of severe dengue cases. Dengue fever patients with warning signs are in danger of experiencing severe dengue and are *placed under strict observation for timely medical intervention if needed. Figure is adopted from (WHO, 2009).

1.4 Pathogenesis of severe dengue

The most widely accepted hypothesis for severe dengue pathogenesis is antibody dependent enhancement (ADE). This phenomenon is well-documented in several clinical studies (reviewed by (Halstead, 2007)). It is known that infection with one dengue serotype provides life-long protection to that serotype (homotypic immunity) and partial immunity to other serotypes in subsequent infection (heterotypic immunity). However, it was also observed in experimental human studies that the incubation period during secondary infection with heterologous serotype is shorter than primary infection, suggesting that a more efficient infection process during

secondary infection (Snow *et al.*, 2014) and this is thought to be mediated by homotypic antibodies that are generated during primary infection, which can enhance the uptake of opsonized virus particles into Fcγ receptor bearing cells (eg. macrophages, monocytes and dendritic cells (DC)) (Figure 1-5) during heterologous secondary infection; this results in increased number of infected cells (Gollins & Porterfield, 1986), which may lead to higher viral load and increased disease severity in dengue infected patients (Libraty *et al.*, 2002a; Simmons *et al.*, 2007; Thomas *et al.*, 2008; Wang *et al.*, 2003; Wang *et al.*, 2006).

Another proposed hypothesis for severe dengue phenomenon is "original antigenic sin", which is mediated by activated T cells (Mongkolsapaya *et al.*, 2003). In this context, it is thought that during secondary infection with a heterologous serotype, re-activation of cross-reactive low avidity T cells from the first exposure results in high level of proinflammatory cytokine secretion and higher level of viremia due to delayed viral clearance (Mongkolsapaya *et al.*, 2003). However, this hypothesis is challenged by the observation that heterologous T-cell responses are not always required to produce severe dengue in infants because when maternal anti-dengue antibody titer drops below the protective level, infants are at increased risk for development of severe dengue even though they have never been exposed to DENV (Weiskopf & Sette, 2014).

In both hypothesis, elevated cytokine (eg. TNF-α, IFN-γ, IL-6, IL-8 and IL-10) levels may play a direct role in immunopathogenesis of severe dengue in secondary infection by increasing vascular permeability (Chakravarti & Kumaria, 2006; Juffrie *et al.*, 2001; Nguyen *et al.*, 2005; Pang *et al.*, 2007; Perez *et al.*, 2004; Raghupathy *et al.*, 1998). However, these theories cannot explain the occurrence of severe dengue during primary infection and other studies have also demonstrated the potential occurrence of severe dengue during primary infection with either certain virus serotypes (Chau *et al.*, 2008; Duyen *et al.*, 2011; Fried *et al.*, 2010; Tricou *et al.*, 2011) or strains that are considered more virulent (Kanakaratne *et al.*, 2009; Rabaa *et al.*, 2010; Vasilakis & Weaver, 2008b) or among at-risk individuals (eg. age, gender, host genetics factors and etc.) (reviewed by (Whitehorn & Simmons, 2011)).

Collectively, there is no clear molecular mechanistic evidence that can specifically pinpoint secondary infection, viral virulence factor or host susceptibility as the major cause for severe dengue pathogenesis, and instead a complex interplay among these factors are probably involved (reviewed by (Acosta *et al.*, 2014; Gubler, 1998; Whitehorn & Simmons, 2011)). Nevertheless, there is an urgent need to understand how these factors interact with the host immune system to cause severe dengue symptoms like increased vascular permeability in order to assist the development of therapeutic intervention for better patient management.

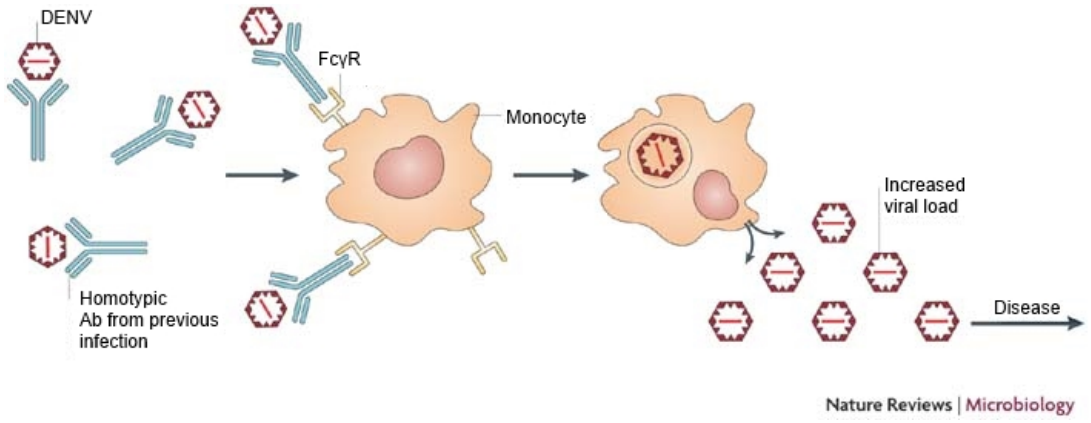

Figure 1-5: Antibody-dependent enhancement phenomenon. ADE typically occurs during secondary infection with heterologous serotype when homotypic antibodies that are generated during primary infection bind to the current infecting DENV particles but cannot neutralize the virus; the antibody-virus complex binds to Fcγ receptor of circulating immune cells (eg. macrophages, monocytes and DC) and this facilitates the uptake of the virus into immune cells that are not readily infected in the absence of antibody. This in turn may lead to higher viral load and increased disease severity in dengue infected patients. Figure is adopted from (Whitehead *et al.*, 2007).

1.5 Genome organization and taxonomy of DENV

DENV is a member of the *Flavivirus* genus, and together with *Pestivirus* and *Hepacivirus*, and the newly approved *Pegivirus* genus (Stapleton *et al.*, 2011; Viruses, 2014), they belong to the *Flaviviridae* family that share some similarities in virion morphology, genome organisation and replication strategy (Lindenbach *et al.*, 2007). Genome organisation is similar among the flaviviruses and yet, distinct from pestiviruses, hepaciviruses and pegiviruses (Hulo *et al.*, 2011; Kapoor *et al.*, 2013; Leyssen *et al.*, 2000; Quan *et al.*, 2013) (Figure 1-6). The flavivirus RNA genome is of positive polarity and it is ~11kb long. It contains a type 1 cap structure at the 5' end but lack a poly A tail at the 3' end. It encodes a single open reading frame that codes for three structural (C (capsid), prM (pre-membrane) and E (envelope)) and seven nonstructural (NS) proteins (NS1, NS2A, NS2B, NS3, NS4A, NS4B and NS5) and is flanked by 5'- and 3'-untranslated regions (UTRs). Both 5′- and 3′-UTRs contain highly structured regulatory RNA elements that are crucial for translation and viral

RNA replication and they interact extensively to form combined secondary structures for efficient replication (also see Figure 1-14, reviewed by (Acosta *et al.*, 2014) and (Villordo *et al.*, 2010)).

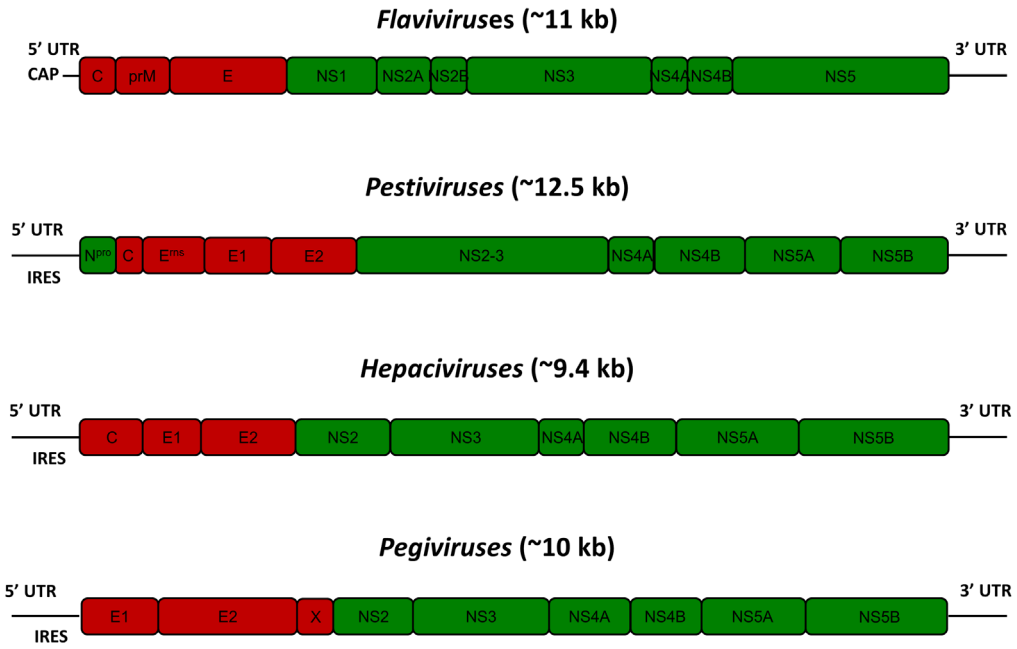

Figure 1-6: Genomic organization of members of the *Flaviviridae* family. The viral genome is a single-stranded positive-sense RNA molecule that is either capped in flaviviruses or contains an IRES (internal ribosome entry site) in pestiviruses, hepaciviruses and pegiviruses in 5'-UTR, at the N-terminal end of the genome. 3'-UTR is also present at the C-terminal end of the genome. The genes that encoded the structural and nonstructural (NS) proteins are indicated in red and green, respectively. The approximate genome size is also indicated. Figure is adapted from (Leyssen *et al.*, 2000), with new information incorporated from (Hulo *et al.*, 2011; Kapoor *et al.*, 2013; Quan *et al.*, 2013).

The *Flavivirus* genus contains at least 70 viral species, many of which are transmitted by arthropod vectors (eg. mosquitoes and ticks). A number of these flaviviruses are medically important human pathogens that are of major global concern, and they include DENV (serotype 1-4) (Figure 1-7, boxed in red), Japanese encephalitis virus (JEV), Tick-borne encephalitis (TBE), Murray Valley encephalitis virus (MVEV), Saint Louis encephalitis virus (SLEV), West Nile virus (WNV) and Yellow fever

virus (YFV) (Figure 1-7, boxed in grey), which cause fevers, encephalitis, and hemorrhagic fevers (Gubler *et al.*, 2007; Lindenbach *et al.*, 2007; Mackenzie *et al.*, 2004). Among the flaviviruses, DENV infection causes the highest morbidity and mortality (Halstead, 1997), and in recent years, a possible fifth serotype that spilled over from a sylvatic cycle has been identified in human, but its impact on public health remains to be determined (Normile, 2013).

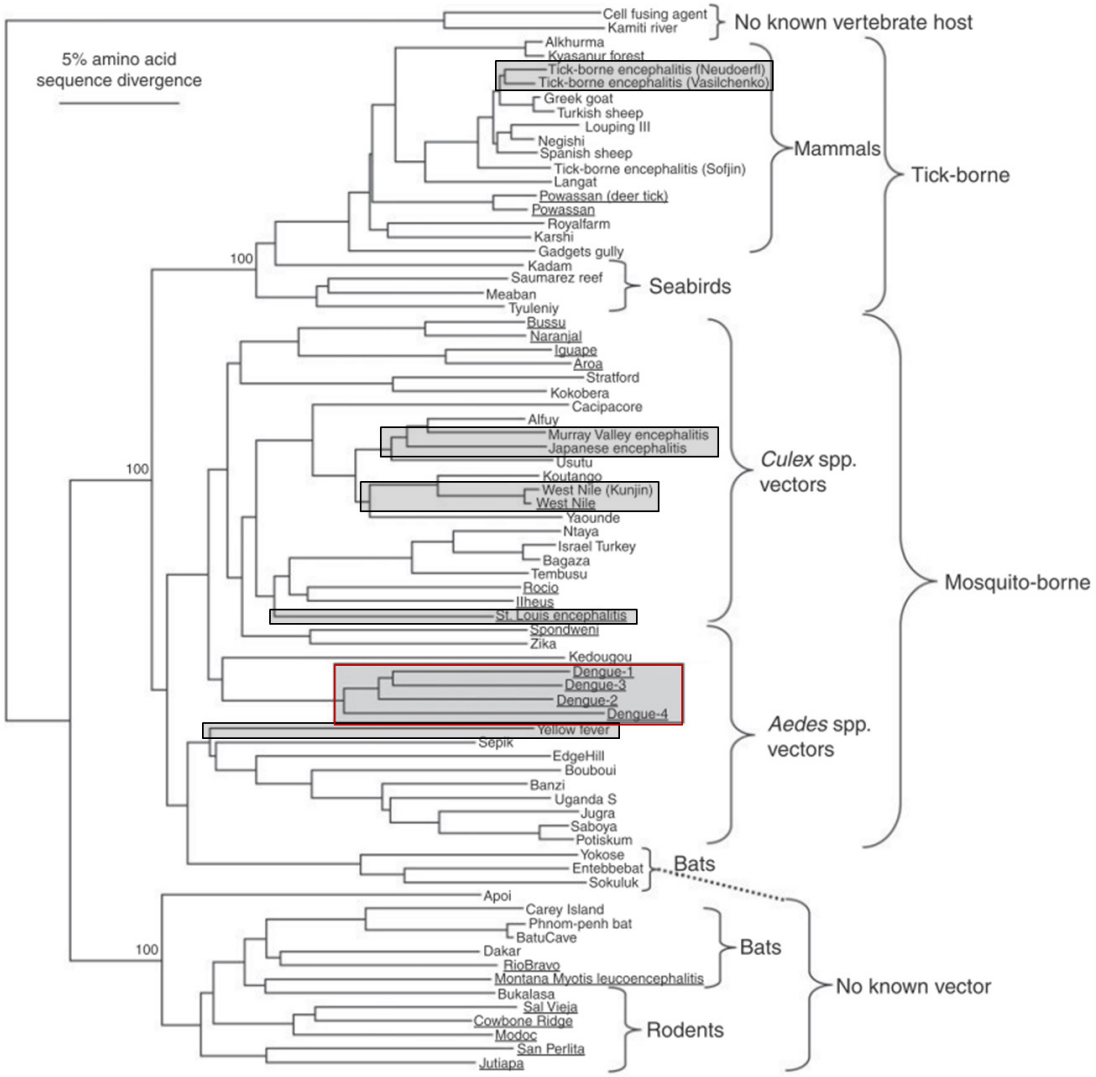

Figure 1-7: Phylogenetic tree of *Flavivirius* genus based on the analysis of partial NS5 amino acid sequences that were obtained from Genbank library. The tree was constructed using neighbor joining method. The bootstrap value for each major clade is indicated. The four serotypes of DENV are boxed in red whereas the other medically important flaviviruses are boxed in grey. Figure is adopted from (Vasilakis & Weaver, 2008a).

Viruses of the *Flavivirus* genus are further classified into three distinct groups depending on their vector association and antigenic relationships: [1] tick-borne, [2] mosquito-borne and [3] viruses with no known arthropod vector (Vasilakis & Weaver, 2008b). DENV is a mosquito-borne flavivirus vectored predominantly by *Aedes* mosquito, contain four antigenically related but genetically distinct dengue viruses, termed as DENV serotype 1-4 (Figure 1-7, boxed in red) (Heinz *et al.*, 2000). The amino acid conservation among four serotypes is 62-67% (Westaway & Blok, 1997). Phylogenetically, DENV1 and 3 are more closely related, whereas DENV4 is the most divergent serotype and it is closer to DENV2 than DENV1 and 3. The advent of full-length genome sequencing has further subdivided each serotype into ~four (DENV 3 & 4) or five (DENV 1 &2) genotypes, where nucleotide sequence divergence is not greater than 6% (Rico-Hesse, 1990; Vasilakis & Weaver, 2008b).

1.6 Molecular biology of DENV

1.6.1 Structure of dengue viral particles

Electron micrographs of mature flavivirus particles showed that these particles have a diameter of ~50 nm and they contain an electron dense ribonuclear core of ~30 nm (Lindenbach *et al.*, 2007). The nucleocapsid is composed of a single molecule of genomic RNA that is associated with ~180 copies of highly basic C protein and it is surrounded by host-derived lipid bilayer (Zhang *et al.*, 2007) that contains ~180 copies of each E and M proteins; the E proteins are organized into 90 tightly packed, head-to-tail dimers (Figure 1-8A) that lie flat on the surface of the viral membrane to form the external protein shell (Figure 1-8B) (Kuhn *et al.*, 2002). The E protein is the major antigenic determinant on virus particles and its role in mediating receptor

binding and membrane fusion to facilitate virus entry and that offers a potential target for antiviral inhibitors or neutralizing antibodies. The M protein is a small proteolytic fragment that is derived from its precursor prM during the maturation of virus particles in trans-Golgi network (TGN) and its role in mature virus is unknown.

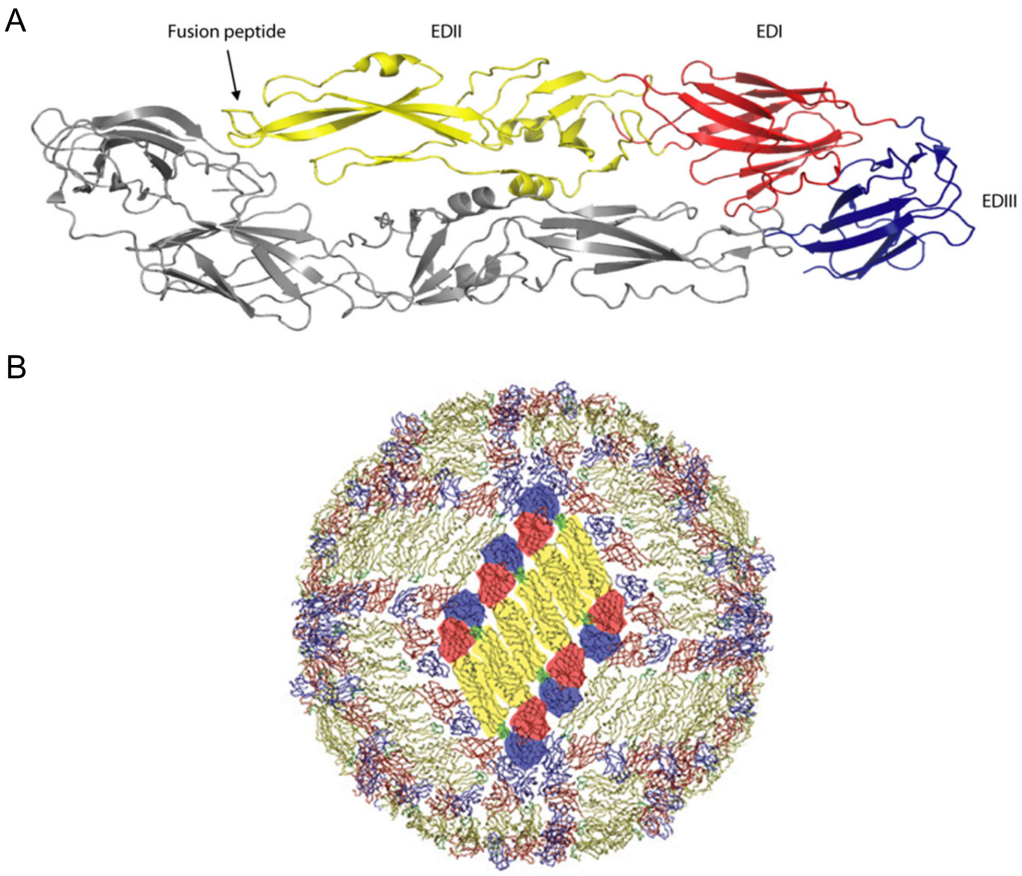

Figure 1-8: DENV envelope protein and its arrangement on mature virion surface. (A) Conformation of soluble E homodimers on mature virion surface at neutral pH. The stem and transmembrane anchor are not shown in the structure. Figure is adopted from (Modis *et al.*, 2004). (C) Packing of E on the surface of a mature virion. 90 E homodimers are arranged on an icosahedral lattice. Figure is adopted from (Zhang *et al.*, 2003).

1.6.2 DENV replication cycle

The infection cycle starts with the attachment of virus particles onto the surface of susceptible cells, which include macrophages, monocytes and DCs (Figure 1-9). This attachment is mediated by the binding of viral envelope (E) protein to a varied array of surface receptors (eg. Fcγ receptor (orange), DC-sign (green), cognate receptor (red, ie heparin sulfate, heat shock proteins, CD14 associated proteins, high-affinity laminin receptor and etc.), reviewed by (Hidari & Suzuki, 2011)) that allows virus entry by receptor-mediated endocytosis. The low pH in late endosome triggers the fusion of the viral envelope and host endosome membrane that is mediated by the structural rearrangement of E proteins and this leads to the release of the nucleocapsid into the cytoplasm. In the cytoplasm, the nucleocapsid dissociates to release viral RNA for translation of polyprotein by ribosomes that are located at the membrane of rough endoplasmic reticulum (ER). The resulting polyprotein is cleaved by a combination of host and viral proteases into three structural proteins (C, prM and E) and seven nonstructural (NS; NS1, NS2A, NS2B, NS3, NS4A, NS4B and NS5) proteins. The NS proteins, possibly together with host proteins, induce membrane invaginations into the ER lumen to generate vesicles that remain connected to the cytoplasm via pore-like openings (Welsch *et al.*, 2009). It is assumed that the vesicle interior contains the replication complex (RC) that is responsible for viral RNA replication. The virus-encoded NS5 RNA-dependent RNA polymerase (RdRP), together with helicase and ATPase activities of NS3, synthesizes a complementary negative-strand that is then used as a template for the amplification of genomic RNAs. The genomic RNA contains a type 1 cap structure ($^{7me}G_{ppp}A_{2'\text{-}O\text{-}me}$, see Figure 1-12A for cap structure) at the 5' end, which is generated by methyltransferase (MTase) and putative guanylyltransferase (GTase) activities of NS5, in conjunction with RNA 5'-

triphosphatase (RTPase) activity of NS3. Newly synthesized viral RNA interacts with C proteins to form nucleocapsid that bud into the ER lumen, at E- and prM-rich microdomains to form immature virions. The immature virions are transported from the ER to TGN via the typical secretory pathway. While passing through the TGN, the host protease furin cleaves prM protein into the pr peptide that remains bound to virion surface under acidic pH to prevent pre-mature fusion before virus release. The secretion of virion into extracellular milieu is accompanied by the release of pr peptide when exposed to neutral pH and this gives rise to mature infectious virions (reviewed by (Acosta *et al.*, 2014; Lindenbach *et al.*, 2007; Sampath & Padmanabhan, 2009)).

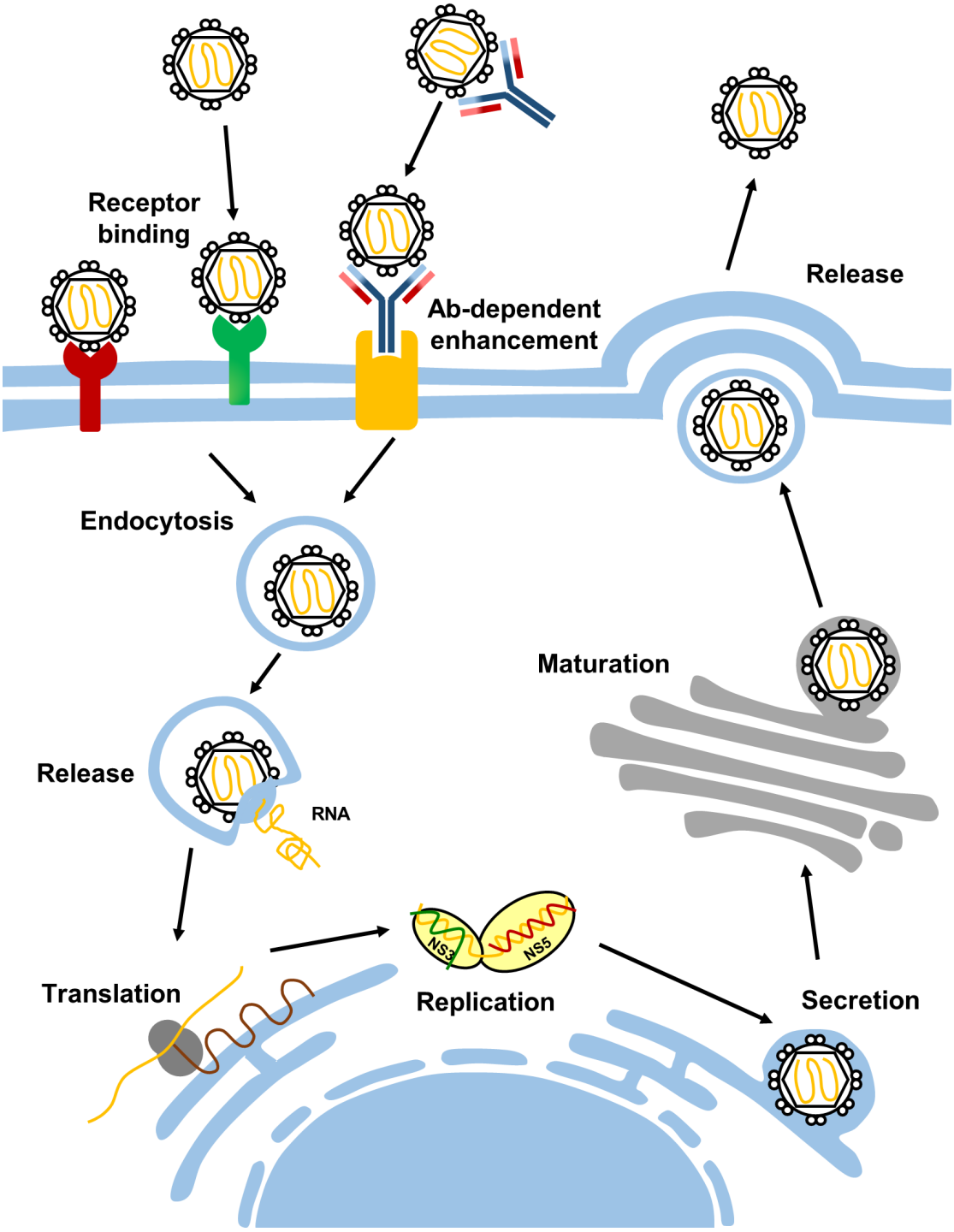

Figure 1-9: Schematic representation of the DENV replication cycle. The virus enters the cell by receptor mediated endocytosis. Membrane fusion between viral envelope and host endosome membrane leads to the release of the nucleocapsid into the cytoplasm. In the cytoplasm, the nucleocapsid dissociates to release viral RNA for translation. The viral RNA is translated by ribosomes to produce a single polyprotein that is being cleaved by viral and host proteases into three structural proteins (C, prM and E) and seven nonstructural (NS; NS1, NS2A, NS2B, NS3, NS4A, NS4B and NS5) proteins. Replication takes place in RCs that reside in virus-induced vesicles. Newly synthesized viral RNA interacts with C proteins to form nucleocapsid that bud into the ER lumen, at E- and prM-rich microdomains to form immature virions. These immature virions are released from the cell via secretory pathway. Virus maturation occurs in TGN where host protease furin cleaves prM protein into the pr peptide. Mature virions are secreted into the extracellular milieu.

1.6.3 Translation and polyprotein processing

Following the uncoating of nucleocapsid in cytoplasm, the 5' capped RNA genome serves as mRNA for translation of viral proteins. Translation from a single ORF produces a ~3300 amino acids long polyprotein that is processed co- and post-translationally by both host and viral proteases into 10 individual proteins. The N-terminal region of the polyprotein encodes structural proteins (C-prM-E) that are involved in the formation of virions whereas the C-terminal region of the polyprotein encodes seven NS proteins (NS1-NS2A-NS2B-NS3-NS4A-NS4B-NS5) that form the RC for genome replication (Lindenbach *et al.*, 2007). The NS3, together with its co-factor, NS2B forms the viral protease that cleaves the protein junctions between C/prM, NS2A/NS2B, NS2B/NS3, NS3/NS4A, NS4A/NS4B and NS4B/NS5 whereas signalase, an ER resident host protease, cleaves the protein junctions between C/prM, prM/E, E/NS1 and NS4A/NS4B (Figure 1-10). Furin, a Golgi-resident endoprotease is involved in virion maturation by cleaving prM to pr peptide and M protein during the transit of the immature virion prior to release. The protease cleaving NS1/2A junction remains to be determined.

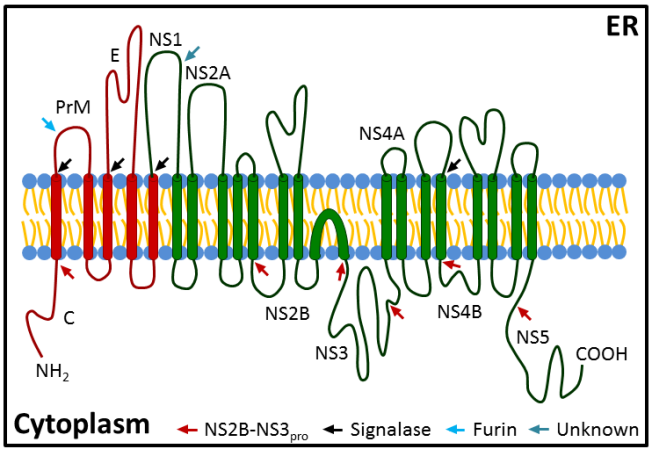

Figure 1-10: Proposed topologies of the viral proteins with respect to the ER membrane and the enzymes that are involved in processing the polyprotein. Structural proteins are shown in red and NS proteins are shown in green. The viral and host proteases that are involved in polyprotein processing are indicated. The NS3, together with its co-factor, NS2B forms the viral protease that cleaves the protein junctions between C/prM, NS2A/NS2B, NS2B/NS3, NS3/NS4A, NS4A/NS4B and NS4B/NS5 whereas signalase, an ER resident host protease, cleaves the protein junctions between C/prM, prM/E, E/NS1 and NS4A/NS4B (Figure 1-10). Furin, a Golgi-resident endoprotease is involved in virion maturation by cleaving prM to pr peptide and M protein during the transit of the immature virion prior to release. The protease cleaving NS1/2A junction remains to be determined.

1.6.4 Functions of dengue viral proteins

Following polyprotein processing, three structural proteins (C, prM and E) and seven NS (NS; NS1, NS2A, NS2B, NS3, NS4A, NS4B and NS5) proteins are released to perform their functions, such as formation of virions and RC, respectively (Lindenbach *et al.*, 2007). The known functions of these proteins are described below.

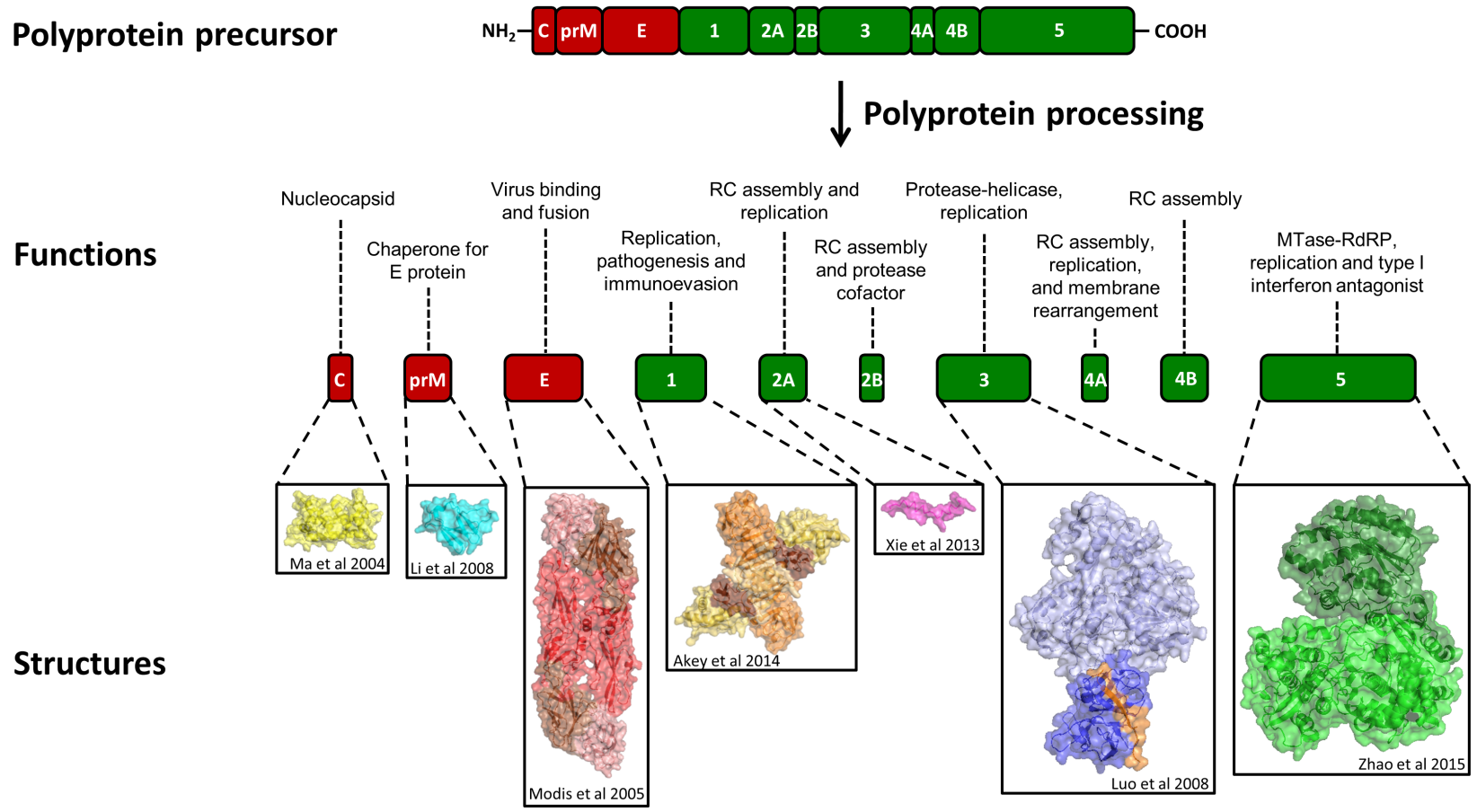

Figure 1-11: Schematic diagram on functions and structures of dengue viral proteins. Following the polyprotein processing by host and viral proteases, three structural proteins (C, prM and E) and seven NS (NS1, NS2A, NS2B, NS3, NS4A, NS4B and NS5) proteins are released to perform their functions, such as formation of virus particles and RC. The representative structure of each viral protein (not solved for NS2B, NS4A and NS4B) is showed. The PBD codes for the following proteins are - C: 1R6R (Ma *et al.*, 2004), prM: 3C6E (Li *et al.*, 2008), E: 1UZG (Modis *et al.*, 2005), NS1: 4O6B (Akey *et al.*, 2014), NS2A: 2M0S (Xie *et al.*, 2013), $NS2B_{18}$NS3: 2VBC (Luo *et al.*, 2008a) and NS5: 4V0Q (Zhao *et al.*, 2015).

1.6.4.1 Structural proteins

a) Capsid protein

Capsid is a ~11 kDa (114 amino acids) highly basic protein that together with the viral RNA genome, forms the nucleocapsid. It can bind viral RNA with high affinity and has RNA chaperone activity (Pong *et al.*, 2011). The capsid protein exists as dimers in solution and each monomer comprises of four alpha helices (Jones *et al.*, 2003). Through nuclear magnetic resonance study, the dimer revealed an asymmetric distribution of basic residues on protein surface; about half of the basic residues lie on one side of the dimer to interact with viral RNA, while the conserved hydrophobic residues form an extensive apolar surface on the opposite side of the dimer to interact with viral membrane (Figure 1-11) (Ma *et al.*, 2004). In infected cells, the protein localizes to the nucleus and nucleoli (Makino *et al.*, 1989; Wang *et al.*, 2002) and it is mediated by two monopartite nuclear localization signals (NLS) (within residues 6-9 and 73-76) and one bipartite NLS (within residues 85-100); mutagenesis study showed that ^{73}KK and ^{85}RK are important for its nuclear localization, interaction with DAXX (Death domain-associated protein 6) and induction of apoptosis (Netsawang *et al.*, 2010). Intriguingly, the protein also localizes to the surface of cytoplasmic lipid droplets and through mutagenesis study, disrupting its lipid droplet targeting ability was shown to affect virus assembly (Samsa *et al.*, 2009).

b) Membrane protein

Precursor of membrane (prM) protein is ~26 kDa and it plays an important regulatory role during virus entry and exit (Hsieh *et al.*, 2011). Uncleaved prM is 166 amino long and the first 91 amino constitutes the pr peptide. Cleavage of prM into soluble pr peptide and membrane-associated M protein is mediated by Golgi-resident endoprotease furin that recognizes the highly conserved RR(D/E)KR sequence in pr domain (Keelapang *et al.*, 2004). The role of pr peptide is thought to prevent the pre-mature fusion of E protein before virus release (Lindenbach *et al.*, 2007) and this is supported by the crystal structure of prM-E protein complex that showed the binding of pr peptide to the fusion loop of E protein (Figure 1-11) (Li *et al.*, 2008). In agreement to that, virus preparations derived from furin-deficient cells contained high numbers of prM-containing viral particles and they were unable to infect (Zybert *et al.*, 2008), which further supports the proposed function of pr peptide. Intriguingly, these immature particles became infective when complexed with anti-prM , which might be Fc receptor mediated (Dejnirattisai *et al.*, 2010; Richter *et al.*, 2014; Rodenhuis-Zybert *et al.*, 2010) and this poses a concern for vaccine development because prM protein is present in DENV vaccine (eg. live attenuated, recombinant or inactivated virus) (Whitehead *et al.*, 2007) and this may increase the risk of ADE in vaccine recipients (Dejnirattisai *et al.*, 2010).

c) Envelope protein

Envelope (E) is a 56 kDa (495 amino acids) membrane-associated glycoprotein and it is the major component of the virion surface. It is involved in virion assembly, receptor binding, membrane fusion and induction of protective anti-DENV antibody. The E protein is synthesized as a type I membrane protein containing twelve conserved cysteines that form six disulphide bonds and it is N-glycosylated (Deubel *et al.*, 1991; Men *et al.*, 1991). The proper folding of E requires co-synthesis with prM (Lindenbach *et al.*, 2007). The N-terminal ectodomain of E contains three β-barrel domains, domain I, II and III (EDI, EDII and EDIII, coloured in red, yellow and blue, respectively (Figure 1-8A and 11). Domain II is involved in the dimerization of E protein, whereas domain III is responsible for receptor binding. The fusion loop is found at the tip of domain II and its role is to interact with host endosomal membrane during fusion (Modis *et al.*, 2005). The C-terminal domain has a stem region containing two α-helices that are connected by a stretch of conserved sequences and an anchor region containing two TM domains (Lin *et al.*, 2011). The glycosylation of E protein has been shown to be important for production of viral particles and infection of DC-SIGN expressing cells (Alen *et al.*, 2012; Bryant *et al.*, 2007; Lee *et al.*, 2010a; Mondotte *et al.*, 2007).

1.6.4.2 Nonstructural proteins

a) NS1

NS1 is a 46 kDa (352 amino acids) glycoprotein that plays an essential yet unclear role in viral replication. In mammalian cells, it exists in two major forms: membrane-associated and secreted forms (Muller & Young, 2013). NS1 monomeric form is water-soluble and it becomes membrane-associated once it dimerizes (Winkler *et al.*, 1989; Winkler *et al.*, 1988). It resides in ER lumen and it co-localizes with double-stranded RNA (dsRNA) in both insect (Mackenzie *et al.*, 1996) and mammalian (Welsch *et al.*, 2009) cells. When NS1 was expressed together with the first 26 amino acids of NS2A, NS1 localized to the plasma membrane via glycosylphosphatidylinositol (GPI) anchor; this is in line with the report that ~20% of surface-expressed NS1 in infected cells were GPI-linked and this linkage may associate NS1 to lipid raft to mediate signaling cascade common to GPI-anchored proteins when specific antibodies are present (Jacobs *et al.*, 2000; Noisakran *et al.*, 2008a; Noisakran *et al.*, 2007). Recently, the crystal structure of NS1 was solved and NS1 was shown to have three domains: β-roll dimerization domain, wing domain and β-ladder domain; the β-roll dimerization domain enables NS1 dimerization and it also forms a hydrophobic protrusion with the connector subdomain of wing domain, which is thought to mediate the interaction of dimeric NS1 with the ER membrane and the RC through transmembrane protein NS4A and NS4B (Figure 1-11) (Akey *et al.*, 2014).

Secreted NS1 is hexametric and inhibition of glycosylation affects the secretion of hexameric form (Flamand *et al.*, 1999; Somnuke *et al.*, 2011). Cryo-electron microscopy study revealed that the secreted NS1 hexamer forms a lipoprotein particle with open-barrel protein shell and a central channel rich of lipids, predominantly triglycerides; interestingly, the composition of these lipids highly resembled high-density lipoprotein and inhibiting lipid biosynthesis reduced NS1 secretion, implying that host lipids may play an essential role in NS1 secretion (Gutsche et al., 2011). The amount of secreted NS1 appears to be significantly higher in sera of patients with DHF rather than DF (Libraty *et al.*, 2002b), which can be a cause or consequence of plasma leakage. In addition, both secreted and surface-expressed NS1 are capable of modulating complement activation pathways through binding to proteins of complement system or the formation of immune complexes (Avirutnan et al., 2010; Avirutnan et al., 2006; Chung et al., 2006; Kurosu et al., 2007).

b) NS2A

NS2A is a 22 kDa (218 amino acids) integral membrane protein that plays an important role in viral RNA replication. According to proposed topology model, NS2A contains five TM helices; the N- and C-terminal faces the ER lumen and cytoplasm, respectively (Xie *et al.*, 2013). Based on nuclear magnetic resonance study, the first TM domain was solved and it was shown to contain two helices that is connected by "helix breaker" (Pro85) (Figure 1-11) (Xie *et al.*, 2013). Through mutagenesis study, NS2A was shown to be important for viral RNA synthesis and virus assembly/maturation (Xie *et al.*, 2013; Xie *et al.*, 2015) but the underlying molecular mechanism for these processes remains to be elucidated.

c) NS2B

NS2B is a 14 kDa (130 amino acids) integral membrane protein that serves as an essential cofactor for NS3 serine protease activity and it recruits NS3 to ER membrane. It was predicted to have two N-terminal TM helices and a membrane-associated C-terminal domain that is connected by hydrophilic cytoplasmic domain; the hydrophilic domain contains a 47 amino acids long region (residues 49-95) that is essential for NS3 folding and activity (Clum *et al.*, 1997; Erbel *et al.*, 2006; Falgout *et al.*, 1991; Luo *et al.*, 2008a). NS2B-NS3 protease interaction via the 47 amino acids long region induces structural remodeling of the protease domain to facilitate cleavage sequence recognition and substrate binding (Zuo *et al.*, 2009). It was suggested that NS2B may play the main role in anchoring NS3 and NS5 to NS2A, NS2B and NS4B in RC (Yu *et al.*, 2013) and this has been evidenced by the co-localization of NS2B with dsRNA in RC (Welsch *et al.*, 2009).

d) NS3

NS3 is a multifunctional protein and it is the second largest (69 kDa, 618 amino acids) viral protein (Lindenbach *et al.*, 2007). It contains a N-terminal protease domain (Li *et al.*, 1999b), and a C-terminal domain that has helicase, RNA-stimulated nucleoside triphosphatase (NTPase), and RNA 5'-triphosphatase (RTPase) activities (Benarroch *et al.*, 2004; Cui *et al.*, 1998; Preugschat *et al.*, 1990; Wengler, 1993; Xu *et al.*, 2005b). The protease domain, works in concert with its NS2B cofactor, is responsible for cleaving the viral polyprotein (see section 1.6.3). On the contrary, its helicase domain, together with NS5 RdRP and MTase activities, is involved in viral RNA replication and type 1 cap formation, respectively. During viral RNA replication, the

helicase activity is thought to be required for unwinding of duplex RNA and/or secondary structure of single-stranded RNA whereas the NTPase activity provides the energy for helicase unwinding activity. During type 1 cap structure formation, the RTPase activity is responsible for removing the γ-phosphate from 5'triphosphorylated RNA, which has to occur before NS5 MTase can catalyze the subsequent reaction (also see Figure 1-12B) (Wang *et al.*, 2009a; Xu *et al.*, 2005b). In infected cells, NS3 co-localises with dsRNA and NS4B proteins in perinuclear region (Welsch *et al.*, 2009) and it was shown to interact with both NS4B (Umareddy *et al.*, 2006a) and hypophorylated NS5 (Kapoor *et al.*, 1995); these findings are consistent with the role of NS3 in viral RNA replication in RC. Apart from its interaction with viral proteins, NS3 has also been shown to interact with the host protein fatty acid synthase (FAS); this interaction is mediated by the protease domain and through this interaction, it enhances the activity of FAS and recruits FAS to areas of viral replication to possibly establish or expand the membranous replication vesicles (Heaton *et al.*, 2010).

The N-terminal of NS3 (residues 1-168) encodes a trypsin-like serine protease that contains the typical catalytic triad of His-53, Asp-77 and Ser-138 in its active site. For it to function as an active protease, it has to interact with the hydrophilic region of NS2B (residues 49-95) (Leung *et al.*, 2001). Without $NS2B_{49-95}$, NS3 is known to be insoluble and hence, in order to obtain soluble active form of NS3 protease for crystallization, NS3 protease was expressed as a fusion construct with $NS2B_{49-95}$ that was connected by flexible glycine linker (G_4SG_4) (Leung *et al.*, 2001; Li *et al.*, 2005). The crystal structure of DENV protease revealed a chymotrypsin-like fold with two β-barrels and each barrel is formed by six β-strands; the barrel interface contains the catalytic triad. In the presence of inhibitor, the C-terminal region of NS2B (residues

67-95) form a conserved β-turn hairpin that wraps around the C-terminal β-barrel of NS3 to form a "closed" conformation and this allows the β-turn hairpin to bind to hydrophobic S2 and S3 pockets in the substrate binding site to interact directly with inhibitor (Aleshin *et al.*, 2007; Erbel *et al.*, 2006; Noble *et al.*, 2012). Hence, this collectively implies that residues 67-95 is needed for NS3 proper folding and catalytic activity.

The C-terminal domain of NS3 is a multifunctional protein (residues 180-618) and it is a member of the superfamily 2 (SF2) that contains the DEAH sequence motif (Gorbalenya *et al.*, 1989). NS3 helicase contains three domains and the crystal structure revealed the RecA-like fold of domain I and II, which is composed of six β-strands that are surrounded by four and three α-helices, respectively (Xu *et al.*, 2005b). For domain III, it is composed of two β-strands and approximately five α-helices. The ATPase and RTPase activities are found in domains I and II whereas the single-stranded RNA binding groove is found at the interface of the three domains. NS3 helicase activity was shown to be ATP- and Mg^{2+}-dependent (Benarroch *et al.*, 2004) and its interaction with NS4B promotes its dissociation from single-stranded RNA, which subsequently enhances its helicase activity (Umareddy *et al.*, 2006a). Its NTPase and RTPase activities were also found to Mg^{2+}-dependent and both activities could be stimulated by NS5 (Cui *et al.*, 1998; Yon *et al.*, 2005); through biochemical and mutagenesis studies, it was suggested that NTPase and RTPase may share a common active site (Bartelma & Padmanabhan, 2002). Similarity, mutations affecting helicase activity also reduced RTPase activity (Benarroch *et al.*, 2004), suggesting that the helicase, NTPase and RTPase activities may be functionally coupled.

The structure of DENV4 full-length NS3 revealed an elongated conformation with protease domain sits underneath the ATP binding site of helicase (Luo *et al.*, 2008a); the protein can also adopt a different relative orientation of the protease and helicase (protease domain rotated by ~161° with reference to the helicase domain) domains due to flexibility of the two domains that is mediated by linker region (residues 169-179) and it appears that the linker region has evolved to an optimum length to confer flexibility to full-length NS3 protein that is required for both polyprotein processing and RNA replication.(Luo *et al.*, 2010). The two conformations of NS3 protein probably reflect the different conformations that are being adopted by the protein to perform its various functions during virus life cycle.

e) NS4A

NS4A is a 16 kDa (150 amino acids) integral membrane protein that plays an important role in viral replication. It was shown to co-localize with dsRNA, NS3 and NS4B in RC (Miller *et al.*, 2007; Welsch *et al.*, 2009; Zou *et al.*, 2015b). It is only viral protein that was demonstrated to have membrane curvature-inducing activity when expressed on its own, suggesting that NS4A may play a major role in replication vesicle formation; biochemical study suggests that NS4A contains three α-helical segments that give rise to its peculiar membrane topology, which may explain its membrane curvature-inducing activity (Miller *et al.*, 2007). A recent study suggests that NS4A contains an N-terminal amphipathic α-helix (residues 3-20) and mutations affecting this helix have reduced ability to oligomerize and have impairment in RNA replication, implying that NS4A self-oligomerization may be important for RC formation (Stern *et al.*, 2013).

f) NS4B

NS4B is a 30 kDa (248 amino acids) integral membrane protein that plays an important role in viral replication. It was shown to co-localize with dsRNA, NS3 and NS4A proteins in RC (Umareddy *et al.*, 2006b; Welsch *et al.*, 2009; Zou *et al.*, 2015b). NS4B exists as dimers in transfected and infected cells (Zou *et al.*, 2014) and it contains three TM segments, as well as N- and C-terminal segments that face ER lumen and cytoplasm (Miller *et al.*, 2007). Mutational studies on NS4B showed that it is crucial for virus replication in cell culture and animal models (Grant *et al.*, 2011; Kelly *et al.*, 2010; Orozco *et al.*, 2012) (Zou *et al.*, 2014). NS4B might be a key determinant of cytokine secretion like TNF-α, IFN-γ, IP-10, IL6 and IL-8 in infected cells (Kelley *et al.*, 2011).

g) NS5

NS5 is the largest (103 kDa, 900 amino acids) and most conserved protein among all viral proteins (Lindenbach *et al.*, 2007). Its N-terminal domain contains MTase (Egloff *et al.*, 2002; Egloff *et al.*, 2007; Kroschewski *et al.*, 2008) and putative GTase activities (Issur *et al.*, 2009) that are involved in type 1 cap formation, whereas its C-terminal harbors RdRP activity that is responsible for viral RNA replication with NS3 (Yap *et al.*, 2007). In infected cell, DENV2 NS5 is known to interact with NS3 (Kapoor *et al.*, 1995) and to also, shuttle between the cytoplasm and nucleus (see section 1.9 for more information) (Brooks *et al.*, 2002; Kumar *et al.*, 2013; Pryor *et al.*, 2007; Rawlinson *et al.*, 2009). NS5 was shown to be a potent TNF-α, IL-6 and IL-8 inducer (Kelley *et al.*, 2011; Medin *et al.*, 2005), and its IL-8 inducing ability seems to correlate with NS5 nuclear localization and infectious virus production (Pryor *et*

al., 2007; Rawlinson *et al.*, 2009). It was demonstrated that DENV2 NS5 can bind to STAT2 to promote UBR4-mediated STAT2 degradation by bridging STAT2 and UBR4, an E3 ligase that recognizes and degrades proteins and this results in inhibition of type I interferon signaling (Ashour *et al.*, 2009; Mazzon *et al.*, 2009; Morrison *et al.*, 2013).

NS5 MTase has two binding sites: a S-adenosyl-L-methionine (SAM) binding site and a RNA cap site for binding to guanosine of the cap structure (Egloff *et al.*, 2007). Its MTase domain possesses two methylation activities: guanine-N7 (Kroschewski *et al.*, 2008) and nucleoside 2'-O methylation (Egloff *et al.*, 2002). The current model for the formation of type 1 cap structure assumes four sequential steps: [1] the RTPase activity of NS3 removes 5′ γ-phosphate from newly synthesized RNA (Benarroch *et al.*, 2004; Xu *et al.*, 2005a), [2] the newly identified GTPase activity of NS5 may cap the RNA 5′-diphosphate end with guanosine monophosphate (GMP) through a 5′ to 5′ phosphodiester bond (Issur *et al.*, 2009), [3] the guanine-N7 methylation activity of NS5 transfers a methyl group to the N7 position of the guanine moiety to form a cap 0 structure ($^{7me}G_{ppp}$A-RNA) (Zhou *et al.*, 2007) and [4] lastly, the 2'-O methylation activity of NS5 catalyzes methylation at the ribose 2′-*O* position of adenosine to form type 1 cap structure ($^{7me}G_{ppp}A_{2'\text{-}O\text{-}me}$-RNA) (Egloff *et al.*, 2002) (Figure 1-12B). Time course experiment showed that N7-methyltion occurs before 2'O-methylation (Selisko *et al.*, 2010) and both use SAM as methyl donor for methylation (Noble *et al.*, 2010). Through mutagenesis study, N7-methyaltion was found to be important for virus replication (Zhou *et al.*, 2007). Recently, a 2'-O MTase mutant virus ($^{216}E\rightarrow A$ in DENV1 and $^{217}E\rightarrow A$ in DENV2) that was shown to replicate like WT in cell culture but poorly in mice and rhesus monkeys were able to induce protection in

rhesus monkeys during homologous challenge, hence demonstrating the potential of using 2'-O MTase mutant virus as a safe and rationally designed vaccine (Zust *et al.*, 2013).

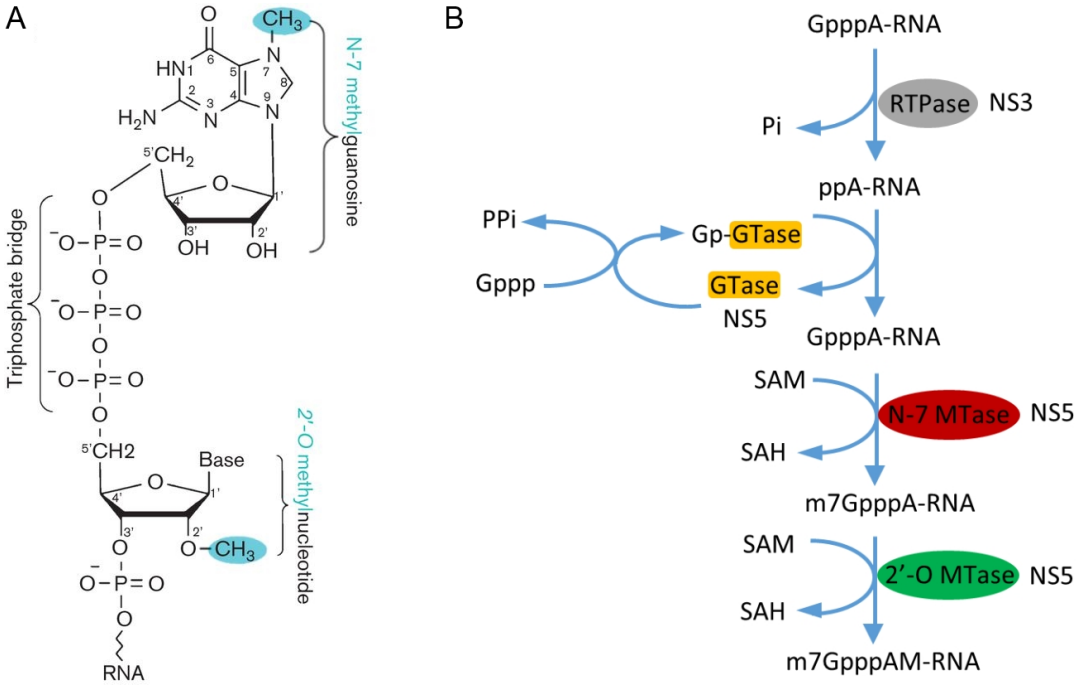

Figure 1-12: Type 1 cap formation by NS5 MTase and NS3 RTPase activities. A) The mRNA cap structure. The cap structure consists of an N-7 methylguanosine, a triphosphate bridge and one or two 2′-*O* methylnucleotide(s). The N-7 and 2′-*O* methyl groups are indicated in blue. B) Four enzymatic activities are required for type 1 cap formation: 5′ RTPase, GTase, N-7 MTase and 2′-*O* MTase. 5′ RTPase activity (blue) is performed by NS3. N-7 MTase (red) and 2′-*O* MTase (green) activities are performed by NS5 and GTase (orange) acitivty is thought to be performed by NS5 too. SAM is the methyl group donor and SAH is the by-product of methylation. Figure is adapted from (Dong *et al.*, 2014).

The RdRP domain of DENV3 has the classical "cupped right hand" architecture with fingers, palm and thumb subdomains that have been described for various flaviviruses (Lim *et al.*, 2013b; Lu & Gong, 2013; Malet *et al.*, 2007; Yap *et al.*, 2007). The βNLS and α/βNLS (reside in residues 320-405), which was originally thought to be an interdomain linker region between MTase and RdRP were found to be an integral part of RdRP domain and is distributed between the fingers and thumb subdomains. The

highly conserved palm domain contains four out of the six conserved sequence motifs that are important for NTP binding and catalysis, including the GDD catalytic active site. Its active site is encircled by several loops to form a tunnel that can direct the RNA template strand to the active site (Yap *et al.*, 2007). The thumb subdomain contains the most structurally variable elements among the known polymerase structures that help to shape the RNA template tunnel and possibly regulate the entry and exit of template into active site, and also the priming loop that is involved in *de novo* initiation (Yap *et al.*, 2007). Functional mutagenesis study of two conserved cavities of thumb subdomain led to the identification of residues K328, Y859 and I863 that are crucial for *de novo* initiation but not elongation, and also residue K330 that is involved in NS3-NS5 interaction (Zou *et al.*, 2011).

Recently, the structure of compact form of DENV3 full-length NS5 was solved and it revealed a different relative orientation of the MTase and RdRP (MTase domain rotated by 105° with reference to the RdRP domain) (Zhao *et al.*, 2015) when compared to extended form JEV full-length NS5 structure (Lu & Gong, 2013), despite the similarity in the overall shape of DENV3 and JEV NS5s.The differences in the length, sequence and structure of linker, as well as the molecular nature of MTase-RdRP binding interface between DENV3 and JEV NS5s led to two NS5 conformations that may reflect the different conformations that are being adopted by the protein with regard to its various functional roles during virus life cycle.

1.6.5 RNA replication in flavivirus replication complex

DENV replication presumably occurs in perinuclear virus-induced vesicles that contain the RC, where viral RNA, viral proteins and host proteins participate in many important RNA-RNA, RNA-protein and protein-protein interactions to ensure efficient viral RNA replication (Chen *et al.*, 1997; Uchil & Satchidanandam, 2003). By electron microscopy and tomography, virus-induced vesicles are shown to be derived from the invagination of ER membrane (Welsch *et al.*, 2009) and they are demonstrated to contain all NS proteins and dsRNA by immuno-electron microscopy and light microscopy (Chen *et al.*, 1997; Uchil & Satchidanandam, 2003; Welsch *et al.*, 2009).

The replication of viral genome starts at the 3'end of the positive-strand genome to synthesize negative-strand RNA that in turn acts as template for additional positive-strand RNA in 10-100 fold excess of negative-strand (Tomassini *et al.*, 2003). Three major species of labeled DENV RNA have been described, including genomic RNA that is RNase sensitive, a double-stranded replicative form (RF) that is RNase resistant and, a heterogeneous population of replicative intermediate (RI) that is partially RNase resistant. RF is composed of genome-length positive- and negative-strand RNAs and it serves as the recycling template for positive-strand production. RI is essentially RF that contains an additional positive-strand RNA molecule and its synthesis is necessary for the progression of replication cycle (Chu & Westaway, 1985; Cleaves *et al.*, 1981).

1.6.6 NS protein-protein interactions within replication complex

Protein-protein interaction between several viral NS proteins of RC have been described, including that of DENV NS2B and NS3 (Phong *et al.*, 2011), NS4A and NS4B (Zou *et al.*, 2015b), and NS1 and NS4B self-dimerization (Figure 1-13) (Akey *et al.*, 2014; Zou *et al.*, 2014) by pulldown assay, NS3 and NS4B (Umareddy *et al.*, 2006b; Zou *et al.*, 2015a), and NS3 and NS5 by yeast two-hybrid (Y2H) and protein-complex immunoprecipitation (co-IP) studies (Brooks *et al.*, 2002; Kapoor *et al.*, 1995; Mairiang *et al.*, 2013; Moreland *et al.*, 2012). *In vitro* binding studies on Kunjin virus proteins showed that NS2A could bind strongly to 3'UTR, NS3 and NS5, while NS4A could bind strongly to itself, NS3 and NS5 strongly and bind weakly to 3'UTR (Mackenzie *et al.*, 1998). Studies on YFV and DENV proteins demonstrated a genetic interaction between NS4A with NS1 and NS4B, respectively (Lindenbach & Rice, 1999; Tajima *et al.*, 2011). A recent study on WNV proteins showed that only four NS proteins, namely the transmembrane proteins, NS2A, NS2B, NS4A and NS4B co-localized with ER membrane protein calnexin, but NS1, NS3 and NS5 did not when these proteins were expressed singly (Yu *et al.*, 2013), which is consistent with the role the NS2A, NS2B, NS4A and NS4B as intergral membrane protein in RC. Through confocal microscopy, fluorescence resonance energy transfer and biologic fluorescence complementation, the authors showed that there were two-way interactions between (1) NS2A and NS4A, (2) NS2B and three other transmembrane proteins (NS2A, NS4A and NS4B), (3) NS2B and NS3, and (4) NS3 and NS5, and three-way interactions between three other transmembrane proteins (NS2A, NS4A and NS4B) and NS3 occurred only when NS2B was present (Yu *et al.*, 2013). This suggests that NS2B may be playing the main role in bringing the three transmembrane proteins together in the RC and in recruiting the key replicative enzymes, NS3 and

NS5 to the replication site. No protein-protein interaction was found between NS1 and the other NS proteins, but fluorescence resonance energy transfer data suggested the formation of NS1 homodimer (Yu *et al.*, 2013), which is the consistent with the observation that intracellular NS1 is predominately dimeric (Akey *et al.*, 2014; Gutsche *et al.*, 2011; Muller *et al.*, 2012; Muller & Young, 2013). Further functional evidence that supports interaction between NS proteins has been demonstrated by the modulation of NS3 enzymatic/functional activity by NS4A (Shiryaev *et al.*, 2009), NS4B (Umareddy *et al.*, 2006a) and NS5 (Cui *et al.*, 1998; Yon *et al.*, 2005).

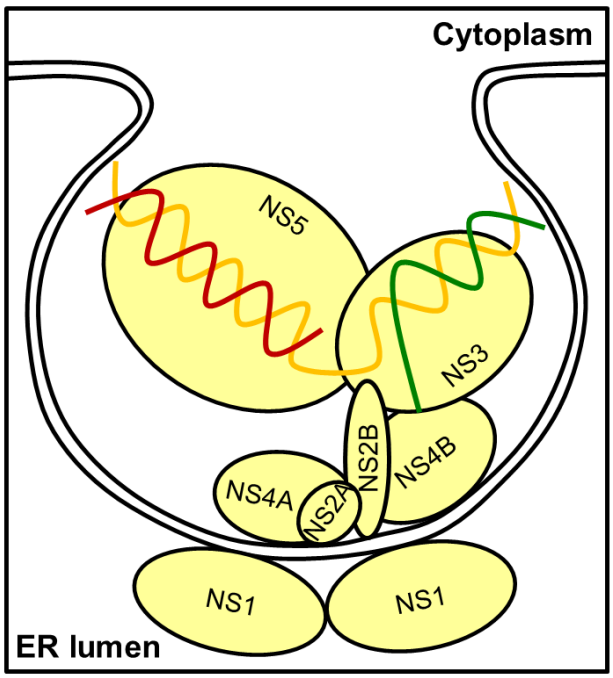

Figure 1-13: Proposed model of flavivirus replication complex in ER. This model was proposed as reviewed in section 1.6.6 and was based on study by (Yu *et al.*, 2013) and reviews by (Muller & Young, 2013; Shi, 2014). The four transmembrane proteins NS2A, NS2B, NS4A and NS4B are proposed to form a transmembrane complex in the ER. NS3 and NS5 are not ER-bound but they are tethered to the ER, together with viral RNAs (yellow line: parental strand that serves as template, green line: unwound parental strand; red line: complementary daughter strand) via interaction between NS2B and NS3. NS3 has been reported to interact with NS4B and NS5. NS1, NS4A and NS4B have the capability to form dimers. The hydrophobic nature of a protrusion that is located at the N-terminal of NS1 is suggested to be involved in interaction with ER and transmembrane proteins NS4A and NS4B.

1.6.7 Role of 5' and 3' untranslated regions in DENV life cycle

Efficient viral RNA replication, translation and viral pathogenicity are regulated by structural elements and conserved sequences in the 5'UTR, capsid-coding region and 3'UTR. It has been shown that DENV genome is a dynamic molecule that adopts at least two different conformations during viral replication - linear and circular (Figure 1-14B); it has also been demonstrated that only the circular forms are capable of viral RNA replication in infected cells (Filomatori *et al.*, 2006) and maintaining a balance between linear and circular forms of the genome is essential for replication, possibly as a control mechanism to limit negative-sense RNA synthesis so as to maintain a 1:10-100 ratio of negative- versus positive-sense RNA found in infected cells (Tomassini *et al.*, 2003; Villordo *et al.*, 2010; Villordo & Gamarnik, 2009). It is known that viral proteins (eg. NS3 and NS5) and host proteins do bind to 5'- and/or 3'-UTR (Anwar *et al.*, 2009; De Nova-Ocampo *et al.*, 2002; Garcia-Montalvo *et al.*, 2004b; Gomila *et al.*, 2011; Paranjape & Harris, 2007; Polacek *et al.*, 2009; Vashist *et al.*, 2009; Vashist *et al.*, 2011; Yocupicio-Monroy *et al.*, 2003) (also see Table 3-5 for the list of these host proteins) and some of the host proteins are shown to modulate viral RNA replication (eg. polypyrimidine tract-binding protein (PTB); (Anwar *et al.*, 2009), Interleukin enhancer-binding factor 3 (ILF3) (Gomila *et al.*, 2011) and Y box-binding protein-1 (YB-1) (Paranjape & Harris, 2007)) but it remains to be determined if viral proteins and host proteins can mediate the switch between linear and circular forms of genome or resolve RNA structural element for efficient viral RNA replication.

a) 5'UTR

DENV has short 5'UTR (96 nucleotides for DENV2) (Figure 1-14A) consisting of two stem loops (SLA and SLB) that is connected by an oligoU spacer. NS5 RdRP domain specifically binds to the genome by SLA, which functions as the promoter element for NS5 RdRP (Villordo & Gamarnik, 2009). SLA alone is inadequate in inducing RdRP activity, and specific nucleotides in SLA are necessary to form an active promoter-polymerase complex for RNA synthesis (Filomatori *et al.*, 2006). SLB contains 5'UAR that interacts with 3'UAR in 3'-UTR (connected by blue line in Figure 1-14A), and together with another two pairs of long range 5'-3' RNA-RNA interactions (5'-3'CS and 5'-3'DAR, connected by orange and grey lines, respectively, in Figure 1-14A), they are required for the circularization of viral genome (Figure 1-14B) to place NS5 to the 3'end of the genome for initiation of negative-strand synthesis (Alvarez *et al.*, 2005b). In addition, the composition of the sequence downstream of 5'CS also influences genome circularization (Friebe *et al.*, 2012). Apart from the crucial role of 5'-UTR in replication, it is also known that the 5'-UTR contains a capsid-coding region hairpin element (cHP) (Figure 1-14B) that is needed for viral RNA synthesis and translation initiation codon selection (Clyde *et al.*, 2008; Clyde & Harris, 2006).

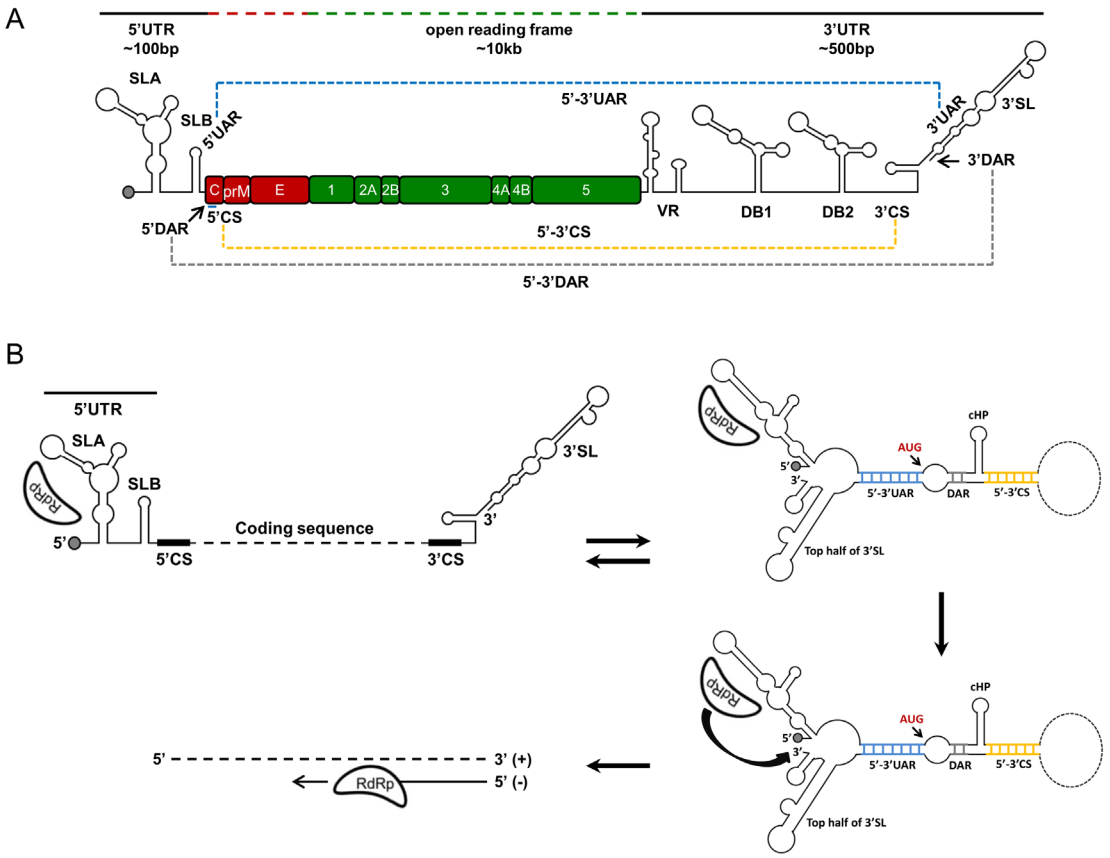

Figure 1-14: Schematic representation of DENV genome circularization and proposed model for negative-sense RNA synthesis. (A) In DENV genome, the 5′- and 3′-UTRs are approximately 100 and 500 nucleotides in length, respectively, and they contain highly structured regulatory RNA elements that are crucial for translation, viral RNA replication and pathogenicity. The 5′- and 3′-UTRs contain sequences, namely 5’ and 3’UAR (connected by blue dotted line), 5’ and 3’DAR (connected by grey dotted line), and 5’ and 3’CS (connected by orange dotted line) that can participate in long-range RNA-RNA interactions to circularize the genome for negative-strand synthesis. (B) Proposed model for negative-sense RNA synthesis. In this model, NS5 binds to 5’ SLA to from promoter-polymerase complex that is far from the 3’ initiation site. Through genome circulation that is mediated by long-range 5’-3’ RNA-RNA interactions, the promoter-polymerase complex is placed in close proximity to the 3’ end of the genome, which the promoter-polymerase complex can use it as a template to initiate negative-strand synthesis. SL = stem loop, VR = variable region, DAR = downstream AUG region, UAR = upstream AUG region, CS = cyclization sequence, DB = dumbbell, UTR = untranslated region and cHP = capsid hairpin. Refer to main text for more information. Figure is adapted from (Acosta *et al.*, 2014) and (Villordo & Gamarnik, 2009).

b) 3'UTR

DENV has a long 3'UTR (454 nucleotides for DENV2) (Figure 1-14A) that contains several important RNA structures/sequences in addition to the three complementary regions (3'CS, 3'UAR and 3'DAR), which are required for genome circularization. The variable region (VR) that is located at the 5'end of 3'UTR contains five stem loop structures (SL-I to V). SL-II forms a pseudo-knot structure in to stall the cellular 5'-3' exonuclease XRN1 to form subgenomic flaviviral RNA (sfRNA) (Chapman *et al.*, 2014); sfRNA has been shown to inhibit XRN1 activity and dysregulate host mRNA stability (Moon *et al.*, 2012), and also to sequester multifunctional RNA-binding proteins G3BP1, G3BP2 and CAPRIN1 to inhibit interferon stimulated genes mRNA translation (Bidet *et al.*, 2014). The middle part of 3'UTR forms two dumb-bell structures that are required for optimal translation (Alvarez *et al.*, 2005a). Finally, the highly conserved 3'SL is crucial for RNA replication and translation (Holden *et al.*, 2006; Tilgner *et al.*, 2005; Zeng *et al.*, 1998) (reviewed by (Selisko *et al.*, 2014)).

1.7 Nuclear-cytoplasmic transport of dengue viral proteins

In DENV life cycle, it is known that DENV2 NS5 protein can undergo nuclear-cytoplasmic trafficking that is mediated through interaction of NS5 with components of host import and export machinery.

For protein to be transported into the nucleus, heterodimer of importin-α and β1 binds specifically to NLS on its respective cargo protein to facilitate the passage of protein across the nuclear pore complex (NPC) (Figure 1-15); importin-α acts as an adaptor molecule that binds cargo protein directly via NLS to form trimeric cargo-importin-α/β1 complex for trafficking (Marfori *et al.*, 2012). Two classical NLSs have been reported that are characterized by the presence of either one (monopartite) or two (bipartite) basic amino acid clusters (Dingwall & Laskey, 1991). The consensus sequences for monopartite and bipartite NLSs are K-K/R-X-K/R and K-R-X_{10-12}K-R-R-K respectively (X represents any amino acids) (Arnold *et al.*, 2006; Matsuura *et al.*, 2003; Moore & Blobel, 1993; Waldmann *et al.*, 2007).

For nuclear-resident proteins to be transported out of the nucleus, CRM1/exportin-1, a member of the importin-β superfamily, binds specifically to nuclear export signal (NES) on its respective cargo protein to facilities the export of protein to the cytoplasm (Figure 1-15). The NES sequence is generally characterized by the presence of regularly spaced, large hydrophobic amino acids (leucine or isoleucine), with intervening amino acids that are small, polar or negatively charged (Fornerod & Ohno, 2002; la Cour *et al.*, 2004). The consensus sequence for NES is ΦX2-3ΦX2-

3ΦXΦ (Φ represents hydrophobic amino acids valine, leucine, isoleucine, phenylalanine and methionine whereas X represents any amino acids) (Hutten & Kehlenbach, 2007).

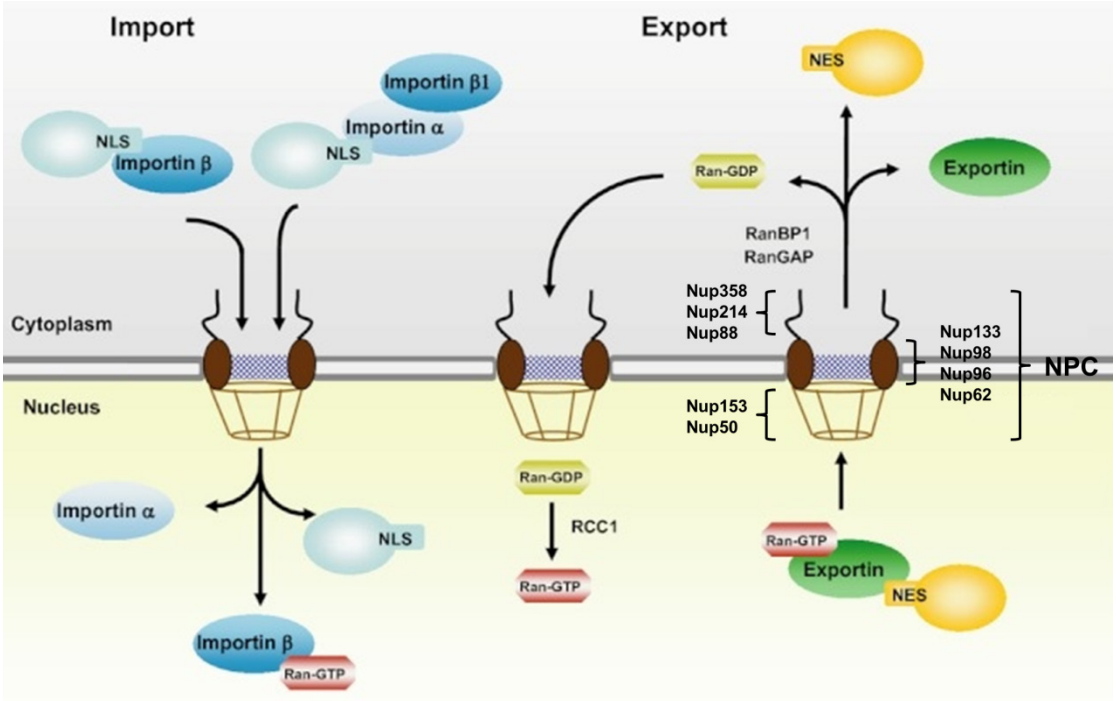

Figure 1-15: Mechanism of nuclear-cytoplasmic trafficking of proteins across nuclear pore complex. The cargo protein that contains NLS is recognized by importin-β alone or importin-α/β heterodimer; the cargo protein that contains NES binds to exportin when complexed with Ran-GTP. The passage of transport complex through the nuclear pore is facilitated by transient interaction of importin-β with Nups. In the cytoplasm, a NLS-containing cargo-importin complex traffics into the nucleus by transient interaction with phenylalanine-glycine-repeat (FG-repeat) domains on Nups of NPC (Pyhtila & Rexach, 2003). After trafficking of cargo protein into the nucleus, the binding of GTP-bound form of Ran (Ran-GTP) to importin-β causes a conformation change in importin-β that dissociates it from cargo-importin complex. The released cargo protein is free to perform its function in the nucleus, and the importins are recycled to the cytoplasm by its export receptor, cellular apoptosis susceptibility (CAS), for next round of transport (Kutay *et al.*, 1997). In the nucleus, a NES-containing cargo-exportin complex forms a trimetric complex with Ran-GTP and traffics out of the nucleus by transient interaction with FG-repeat domains on Nups (Kutay & Guttinger, 2005). In the cytoplasm, the conversion of Ran-GTP to Ran-GDP by guanine nucleotide exchange factor RCC1 to trigger the dissociation of the export complex (Melchior & Gerace, 1998). The relative position of several Nups within the NPC is listed. Figure is adapted from (Sekimoto & Yoneda, 2012).

1.8 Identification of DENV host factors via viral-protein interaction screens

The analysis of viral-protein interaction network in DENV is being intensively investigated as a means to identify both human and mosquito host factors that are involved in mediating replication and pathogenesis. The two approaches that are commonly used for such screen are high-throughput Y2H assay (Bhuvanakantham *et al.*, 2010; Brault *et al.*, 2011; Chua *et al.*, 2004; Duan *et al.*, 2008; Folly *et al.*, 2011; Gao *et al.*, 2010; Jiang *et al.*, 2009; Khadka *et al.*, 2011; Le Breton *et al.*, 2011; Li *et al.*, 2012; Limjindaporn *et al.*, 2007; Limjindaporn *et al.*, 2009; Mairiang *et al.*, 2013; Silva *et al.*, 2013), or co-affinity purification or co-IP that is coupled to mass spectrometry (MS) (Colpitts *et al.*, 2011a; Colpitts *et al.*, 2011b; Kurosu *et al.*, 2007; Noisakran *et al.*, 2008b).

The first genome-wide analysis of viral-protein interactions between DENV and human proteins was reported by Khadka and colleagues via Y2H screening with human liver cDNA library (Khadka *et al.*, 2011). They identified a total of 139 interactions between 105 human proteins and 8 dengue viral proteins (M protein and all NS proteins). Among the 105 human proteins, six were previously implicated in DENV infection whereas 45 were associated with replication of other viruses. The authors found enrichment among human proteins that are related to cell/centrosome, coagulation cascade, Golgi apparatus, complement and cytoskeleton (Khadka *et al.*, 2011). In the same year, two additional Y2H screens were published to identify interactions between structural or NS proteins of DENV with human proteins (Folly *et al.*, 2011; Le Breton *et al.*, 2011). Folly *et al*. identified 31 human proteins to be

interacting with E, prM or C and these proteins are involved in distinct biological process that are related to immune response and homeostatic balance (Folly *et al.*, 2011). Similarly, Le Breton and coworkers identified 108 human proteins to be interacting with NS3, NS5 or both and host proteins related to the regulation of innate immune response, transcription regulation, RNA binding and vesicular transport. Topological analysis of this interaction network revealed that NS3 and NS5 have a strong tendency to interact with human proteins that highly connected within the human interactome and this further support Khadka *et al*'s conclusion (Le Breton *et al.*, 2011).

The first genome-wide analysis of viral-protein interactions between DENV and human or mosquitoes proteins was reported by Mairiang and coworkers via Y2H screening with human peripheral blood leukocytes or *Aedes aegypti* cDNA library (Mairiang *et al.*, 2013). They have identified 102 interactions between 93 mosquito proteins and four dengue viral proteins (C, prM, NS3 and NS5) and 46 interactions between 35 human proteins and three dengue viral proteins (C, NS3 and NS5). Out of 93 mosquito proteins, 54 were identified to have human orthologs but only four of these proteins were observed to have conserved interactions among mosquito and human with same dengue proteins. NS3-mosquito protein-protein interactions were enriched by proteins that are implicated in response to heat shock and stress, whereas C typically interacted with nucleic acid binding proteins.

A recent co-IP experiment coupled with MS study with GFP-NS3 and GFP-NS5 transfected cells that were also infected with DENV2 by Carpp et al has identified 41 and 53 host proteins to be interacting with GFP-NS3 and GFP-NS5, respectively, and 13 of them were common to both. Analysis of interaction network revealed biological processes or cellular components like viral infectious cycle, reproductive process, major histocompatibility complex class I protein binding, protein folding and unfolded protein response to be enriched in GFP-NS3 interaction network, whereas nuclear pore, nuclear envelope and Golgi-to-ER retrograde vesicle-mediated transport to be enriched in GFP-NS5 interaction network. Lastly, lipid metabolism and transmembrane transporter activity for organic acids and carboxylic acids were enriched in both GFP-NS3 and GFP-NS5 interaction networks (Carpp *et al.*, 2014).

1.9 Dengue control

Currently, there is no licensed vaccine and antiviral drug that can be used to prevent or treat dengue infection and vector control remains the cornerstone in preventing transmission. The current treatment for dengue infection is mainly supportive. Patients with DF are encouraged to take oral fluids to replace losses from vomiting and fever and antipyretics (eg. paracetamol) is given for fever. The treatment for DHF requires timely fluid support to prevent the progression to DSS and this involves prompt diagnosis, monitoring for warning signs, providing supportive care and fluid resuscitation when needed.

1.9.1 Vector control

Traditional -based vector control methods rely on surveillance, public education and removal of mosquito breeding habitats to control the abundance of mosquito (NEA, 2015; Ooi *et al.*, 2006). However, in recent years, there has been increased interest in the use of *Wolbachia*-infected mosquito in natural setting as a population replacement strategy to biologically control DENV transmission by targeting mosquito longevity (Hancock *et al.*, 2011). As of current, there have been several *Wolbachia* field trials in Australia and Vietnam and its impact on DENV transmission in natural setting is currently being evaluated.

1.9.2 Dengue vaccine

Vaccine research and development for DENV have been ongoing since the 1940s (Mahoney *et al.*, 2011) and yet, there is still no approved vaccine against DENV infection because of the difficulty in mounting sufficient tetravalent protection against all four DENV serotypes to deal with the ADE phenomenon (Figure 1-5) where the major risk is that presence of subneutralizing concentrations of neutralizing antibodies may increase the risk of ADE (Thisyakorn & Thisyakorn, 2014). At present, several vaccine candidates are under development and they include live attenuated vaccine, recombinant chimeric vaccine, inactivated virus vaccine, recombinant protein vaccine and DNA vaccine (reviewed by (Murrell *et al.*, 2011). Among them, only the recombinant chimeric vaccine from Sanofi Pasteur has made it to phase III clinical trial.

1.9.3 Antiviral development

In recent years, a greater molecular understanding of viral protein roles in replication and pathogenies enables a new range of targets to be identified for potential therapeutic intervention. Extensive effort has been invested to discover new small-molecule antiviral drug against DENV.

1.9.3.1 Discovery of new antiviral agents

Searching for anti-dengue inhibitors against viral and host proteins that are implicated in viral replication or pathogenesis and obtaining crystal structures of viral proteins (Figure 1-11, representative crystal structures of DENV proteins) are the general approaches that have been taken to identify potential targets for antiviral therapy and obtaining key information for rational design of novel anti-dengue agents. Various strategies have been frequently used to identify such inhibitors and they include (1) high-throughput cell-based infection assays, (2) high-throughput cell-based infection assays coupled with viral enzyme assay or functional characterization assay, (3) structure-based *in silico* docking and rational design, and (4) repurposing of HCV inhibitors for DENV (reviewed comprehensively by (Lim *et al.*, 2013c).

For the viral proteins, the receptor binding property of E and the enzymatic functions of NS3 (protease/helicase) and NS5 (MTase/RdRP) (refer to section 1.6.4 on details of functions) have always been attractive antiviral targets and several compounds have been identified via the above strategies; however, in recent years, new antiviral targets that include NS3 RTPase activity, NS5 RNA binding and viral-viral protein

interaction (both structural and NS, refer to section 1.6.6 for known NS protein-protein interactions) have also been proposed to be promising new targets and they remained to be further explored (Geiss *et al.*, 2009). For the host proteins, those that are involved in viral protein trafficking, viral glycoprotein modification, viral replication (eg. pyrimidine biosynthesis) and severe dengue pathogenesis are worth to be further pursued. Collectively, among the identified compounds, very few inhibitors have advanced to the point of clinical trial (see 1.8.3.1) because of their poor selectivity, physiochemical or pharmacokinetic properties (Lim *et al.*, 2013c).

1.9.3.2 Therapeutic trial of small molecules

As of now, several clinical studies have been conducted to test the efficacy of small inhibitors that are either targeting the NS5 protein (eg. balapiravir) or host protein (eg. celgosivir, chloroquine and prednisolone) in conventional randomized controlled trial (Low *et al.*, 2014; Nguyen *et al.*, 2013a; Tam *et al.*, 2012; Tricou *et al.*, 2010; Whitehorn *et al.*, 2012).

Balapiravir is a prodrug of a nucleoside analogue that was initially developed for treatment of chronic HCV infection; despite its antiviral potential *in vitro*, balapiravir was unable to improve clinical outcome when tested in a trial (Nguyen *et al.*, 2013a). Celgosivir is a prodrug of castanospermine that inhibits host alpha-glucosidase I. It was shown *in vitro* to be effective against all four serotypes and further *in vivo* study with mouse model shown antiviral activity against DENV2 (Rathore *et al.*, 2011b). Celgosivir was demonstrated to be safe and well tolerated but there was no clear

evidence to suggest protection at recommended doses (Low *et al.*, 2014). Chloroquine was evaluated for both its anti-dengue properties and its ability to potentially modulate immune response during infection; however, the trial did not show any obvious antiviral or clinical benefits (Tricou *et al.*, 2010). Prednisolone was tested for its ability to modulate immune-mediated response with the hope that through early administration of prednisolone, severe dengue could be prevented; the trial was safe but it was not effective (Tam *et al.*, 2012) and there were very little evidence to suggest the attenuation of host immune response (Nguyen *et al.*, 2013b).

1.10 Dual faces of NS5 in DENV life cycle

In DENV infected cells, NS5 exists in two forms; a hypo- and hyper-phosphorylated forms. The hypo-phosphorylated form is localized to the cytoplasm where it interacts with NS3; the hyper-phosphorylated form is predominately localized to nucleus and is thought not to interact with NS3 (Kapoor *et al.*, 1995; Welsch *et al.*, 2009).

1.10.1 Cytoplasmic NS5

Among the NS proteins, NS3 and NS5 contain the enzymatic activities, namely NTPase/RTPase/helicase and MTase/RdRP activities, respectively, which are crucial for viral RNA replication in cytoplasmic RC. Further evidence for the roles of NS3 and NS5 proteins in the RC have been demonstrated by the specific interactions of NS3 and NS5 with flavivirus 5' and 3'UTR (Chen *et al.*, 1997; Cui *et al.*, 1998; Garcia-Montalvo *et al.*, 2004b; Khromykh *et al.*, 1996; Mackenzie *et al.*, 1998; You *et al.*, 2001), the stimulation of NS3 NTPase and RTPase activities by NS5 (Cui *et al.*,

1998; Yon *et al.*, 2005) and the addition of anti-NS3 and anti-NS5 inhibited the reaction that converts RF to RI (Bartholomeusz & Wright, 1993); these findings are consistent with the functional roles of both proteins in the RC.

NS3 and NS5 have been demonstrated to co-localized at RC in infected cells (Kapoor *et al.*, 1995; Uchil *et al.*, 2006; Welsch *et al.*, 2009; Westaway *et al.*, 1997). There have been several reports on NS3-NS5 interaction that include co-IP assays from infected cell extracts (Chen *et al.*, 1997; Garcia-Montalvo *et al.*, 2004b; Kapoor *et al.*, 1995; Moreland *et al.*, 2012), *in vitro* direct-binding assays (Moreland *et al.*, 2012; Takahashi *et al.*, 2012) and Y2H studies (Brooks *et al.*, 2002; Johansson *et al.*, 2001a; Mairiang *et al.*, 2013). Through Y2H studies, their interaction has been mapped to C-terminal region of NS3 helicase (residues 303-618) and the N-terminal region of NS5 RdRP (residues 320-368) (Figure 1-16) (Brooks *et al.*, 2002; Johansson *et al.*, 2001b). Interestingly, the region of NS5 also binds to importin-β1 and hence, known as βNLS (Brooks *et al.*, 2002). The binding site on NS5 seems to be centered on residue K330 because the mutation of this residue to alanine reduced its interaction with NS3 and abolished infectious virus particle production, although the *in vitro de novo* RdRP activity remained unaffected (Zou *et al.*, 2011). Based on structure-guided mutational analysis of two cavities in DENV NS5, it was hypothesized that the cavity occupied by K330 may be a potential target for antiviral drug design by blocking NS3-NS5 interaction (Zou *et al.*, 2011).

1.10.2 Nuclear NS5

During infection, DENV2 NS5 accumulates in the nucleus (Kapoor *et al.*, 1995). The functional bipartite NLS (α/βNLS) that is responsible for mediating NS5 nuclear-localization is found within residues 369-405 (Figure 1-16) (Brooks *et al.*, 2002; Forwood *et al.*, 1999) and it has been shown experimentally that the α/βNLS is capable of targeting β-galactosidase into the nucleus by interacting with importin-α/β1 complex (Forwood *et al.*, 1999). Mutations in NS5 α/βNLS (^{387}KKK→AAA and ^{371}KK→AA+^{387}KKK→AAA) reduced NS5 nuclear accumulation and virus release and this correlates well with increased IL-8 secretion (Pryor *et al.*, 2007). Apart from a well-characterized NLS, a consensus casein kinase 2 (CK2) site (^{395}TREE) was also identified in this region and *in vitro* phosphorylation of site by CK2, possibly at T395, was shown to be negatively regulating DENV2 NS5 nuclear import (Forwood *et al.*, 1999). Subsequently, a NES sequence (residues 327-343) was identified to be responsible for shuttling DENV2 NS5 into cytoplasm and it was shown to bind to CRM-1 (Rawlinson *et al.*, 2009). Blocking nuclear export with CRM-1 inhibitor leptomycin B (LMB) increased NS5 nuclear accumulation and virus release and this also correlates with decreased IL-8 secretion (Rawlinson *et al.*, 2009), which collectively implies that nuclear NS5 is important for efficient virus production. Recently, it was demonstrated that NS5 residues 529-740 interacts with DAXX in the nucleus to modulate RANTES (CCL5) production, which is a DHF-associated cytokine (Khunchai *et al.*, 2012). Taken together, it seems to suggests that the role of nuclear NS5 is to modulate host transcription to create a permissive environment for virus infection to proceed (Caly *et al.*, 2012a).

1.11 Aim of the thesis

Given the worldwide re-emergence of epidemic dengue, there is an urgent need for the development of prophylactic vaccine or effective antiviral agent to control dengue infection. Knowledge of dengue pathogenesis, especially in the molecular aspects of virus-virus protein and virus-host protein interactions that are important for virus replication and pathogenesis will contribute to the identification of potential targets for antiviral therapy and obtainment of key information for rational design of novel anti-dengue agents. The enzymatic activities of two major replicative proteins of DENV, NS3 and NS5 proteins, and the membrane fusion ability of E have formed important targets for anti-dengue drug design (Geiss *et al.*, 2009; Lim *et al.*, 2013c). However, in recent years, virus-virus protein interaction between the two major replicative proteins of DENV, NS3 and NS5, as well as virus-host protein interaction between DENV NS5 and its nuclear importer, importin α/β1 have also become attractive targets for antiviral drug development (also see section 1.9.3.1) (Caly *et al.*, 2012b; Geiss *et al.*, 2009). In order to facilitate the drug discovery process, an in-depth understanding of their molecular interactions and the consequence of their interactions on viral replication is needed; the quest of such knowledge constitutes the basis of this thesis, with specific aims that are directed at dissecting the details of molecular interaction between NS5 and its viral-partner, NS3 and host-protein, importin-α/β1.

The specific aims of this thesis are:

1. To fine map the interaction region between NS3 and NS5 and investigate its impact on virus replication

We set out to investigate the details of molecular interaction between NS3 and NS5, with more emphasis from the NS3 perspective as it was not fully characterized. Biochemical pull-down assays from infected cell lysates have demonstrated the existence of NS3-NS5 interaction (Chen et al., 1997; Kapoor et al., 1995). Previous Y2H studies have narrowed down the region on NS3 and NS5 to residues 303-618 and residues 320-368 respectively (Figure 1-16) (Brooks *et al.*, 2002; Johansson *et al.*, 2001a; Vasudevan *et al.*, 2001). Reverse genetics study with mutation in NS5, residue K330 to alanine abolished viral replication via reducing NS3-NS5 interaction, while the RdRP activity of NS5 remained unaffected, suggesting that interaction between NS3 and NS5 may be a potential antiviral target (Zou et al., 2011). These studies suggest a crucial role of this interaction in viral replication.

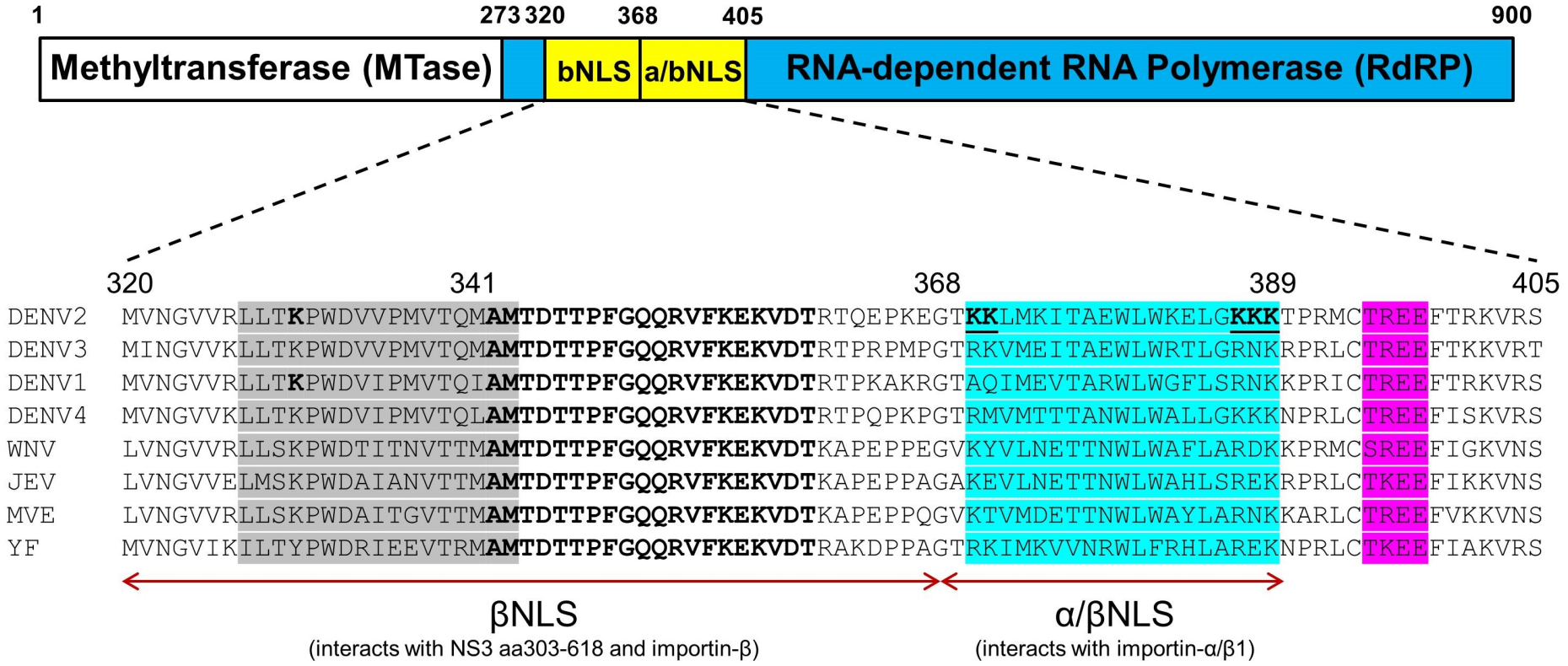

Figure 1-16: Sequence alignment of residues 320-405 of NS5 RdRP domain of DENV2 with other DENV serotypes and representative members of the Flavivirus genus. βNLS (residues 320-368) denotes the region where NS5 was reported to interact with NS3 and importin-β, whereas α/βNLS (residues 369-389; highlights in cyan) denotes the region where NS5 was reported to interact with importin-α/β1. Within α/βNLS, contains a classical bipartite NLS sequence that targets DENV2 NS5 into nucleus and the basic residues that make up the NLS are underlined and bold (Brooks *et al.*, 2002; Pryor *et al.*, 2007). Within βNLS, contain a NES sequence (residues 327-343; highlights in grey) (Rawlinson *et al.*, 2009) and a region that is totally conserved in Flavivirus NS5 (residues 342-361, bold). Within NES, K330 (bold) is important for NS3-NS5 interaction (Zou *et al.*, 2011). Phosphorylation of threonine within ^{395}TREE region (highlights in magenta) by protein kinase CK2 is believed to reduce nuclear import (Forwood *et al.*, 1999). The numbering of residues is based on DENV2 protein sequence. The virus sequences and their GenBank accession numbers are as follows: DENV2 (AF038403), DENV1 (U88535), DENV3 (M93130), DENV4 (AF326573), Yellow Fever virus (YFV; X15062), Japanese Encephalitis virus (JEV; M55506), Murray Valley Encephalitis virus (MVEV; AF161266) and West Nile virus (WNV; M12294).

2. To investigate the subcellular localization pattern of NS5 for DENV1-4 serotypes and its impact on virus replication

Flavivirus NS5 subcellular localization has been reported for DENV2, YFV, JEV and WNV. In the case of DENV, it was only formally shown for DENV2 NS5 that its nuclear-cytoplasmic trafficking ability was mediated by both well-characterized NLS and NES sequences that also reside within residues 320-405 (Figure 1-16) (Brooks et al., 2002; Pryor et al., 2007; Rawlinson et al., 2009; Vasudevan et al., 2001). In order to determine if similar nuclear-cytoplasmic trafficking ability was observed in NS5 in infected cells of other serotypes, anti-NS5 antibodies that could cross-react with all serotypes were developed in-house as such antibody was unavailable commercially. Using a uniquely available anti-NS5 antibody, we found that DENV2 and 3 NS5 are predominately nuclear while DENV1 and DENV4 NS5 are mostly cytoplasmic. A small molecule screen based on interaction of NS5 with importin-α/β1 identified ivermectin as a potential inhibitor. In spite of the differences in the NS5 subcellular localization, the IC_{50} for ivermectin in a cell-based infection assay was similar.

3. To identify potential nuclear or cytoplasmic binding partners that are unique to DENV1 and 2 NS5 by co-immunoprecipitation coupled to mass spectrometry

Even though it has been known for two decades that DENV2 NS5 localizes to the nucleus of infected cell, the significance of NS5 protein nuclear localization remains poorly understood. In comparison to DENV capsid protein, which is also known to nuclear-localized, research in recent years has shed some light on its possible functions in nucleus (Colpitts *et al.*, 2011a; Netsawang *et al.*, 2010). Apart from that, several proteomics screens were performed to identify host proteins that physically interact with DENV capsid protein, either by Y2H (Li *et al.*, 2012) (Bhuvanakantham *et al.*, 2010; Bhuvanakantham & Ng, 2013; Limjindaporn *et al.*, 2007) or tandem affinity purification-MS (Colpitts *et al.*, 2011a), and all of them have successfully led to the identification of several host proteins that interact with capsid and are implicated in DENV life cycle. With this notion, we set out to isolate and identify binding partners to DENV1 and 2 NS5 by co-IP coupled to MS.

4. To characterize a newly discovered C-terminal NLS of DENV2 NS5 and study its importance in virus replication

While searching for a cytoplasmic retention signal (CRS) in DENV1 NS5 through gene shuffling with DENV2 NS5, we unexpectedly discovered a new C-terminal NLS in DENV2 NS5. This finding was studied comprehensively to prove the functionality of this NLS in targeting NS5 and unrelated protein into nucleus. The implication of this discovery on our understanding of NS5 subcellular localization is discussed in detail.

Chapter 2: Methods and Materials

2.1 Materials

2.1.1 Antibodies

Table 2-1: Primary antibodies used in the course of this work

Antibody	Name	From (Organism)	Type	Source
Anti-dsRNA	J2	Mouse	Monoclonal	Scicons, Hungary
Anti-E	4G2	Mouse	Monoclonal	HB-112, ATCC, USA
Anti-NS2B	3F10	Human	Monoclonal	This work; (Moreland *et al.*, 2012)
Anti-NS3	3F7	Human	Monoclonal	This work; (Moreland *et al.*, 2012)
Anti-NS3	3F8	Human	Monoclonal	This work; (Moreland *et al.*, 2012)
Anti-NS5	5M1	Human	Monoclonal	This work; (Zhao *et al.*, 2014)
Anti-NS5	5R3	Human	Monoclonal	This work; (Zhao *et al.*, 2014)
Anti-actin	A2066	Rabbit	Polyclonal	Sigma-Aldrich, USA
Anti-STAT2	4594	Rabbit	Polyclonal	Cell Signaling Technology, USA
Anti-DDX3X	A300-474A	Rabbit	Polyclonal	Bethyl Laboratories Inc, USA
Anti-DDX5	A300-523A	Rabbit	Polyclonal	Bethyl Laboratories Inc, USA
Anti-MATR3	A300-591A	Rabbit	Polyclonal	Bethyl Laboratories Inc, USA
Anti-GFP	ab6556	Rabbit	Polyclonal	Abcam, USA
Anti-M13 HRP	27942101	Mouse	Monoclonal	GE Healthcare, USA

Table 2-2: Secondary antibodies used in the course of this work

Antibody	From (Organism)	Source
Anti-human Alexa Fluor 488	Goat	Invitrogen, USA
Anti-mouse Alexa Fluor 488	Goat	Invitrogen, USA
Anti-rabbit Alexa Fluor 488	Goat	Invitrogen, USA
Anti-human Alexa Fluor 594	Goat	Invitrogen, USA
Anti-mouse Alexa Fluor 594	Goat	Invitrogen, USA
Anti-mouse IgG HRP	Goat	Dako, USA
Anti-rabbit IgG HRP	Goat	GE Healthcare, USA
Anti-human IgG HRP	Goat	MyBiosource, USA

2.1.2 Bacterial strains

Table 2-3: Bacterial strains used in the course of this work

E. coli strain	Genotype	Source
XL1-blue	endA1 gyrA96(nal^R) thi-1 recA1 relA1 lac glnV44 F'[::Tn10 proAB$^+$ lacI^q Δ(lacZ)M15] hsdR17(r_K^- m_K^+)	Stratagene, USA
BL21-Codon Plus(DE3)-RIL	F- *ompT hsdS*(rB- mB-) *dcm*+ Tet^r *gal* l (DE3) *endA* Hte [*argU ileY leuW* Cam^r]	Stratagene, USA

2.1.3 DNA oligonucleotides

The DNA oligonucleotides that were used in this work were synthesized by Integrated DNA Technologies (IDT; Singapore). The oligonucleotides were provided as lyophilized powder, which were resuspended in DNase/RNase-free distilled water prior to use. The sequences of all synthesized DNA oligonucleotides were listed in the respective tables.

2.1.4 Cloning vectors

Table 2-4: Cloning vectors used in the course of this work

Vector	Tag	Cleavage site	Type	Source
pEGFP-C1	N-terminal GFP	-	Mammalian	Clontech, Japan
pET14b	N-terminal His_6	Thrombin	Bacterial	Novagen, Germany
pET15b	N-terminal His	Thrombin	Bacterial	Novagen, Germany
pET32b	N-terminal His and thioredoxin	Thrombin	Bacterial	Novagen, Germany
pGEX-4T-1	N-terminal GST	Thrombin	Bacterial	GE Healthcare, USA
pPROEX HTb B	N-terminal His	TEV	Bacterial	Invitrogen, Thermo Fisher Scientific, USA

2.1.5 Enzymes, kits and other reagents

Table 2-5: List of kits, enzymes and other reagents used in the course of this work

Product	Manufacturer
Protein expression and purification	
IPTG	Thermo Fisher Scientific, USA
Protein G-Sepharose 4B	Sigma-Aldrich, USA
HisTrap HP column	GE Healthcare, UK
Amicon® Ultra-15 Centrifugal Filters	Millipore, Merck, USA
DNA cloning and purification	
T4 DNA-Ligase	NEB, USA
PfuUltra II Fusion HS DNA Polymerase	Agilent Technologies, USA
QuikChange II Site-Directed Mutagenesis Kit	Agilent Technologies, USA
dNTPs	Promega, USA
QIAGEN Plasmid Mini Kit	Qiagen, Germany
QIAquick Gel Extraction Kit	Qiagen, Germany

UltraPure Phenol:Chloroform:Isoamyl Alcohol (25:24:1, v/v)	Life Technologies, Thermo Fisher Scientific, USA
Transfection reagent	
jetPRIME transfection reagent	Polyplus-transfection SA, France
Lipofectamine 2000	Invitrogen, Thermo Fisher Scientific, USA
***In vitro* transcription**	
$m^7G(5')ppp(5')A$ RNA Cap Structure Analog	NEB, USA
mMESSAGE mMACHINE T7 Transcription Kit	Ambion, Thermo Fisher Scientific, USA
Improm II reverse transcription system	Promega, USA
Real time RT-PCR	
iQ SYBR Green supermix	Biorad, USA
iTaq Universal SYBR Green One-Step Kit	Biorad, USA
SDS-PAGE and western blot	
Prestained SDS-PAGE standards	Biorad, USA
Silver Stain kit	Thermo Fisher Scientific Pierce, USA
Nitrocellulose transfer membrane	Milipore, Merck, USA
Amersham Hybond-P polyvinylidene fluoride (PVDF) transfer membrane	GE Healthcare, UK
WesternBright *Sirius HRP substrate*	Advansta, USA
Immunoprecipitation	
Protease Inhibitor Cocktail (Complete)	Roche, Switzerland
GFP-Trap_A resin	Chromotek, Germany
Protein A/G agarose	Thermo Fisher Scientific Pierce, USA
*Rapi*Gest SR surfactant reagent	Waters, USA
RNA extraction and purification	
QIAamp Viral RNA Mini kit	Qiagen, Germany
TRIzol reagent	Life Technologies, Thermo Fisher Scientific, USA
Immunofluorescence assay	
ProLong Gold antifade reagent with DAPI	Life Technologies, Thermo Fisher Scientific, USA
Restriction enzymes	
*Acc65*I, *Bam*HI, *Bsp*EI, *Eag*I, *Nae*I, *Nde*I, *Sal*I, *Sph*I, *Xho*I and *Xma*I	NEB, USA
Others	
Ph.D.™ Peptide Display Cloning System	NEB, USA
Fab-phage display library	Humanyx Pte Ltd, Singapore
Malachite Green Phosphate Assay Kit	BioAssay Systems,

2.1.6 Buffers and solutions

Table 2-6: Buffers and solutions used in the course of this work

DNA and RNA work	
3M Sodium Acetate	3 M Sodium Acetate (pH 5.2)
6× DNA loading dye	0.4% orange G, 0.03% bromophenol blue, 0.03% xylene cyanol FF, 15% Ficoll® 400, 10 mM Tris-HCl (pH 7.5) and 50 mM EDTA (pH 8.0) (Promega, USA)
NEB buffer 4 (NEB, USA)	20 mM Tris-acetate, 10 mM magnesium acetate, 50 mM potassium acetate and 1 mM DTT (pH 7.9)
10× T4-DNA Ligase Buffer (NEB, USA)	500 mM Tris-HCl, 100 mM $MgCl_2$, 10 mM ATP and 100 mM DTT (pH 7.5)
50× TAE	2 M Tris, 2 M Acetic Acid, and 50 mM EDTA (pH 8.3)

SDS page and western blot	
30% acrylamide/bis Solution 29:1	30% acrylamide/bis-acrylamide (29:1) solution with 3.3% cross-linker concentration (Biorad, USA)
Western blot blocking and antibody binding buffers (PBST-M)	PBS pH 7.2 with 0.1% (v/v) of Tween 20, and 3% (w/v) milk powder
Coomassie blue staining solution	0.25% (w/v) Coomassie Brilliant Blue R-250, 50% (v/v) Methanol, 10% Glacial Acetic acid
Destaining solution	5% (v/v) Methanol, 5% (v/v) Glacial acetic acid
4× SDS-PAGE sample loading buffer	200 mM Tris-HCl pH 6.8 , 8% (w/v) SDS, 40% (v/v) glycerol, 4% β-mercaptoethanol (v/v), and 0.08 % bromophenol blue
Stacking gel buffer	1M Tris-HCl (pH 6.8)
Resolving gel buffer	1.5M Tris-HCl (pH 8.8)
Western blot stripping buffer	2% (v/v) SDS, 62.5 mM Tris HCl pH 6.8 and 0.8% (v/v) β-mercaptoethanol
Western blot wash buffer (PBST)	PBS pH 7.2 with 0.1% (v/v) of Tween 20
Immunofluorescence assay	
4% paraformaldehyde	PBS pH 7.4 with 4% (w/v) paraformaldehyde. Heat to 60°C, with continuous stirring to promote dissolution. Filter sterilized and stored at -20°C.
Blocking and antibody binding buffers	PBS pH 7.4 with 2% (w/v) bovine serum albumin (BSA)
Antibiotics and bacterial culture medium	
1000× ampicillin stock	100mg/ml in double distilled water, filter sterilized and stored at -20°C (Sigma-Aldrich, USA)
1000× kanamycin stock	50mg/ml in double distilled water, filter sterilized and stored at -20°C (Sigma-Aldrich, USA)
1000× chloramphenicol	34mg/ml in 100% ethanol and stored at -20°C (Sigma-Aldrich, USA)
Luria Broth (LB) medium	BD, USA
LB-agar	BD, USA
Cell culture medium (Gibco, Thermo Fisher Scientific, USA)	
Dulbecco's Modified Minimal Eagle Medium (DMEM), high glucose	L-Glutamine DMEM with 4.5g/L glucose.
Roswell Park Memorial Institute (RPMI) 1640 Medium	L-Glutamine RMPI.
RPMI 1640 Medium, HEPES	RPMI 1640 medium with 5.958g/L Hepes.
100× penicillin-streptomycin (P/S) (10,000U/ml)	Used at a final concentration of 100U/ml.
Fetal bovin serum (FBS)	Heat-inactivated at 56°C for 30 minutes. Used to supplement cell culture medium at 2, 5 or 10%.
Opti-MEM	Reduced serum medium that was derived from modification of DMEM for transfection use.
Other solutions/buffers	
ATPase assay buffer	50 mM Tris-HCl, pH 7.5, 2 mM $MgCl_2$, 1.5 mM dithiothreitol, 0.05% Tween 20 and 0.25 μg/ml BSA
BSA (Sigma-Aldrich, USA)	5% (w/v) BSA in PBS pH 7.2. Filter sterilized and stored at -20°C.
Carboxymethyl cellulose	0.8% (w/v) aqualite II dissolved in RPMI media supplemented with 2% FBS, 1% P/S , 0.0375% (v/v) $NaHCO_3$ and 25 mM HEPES
Crystal violet solution	1% (w/v) crystal violet dissolved in 20% (v/v) ethanol
CCMB80 buffer (modified)	80 mM $CaCl_2$, 10 mm$MgCl_2$. 10% (v/v) glycerol and 10 mM potassium acetate pH 7.0. Adjusted pH to 6.4 with HCl. Filter sterilized and stored at 4°C.
Lysis buffer with 1% triton X-100	50 mM Tris pH 7.4, 150 mM NaCl, 1mM EDTA, 1% (v/v) triton X-100
PBS pH 7.2	137 mM NaCl, 2.7mM KCl, 10 mM Na_2HPO_4 and 1.8 mM and KH_2PO_4
NP-40	AnalytiCon Discovery, Germany

2.1.7 Cell lines

All cell lines were obtained from ATCC.

Table 2-7: Cell lines used in the course of this work

Cell lines	Description
BHK-21	Baby hamster kidney cell (Fraser & Gharpure, 1962; Stoker, 1962)
Huh-7	Human hepatoma cell (Nakabayashi *et al.*, 1982)
Vero	African green monkey kidney cell (Mosca & Pitha, 1986)
HEK293T	Human embryonic kidney cells expressing the SV40 large T-antigen (Graham *et al.*, 1977)
C6/36	*Aedes albopictus* fibroblast (Igarashi, 1978)

2.1.8 Viruses

DENV1-4 of GenBank accession number: EU081230, EU081177, EU081190 and GQ398256 respectively were grown in C6/36 cells, and titered in BHK-21 cells before storage at -80°C (Christenbury *et al.*, 2010; Schreiber *et al.*, 2009a). These viruses were isolated during a local dengue outbreak that occurred in 2005 as part of Early Dengue infection and outcome (EDEN) study in Singapore (Schreiber *et al.*, 2009a).

2.2 Methods

Standard molecular cloning techniques, and protein expression and purification methods were carried out as described in reference manuals, namely "Molecular Cloning: A Laboratory Manual" (Sambrook, 2001) and "Current Protocols: Molecular Biology" (Ausubel, 2010), and references that were cited in this work. Unless mentioned otherwise, all routine practises like DNA and RNA purification, restriction

enzyme digestion, ligation, transfection and etc. were carried out according to the protocol provided by the respective manufacturers.

All centrifugation steps mentioned in this work were done in bench top or floor standing refrigerated centrifuge at specified temperatures.

2.2.1 Cell culture and viruses

2.2.1.1 Cell culture

Huh-7 cells were cultured in DMEM high glucose medium supplemented with 10%FBS and 1% penicillin-streptomycin (P/S). Vero and HEK293T cells were MEM high glucose medium supplemented with 10%FBS. BHK-21 cells were maintained in RPMI 1640 medium supplemented with 10% FBS and 1% P/S. These cells were maintained at 37°C with 5% CO_2.

C6/36 cells were maintained in RPMI 1640 medium, supplemented with 25 mM HEPES, 10% FBS and 1% P/S at 28°C in the absence of CO_2.

Depending on the cell types, these cells were re-plated every 3 to 4 days, and with a split ratio of 1:10 to 1:20 for maintenance.

2.2.1.2 Transfection of eukaryotic cells with plasmid DNA

One day prior to transfection, 1.6×10^5 Vero cells were seeded into 12-well plate, with glass cover slips, and incubated overnight at 37°C with 5% CO_2. On the following day, Vero cells were transfected using Lipofectamine 2000 with 2 μg of plasmid per well respectively, according to the manufacturer's recommendations.

2.2.1.3 Passaging viruses

The virus supernatants from C6/36 cells that were infected with DENV (serotypes 1-4) were harvested either on day 7 post-infection, or when infected cells showed ~75% cytopathic effect under a microscope, whichever came first. The harvested virus supernatants were filtered through a 0.22μm pore size filter and stored at -80ºC as small aliquots. Plaque assays of virus stocks were carried on BHK-21 cells to determine viral titer prior to use.

2.2.1.4 Plaque assay

One day prior to experiment, 2×10^5 BHK-21 cells were seeded in a 24-well plate. On the day of experiment, medium was aspirated and 10-fold serial dilutions of virus in RPMI medium were added to BHK-21 cells. After 1 hour incubation at 37°C, virus inoculum was removed and replaced with 0.8% methyl-cellulose in maintenance medium (RPMI 1640 medium supplemented with 2% FCS and 1% P/S). The plate was kept at 37°C for at least 4 days (typically 5 days but not more than 7 days) and fixed with 4% formaldehyde at RT for 20 minutes when the plaque was visible to

eyes. After fixing, the plate was washed thoroughly with water, and 0.5 ml of 1% (w/v) crystal violet was added to stain fixed cells for 20 minutes. After staining, the plate was washed, dried and the plaque forming units per ml (pfu/ml) was calculated.

2.2.1.5 Immunofluorescence assay

At an appropriate time post-transfection/infection, cells that were either transfected with mammalian expression plasmids, infected with DENV, or mock-transfected/infected were fixed with ice-cold methanol: acetone (1:1) for 15 minutes at -20ºC. Following fixation, cells were washed once by PBS and analyzed by IFA, using primary antibodies against GFP (ab6556, 1:1000; Abcam), dsRNA (J2, 1:300; Scicons), E (4G2, 1:1000; HB-112, ATCC) or NS5 (5M1, 20 nM and 5R3, 30 nM (Zhao *et al.*, 2014)), and secondary antibodies coupled to Alexa-Fluor 488 or Alexa-Fluor 594 (Invitrogen). Coverslips were mounted using ProLong Gold antifade reagent with DAPI (Invitrogen).

2.2.1.6 Fluorescence microscopy and confocal laser scanning microscopy

Digitized images were captured on inverted fluorescence microscope (Olympus IX71, USA) and Zeiss LSM 710 upright confocal microscope (Carl Zeiss, Germany) at 20× and 40/64× magnification, respectively. Image processing was performed with ImageJ software (Collins, 2007).

2.2.1.7 Computation of nuclear to cytoplasmic fluorescence ratio ($F_{n/c}$)

Image analysis was performed on digitized images with ImageJ software (Collins, 2007) to determine nuclear to cytoplasmic fluorescence ratio ($F_{n/c}$) of each cell using the following formula: $F_{n/c} = (F_n-F_b)/(F_c-F_b)$, where F_n is the nuclear fluorescence, F_c is the cytoplasmic fluorescence and F_b is the background fluorescence (Kumar *et al.*, 2013; Pryor *et al.*, 2007; Rawlinson *et al.*, 2009; Tay *et al.*, 2013). The mean $F_{n/c} \pm$ SEM was calculated for ≥ 25 cells.

2.2.2 Working with DNA and RNA

2.2.2.1 Site-directed mutagenesis

Site-directed mutagenesis (SDM) was carried out using with QuikChange II SDM Kit with appropriate forward and reverse primers, according to manufacturer's instructions. Sequencing was done to confirm the presence of mutation.

2.2.2.2 Polymerase chain reaction

The polymerase chain reaction (PCR) for generating DNA fragments for cloning contained of 30-50 ng template DNA, 200 nM forward and reverse primer, 300 µm dNTPs, 1×PCR buffer and 1 µl PfuUltra II Fusion HS DNA Polymerase in a reaction volume of 50µl. The PCR cycling conditions were: 1 cycle of 95°C 2 minutes, followed by 30 cycles of 95°C 20 seconds, 55-58°C 20 seconds, 72°C 15 seconds per kb and a last cycle of 72°C for 10 minutes.

2.2.2.3 Overlap extension polymerase chain reaction

The first step involved two independent PCRs that generated two PCR products that were subjected for joint in the second PCR (Figure 2-1; primers a and b for first fragment, and primers c and d for second fragment). Primers for the joining position (primer b and c) were designed in a way that they overlapped with each other by at least 30 base pairs. Following purification of both fragments, 1:1 molar ratio of purified fragments were mixed together and heated at 95°C in a heat block for 5 minutes. The mixture was allowed to cool to RT to promote annealing of both fragments. Following annealing, the mixture underwent extension at 72°C for 30 minutes by adding polymerase and dNTPs. After extension, 1/3rd of the extension mix was used for the last PCR, with the addition of primer a and d and fresh polymerase and dNTPs for amplification of more overlapped products.

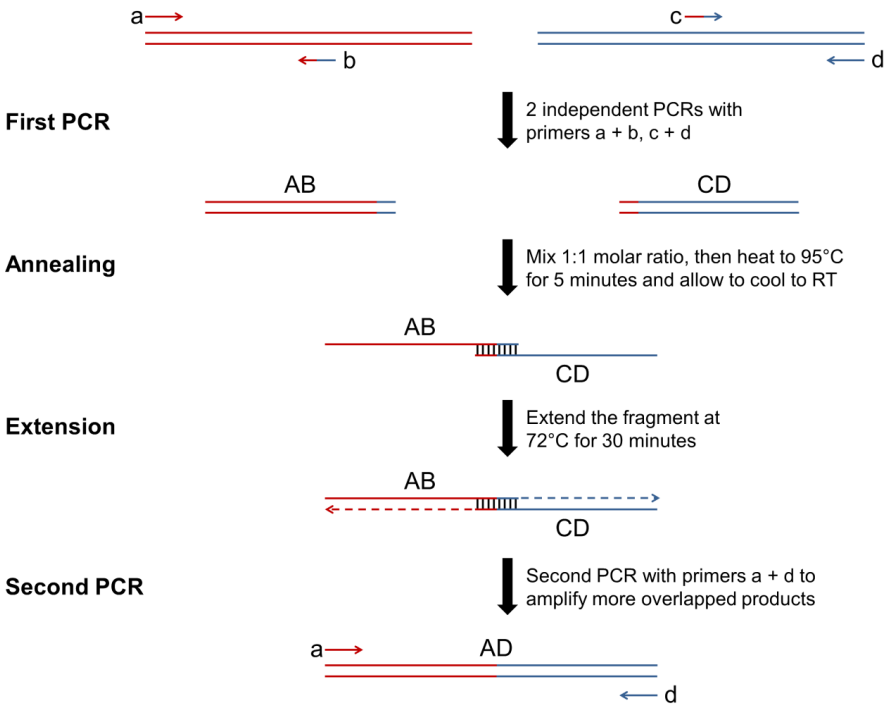

Figure 2-1: Schematic representation of the PCR products that were generated for overlap extension PCR. AB: segment synthesized by primers a + b; CD: segment synthesized by primers c + d; AD: segment synthesized by primers a + d after overlapping.

2.2.2.4 DNA extraction from agarose gel

Following DNA gel electrophoresis, gel slides containing DNA were cut and subjected to DNA purification by QIAquick Gel Extraction Kit, following supplier's protocol.

2.2.2.5 Transformation of competent bacteria

Competent *E.coli* XL1-blue and BL21-Codon Plus(DE3)-RIL were made in CCMB80 buffer (Table 2-6) (Sambrook, 2001). DNA plasmid (≥50 ng/µl) or ligation reaction was mixed with 100 µl of competent bacteria and incubated on ice for 5 minutes. Afterwards, the cells were heat-shocked at 42°C for 1.5 minutes and incubated on ice for 2 minutes. The bacteria was resuspended in 500 µl LB and incubated at 37°C with shaking for 1 h. After 1 h, the cells were pelleted and plated on LB-agar plates containing appropriate antibiotics and grown overnight at 30 or 37°C for colony development.

2.2.2.6 DNA plasmid purification

Plasmids were prepared from 5-10ml (high copy plasmids) or 100 ml (low copy plasmids) overnight cultures that were inoculated with a single colony in LB medium, which contained the appropriate antibiotics. The plasmids were extracted with QIAGEN Plasmid Mini Kit according to manufacturer's instructions. The reagent volumes were adjusted according to the volume of overnight culture. DNA was eluted in nuclease-free water and the concentration was quantified by NanoDrop 2000 UV-Vis Spectrophotometer (Thermo Fisher Scientific, USA).

2.2.2.7 DNA sequencing

Purified DNA plasmids or fragments were sent to First Base (Singapore) for sequencing. The sequencing results were analysed by ClustalW2 (http://www.ebi.ac.uk/Tools/msa/clustalw2/) (Thompson *et al.*, 1994).

2.2.2.8 Quantitative real time RT-PCR

For intracellular viral RNA quantification, total cellular RNA was extracted from infected cells by TRIzol reagent according to supplier's protocol. 500 ng of viral RNA was used for cDNA synthesis with Improm II reverse transcription system with random primer in a 10 µl reaction according to manufacturer's instructions. Following cDNA synthesis, 40 ng of cDNA was used for quantitative real time RT-PCR analysis of viral RNA with the use of iQ SYBR Green supermix and NS1 gene primers DENV2 NS1 (forward: 5'- CCGCTGACATGAGTTTTGAGTC-3; and reverse: 5'-CATGACAGGAGACAT CAAAGGA-3' (Paradkar *et al.*, 2011a). Absolute copy numbers of viral RNA was calculated based on DENV2 standard curve and normalized to actin level that was also quantified (forward: 5'-CAGGGGAACCGCTCATTGC CAATGG-3' and reverse: 5'-TCACCACACACTGTGCCCATCTACGA'-3) and reported as absolute copy numbers of viral RNA per µg of RNA used for real-time RT-PCR.

For extracellular viral RNA quantification, viral RNA from supernatant was extracted by QIAamp Viral RNA Mini kit according to manufacturer's instructions and for its quantification, a SYBR green one-step real-time RT-PCR (Bio-Rad) was conducted

using the same PCR conditions as cellular RNA quantification, with primers that bind to NS1 gene (as mentioned above). Absolute copy numbers of viral RNA was calculated based on DENV2 standard curve and reported as absolute copy numbers of viral RNA in log scale per ml of supernatant used for real-time RT-PCR.

2.2.3 Working with proteins

2.2.3.1 Standard SDS-PAGE

Protein samples were mixed with sample loading dye and were heated at 95ºC for 5 minutes. The polyacrylamide gels were prepared according to standard protocols (Sambrook, 2001) and gel electrophoresis was carried out at a constant voltage of 100-120 for 1-2 hours (10×7.5 cm). Prestained SDS-PAGE standard was used as molecular size marker.

2.2.3.2 Western blot analysis

Following gel electrophoresis, the proteins were transferred to Amersham Hybond-P PVDF transfer membrane with wet transfer apparatus (Biorad, USA) for 2 hours at a constant voltage of 80. The membrane was blocked with PBST-M for 1 hour at RT and was incubated overnight with the primary antibody diluted in PBST-M at 4°C. Following overnight incubation, the membrane was washed 3× for 10 minutes with PBST. Afterwards, the appropriate secondary antibody was diluted in PBST-M and incubated for 1-2 hours at RT with membrane. Following incubation, the membrane was washed 3× with PBST and WesternBright Sirius HRP substrate was added for

signal development. Image was acquired using an ImageQuant LAS 4000 (GE Healthcare, UK).

2.2.4 Working with DENV2 cDNA infectious clone

DENV2 of cosmopolitan genotype (GenBank™ accession number: EU081177, as mentioned in section 2.1.8) was selected to be the template for generation of cDNA infectious clone (developed in collaboration between Dr Subhash G. Vasudevan and Dr Eng Eong Ooi; clone was generated by Dr Yuwen Chong) because of its well-documented patient's history (Schreiber *et al.*, 2009a). The overall schematic representation of cloning strategy is shown in Figure 2-2A. The infectious clone was divided into three separate fragments (fragment 1: nucleotide position 1-4,498, fragment 2: nucleotide position 4,493-6008 and fragment 3: nucleotide position 6,003-10,723) and each fragment was maintained as a subclone in low-copy plasmid pWSK29 (Wang & Kushner, 1991) (pWSK29 D2 fragment 1, 2 and 3 respectively). These three fragments were also assembled into full-length clone, which was maintained in the same plasmid (Tay *et al.*, 2014b). Depending on the site the mutation, the respective subclone was selected for SDM.

2.2.4.1 Generation of mutant virus

In the course of this work, all mutations were made in pWSK29 D2 fragment 3 subclone, according to manufacturer's protocol.

After transformation of *Dpn*I digested site-directed mutagenesis reaction mix into *E. coli* XL-1 blue chemically competent cell, the cells were grown at 30°C for at least 20 hours. Colonies were picked to inoculate 100ml Luria Broth (LB) culture for overnight growth at 30°C. On the next day, cells were harvested and lysed with QIAprep Spin Miniprep Kit (Qiagen) for isolating dengue cDNA plasmid. The plasmid was sent for automated DNA sequencing (1st BASE DNA Sequencing Services [Singapore]) to confirm the presence of mutation. Once the mutation was confirmed, fragment 3 was cut from the plasmid by *Xba*I and *Sac*I and inserted into subclone pWSK29 D2 fragment 1+2 that were similarly cut with *Xba*I and *Sac*I to generate full-length DENV2 cDNA infectious clone, which contained the intended mutation. All enzymes were purchased from NEB.

2.2.4.2 Linearization and purification of linearized infectious clone plasmid

10 µg of full-length DENV2 cDNA infectious clone plasmid was digested by *Sac*I (NEB) in the presence of BSA and buffer 4 in a 100µl reaction for 2 hours at 37°C for linearization. After digestion, 100µ1 of phenol/chloroform/isoamylalcohol (25:24:1) was added and mixed thoroughly. The mixture was spun at 13,200 rounds per minute (rpm) for 2 minutes and 100µl was transferred to a new eppendorf tube. 100µl of chloroform was added to the supernatant and mixed thoroughly. The mixture was spun at 13,200rpm for 2 minutes and 60µl of supernatant was transferred to a new eppendorf tube. The remaining 40ul of supernatant was mixed thoroughly with 140µl of water and allowed to spin at 13,200 rpm for 2 minutes. 140µl of diluted supernatant was removed and combined with the initial 60µl of supernatant to give 200µl. 20µl of 3M sodium acetate pH 5.2 (1/10th volume of combined supernatant) and 500µl of 100%

ethanol (2.5×volume of combined supernatant) were added to precipitated DNA at -80°C for at least 1 hour. The mixture was spun at 13,200 rpm at 4°C for 10 minutes and the supernatant was discarded. The DNA pellet was washed with 1ml of 70% ethanol and the mixture was spun at 13,200 rpm at 4°C for 10 minutes. The 70% ethanol was removed and the DNA pellet was allowed to air-dry at RT. The dried DNA pellet was resuspended in RNase-free water and the concentration was measured by NanoDrop 2000 Spectrophotometer.

2.2.4.3 *In vitro* transcription

Linearized full-length DENV2 cDNA infectious clone plasmid that was purified was used as template for *in vitro* transcription by Ambion MEGAscript® T7 Transcription Kit. The reaction mix contained 5.6 μl of linearized DNA (≤3 μg), 2 μl of rGTP, rCTP and rUTP, 0.4 μ1 of rATP, 3 μl of m7G(5')ppp(5')A RNA Cap Structure Analog (total 2.5 units), 1 μ1 RNAse inhibitor, 2 μ1 T7 RNA polymerase and 2 μ110× reaction buffer. The reaction mix was incubated at 37°C for 30 minutes. Following 30 minutes incubation, the reaction was spiked with additional 1.8 μl rATP and 0.2 μl 10× buffer and allowed to incubate for another 2 hours at 37°C. 1 μl of TURBO DNase was added and the reaction was incubated at 37°C for 15 minutes to remove DNA template. Following the addition of 27 μL Nuclease-free water and 30 μL lithium chloride, RNA was allowed to precipitate overnight at -80°C. After overnight incubation, the reaction mix was spun at 13,200 rpm at 4°C for 15 minutes to pellet RNA. The supernatant was removed carefully and the RNA pellet was resuspended in 1 ml of 70% ethanol. The mixture was spun at 13,200 rpm at 4°C for 10 minutes to pellet RNA and the 70% ethanol was removed. The RNA pellet was allowed to air-

dry at RT. The dried RNA pellet was resuspended in RNase-free water and the concentration was measured by NanoDrop 2000 UV-Vis Spectrophotometer. 0.6% DNA agarose gel was used to check RNA integrity.

2.2.4.4 Electroporation of DENV RNAs into mammalian cells

BHK-21 or C6/36 cells cells in the log phase of growth were trypsinized and washed 2× with cold PBS pH 7.4. The cells were resuspended in Opti-MEM® (Gibco) to a cell density of 1×10^7 cells/ml. 10 μg of *in vitro* transcribed RNA was mixed with 800 μl of the cell suspension and was transferred into a pre-chilled 4mm curvette (Bio-rad, Germany). The cells were electroporated with a Gene Pulser Xcell system (Bio-rad) at 850V and 25μF, for 2 pluses at an interval of 3 seconds. The cells were allowed to recover at RT for 10 minutes.

For BHK-21 cells, cells were diluted to a cell density of 3×10^5 cells/ml in RPMI 1640 medium supplemented with 10% FBS and 1% P/S, and 1ml of cells were seeded into each well of a 12-well plate. The medium was changed 6 hours post-seeding to RPMI 1640 medium supplemented with 2% FBS and 1% P/S, and the supernatants and cells were harvested at 24, 48, 72, 96 and 120 hours.

For C6/36 cells, cells were diluted to a cell density of 1×10^5 cells/ml in RPMI 1640 medium supplemented with 25 mM HEPES, 10% FBS and 1% P/S and 10 ml of cells were seeded into a T25 flask. The medium was changed 24 hours post-seeding to RPMI 1640 medium supplemented with 25 mM HEPES, 2% FBS and 1% P/S, and

the supernatants were harvested at 7 days post-seeding. The harvested samples were kept at -80^{o}C till further processing.

2.2.5 Statistical analysis

Two-tailed unpaired Student t-test was used to determine if the difference in mean observed was statistically significant. P values < 0.05 were considered as significant. All calculations were done using GraphPad Prism v5.0 (GraphPad Software Inc).

2.3 Material and Methods that were used in section 3.1

2.3.1 Peptide synthesis

DENV3 and 4 NS3 and NS5 peptides (Table 2-8) that were used for SPR assay, competitive NS3-NS5 interaction ELISA and viral inhibition assay were synthesized by NTU peptide synthesis core facility (Singapore).

Table 2-8: List of peptides used in SPR assay, competitive NS3-NS5 interaction ELISA and viral inhibition assay. The residue numbers in peptide name indicate the region on NS3 or NS5 that was synthesized. The peptides were synthesized with either biotin or NH_2 group at N-terminal and $CONH_2$ group at C-terminal. "s" indicates scrambled sequence.

	Peptide name	Sequence
DENV3	$NS3_{566-585}$	^{NH2}CGQRNNQILEENMDVEIWTKEC^{CONH2}
	$NS3_{566-585(N570A)}$	^{NH2}CGQRNAQILEENMDVEIWTKEC^{CONH2}
	$NS3_{86-100}$	^{NH2}EGEWKEGEEVQVLAL^{CONH2}
	$NS3_{570-585}$	^{NH2}QILEENVEVEIWTKE^{CONH2}
	Penetratin	^{biotin}RQIKIWFQNRRMKWKK^{CONH2}
	$_{pene}NS5_{320-341}$	^{biotin}RQIKIWFQNRRMKWKKMINGVVKLLTKPWDVVPMVTQM^{CONH2}
	$_{pene}NS5_{s320-341}$	^{biotin}RQIKIWFQNRRMKWKKMVTPKTLIVDWMNMLVQKVPVG^{CONH2}
DENV4	$NS5_{320-368}$	^{Biotin}MVNGVVKLLTKPWDVIPMVTQLAMTDTTPFGQQRVFKEKVDTRT PQPKP^{CONH2}
	$NS5_{320-341}$	^{Biotin}MVNGVVKLLTKPWDVIPMVTQL^{CONH2}
	$NS5_{342-368}$	^{Biotin}AMTDTTPFGQQRVFKEKVDTRTPQPKP^{CONH2}

2.3.1 NS5 peptide-phage clone construction

DENV3 NS5 peptide-phage clones were constructed using Ph.D.™ Peptide Display Cloning System (NEB) according to the manufacturer's instructions. Templates encoding the sequence of DENV3 $NS5_{320-368}$, $_{320-341}$ and $_{342-368}$ (Table 2-9) were synthesized by IDT. Transformant with NS5 insert was confirmed by sequencing, and was used to prepare NS5 peptide-phage stock as instructed by NEB for peptide-phage ELISA. The phage titre was determined prior to ELISA.

Table 2-9: Sequences of NS5 template used in cloning of NS5 peptide-phage clones for NS5 peptide-phage ELISA. The residue numbers in template name indicate the region on NS5 that was cloned. Underlined nucleotides within primers indicate *Acc65*I and *Eag*I sites respectively.

Template name	Sequence
$NS5_{320-368}$	5'-CCCGGGTACCTTTCTATTCTCACTCTATGATAAATGGAGTCGTGAA ACTCCTCACCAAACCATGGGATGTGGTGCCCATGGTGACACAGATG GCAATGACAGACACAACTCCATTTGGCCAGCAGAGAGTCTTTAAAG AGAAAGTGGACACCAGGACGCCCAGGCCCCTGCCAGGCGGCGGCTC GGCCGAAACATG-3'
$NS5_{320-341}$	5'-CCCGGGTACCTTTCTATTCTCACTCTATGATAAATGGAGTCGTGAA ACTCCTCACCAAACCATGGGATGTGGTGCCCATGGTGACACAGATG GGCGGCGGCTCGGCCGAAACATG-3'
$NS5_{342-368}$	5'-CCCGGGTACCTTTCTATTCTCACTCTGCAATGACAGACACAACTCC ATTTGGCCAGCAGAGAGTCTTTAAAGAGAAAGTGGACACCAGGACG CCCAGGCCCCTGCCAGGCGGCGGCTCGGCCGAAACATG-3'

2.3.2 NS3 bacterial expression plasmid construction

Plasmids for the expression of DENV3 NS5 RdRP *(*residues 273-900), DENV3 and 4 NS3 full-length protein ($NS2B_{49-66}NS3_{FL}$; residues 49-66 of NS2B and 1-618 of NS3 connected by a flexible glycine linker G_4SG_4), DENV 3 protease domain ($NS2B_{49-95}NS3_{1-185}$; residues 49-95 of NS2B and 1-185 of NS3 connected by a flexible glycine linker G_4SG_4) and DENV4 NS3 helicase domain ($NS3_{172-618}$) had been described previously (Li *et al.*, 2005; Luo *et al.*, 2008a; Yap *et al.*, 2007) (Table 2-10).

DENV3 $NS2B_{49-66}NS3_{FL}$ construct (as mentioned above) was used as template to amplify the PCR fragments of DENV3 $NS3_{172-618}$, $_{482-618}$ and $_{566-618}$ by primers in Table 2-10. DENV3 $NS3_{172-618}$ and $_{482-618}$ fragments were digested with *Nde*I and *Bam*HI, and ligated into pET14b vector that was pre-cut with *Nde*I and *Bam*HI. $NS3_{482-618}$ and $_{566-618}$ fragments were digested with *Bam*HI and *Xho*I, and ligated into pGEX-4T-1 vector that was pre-cut with *Bam*HI and *Xho*I.

DENV4 $NS2B_{49-66}NS3_{FL}$ construct (Luo *et al.*, 2008a) was used as template to amplify the PCR fragment that encoded helicase of DENV4 $NS3_{172-618}$-$NS5_{320-341}$ (connected by a flexible glycine linker G_4SG_4) (Figure 3-6A) by primers in Table 2-10. The flexible linker sequence and $NS5_{320-341}$ sequence were then added by two separate PCR reactions to the helicase fragment, and the full-length fragment was cut by *Nae*I and *Sal*I and ligated into pProEx HTb vector that was pre-cut with *Nae*I and *Sal*I.

Mutation of NS3 N570 to alanine in DENV3 $NS2B_{49-66}NS3_{FL}$ protein was done using using QuikChange II SDM kit, according to manufacturer's instruction. The following primers were used: NS3_N570A_forward (5'-GATGGGCAACGCAATGCTCAAA TTTTAGAGGAG-3') and _reverse (5'-CTCCTCTAA AATTTGAGCATTGCGTTG CCCATC-3'). The underlined nucleotide corresponds to the mutation that was being made. Sequencing was done to confirm the presence of mutation.

Table 2-10: List of NS3 and NS5 constructs used for competitive NS3-NS5 interaction ELISA, peptide phage ELISA and SPR assay. The residue numbers in construct name indicate the region on NS3 and NS5 that was cloned. Primers and restriction sites (underlined) that were used to make new NS3 constructs were listed. "N" indicates No and "Y" indicates Yes.

Construct name	Primer sequence (5'→3')	Restriction site used	Cloning vector	Expressed and purified	Reference
DENV3 $NS5_{273-900}$ (RdRP)	-	-	pET15b	Y	(Yap *et al.*, 2007)
DENV3 $NS2B_{49-95}NS3_{1-185}$	-	-	pET15b	Y	(Li *et al.*, 2005)
DENV3 and 4 $NS2B_{49-66}NS3_{FL}$	-	-	pET32b	Y	(Luo *et al.*, 2008a)
DENV4 $NS3_{172-618}$ (helicase)	-	-			(Luo *et al.*, 2008a)
DENV4 $NS3_{172-618}$-G_4SG_4-$NS5_{320-341}$	Forward: GAAAACCTGTATTTTCAGGGCGCCGGCGGTGAGCCAGATTATGAAGTGG	*Nae*I	pPROEX HTb B	Y	In this study
	Reverse: CTCCATTCACCATTCCTCCTCCTCCTGATCCTCCTCCTCCCTTTCTTCCACTGGC	-			
	Reverse: GGAATCACATCCCAGGGTTTTGTCAGCAGTTTCACCACTCCATTCACCATTCCTC	-			
	Reverse: GCGGCCGCGACTAGTGAGCTCGTCGACTTACTGGGTCACCATTGGAATCACATCCCAGGG	*Sal*I			
DENV3 $NS3_{172-618}$ (helicase)	Forward: CAAACAAATGCACATATGGATGGACCGACACC	*Nde*I	pET14b	Y	
	Reverse: GTGCTCGAGTGCGGATCCAAGCTTTTACTTTC	*Bam*HI			
DENV3 $NS3_{172-481}$	Forward: CAAACAAATGCACATATGGATGGACCGACACC	*Nde*I	pET14b	N	
	Reverse: GCAGCCGGATCCCTAATTGTTGAGAGGCTGGCCCG	*Bam*HI			
DENV3 $NS3_{307-618}$	Forward: CAACTCGTGTTCATATGGGAGAAGCAGCC	*Nde*I	pET14b	N	
	Reverse: GTGCTCGAGTGCGGATCCAAGCTTTTACTTTC	*Bam*HI			
DENV3 $NS3_{482-618}$	Forward: CCAGCCTCTCCATATGGATGAAGACCATG	*Nde*I	pET14b	Y	
	Reverse: GTGCTCGAGTGCGGATCCAAGCTTTTACTTTC	*Bam*HI			
GST DENV3 $NS3_{482-618}$	Forward: CCAGCCTCTCGGATCCGATGAAGACCATG	*Bam*HI	pGEX-4T-1	Y	
	Reverse: CACAAGATCAAGCTCGAGTCACTTTCTGCC	*Xho*I			
GST DENV3 $NS3_{566-618}$	Forward: GAAAATGGTGCGGATCCGGGCAACGCAATAATC	*Bam*HI	pGEX-4T-1	Y	
	Reverse: CACAAGATCAAGCTCGAGTCACTTTCTGCC	*Xho*I			
GST DENV3 $NS3_{172-565}$	Forward: CAAATGCAGGATCCGATGGACCGACACC	*Bam*HI	pGEX-4T-1	N	
	Reverse: GATTATTCTCGAGCTAATCAAAGCACCATTTTCTATCTGTG	*Xho*I			

2.3.3 *E. coli* protein expression and purification

All NS3 and NS5 bacterial expression constructs (Table 2-3) were transformed into *E. coli* BL21 CodonPlus (DE3)-RIL cells for protein expression and were purified as previously published (Li *et al.*, 2005; Luo *et al.*, 2008a; Moreland *et al.*, 2010; Tay *et al.*, 2014b; Yap *et al.*, 2007).

2.3.4 Competitive NS3-NS5 interaction ELISA

Maxisorp 96-well Immunoplate (Thermo Scientific Nunc) was coated with 100 µl of NS5 RdRP (5 µg/mL) in PBS (pH 7.2) overnight at 4ºC (Figure 3-2A). Prior to blocking of each well by 300 µl of 5% skim milk in PBST for 1 hour at 37ºC, the plate was washed 2× with PBS. After blocking, the plate was washed 3× with PBST and 35 µl of either DENV3 $NS2B_{49\text{-}66}NS3_{FL}$ or $NS2B_{47}NS3_{1\text{-}185}$ protein (control) that was diluted in PBST with 0.5% BSA was added for 1 hour incubation at 37ºC. After which, the plate was washed 4× with PBST and bound NS3 proteins were detected by 1 hour incubation at 37ºC with 50 µl of 3F10 IgG (1 nmol/L) that was diluted in PBST-M. Plates were again washed 5× with PBST and incubated with 100 µl of anti-human IgG HRP conjugate (1:1000 in PBST-M) for 1 hour at RT. Prior to colour development with 35 µl of colorimetric substrate TMB (3,3′,5,5′-tetramethylbenzidine; Sigma), the plate was washed with 2×PBST and 1×PBS. Colour development was stopped with addition of 12.5 µl of 3M HCl and the plate was read at 450 nm on an optical density plate reader.

For competitive NS3-NS5 interaction ELISA, the concentration of $NS2B_{49-66}NS3_{FL}$ was fixed at either 60 nM when NS3 peptide was added (starting from 60 to 480 μM) or 80 nM when NS3 protein was added (starting from 1 to 20 μM). The concentration of NS3 peptide or protein at which 50% inhibition of $NS2B_{49-66}NS3_{FL}$ protein binding occurs corresponds to the K_d. Data was subjected to nonlinear regression analysis by GraphPad Prism 5 software and an apparent K_d was obtained.

2.3.5 ATPase assay

The assay was carried out as described (Xu *et al.*, 2005a), with slight modification. 2.5 nM of purified $NS2B_{49-66}NS3_{FL}$ WT or N570A protein was pre-incubated at 37°C with poly U (10 μg/ml) in 40 μl ATPase assay buffer (section 2.1.6) for 5 minutes. The reaction was initiated by the addition of 10 μl of increasing ATP concentrations (2-fold serial dilution, starting from 2000 μM) and carried out for 10 minutes at 37°C. 10 μl of Malachite green reagent was added to stop the reaction. Absorbance was read at 635 nm after 30 minutes at RT. The K_m of the protein was determined with GraphPad Prism 5, with Michaelis-Menten equation, $V_o = (V_{max}[S])/(K_m+[S])$.

2.3.6 Surface plasmon resonance assay (did in collaboration with Drs Luo Dahai and Julien Lescar in NTU)

Surface plasmon resonance (SPR) measurements were performed on ProteOn XPR36 instrument (Bio-Rad Laboratories, Inc). All experiments were carried out with a constant flow rate of 25µl/minutes (20 mM Tris-HCl pH 7.4, 0.2 M NaCl, 1 mM dithiothreitol, 5% glycerol, 0.005% NP-20). Both DENV4 $NS2B_{49\text{-}66}NS3_{FL}$ and $NS3_{172\text{-}618}$ were amine-coupled to a carboxylated sensor surface (GLM sensor chip) to a final immobilized level of 10000 and 15000RU respectively. A 2-fold serially diluted biotinylated NS5 peptides (starting from 120 µM) was injected in duplicate across the chip for four minutes and dissociation was monitored for ten minutes. Data were analyzed in ProteOn Manager version 2.0.

2.3.7 NS5 peptide-phage ELISA

The ELISA binding assay was performed as instructed by NEB. In brief, Maxisorp 96-well Immunoplate was coated with either 100 µl of DENV3 $NS2B_{49\text{-}66}NS3_{FL}$, $NS3_{172\text{-}618}$, $NS3_{482\text{-}618}$, $NS2B_{49\text{-}95}NS3_{1\text{-}185}$ or BSA (control) protein (5 µg/mL) in PBS (pH 7.2) overnight at 4°C. Prior to blocking of each well by 300 µl of 5% skim milk in PBST (PBS pH 7.2 supplemented with 0.1% Tween 20; PBST-M) for 1 hour at RT, the plate was washed 2× with PBS. After blocking, the plate was washed 3× with PBST and 100 µl (5×10^9 phage particles) of either DENV3 $NS5_{320\text{-}368}$, $NS5_{320\text{-}341}$, $NS5_{342\text{-}368}$ peptide-phage or WT phage (control) that was diluted in PBST-M was added for 2 hours incubation at RT. After which, the plate was washed 5× with PBST and bound phages were detected by 1 hour incubation at RT with 100 µl of anti-M13

HRP conjugate polyclonal antibody (1:1000; PBST-M) for 1 hour at RT. Prior to colour development with 35 µl of colorimetric substrate TMB, the plate was washed with 2×PBST and 1×PBS. Colour development was stopped with addition of 12.5 µl of 3M HCl and the plate was read at 450 nm on an optical density plate reader.

2.3.8 Small angle X-ray scattering data collection and processing (did in collaboration with Saw Wuan Geok and Dr Gerhard Grüber from NTU)

Small angle X-ray scattering (SAXS) data of the $NS3_{172-618}$ and $NS3_{172-618}$-$NS5_{320-341}$ were collected and analysed as described (Tay *et al.*, 2014b). Briefly, SAXS experiments for both $NS3_{172-618}$ and $NS3_{172-618}$-$NS5_{320-341}$ proteins were collected with a NANOSTAR instrument (Bruker AXS, USA) that was equipped with a Metaljet X-ray source and a 2D Vantee-2000 detector. Data was collected at 15°C, a wavelength of λ = 1.34 Å and a source-to-sample and sample-to-detector distance of 145 and 67 cm, respectively. To exclude concentration-dependence effect, 3 different concentrations of each protein, namely 1.2, 2.2 and 4 mg/ml, were prepared. Nine measurements were recorded for each sample with a 5 minutes interval. The data were flood-field, spatially corrected and processed using the in-built SAXS software. No radiation damage was detected as comparison of all datasets revealed no changes in data. The scattering intensity of the buffer was subtracted from the scattering intensity of each protein solution. All the data processing steps were performed automatically using the program package PRIMUS (Svergun, 1993). The radius of gyration *Rg* and forward scattering *I(0)* were evaluated using the Guinier approximation (Lipson, 1956). These parameters were also computed by the indirect transform package

GNOM (Svergun, 1992), which also provide the distance distribution function p(r). Ten low-resolution models of $NS3_{172-618}$ or $NS3_{172-618}$-$NS5_{320-341}$ were independently built by the program GASBOR (Svergun *et al.*, 2001). The normalized spatial discrepancy (NSD), which is a measure of similarity between sets of 3D points was computed for all ten reconstructions using the DAMAVER program (Kozin & Svergun, 2001); the reconstruction with the least NSD was selected for both proteins. Ensemble Optimization Method (EOM) suite was employed to select an ensemble of conformations that best fits the experimental data, and the dimensions of selected conformations were compared with the random pool to evaluate the compactness and flexibility of $NS3_{172-618}$-$NS5_{320-341}$ (Bernado *et al.*, 2007; Petoukhov *et al.*, 2012).

2.3.9 Viral inhibition assay

One day before infection, Huh-7 cells were seeded in 12 well plates at a density of 2×10^5 cells/well. On the following day, cells were infected with DENV2 (MOI = 1) for 1 hour at 37°C, and after which, virus inoculums were removed and replaced with 5% FBS DMEM media. At 6 hours post-infection, the infected cells were treated with 7.5 μM NS3 peptides complexed with 22.5 μM penetratin (molar ratio = 1:3) or 7.5 μM NS5-penetratin fusion peptides. At 24 hour post-infection, cells were washed once with PBS pH 7.4 prior to lysis by TRIzol for extraction of total cellular RNA for viral RNA quantification by real-time RT-PCR analysis with primers that binds NS1 gene (see section 2.2.2.8). Absolute copy numbers of viral RNA was calculated based on DENV2 standard curve and normalized to actin level that was also quantified. The data was reported as fold-change that was normalized to 24 hour control.

2.3.10 NS3-NS5 co-IP from infected cells

One day prior to infection, 2.4×10^6 Huh-7 cells were seeded in a 10-cm plate. On the following day, medium was removed and cells were infected with either DENV1 or 2 at a multiplicity of infection (MOI) of 10 (2 plates per serotype). After 1 hour incubation at 37°C, virus inoculum was removed and replaced with 5% FBS DMEM medium. The plates were kept at 37°C with 5% CO_2 for 24 hours. After 24 hours, the medium was removed and the cells were harvested by trypsinization. The cells were washed 2× with 5ml cold PBS pH 7.4 and the cell pellet was resuspended in 600 µl of lysis buffer with 1% triton X-100 that was supplemented with protease inhibitor). The cells were allowed to lyse on ice for 30 minutes with occasional mixing. The lysed cells were centrifuged at 13,200 rpm for 10 minutes in a 1.5ml eppendorf tube, and supernatant was transferred to new eppendorf tube. 2µg of each dengue antibody (mouse anti-E 4G2, human anti-NS3 3F7 (Moreland *et al.*, 2012), anti-NS3 3F8 (Moreland *et al.*, 2012) or anti-NS5 5R3 (Zhao *et al.*, 2014)) was incubated with 135 µl of supernatant overnight at 4°C with continuous rotation. Following overnight incubation, 10µl of equilibrated protein A/G resin (washed 3× with lysis buffer) was added to each antibody-supernatant mixture and allowed to incubate for at least 2 hours at 4°C with continuous rotation. After incubation, the resin was washed with 3× with 1ml TBST (25 mM Tris pH 7.2, 100 mM NaCl and 0.1% Tween 20). Bound proteins were eluted from resin by boiling at 95ºC for 5 minutes with 45 µl of 2× loading dye and 15 µl of elutant was loaded onto 10% gel for western blot analysis.

2.3.11 Generation of NS3:N570A and NS5:K330A mutant viruses

For NS3:N570A and NS5:K330A, mutation was done in pWSK29 D2 fragment 3 subclone. SDM was performed with QuikChange II SDM Kit, according to the manufacturer's instructions. The following primers were used for the generation of both mutants: NS3:N570A_forward (5'-CTTTGATGGAGTCAAGAACGCCCAAA TCTTGGAAGAAAATG-3') and _reverse (5'-CATTTTCTTCCAAGATTTGGGCG TTCTTGACTCCATCAAAG-3') and NS5:K330A_forward (5'-GTGGTTAGGCTG CTAACAGCACCTTGGGATGTCATCCCC-3') and _reverse (5'- GGGGATGACA TCCCAAGGTGCTGTTAGCAGCCTAACCAC-3'). The underlined nucleotide corresponds to the mutation that was being made.

2.3.12 Strand-specific quantitative RT-PCR assay

For intracellular viral RNA quantification of both negative- and positive-strand, *5'*-tagged primers (Plaskon *et al.*, 2009) that bind to E gene (Johnson *et al.*, 2005) were used for transcribing cDNAs of both polarities (Table 2-11). Forward primer (Eden2_E_FP_RT) was used to transcribe cDNA from negative-strand RNA, while reverse primer (Eden2_E_RP_RT) was used to transcribe cDNA from positive-strand RNA by using Improm II reverse transcription system. 40 ng of cDNA was used for real-time RT-PCR analysis of viral RNA with the use of iQ SYBR Green supermix and the appropriate primer pair for either negative-strand (Eden2_E_RP_qPCR and Tag_S_qPCR) or positive-strand (Eden2_E_FP_qPCR and Tag_S_qPCR) for detection. Absolute negative- and positive-strand copy numbers were quantitated with DENV2 standard curve that used *in vitro* RNA transcripts (nucleotide number 1450 to

1739 of DENV2 genome) that were synthesized by T7 RNA polymerase, and reported as described in section 2.2.2.8.

Table 2-11: Primers used for intracellular viral RNA quantification of both negative- and positive-strand by real-time RT-PCR. The underlined sequence corresponds to unique tag sequence that was incorporated into cDNA and was responsible for binding to tag primer during real-time RT-PCR.

Primer name	Sequence (5'→3')	Reference
Eden2_E_FP_RT	GGCCGTCATGGTGGCGAATAACAGGCTATGGCACTGTCACGAT	This study
Eden2_E_RP_RT	GGCCGTCATGGTGGCGAATAACCATTTGCAGCAACACCATCTC	
Eden2_E_FP_qPCR	CAGGCTATGGCACTGTCACGAT	
Eden2_E_RP_qPCR	CCATTTGCAGCAACACCATCTC	
Tag_S_qPCR	GGCCGTCATGGTGGCGAATAA	

2.4 Materials and Methods that were used in section 3.2

2.4.1 Biopanning of naïve human Fab-phage display library

The biopanning was performed as described previously (Moreland *et al.*, 2010; Tay *et al.*, 2014a) (Figure 2-2). Briefly, Fab-phage display library (Humanyx Pte Ltd, Singapore) was biopanned against either biotinylated DENV2 or 3 NS5 MTase and RdRP proteins for four rounds, with increased stringency after each round, by reducing the amount of biotinylated protein and increasing the number of washes. After the last round of panning, individual phage colony was picked to produce phage particles for screening of positive phage clone that could bind to unbiotinylated DENV2 or 3 NS5 MTase and RdRP by ELISA. Upon confirmation of positive phage clone that bound NS5, the Fab-phage clone was converted to human IgG by cloning the variable light and heavy chain sequences into an IgG vector containing human constant region sequences via ApaL1 and BsmB1 sites as previously described (Lim *et al.*, 2008). IgG was produced by transfection of full-length IgG vector via

jetPRIME reagent (Polyplus) into HEK293T cells as previously described (Moreland *et al.*, 2012).

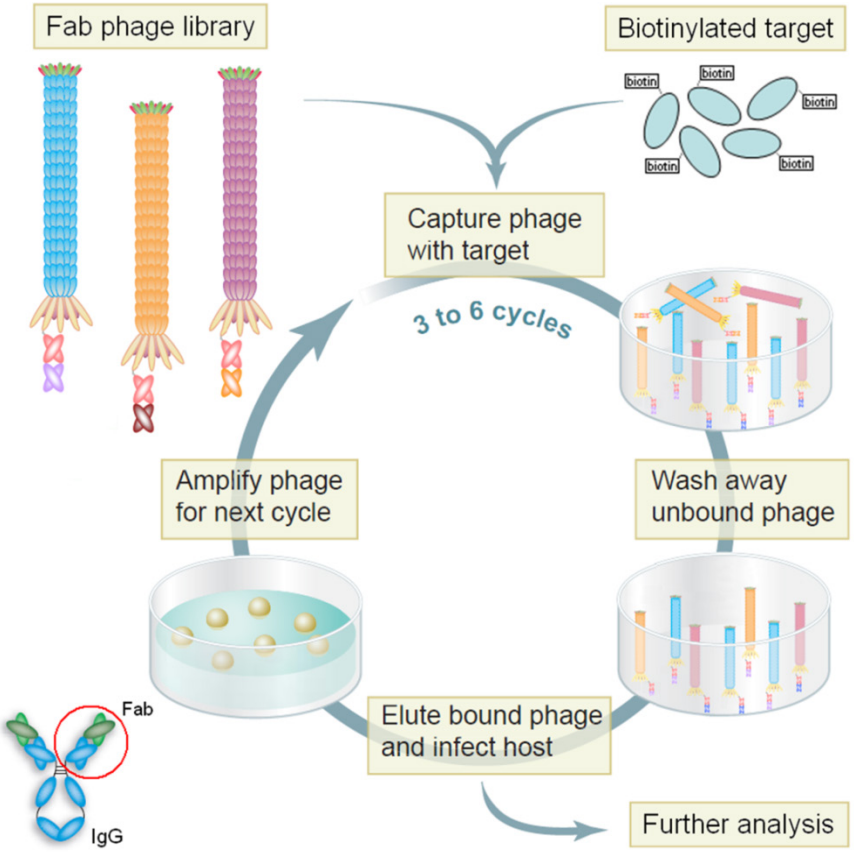

Figure 2-2: Schematic representation of biopanning against Fab-phage display library. Humanyx library was constructed by introducing cloned Fab fragment into phagemid that fused the cloned Fab fragment to gene *III*. Fabs are displayed on surface of M13 phage as Fab-protein *III* fusion protein. During biopanning, Fab-phage are mixed with biotinylated target to allow binding and unbound phage are removed by washing. Bound phage are eluted by a short exposure to extreme pH and amplified overnight for subsequent rounds of biopanning. Figure is modified from (Smothers *et al.*, 2002).

2.4.2 Characterization of anti-NS5 by ELISA and dot blot

The ELISA was performed as described previously (Moreland *et al.*, 2012). Briefly, either DENV2 or 3 NS5 MTase or RdRP protein was coated overnight in PBS pH 7.5, 5 µg/ml, at 4ºC. On the following day, the plate was washed and blocked in PBST-M for 1 hour at RT. After blocking, 2-fold serially diluted anti-NS5 Fab or IgG in PBST-

M (starting from 200 nM; 5M1 or 5R3) was added and incubated for 1 hour at RT. After primary antibody incubation, plate was washed with PBST and incubated with an anti-human HRP conjugate (MyBiosource, USA) for detection.

The dot blot was performed as described previously (Zhao *et al.*, 2014). Briefly, either boiled or native DENV3 NS5 protein was spotted onto nitrocellulose western blot membrane at various amounts (2-fold serially diluted, starting from 2.5 μg). The membrane was allowed to dry prior to blocking in PBST-M. After blocking, the blot was incubated with 10 nM of anti-NS5 IgG for 1 hour at RT. After primary antibody incubation, bolt was washed with PBST and incubated with an anti-human HRP conjugate for detection.

2.4.3 Mammalian expression plasmid construction

2.4.3.1 DENV1-4 GFP-NS5 constructs

DENV1-4 NS5 genes were amplified by PCR from DENV1-4 cDNA clones (GenBank accession numbers for the relevant sequences are: DENV1 (EU081230), DENV2 (EU081177), DENV3 (EU081190) and DENV4 (GQ398256)) (Christenbury *et al.*, 2010; Schreiber *et al.*, 2009b) with the primer pairs listed in Table 2-12 for each construct. The PCR products were digested with *Xho*I and *Xma*I and cloned in similarly cut pEGFP-C1 vector (Clontech).

Table 2-12: Primers used to clone NS5 full-length proteins of DENV1-4 into pEGFP-C1 vector, which is an N-terminal GFP tag mammalian expression vector. FP indicates forward primer; RP indicates reverse primer; **CTCGAG** in FP indicates *Xho*I site; **CCCGGG** indicates *Xma*I site; ~~**CC**~~ indicates extra nucleotide added for in-frame cloning.

Construct name	Primer name	Primer sequence
D1 NS5	D1NS5_FP	CAAGTCCGGACTCAGAT**CTCGAG**~~**CC**~~GGTACGGGAGCCCAAGGGG
	D1NS5_RP	CTAGATCCGGTGGAT**CCCGGG**TCACCAGAGTGCCCCTTCGGG
D2 NS5	D2NS5_FP	CAAGTCCGGACTCAGAT**CTCGAG**~~**CC**~~GGAACTGGCAACACAGGAGAG
	D2NS5_RP	CTAGATCCGGTGGAT**CCCGGG**CTACCACAAGACTCCTGCCTC
D3 NS5	D3NS5_FP	CAAGTCCGGACTCAGAT**CTCGAG**~~**CC**~~GGAACAGGCTCACAAGGTG
	D3NS5_RP	CTAGATCCGGTGGAT**CCCGGG**TTACCAAATGGCTCCCTCCAAC
D4 NS5	D4NS5_FP	CAAGTCCGGACTCAGAT**CTCGAG**~~**CC**~~GGAACTGGGACCACAGGAG
	D4NS5_RP	CTAGATCCGGTGGAT**CCCGGG**TTACAGAACTCCTTCACTTTCGG

2.4.3.2 DENV1 and 2 GFP-NS5 domain-swapped constructs

DENV1 and 2 GFP-NS5 domain-swapped genes were generated by overlap extension PCR with the primer pairs listed in Table 2-12 and 2-13. DENV1 and 2 GFP-NS5 constructs (mentioned above) were used as templates for overlap extension PCR. The PCR products were digested and cloned in pEGFP-C1 vector as described in section 3.2.5.1.

Table 2-13: Primers used to clone NS5 full-length proteins that were domain-swapped between DENV1 and 2 into pEGFP-C1vector (together with those primers listed in Table 2-12). The residue numbers in construct name indicate the region on DENV1 and 2 NS5 that were being swapped. FP indicates forward primer; RP indicates reverse primer.

Construct name	Primer name	Sequence
D2 1-319 D1 320-405 D2 406-900	D2_320_D1 FP	CAGACTGGATCAGCATCATCCATGGTCAATGGTGTGGTGAAAC
	D2_320_D1 RP	GTTTCACCACACCATTGACCATGGATGATGCTGATCCAGTCTG
	D1_405_D2 FP	GGAGTTCACAAGAAAAGTTAGGTCAAATGCAGCCTTAGGTGCC
	D1_405_D2 RP	GGCACCTAAGGCTGCATTTGACCTAACTTTTCTTGTGAACTCC
D1 1-319 D2 320-405 D1 406-900	D1_320_D2 FP	GCCATCAGGATCAGCCTCATCCATGGTGAACGGAGTGGTTAGGC
	D1_320_D2 RP	GCCTAACCACTCCGTTCACCATGGATGAGGCTGATCCTGATGGC
	D2_405_D1 FP	GAATTCACAAGAAAGGTGAGAAGCAACGCAGCCATTGGAGCAGTG
	D2_405_D1 RP	CACTGCTCCAATGGCTGCGTTGCTTCTCACCTTTCTTGTGAATTC

2.4.3.3 DENV1 and 2 GFP-NS3 constructs

DENV1 and 2 NS3 genes were amplified by PCR from pET32b plasmids that encoded DENV1 and 2 $NS2B_{49\text{-}66}NS3$ (GenBank accession numbers for the relevant sequences are: DENV1 Hawaii strain (EU848545) and DENV2 TSV01 strain (AY037116)) (Moreland et al., 2010) with the primer pairs listed in table 2-14. The PCR products were digested and cloned in pEGFP-C1 vector as described in section 3.2.5.1.

Table 2-14: Primers used to clone NS3 full-length proteins of DENV1 and 2 into pEGFP-C1 vector. FP indicates forward primer; RP indicates reverse primer; **CTCGAG** in FP indicates *Xho*I site; **CCCGGG** indicates *Xma*I site; ~~**CC**~~ indicates extra nucleotide added for in-frame cloning.

Construct name	Primer name	Sequence
D1 NS3	D1NS3_FP	CAAGTCCGGACTCAGAT**CTCGAG**~~**CC**~~GCCGATTTATCACTGGAGAAAGC
	D1NS3_RP	CTAGATCCGGTGGAT**CCCGGG**TTATCTTCTTCCTGCTGCAAACTC
D2 NS3	D2NS3_FP	CAAGTCCGGACTCAGAT**CTCGAG**~~**CC**~~GCTGATTTGGAACTGGAGAGAG
	D2NS3_RP	CTAGATCCGGTGGAT**CCCGGG**TTACTTTCTTCCAGCTGCGAATTCCTTG

All plasmids produced in the study were verified by sequencing (First Base, Singapore) before use.

2.4.4 Virus infection in Huh-7 cells

One day prior to infection, 7.5×10^4 Huh-7 cells were seeded into 24-well plate, with glass cover slips, and incubated overnight at 37^oC with 5% CO_2. On the following day, the cells were infected with either DENV1, 2, 3 or 4 at a MOI of 10 for 1 hour and after which, virus inoculums were removed and replaced with 5% FBS DMEM media.

2.4.5 Cell-based flavivirus immunodetection assay

The cell-based flavivirus immunodetection (CFI) assay was carried out essentially as described elsewhere (Tan *et al.*, 2014). Briefly, one day before the experiment, 1.3×10^4 BHK-21 cells were seeded into 96-well plate and incubated overnight at 37ºC with 5% CO_2. On the following day, the cells were infected with DENV2 at a MOI of 0.3, in the presence of different concentrations of the test compounds for 1 hour at 37°C. The virus inoculums were removed and replaced with fresh 2% FBS RMPI media containing the test compounds, and the cells were incubated for 48 hours, at 37°C with 5% CO_2. The cells were washed once with phosphate-buffered saline (PBS) and fixed with ice-cold methanol for 15 minutes at -20ºC. Following fixation, cells were washed 2× by PBS and blocked for 1 hour at RT in PBS that contained 1% FBS and 0.1%Tween 20. After blocking, fixed cells were analyzed by IFA by using primary antibody against E (4G2) and secondary antibody coupled to Alexa-Fluor 488 (Invitrogen). Cells were counterstained with DAPI prior to high-content fluorescence microscopy by imaging at channels that detected both DAPI and Alexa Fluor 488 at 4× magnification. Dose-response curves were plotted (log concentration of test compound versus mean percentage infection) by nonlinear regression analysis in GraphPad Prism 5 software and the concentration of the test compound that decreased the level of viral E protein production by 50% (EC_{50}; 50% effective concentration) was calculated.

2.5 Material and Methods that were used in section 3.3

2.5.1 NS3- or NS5-host protein co-IP from transfected cells

One day prior to transfection, 5×10^6 HEK293T cells were seeded into 10-cm plate and incubated overnight at 37°C with 5% CO_2. On the following day, cells were transfected using jetPRIME reagent (Polyplus) with 10 μg of plasmid per plate (2 plates per GFP construct), according to the manufacturer's recommendations. After 24 hours, the medium was removed and the cells were harvested by trypsinization. The cells were washed 2× with 5ml cold PBS pH 7.4 and the cell pellet was resuspended in 200 μl of lysis buffer (10 mM Tris pH 7.5, 150 mM NaCl, 0.5 mM EDTA, 0.5% (v/v) NP-40) in the presence of protease inhibitor (Sigma)). The cells were allowed to lyse on ice for 30 minutes with occasional mixing. The lysed cells were centrifuged at 13,200 rpm for 10 minutes in a 1.5ml eppendorf tube, and supernatant was transferred to new eppendorf tube. The supernatant was diluted with dilution buffer (10 mM Tris pH 7.5, 150 mM NaCl, 0.5 mM EDTA) to achieve a final concentration of 0.2% NP-40. 15 μl of equilibrated GFP-Trap_A resin (washed 3× with lysis buffer) was incubated with diluted supernatant overnight at 4°C with continuous rotation. Following overnight incubation, the resin was washed with 2× with 500 μl of lysis buffer and once with 500 μl of 50 mM ammonium bicarbonate. Bound proteins were eluted from resin by 70 μl of 0.2% (w/v) *Rapi*Gest SR surfactant reagent (Waters) that was made up in 50 mM ammonium bicarbonate via vigorous vortexing for 5 minutes at RT. The elutant was removed and fresh 70 μl of 0.2% *Rapi*Gest SR reagent was added to elute the remaining bound proteins via heating at 95ºC for 5 minutes. Elutants were kept at -80°C till further analysis.

2.5.2 Silver staining and western blot analysis

Elutants from co-IP experiment were nanodropped to quantify the amount of protein present. After quantification, appropriate amount of elutants were mixed with 4×LD and boiled, prior to loading on two 8% SDS PAGE for silver staining (Thermo Scientific Pierce) and western blot analysis. Western blot was performed as described using primary antibodies against GFP, STAT2, DDX3X, DDX5 and MATR3 and the respective HRP conjugated secondary antibodies were added for detection.

2.5.3 LC/ESI/MS/MS analysis and MS data analysis

Elutants were quantified by BCA assay (protein total amount is listed in Table 3-2) prior to mass spectrometry (MS) analysis to ensure that a fixed percentage (≤ 1 μg) of each elutant was injected for analysis. After BCA quantification, elutants were digested with trypsin and digested peptides were subjected to liquid chromatography (LC)/electrospray ionization (ESI)/MS/MS for host protein identification; this service was provided by Proteomics and Metabolomics Shared Resource of Duke University (http://www.genome.duke.edu/cores/proteomics/).

For MS data analysis, trypsin-digested peptides were searched against the Swiss-Prot 2013× database using the 'Mascot' database search algorithm. Search parameters in Mascot were as follows: an initial MS tolerance of 10 ppm and an MS/MS tolerance at 0.04 Da, full tryspin specificity and allowing at most 2 missed cleavages. Carbamidomethylation of cysteine was included as a fixed modification, and oxidation of methionines and deamidation of asparagine and glutamine were included

as variable modifications. Scaffold Proteome software (version 4.3.4) was used to validate MS/MS-based peptide and protein identification (available from http://www.proteomesoftware.com/products/free-viewer/). Peptide and protein identifications were validated with the PeptideProphet algorithm with decoy database validation, and the final database set was curated based on the following parameters: peptide thresholds: 95.0% minimum, protein thresholds: 99.0% minimum and at least two exclusive unique peptide count (the number of different amino acid sequences, regardless of any modification that are associated with a single protein group).

2.5.4 Enrichment of annotation terms and pathways

The set of human proteins that bound to either GFP-NS2B$_{18}$NS3 (DENV1 or 2) or GFP-NS5 (DENV1 or 2) was submitted to GeneMANIA (Warde-Farley *et al.*, 2010) with the following parameters: (1) all networks enabled, (2) equal weighting by network, and (3) 20 related genes displayed. GeneMANIA performed a false discovery rate-corrected hypergeometric test to test for enrichment of gene ontology (GO) features in the query/input dataset by comparing with the entire database of GO terms in the Homo sapiens proteome. Significantly enriched GO features, together with their associated q-values are reported. For each enriched GO feature that is associated with the generated interaction network, the number of proteins in the interaction network listed in that group, as well as the number of total proteins in the Homo sapiens proteome associated with the same GO feature, are also reported.

2.6 Materials and Methods that were used in section 3.4

2.6.1 Mammalian expression plasmid construction

Two types of mammalian expression plasmids were used for cloning: [1] pEGFP-C1 vector (Clontech) and [2] pEGFP-C1 vector with additional GFP gene cloned in (2×GFP vector) that was generated in this study (see below for details). Gene fragments were generated either by PCR or overlap extension PCR (see below for details) and were digested by *Xho*I and *Xma*I prior to ligation into pre-cut vectors.

2.6.2 DENV1 and 2 GFP-NS5 domain-swapped constructs

DENV1 and 2 GFP-NS5 domain-swapped genes were generated by overlap extension PCR with the primer pairs listed in Table 2-12 and 2-15. DENV1 and 2 GFP-NS5 constructs (mentioned above) were used as templates for overlap extension PCR. The PCR products were digested and cloned in pEGFP-C1 vector as described in section 2.4.3.1.

Table 2-15: Primers used to clone NS5 full-length proteins that were domain-swapped between DENV1 and 2 into pEGFP-C1vector (together with those primers listed in Table 2-12). The residue numbers in construct name indicate the region on DENV1 and 2 NS5 that were being swapped. FP indicates forward primer; RP indicates reverse primer.

Construct name	Primer name	Sequence
D2 1-272 D1 273-900	D2_272_D1 FP	CGGAATTGAAAGTGAGACACCAAACCTAGATATCATTGGCCAG
	D2_272_D1 RP	CTGGCCAATGATATCTAGGTTTGGTGTCTCACTTTCAATTCCG
D2 1-319 D1 320-900	D2_320_D1 FP	CAGACTGGATCAGCATCATCCATGGTCAATGGTGTGGTGAAAC
	D2_320_D1 RP	GTTTCACCACACCATTGACCATGGATGATGCTGATCCAGTCTG
D2 1-405 D1 406-900	D2_405_D1 FP	GAATTCACAAGAAAGGTGAGAAGCAACGCAGCCATTGGAGCAGTG
	D2_405_D1 RP	CACTGCTCCAATGGCTGCGTTGCTTCTCACCTTTCTTGTGAATTC
D1 1-272 D2 273-900	D1_272_D2 FP	GCAGTGGAACCAGAGGTAGCCAATTTAGACATAATTGGGAAAAG
	D1_272_D2 RP	CTTTTCCCAATTATGTCTAAATTGGCTACCTCTGGTTCCACTGC
D1 1-319 D2 320-900	D1_320_D2 FP	GCCATCAGGATCAGCCTCATCCATGGTGAACGGAGTGGTTAGGC
	D1_320_D2 RP	GCCTAACCACTCCGTTCACCATGGATGAGGCTGATCCTGATGGC
D1 1-405 D2 406-900	D1_405_D2 FP	GGAGTTCACAAGAAAAGTTAGGTCAAATGCAGCCTTAGGTGCC
	D1_405_D2 RP	GGCACCTAAGGCTGCATTTGACCTAACTTTTCTTGTGAACTCC

2.6.2.1 DENV1 and 2 GFP-NS5 motif-swapped constructs

DENV1 and 2 GFP-NS5 motif-swapped genes were generated by overlap extension PCR with the primer pairs listed in Table 2-12 and 2-16. DENV1 and 2 GFP-NS5 constructs (mentioned above) were used as templates for overlap extension PCR. The PCR products were digested and cloned in pEGFP-C1 vector as described in section 2.4.3.1.

Table 2-16: Primers used to clone NS5 full-length proteins that were motif-swapped between DENV1 and 2 into pEGFP-C1 vector (together with those primers listed in Table 2-12). The residue numbers in construct name indicate the region on DENV1 and 2 NS5 that were being swapped. FP indicates forward primer; RP indicates reverse primer.

Construct name	Primer name	Sequence
D2 1-361 D1 362-393 D2 394-900	D2_362_D1 FP	CAAAGAGAAGGTGGACACGAGAACACCAAAAGCAAAACGAGG
	D2_362_D1 RP	CCTCGTTTTGCTTTTGGTGTTCTCGTGTCCACCTTCTCTTTG
	D1_393_D2 FP	GAAACAAGAAGCCAAGAATTTGTACCAGAGAAGAATTCACAAG
	D1_393_D2 RP	CTTGTGAATTCTTCTCTGGTACAAATTCTTGGCTTCTTGTTTC
D2 1-393 D1 394-496 D2 497-900	D2_394_D1 FP	GAAAAAGACACCTAGGATGTGCACAAGAGAGGAGTTCACAAG
	D2_394_D1 RP	CTTGTGAACTCCTCTCTTGTGCACATCCTAGGTGTCTTTTTC
	D1_496_D2 FP	CATGAACGAAGACCACTGGTTTTCCAGAGAGAACTCCC
	D1_496_D2 RP	GGGAGTTCTCTCTGGAAAACCAGTGGTCTTCGTTCATG
D2 1-507 D1 508-536 D2 537-900	D2_508_D1 FP	CCCTGAGTGGAGTGGAAGGAGAAGGACTCCACAAAC
	D2_508_D1 RP	GTTTGTGGAGTCCTTCTCCTTCCACTCCACTCAGGG
	D1_536_D2 FP	CAGATGACACAGCCGGATGGGACACAAGAATCACAC
	D1_536_D2 RP	GTGTGATTCTTGTGTCCCATCCGGCTGTGTCATCTG
D2 1-551 D1 552-585 D2 586-900	D2_552_D1 FP	CAGGATGGGACACAAGAATCACAGAGGATGATCTTCAGAATG
	D2_552_D1 RP	CATTCTGAAGATCATCCTCTGTGATTCTTGTGTCCCATCCTG
	D1_585_D2 FP	CTTCAAGCTAACCTACCAAAATAAAGTGGTGCGTGTACAAAGAC
	D1_585_D2 RP	GTCTTTGTACACGCACCACTTTATTTTGGTAGGTTAGCTTGAAG
D2 1-574 D1 575-595 D2 596-900	D2_595_D1_FP	AAATTAACGTACCAAAACAAAGTGGTAAGGGTACAGAGACCAG CAAAAAATGGAACCGTG
	D2_575_D1 RP	GTTTTGGTACGTTAATTTGAAAATGGCTTCAGCAAG
D2 1-625 D1 626-657 D2 658-900	D2_626_D1 FP	CAGACAGATGGAGGGAGAAGGAATCTTTTCACCCAGTG
	D2_626_D1 RP	CACTGGGTGAAAAGATTCCTTCTCCCTCCATCTGTCTG
	D1_657_D2 FP	CGTCGAAAGGCTAAAAAGAATGGCCATCAGTGGAGATGATTG
	D1_657_D2 RP	CAATCATCTCCACTGATGGCCATTCTTTTTAGCCTTTCGACG
D2 1-625 D1 626-708 D2 709-900	D2_626_D1 FP	CAGACAGATGGAGGGAGAAGGAATCTTTTCACCCAGTG
	D2_626_D1 RP	CACTGGGTGAAAAGATTCCTTCTCCCTCCATCTGTCTG
	D1_708_D2 FP	GGAATGATTGGCAACAAGTGCCTTTTTGTTCACACCATTTCCATGAGTTAATCATGAAG
	D1_708_D2 RP	CTTCATGATTAACTCATGGAAATGGTGTGAACAAAAAGGCACTTGTTGCCAATCATTCC
D2 1-625 D1 626-900	D2_626_D1 FP	CAGACAGATGGAGGGAGAAGGAATCTTTTCACCCAGTG
	D2_626_D1 RP	CACTGGGTGAAAAGATTCCTTCTCCCTCCATCTGTCTG
D2 1-657 D1 658-900	D2_658_D1 FP	GCGTGAGAGGTTATCAAGAATGGCAATCAGTGGAGATGACTGCG
	D2_658_D1 RP	CGCAGTCATCTCCACTGATTGCCATTCTTGATAACCTCTCACGC
D2 1-708 D1 709-900	D2_709_D1 FP	CGATTGGACACAAGTGCCCTTTTGTTCACACCACTTCCACCAGCTG
	D2_709_D1 RP	CAGCTGGTGGAAGTGGTGTGAACAAAAGGGCACTTGTGTCCAATCG

2.6.2.2 DENV1-4 GFP-NS5 C-terminal-swapped constructs

DENV1 and 2 GFP-NS5 C-terminal-swapped genes were generated by PCR or overlap extension PCR with the primer pairs listed in Table 2-12 and Table 2-17. DENV1-4 GFP-NS5 constructs (mentioned above) were used as templates for PCR. The PCR products were digested and cloned in pEGFP-C1 vector as described in section 2.4.3.1.

Table 2-17: Primers used to clone NS5 full-length proteins that were C-terminal-swapped between DENV1-4 into pEGFP-C1vector (together with those primers listed in Table 2-12). The residue numbers in construct name indicate the region on DENV1 and 2 NS5 that was being swapped. FP indicates forward primer; RP indicates reverse primer.

Construct name	Primer name	Sequence
D2 1-888 D1 889-900	D2_899_D1 RP	CACCAGAGTGCCCCTTCGGGATCACTCTCGTTCTTAAATCTTTTC ATGGATGGCATGTAG
D2 1-888 D3 889-900	D2_899_D3 RP	ACCAAATGGCTCCCTCCAACTCCTCTTCCTTCCTAAATCTTTTCA TGGATGGCATGTAG
D2 1-888 D4 889-900	D2_899_D4 RP	TTACAGAACTCCTTCACTTTCGGAAGGAGCGCTAAATCTTTTCA TGGATGGCATGTAG
D1 1-882 D2 883-900 (also known as D1 NS5 with D2 883-900)	D1_883_D2 FP	GGGAATGAGAATTATCTAGATTACATGCCATCCATGAAAAGAT TTAGAAG
	D1_883_D2 RP	CTTCTAAATCTTTTCATGGATGGCATGTAATCTAGATAATTCTC ATTCCC
D2 1-882 D1 883-900 (also known as D2 NS5 with D1 883-900)	D2_883_D1 FP	TAGGCAATGAGGAATACACAGACTACATGACATCAATG AAGAGATTCAAGAAC
	D2_883_D1 RP	GTTCTTGAATCTCTTCATTGATGTCATGTAGTCTGTGTAT TCCTCATTGCCTA

2.6.2.3 DENV1 and 2 GFP-NS5 C-terminal truncated constructs

DENV1 and 2 GFP-NS5 C-terminal truncated genes were generated by PCR with the primer pairs listed in table 2-12 and 2-18. DENV1 and 2 GFP-NS5 constructs (mentioned above) were used as templates for PCR. The PCR products were digested and cloned in pEGFP-C1 vector as described above.

Table 2-18: Primers used to clone DENV1 and 2 NS5 proteins that were C-terminal truncated into pEGFP-C1 vector (together with those primers listed in Table 2-12). The residue numbers in construct name indicate the region on DENV1 and 2 NS5 that were being cloned. FP indicates forward primer; RP indicates reverse primer; **CCCGGG** indicates *Xma*I site.

Construct name	Primer name	Sequence
D1 1-882	D1_882_RP	CTAGATCCGGTGGAT**CCCGGG**TCAGTAATCTAGATAATTCTCATTCC CAATTAG
D2 1-882	D2_882_RP	CTAGATCCGGTGGAT**CCCGGG**CTAGTAGTCTGTGTATTCCTCATTGCC
D2 1-888	D2_888_RP	CTAGATCCGGTGGAT**CCCGGG**CTATCTTTTCATGGATGGCATGTAGT C
D2 1-891	D2_891_RP	CTAGATCCGGTGGAT**CCCGGG**CTATCTTCTAAATCTTTTCATGGATGG CATG

2.6.2.4 Generation of 2×GFP construct

GFP gene was amplified by PCR from pEGFP-C1 plasmid with the following primer pair (forward: 5'-GTACAAG**TCCGGA**ATGGTGAGCAAGGGCGAGGAGC-3' and reverse: 5'- CGCCGC**CTCGAG**CCTTGTACAGCTCGTCCATGCCGAG-3'). The underlined sequences correspond to *Bsp*EI and *Xho*I, respectively. The PCR product was digested with *Bsp*EI and *Xho*I and cloned into pre-cut pEGFP-C1 vector.

2.6.2.5 DENV1-4 2×GFP-NS5 constructs

DENV1-4 NS5 gene fragments that corresponded to the indicated NS5 gene segment (denote by the residue numbers in construct name) were amplified from the respective DENV1-4 GFP-NS5 constructs with the primer pairs listed in Table 2-19. The PCR products were digested and cloned in 2×GFP vector as described above. $SV40_{NLS}$ gene fragment (sequence) was also cloned into 2×GFP vector to serve as a positive control for monopartite NLS.

Table 2-19: Primers used to clone DENV1-4 NS5 gene fragments into 2×GFP vector. The residue numbers in construct name indicate the region on DENV1-4 NS5 that were being cloned. FP indicates forward primer; RP indicates reverse primer. **CTCGAG** in FP indicates *Xho*I site; **CCCGGG** in RP indicates *Xma*I site in RP; ~~**GCGGCGGC**~~ indicates extra nucleotide added for in-frame cloning and with the addition of three glycine residues.

Construct name	Primer name	Sequence
$D2_{320-405}$	D2NS5_320_FP	TCAGAT**CTCGAG**~~**GCGGCGGC**~~CATGGTGAACGGAGTGGTTAG
	D2NS5_405_RP	GTGGAT**CCCGGG**CTAGCTTCTCACCTTTCTTGTGAATTC
$D2_{320-367}$	D2NS5_320_FP	TCAGAT**CTCGAG**~~**GCGGCGGC**~~CATGGTGAACGGAGTGGTTAG
	D2NS5_367_RP	GTGGAT**CCCGGG**CTATTTCGGTTCTTGGGTTCTCG
$D2_{368-405}$	D2NS5_368_FP	TCAGAT**CTCGAG**~~**GCGGCGGC**~~GAAGGCACGAAAAAGCTAATG
	D2NS5_405_RP	GTGGAT**CCCGGG**CTAGCTTCTCACCTTTCTTGTGAATTC
$D2_{368-389}$	D2NS5_368_FP	TCAGAT**CTCGAG**~~**GCGGCGGC**~~CGAAGGCACGAAAAAGCTAATG
	D2NS5_389_RP	GTGGAT**CCCGGG**CTACTTTTTCTTTCCTAGTTCTTTCC
$D2_{387-405}$	D2NS5_387_FP	TCAGAT**CTCGAG**~~**GCGGCGGC**~~CAAGAAAAAGACACCTAGGATGTGC
	D2NS5_405_RP	GTGGAT**CCCGGG**CTAGCTTCTCACCTTTCTTGTGAATTC
$D2_{883-900}$	D2NS5_883_FP	TCAGAT**CTCGAG**~~**GCGGCGGC**~~CATGCCATCCATGAAAAGATTTAG
	D2NS5_900_RP	GTGGAT**CCCGGG**CTACCACAAGACTCCTGCCTC
$D1_{883-900}$	D1NS5_883_FP	TCAGAT**CTCGAG**~~**GCGGCGGC**~~CATGACATCAATGAAGAGATTCAAGAACG
	D1NS5_900_RP	CTAGATCCGGTGGAT**CCCGGG**TCACCAGAGTGCCCCTTCGGG
$D3_{883-900}$	D3NS5_883_FP	TCAGAT**CTCGAG**~~**GCGGCGGC**~~CATGAAGAGATTCAGGAAGGAAGAGG
	D3NS5_900_RP	CTAGATCCGGTGGAT**CCCGGG**TTACCAAATGGCTCCCTCCAAC
$D4_{883-900}$	D4NS5_883_FP	TCAGAT**CTCGAG**~~**GCGGCGGC**~~CATGCCAGTCATGAAAAGATACAGC
	D4NS5_900_RP	CTAGATCCGGTGGAT**CCCGGG**TTACAGAACTCCTTCACTTTCGG
$SV40_{NLS}$	SV40_NLS_FP	TCAGAT**CTCGAG**~~**GCGGCGGC**~~CCCAAAAAAGAAGAGAAAGG
	SV40_NLS_RP	GTGGAT**CCCGGG**CTATACCTTTCTCTTCTTTTTTGGGCC

All plasmids produced in the study were verified by sequencing (First Base, Singapore) before use.

2.6.3 Site-directed mutagenesis

2.6.3.1 DENV2 GFP-NS5 with α/β and C-terminal NLS mutation constructs

Mammalian GFP plasmid encoding DENV2 NS5 (mentioned above) was subjected to SDM with the primer pairs listed in Table 2-21 to generate alanine mutation at residue 371-372, 387-389, 887-888 and 890-891. SDM was performed according to the manufacturer's instructions.

Table 2-21: Primers used for SDM of DENV2 pEGFP-C1 GFP-NS5 plasmid. FP indicates forward primer; RP indicates reverse primer.

Construct name	Site of mutation	Sequence
D2 α/β NLS A2	Residues 387-389, KKK→AAA	FP: GAACCGAAAGAAGGCACGGCAGCGCTAATGAAAATCACGGCAG
		RP: CTGCCGTGATTTTCATTAGCGCTGCCGTGCCTTCTTTCGGTTC
D2 α/β NLS A1+2	Residues 371-372 and 387-389, KK→AA and KKK→AAA	FP: CTGGAAAGAACTAGGAGCGGCAGCGACACCTAGGATGTGCACC
		RP: GGTGCACATCCTAGGTGTCGCTGCCGCTCCTAGTTCTTTCCAG
D2 C-term NLS A1	Residues 887-888, KR→AA	FP: ACTACATGCCATCCATGGCAGCATTTAGAAGAGAAGAGG
		RP: CCTCTTCTCTTCTAAATGCTGCCATGGATGGCATGTAGT
D2 C-term NLS A2	Residues 890-891, RR→AA	FP: TCCATGAAAAGATTTGCAGCAGAAGAGGAAGAGGCA
		RP: TGCCTCTTCCTCTTCTGCTGCAAATCTTTTCATGGA
D2 C-term NLS A1+A2	Residues 887-888 and 890-901, KR→AA and RR→AA	FP: TACATGCCATCCATGGCAGCATTTGCAGCAGAAGAGGAAGAGGCA
		RP: TGCCTCTTCCTCTTCTGCTGCAAATGCTGCCATGGATGGCATGTA

All mutations were verified by sequencing (First Base, Singapore) before use.

2.6.3.2 DENV2 cDNA with C-terminal NLS mutation in NS5 gene

Subclone pWSK29 fragment 3 (see section 2.2.4.1) was subjected to SDM with the primer pairs listed in Table 2-21 to generate alanine mutation at residue 887-888 and 890-891. SDM was performed according to the manufacturer's instructions. Mutation in fragment 3 clone was confirmed by sequencing and was excised from the vector by *Xba*I and *Sac*I and cloned into subclone pWSK29 D2 fragment 1+2 that were similarly cut with *Xba*I and *Sac*I.

Chapter 3: Results

3.1 Fine mapping the interaction region between NS3 and NS5 and investigating its impact on virus replication

3.1.1 NS3 and NS5 interact *in vivo* and *in vitro*

NS3 and NS5 were previously reported to interact in DENV2 infected cells via co-IP (Kapoor *et al.*, 1995). To demonstrate that NS3 and NS5 can also interact in DENV1 infected cells, we used our in-house cross-reactive human anti-NS3 (3F7 and 3F8) (Moreland *et al.*, 2012) and NS5 (5R3) (Zhao *et al.*, 2014) IgG antibodies for co-IP experiment. We first infected Huh-7 cells with either DENV1 or 2 at MOI = 10 and lysed the cells at 24 hours post-infection to obtain the supernatant for co-IP with antibodies mentioned above. The elutants from co-IP were subjected to western blot analysis with anti-NS3 (3F8) (Moreland *et al.*, 2012) and anti-NS5 (5M1) (Zhao *et al.*, 2014) antibodies to check for presence of NS3 and NS5 proteins.

When IP was performed with anti-NS5 5R3, both DENV1 and 2 NS3 and NS5 were detected by anti-NS3 and anti-NS5 in western blot (Figure 3-1). This demonstrated that anti-NS5 5R3 could immunoprecipitate NS3-NS5 complex from both DENV1 and 2 infected cells and this is consistent with previous publication that NS3-NS5 complex could be isolated from infected cells via anti-NS5 (Kapoor *et al.*, 1995). However, when IP was carried out with anti-NS3 3F7 and 3F8, only DENV1 and 2 NS3 were detected by western blot. This showed that anti-NS3 3F7 and 3F8 could only immunoprecipitate NS3 from both DENV1 and 2 infected cells, suggesting that the interaction between NS3 and NS5 may block the accessibility of NS3 epitope to

anti-NS3 (previously mapped to residues 526-531 of NS3) (Moreland *et al.*, 2010) and it is the free form of NS3 (those that are not interacting with NS5) that was being immunoprecipitated.

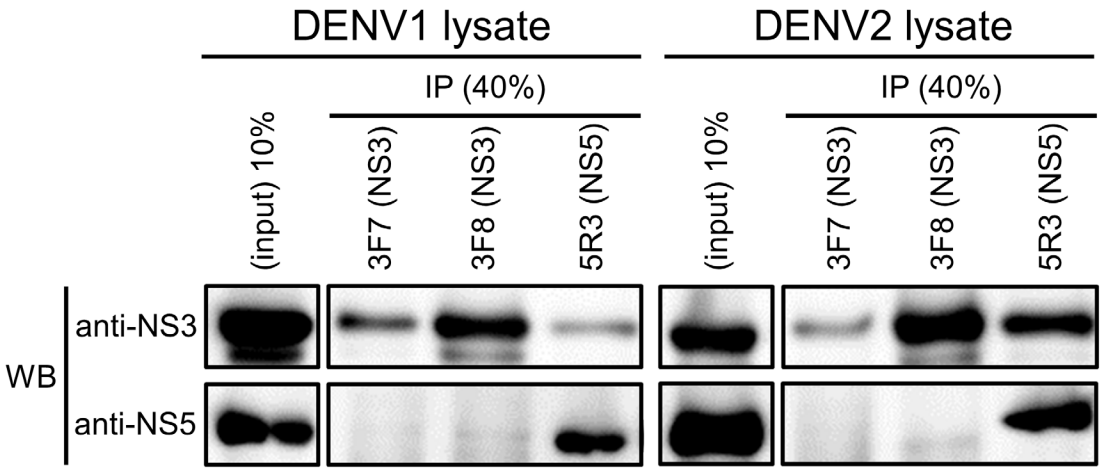

Figure 3-1: Co-IPs with lysates from DENV1 and 2 infected cells show that NS3 and NS5 interact *in vivo*. Cell lysates from DENV1 and 2 Huh-7 infected cells were subjected to immunoprecipitation with anti-NS3 (3F7 and 3F8) and anti-NS5 (5R3) IgGs. 10% of the total lysate were subjected to western blot analysis by anti-NS3 3F8 IgG at 0.2 nM and anti-NS5 5M1 IgG at 25 nM to indicate the amount of input NS3 or NS5 from infected cell lysate. 40% of the elutant from beads with the respective Abs were also subjected to western blot analysis by the same antibodies.

Since NS3 and NS5 can interact *in vivo*, we next asked the question if NS3 and NS5 can interact *in vitro*. To address that, we established an ELISA-based binding assay with NS3 and NS5 recombinant proteins to measure NS3-NS5 interaction *in vitro*. (Figure 3-2A). In-house anti-NS2B 3F10 IgG was used as detection reagent in this ELISA because anti-NS3 3F8 IgG could block NS3 binding to NS5, as shown in Figure 3-1. Furthermore, the binding of 3F10 to NS2B was less likely to block NS3-NS5 interaction as NS2B is located at the opposite end of the elongated $NS2B_{49}$-$_{66}NS3_{FL}$ (residues 49-66 of NS2B fused to NS3 full-length protein, residues 1-618 via glycine flexible linker) protein from the C-terminal region that contains NS5 binding site. In the assay, we coated DENV3 NS5 RdRP (residues 273-900) protein onto

ELISA plate, incubated with increasing concentration of $NS2B_{49-66}NS3_{FL}$ and bound $NS2B_{49-66}NS3_{FL}$ was detected by a fixed concentration of 3F10 IgG (1 nM). To test the specificity of 3F10-NS3-NS5 ELISA, $NS2B_{49-95}NS3_{1-185}$ (residues 49-95 of NS2B fused to NS3 protease domain, residues 1-185 via glycine flexible linker) that only contained NS3 protease domain, which was fused to NS2B, was included as a negative control. As expected, only $NS2B_{49-66}NS3_{FL}$ that contained full-length NS3 protein, but not the protease domain, bound to coated NS5 RdRP in a dose-dependent manner (Figure 3-2B) (Moreland *et al.*, 2012). Collectively, these results demonstrate that NS3-NS5 interaction can occur *in vivo* and *in vitro*.

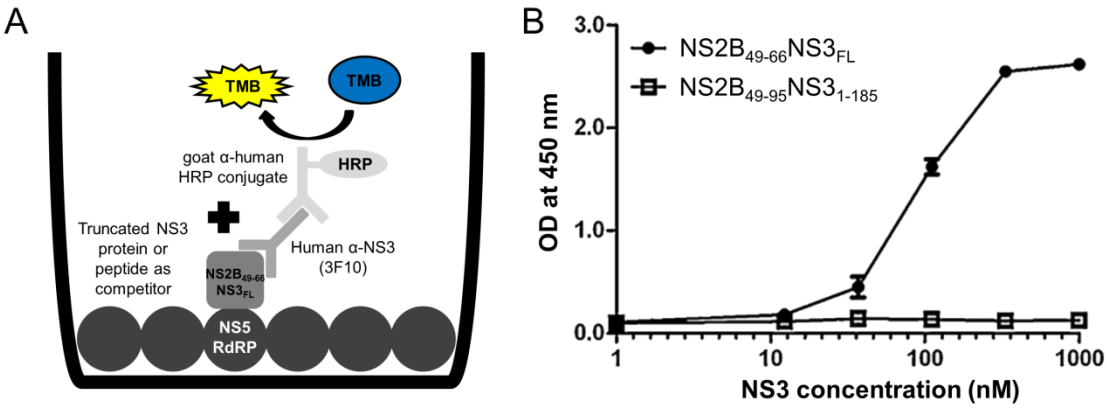

Figure 3-2: Interaction ELISA with recombinant NS3 and NS5 proteins shows that NS3 and NS5 can interact *in vitro*. (A) Illustration of NS3-NS5 interaction ELISA. (B) Typical binding curve of $NS2B_{49-66}NS3_{FL}$ protein (NS3 full-length protein, closed circles) to coated NS5 RdRP protein by interaction ELISA. $NS2B_{49-95}NS3_{1-185}$ (protease domain, open squares) was included as a negative control. Bound NS2B/NS3 proteins were detected by anti-NS2B 3F10 IgG at 1 nM.

3.1.2 $NS3_{566-618}$ interacts with NS5 RdRP

Even though residues 303-618 of DENV2 NS3 helicase domain was previously shown by Y2H study to interact with residues 320-368 (bNLS) of DENV2 NS5 RdRP domain (Brooks *et al.*, 2002; Johansson *et al.*, 2001b), the amino acid residues on NS3 helicase that are involved in binding to NS5 RdRP have not been identified. However based on 3D structure, it was predicted that subdomain III of NS3 helicase, residues 482-618, contained the NS5 binding site (Wu *et al.*, 2005; Xu *et al.*, 2005a). Therefore, in order to prove that the NS5 binding site resides within the NS3 helicase domain, we decided to express a panel of truncated proteins of helicase protein for testing in the NS3-NS5 interaction ELISA that we had developed (Figure 3-2A). NS3 helicase protein has three subdomains, namely I, II and III that are within residues 172-326, 327-481 and 482-618 (residue numbers are based on DENV2 sequence, Figure 3-3A), repsectively, and based on that, we cloned six NS3 gene fragments that spanned different subdomains into either His or GST tagged vector for protein expression. Among these proteins, only $NS3_{172-618}$, GST $NS3_{482-618}$ and GST $NS3_{566-618}$ (labels as red in Figure 3-3A) were expressed and purified to adequate amount for testing in ELISA. Due to (i) protein stickiness, (ii) protein instability or (iii) low protein yield, $NS3_{172-482}$, $NS3_{307-619}$ and GST-$NS3_{172-566}$ (labels as black in Figure 3-3A) could not be purified to sufficient quantity for the competition assay.

Following the purfiication and quantification of proteins, we used $NS3_{172-618}$, GST-$NS3_{482-618}$ and GST-$NS3_{566-618}$ to compete with NS3 full-length protein for binding to NS5 RdRP in competitive NS3-NS5 interaction ELISA. Briefly, these proteins were serially diluted 2-fold starting with a concentration of 20 μM, and added together with 80 nM of NS3 full-length protein to ELISA plate that was coated by NS5 RdRP proteins. NS3 full-length protein that was bound to NS5 RdRP was detected by anti-NS2B 3F10. As indicated in Figure 3-3B, all the three NS3 truncated proteins were able to compete with NS3 full-length protein to bind to coated NS5 RdRP in a dose dependent manner. The apparent K_d for NS3-NS5 interaction for $NS3_{172-618,}$ GST-$NS3_{482-618}$ and GST-$NS3_{566-618}$ were found to be comparable (5.33 ± 0.35 μM, 10.18 ± 0.91 μM and 10.25 ± 1.14 μM (mean ± S.D, n = 3), respectively), and was also similar to the K_d for $NS3_{172-618}$ that was reported previously (Moreland *et al.*, 2012; Zou *et al.*, 2011). Next, we also computed the IC_{50} value for $NS3_{172-618}$ to be 6.07 ± 2.60 μM. The IC_{50} values for GST-$NS3_{482-618}$ and GST-$NS3_{566-618}$ were not computed as we were unable to reach 100% inhibition due to limited amount of truncated protein. Taken together, these data indicate that the NS5 binding site resides within residues 566-618 of NS3 helicase subdomain III.

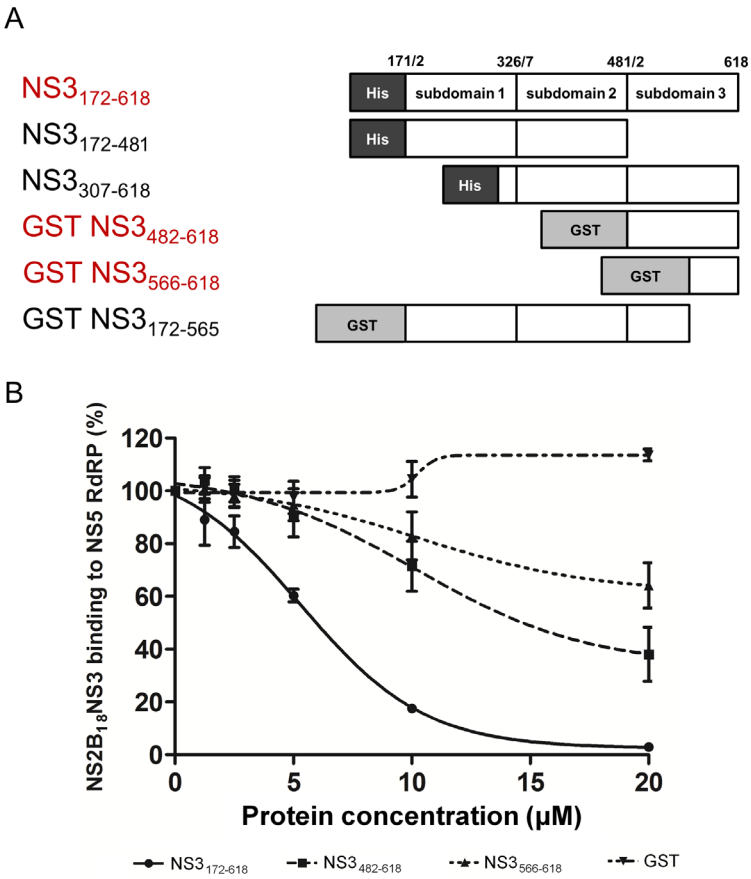

Figure 3-3: Competitive NS3-NS5 interaction ELISA shows that residues 566-618 of NS3 are responsible for binding to NS5 RdRP. (A) Schematic representation of the NS3 constructs that were being made in this study. The residues numbers are shown above each construct. Construct name in red indicates that the protein was expressed and purified for this study. Construct name in black indicates that the protein was not expressed and/or purified for this study. (B) During incubation of $NS2B_{49-66}NS3_{FL}$ protein with coated NS5 RdRP, 2-fold serial dilution of various NS3 proteins (starting from 20 μM) was added in triplicate during competitive ELISA. GST protein was included as negative control. Data are shown as the mean ± SD of triplicates from two independent experiments.

3.1.3 NS3 N570 is critical for NS3-NS5 interaction

To narrow down the NS3 region that interacts with NS5, we went on to screen an array of overlapping 15-mer peptides (Mimotopes) (Moreland *et al.*, 2010; Rivino *et al.*, 2013) that spanned subdomain III of helicase in the same competitive ELISA (Figure 3-4A). We identified two consecutive peptides ($NS3_{566-580}$ and $NS3_{571-585}$) that moderately (p-value = 0.06 and 0.009, respectively) blocked NS3-NS5 interaction, therefore narrowing down the interaction site to residues 566-585. We next tested the

synthetic peptide $NS3_{566-585}$ in competitive ELISA and showed that it could also prevent NS3-NS5 interaction in a dose-dependent manner with an IC_{50} value of 128.8 ± 2.57 μM (Figure 3-4B); the same peptide also inhibited NS3-NS5 interaction when tested in an AlphaScreen-based NS3-NS5 binding assay (Takahashi *et al.*, 2012) (data not shown). To assess the specificity of peptide $NS3_{566-585}$ in blocking the interaction, we also included another peptide, $NS3_{86-100}$ that had similar charge as $NS3_{566-585}$ in the experiment and we could show that this peptide did not compete. This implies that NS3-NS5 interaction involves sequence-specific residues on NS3 protein for interaction.

Sequence alignment of $NS3_{566-585}$ of DENV1-4 and other flaviviruses (Figure 3-4C) suggests that N570 (highlighted in grey) is highly conserved within this region and may be critical for NS3-NS5 interaction. To test this, we synthesized $NS3_{566-585(N570A)}$ peptide and carried out the same competitive ELISA. We found that the replacement of asparagine by alanine at position 570 of NS3 resulted in a null-peptide with respect to its ability to block NS3-NS5 interaction (Figure 3-4B). Next, we expressed and purified both $NS2B_{49-66}NS3_{FL}$ WT and N570A full-length protein to measure their ATPase activity (Luo et al., 2010) (Figure 3-4D) to determine if residue N570 is important for ATPase activity. The ATPase activity of NS3 N570A protein was comparable to $NS2B_{49-66}NS3_{FL}$ WT protein; both proteins also had similar affinity to ATP (K_m = 185.8 ± 10.86 μM and 176.1 ± 8.73 μM for $NS2B_{49-66}NS3_{FL}$ WT and N570A, respectively) and similar turnover numbers (k_{cat} = 3.15 s^{-1} and 3.11 s^{-1} for $NS2B_{49-66}NS3_{FL}$ WT and N570A, respectively). From these results, we concluded that N570 in subdomain III of NS3 helicase appears to be critical for NS3-NS5 interaction, without affecting the *in vitro* ATPase activity.

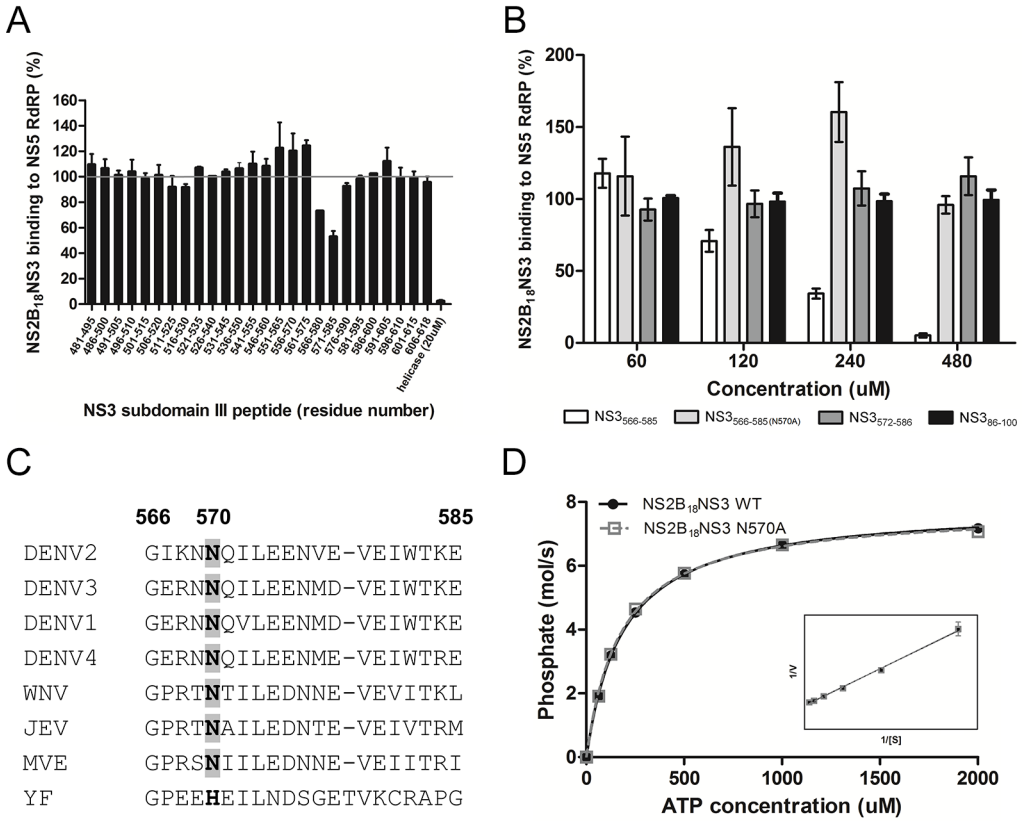

Figure 3-4: *In vitro* functional characterization of NS3 residue N570. An array of overlapping 15-mer peptides that spanned subdomain III of NS3 helicase were tested in competitive ELISA as shown in Figure 3-2A. 20 μM of helicase was included as negative control. Data are shown as the mean ± SD of duplicates from one experiment. (B) 2-fold serial dilution of 20-mer $NS3_{566-585}$ or $NS3_{566-585(N570A)}$ peptide (starting from 480 μM) was tested in the competitive ELISA. $NS3_{86-100,}$ which has similar net charge as $NS3_{566-585}$ and $NS3_{571-585}$ were included as negative controls. Data are shown as the mean ± SD of triplicates from two independent experiments. (C) Sequence alignment of NS3 residues 566-585 of DENV2 with other DENV serotypes and representative members of the Flavivirus genus. NS3 residue N570 that is critical for NS3-NS5 interaction is highlighted in grey and bold. The alignment was performed using ClustalW (Thompson *et al.*, 1994). The virus sequences and their GenBank accession numbers are as follows: DENV2 (AF038403), DENV1 (U88535), DENV3 (M93130), DENV4 (AF326573), Yellow Fever virus (YFV; X15062), Japanese Encephalitis virus (JEV; M55506), Murray Valley Encephalitis virus (MVEV; AF161266) and West Nile virus (WNV; M12294). The numbering of residues is based on DENV2 protein sequence. (D) ATPase assay was carried out with 2.5 nM of $NS2B_{49-66}NS3_{FL}$ WT and N570A proteins, in the presence of increasing concentrations of ATP. The amount of inorganic phosphate released during reaction was detected with Malachite green reagent and the initial rates were calculated (mol of phosphate released per second). The data points were fitted using Michaelis-Menten equation by Prism software (see Materials and Methods).

3.1.4 $NS5_{320-341}$ interacts with NS3 helicase

While we were trying to identify the region on NS3 helicase that contributes to NS3-NS5 interaction, we also tried to narrow down the region on NS5 RdRP that is involved in the interaction. The NS3 binding site on NS5 was shown by Y2H to reside within residues 320-368 (Brooks *et al.*, 2002; Johansson *et al.*, 2001b) and upon sequence inspection of this region within Flavivirus NS5, we identified a 20 amino acid sequence (residues 342-361) that is highly conserved among the Flaviviruses (Figure 3-5A). With this observation in mind, we decided to determine if residues 320-341 or residues 342-368 of NS5 contains the NS3 binding site by two binding assays, namely peptide-phage ELISA and surface plasmon resonance (SPR).

For peptide-phage ELISA, we first cloned DENV3 NS5 gene fragments the encoded $NS5_{320-368}$, $NS5_{320-341}$ or $NS5_{342-368}$ into the genome of M13 phage to make phage that could express NS5 peptide on virus surface. Following that, phages were grown and concentrated to obtain high titre stock ($\geq 10^{11}$ particles/ml). In parallel, we coated the ELISA plated with DENV3 [1] NS3 full-length protein ($NS2B_{49-66}NS3_{FL}$), [2] helicase ($NS3_{172-618}$), [3] helicase subdomain III ($NS3_{482-618}$), [4] protease ($NS2B_{49-95}NS3_{1-185}$; as negative control) and [5] BSA (as negative control) (Figure 3-5B). Next, we diluted the phage and added 5×10^9 phage particles to each coated well. Bound phages were detected by anti-M13 antibody. From the ELISA result, NS3 proteins that contained residues 566-585, namely NS3 full-length protein, helicase and helicase subdomain III, were shown to bind to $NS5_{320-368}$ and $NS5_{320-341}$ peptide-phages but not $NS5_{342-368}$ peptide phage (Figure 3-5C); none of the phages bound to

NS3 protease and BSA. This result supported the ELISA data in Figure 3-3B that the NS5 binding site is indeed found in NS3 helicase subdomain III.

For SPR, we first immobilized either DENV4 NS3 full-length ($NS2B_{49\text{-}66}NS3_{FL}$) or helicase ($NS3_{172\text{-}618}$) (Figure 3-5B) on SPR chip and passed through serially diluted (2-fold) $NS5_{320\text{-}368}$, $NS5_{320\text{-}341}$ or $NS5_{342\text{-}368}$ peptides to measure real-time binding of NS5 peptides to mobilized NS3 proteins; this enables us to compute K_D value for the interaction. $NS5_{320\text{-}368}$ and $NS5_{320\text{-}341}$ (Figure 3-5D), but not $NS5_{320\text{-}341}$ (data not shown), were detected to bind to NS3. After analysis of binding data, we determined the K_D for $NS5_{320\text{-}368}$ and $NS5_{320\text{-}341}$ 10-50 μM and 100-400 μM, respectively. This result was in agreement with the ELISA data that supported the presence of NS3 binding site to be within residues 320-341 of NS5, but not residues 342-368. Taken together, we can conclude that the interaction between NS3 helicase and NS5 RdRP is mediated by residues 566-585 of NS3 and residues 320-341 of NS5.

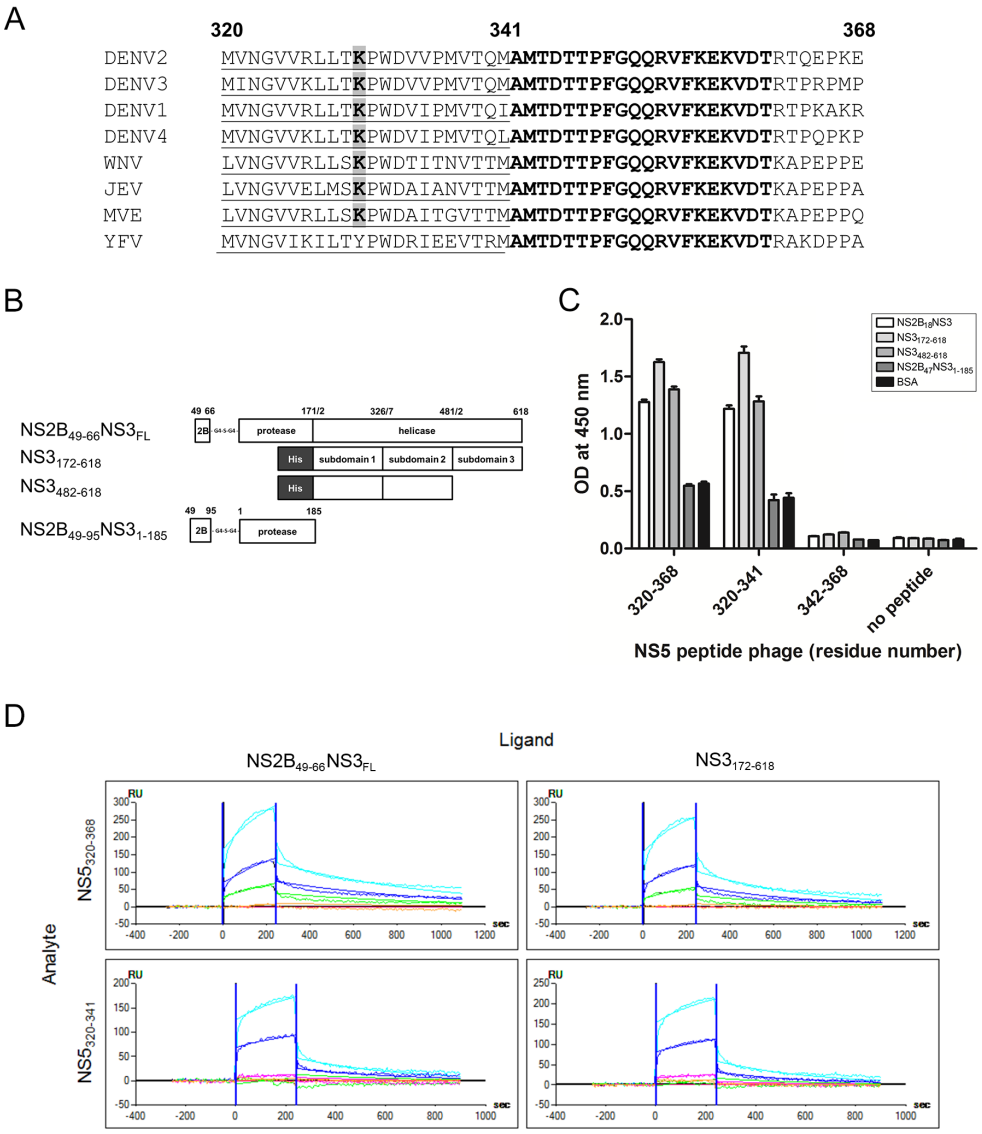

Figure 3-5: Sequence alignment of Flavivirus NS5 residues 320-368, SPR and NS5 peptide-phage ELISA. (A) Sequence alignment of NS5 residues 320-368 (bNLS) of DENV2 with other DENV serotypes and representative members of the Flavivirus genus. The highly conserved 20-amino acid region within bNLS is bold. $NS5_{320-341}$ that was fused to $NS3_{172-618}$ is underlined and K330 that is important in NS3-NS5 interaction is bold and is highlighted in grey (Zou *et al.*, 2011). The alignment was performed using ClustalW (Thompson *et al.*, 1994). The virus sequences and their GenBank accession numbers are as described in Figure 3-4C. (B) Schematic representation of the NS3 constructs that were being used in this study. The residues numbers are shown above each construct. (C) NS3-NS5 interaction data by peptide-phage ELISA. NS5 peptide sequence ($NS5_{320-368}$, $_{320-341}$ and $_{342-368}$) was cloned directly into phage genome, which expressed as fusion peptide to protein III and was displayed on phage surface. NS3 ($NS2B_{49-66}NS3_{FL}$, $NS3_{172-618}$, $NS3_{482-618}$ or $NS2B_{47}NS3_{1-185}$) or BSA (negative control) protein was coated onto ELISA plate and NS5 peptide phage ($NS5_{320-368}$, $NS5_{320-341}$ and $NS5_{342-368}$; 5×10^9/well) was added to coated wells. No peptide/WT phage was included as negative control. Data are shown as the mean ± SD of triplicates from one representative experiment out of two independent studies. (D) NS3-NS5 interaction data by SPR assay. DENV4 NS3 protein ($NS2B_{49-66}NS3_{FL}$ or $NS3_{172-618}$) was mobilized on chip and NS5 biotinylated peptide ($NS5_{320-368}$, $NS5_{320-341}$ and $NS5_{342-368}$) was passed through to measure real-time interaction. The resultant affinity for interaction was calculated using the ratio of k_d/k_a from the SPR assay and was reflected as K_D (equilibrium dissociation constants). Data are shown as the mean ± SD of duplicate from one independent experiment. The experiment in D was done in collaboration with Drs Luo Dahai, Julien Lescar and Susana Geifman-Shochat from NTU.

3.1.5 $NS5_{320-341}$ binds to NS3 helicase in solution

To gain some structural insights on the binding between NS3 and NS5, we made a construct that fused DENV4 NS3 helicase to residues 320-341 of DENV4 NS5 (within bNLS) via a flexible glycine linker (G_4SG_4, $NS3_{172-618}$-$NS5_{320-341}$; Figure 3-6A) for crystallization study. The construct was designed based on the experience with the dengue NS3 protease where the covalent attachment of NS2B cofactor region to NS3 protease domain permitted extensive biochemical and biophysical studies (Erbel *et al.*, 2006; Li *et al.*, 2005; Luo *et al.*, 2008a). Also, we have prior knowledge that NS3 helicase crystallises easily. We managed to crystallize the fusion protein that was made from this construct. However, X-ray diffraction data of the crystal only showed electron density from NS3 helicase but not $NS5_{320-341}$. Therefore, we employed small angle X-ray scattering (SAXS) as an alternative approach to X-ray crystallography, in hope of obtaining a low resolution, 3D molecular envelope of this protein in solution (Svergun *et al.*, 2013). SAXS study was done with highly purified $NS3_{172-618}$ and $NS3_{172-618}$-$NS5_{320-341}$ proteins at three different concentrations, namely 1.2 mg/ml, 2.1 mg/ml and 4 mg/ml for data collection. The data were processed by subtracting the scattering intensities of the buffer from that of the protein to yield the final composite scattering curve (Figure 3-6B and C). Inspection of the Guinier plots at low angles revealed that the protein samples were monodispersed and not aggregated, and the dataset was of good quality (inset of Figure 3-6B and C). $NS3_{172-618}$ has a radius of gyration (R_g, defined as the root mean square average of the distance of the electrons from the center of the particle) of 25.16 ± 0.6 Å and a maximum dimension (D_{max}) of 72.95 Å, while the $NS3_{172-618}$-$NS5_{320-341}$ has a R_g of 25.42 ± 0.6 Å and a D_{max} of 75.64 Å. The distance distribution function curves for both proteins are "bell-shape", indicates that the protein is globular (Figure 3-6D). Comparison of the forward

scattering of both proteins with the values obtained from a reference solution of lysozyme (14.4 kDa) produced a molecular weight of 44.4 kDa for $NS3_{172-618}$ and 47.7 kDa for $NS3_{172-618}$-$NS5_{320-341}$, implying that both proteins are monomeric at all concentrations.

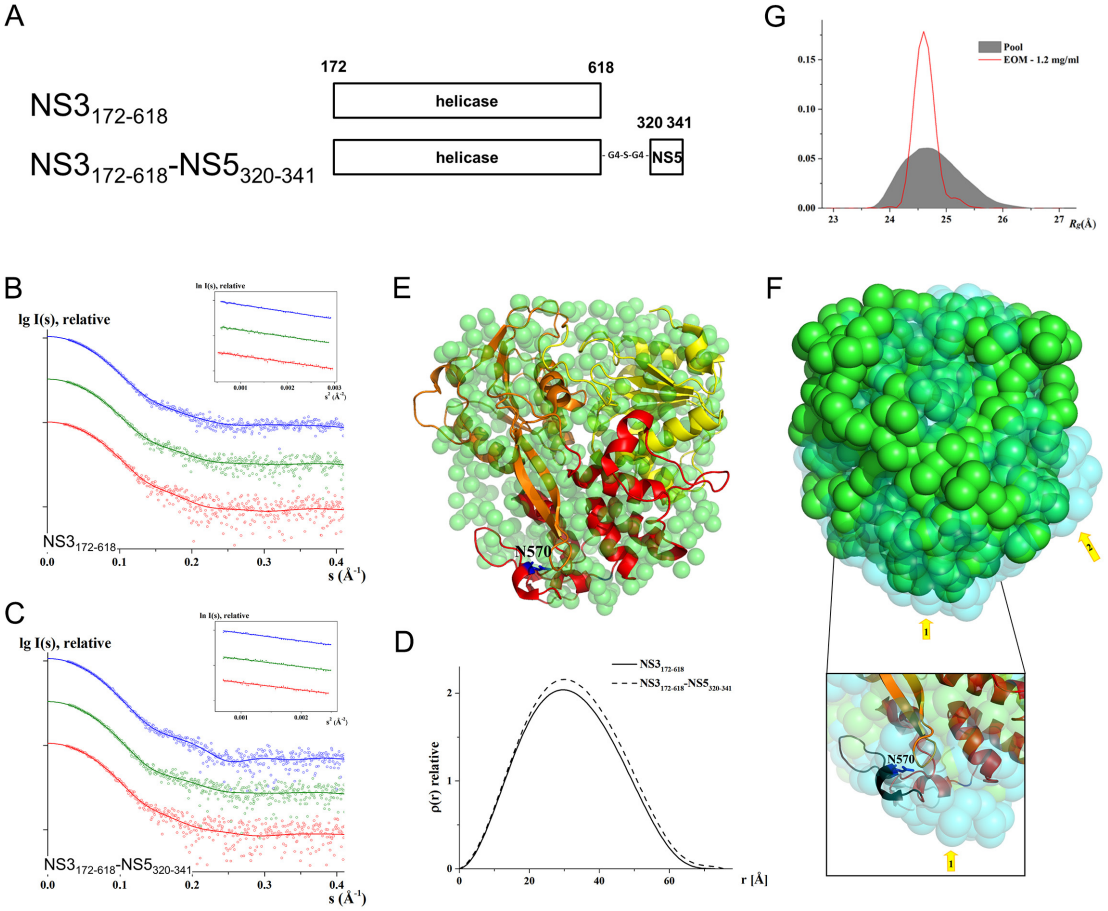

Figure 3-6: SAXS of $NS3_{172-618}$-$NS5_{320-341}$ indicates NS3-NS5 interaction. (A) Schematic representation of recombinant $NS3_{172-618}$ and $NS3_{172-618}$-$NS5_{320-341}$ proteins that were expressed in *E. coli* and used in SAXS study. SAXS scattering pattern (○) and its corresponding experimental fit (—) of (B) $NS3_{172-618}$ and (C) $NS3_{172-618}$-$NS5_{320-341}$ at protein concentrations of 1.2 mg/ml (*red*), 2.1 mg/ml (*olive*) and 4 mg/ml (*blue*). The curves are displayed in logarithmic unit for clarity. The inserts in (B) and (C) show the respective Guinier plots. (D) Distance distribution functions of $NS3_{172-618}$ (—) and $NS3_{172-618}$-$NS5_{320-341}$ (- -). (E) Superimposition of crystallographic structure of $NS3_{172-618}$ (PDB ID: 2JLS (Luo *et al.*, 2008b)) with the determined solution shape of $NS3_{172-618}$ (green). Ribbon representation of subdomain I, II and III of $NS3_{172-618}$ are coloured in yellow, orange and red, respectively. (F) Superimposition of $NS3_{172-618}$ and (*green*) and $NS3_{172-618}$-$NS5_{320-341}$ (*cyan*) solution shapes. The *Rg* of the $NS3_{172-618}$ and $NS3_{172-618}$-$NS5_{320-341}$ were 25.2 Å and 25.4 Å, respectively. The arrows indicate two protrusions: the first protrusion is at the bottom of the $NS3_{172-618}$-$NS5_{320-341}$ solution shape and the second protrusion may be caused by a conformational alteration due to $NS3_{172-618}$-$NS5_{320-341}$ interaction. (G) The EOM *Rg*-distribution of the selected ensemble (*red line*) contains a narrow peak at 24.6 Å, which is slightly smaller than the center *Rg* of random pool (*grey filled area*), 24.8 Å, suggesting $NS3_{172-618}$-$NS5_{320-341}$ is rigid and compact in solution, and peptide $NS5_{320-341}$ is bound to $NS3_{172-618}$. This experiment was done in collaboration with Wuan Geok Saw and Dr Gerhard Grüber from NTU.

The low resolution solution structure of $NS3_{172-618}$ and $NS3_{172-618}$-$NS5_{320-341}$ were restored *ab initio* using program GASBOR (Svergun *et al.*, 2001). The normalized spatial discrepancy (NSD) of ten independent reconstructions of $NS3_{172-618}$ and $NS3_{172-618}$-$NS5_{320-341}$ are 0.95 ± 0.02 Å and 0.99 ± 0.03 Å, respectively. The reconstructions with the least NSD from both proteins were selected, and the obtained solution shapes for both proteins produced a good fit to the experimental data in the entire scattering range. The corresponding fits for $NS3_{172-618}$ and $NS3_{172-618}$-$NS5_{320-341}$ had discrepancies of χ = 1.15 and 1.04, respectively. Both $NS3_{172-618}$ and $NS3_{172-618}$-$NS5_{320-341}$ were globular shapes, with the dimensions of about 59.9 × 54.4 × 34 Å and 65.6 × 57.7 × 36.8 Å, respectively. When the solution form of $NS3_{176-618}$ (*green*) was superimposed with the crystal structure of $NS3_{176-618}$ (PDB ID: 2JLS), it accommodated very well into the solution form of the protein (Figure 3-6E), implying that the solution data is of high quality and the crystal structure is likely to exist in solution. When the solution forms of $NS3_{172-618}$ (*green*) and $NS3_{172-618}$-$NS5_{320-341}$ (*cyan*) were superimposed (Figure 3-6F), two protrusions were observed and were denoted by arrows in Figure 3-6F. Protrusion 1 is at the bottom of $NS3_{172-618}$-$NS5_{320-341}$ solution shape and this leads to a more elongated conformation in $NS3_{172-618}$-$NS5_{320-341}$ than $NS3_{172-618}$, which is also reflected by the increased D_{max} in $NS3_{172-618}$-$NS5_{320-341}$ (75.64 Å) when compared to $NS3_{172-618}$ (72.95 Å) (Figure 3-6D). The protrusion is in close proximity to residue N570 (showed as *blue stick representation* in the inset of Figure 3-6F) and to the peptide $NS3_{566-585}$ that was used in ELISA (showed as *black cartoon representation* in the inset of Figure 3-6F). Protrusion 2 of $NS3_{172-618}$-$NS5_{320-341}$ may occur due to a conformational alteration that was induced by $NS3_{172-618}$ and $NS5_{320-341}$ interaction. Taken together, these results appear to be

consistent with the ELISA data and suggest a physical interaction between $NS3_{172-618}$ and $NS5_{320-341}$ in solution.

To eliminate the possibility that $NS5_{320-341}$ may be flexible in solution, the scattering dataset of $NS3_{172-618}$-$NS5_{320-341}$ were further analyzed by EOM (Bernado *et al.*, 2007; Petoukhov *et al.*, 2012) to assess the flexibility and compactness of $NS3_{172-618}$-$NS5_{320-341}$ in solution (Figure 3-6G). Based on the width and position of the selected ensemble peak relative to random pool in *Rg*-distribution, the flexibility and compactness of the protein in solution can be determined. With respect to $NS3_{172-618}$-$NS5_{320-341}$, the *Rg*-distribution of the ensemble contained a narrow peak, indicating that $NS3_{172-618}$-$NS5_{320-341}$ is rigid in solution. This peak is centered at 24.6 Å, which is slightly smaller than the center *Rg* of a random pool, 24.8 Å, suggesting that $NS3_{172-618}$-$NS5_{320-341}$ is compact in solution. The EOM data demonstrate that peptide $NS5_{320-341}$ is bound to $NS3_{172-618}$.

3.1.6 NS3:N570A mutant has reduced infectious virus production and viral protein synthesis

To study the impact of NS3:N570A mutation on NS3-NS5 interaction during the virus life cycle, we first characterized DENV2 cDNA infectious clone (Figure 3-7A, a kind gift from Assoc Prof Eng Eong Ooi (Duke-NUS Graduate Medical School)) in term of its ability to produce viral protein and infectious virus. Following the transfection of *in vitro* transcribed DENV2 RNA into BHK-21 cells, IFA of BHK-21 cells showed increasing number of E-positive cells from day 1 to 3 post-transfection, with ~50-60% of cells being E-positive on day 3 (Figure 3-7B). Plaque assay with supernatant showed an increase in infectious virus particle production from day 1 to 3, peaking at 1×10^5 pfu/ml on day 3 (Figure 3-7C). The size of plaque on BHK-21 cells that was produced by the supernatant of BHK-21 transfected cells was comparable to those produced by the supernatant of C6/36 transfected cells (left and right inset of Figure 3-7C, respectively). These results indicate that the RNA transcribed from DENV2 cDNA clone is infectious and that infectious virus particle can be produced in both BHK-21 mammalian cells and C6/36 mosquito cells.

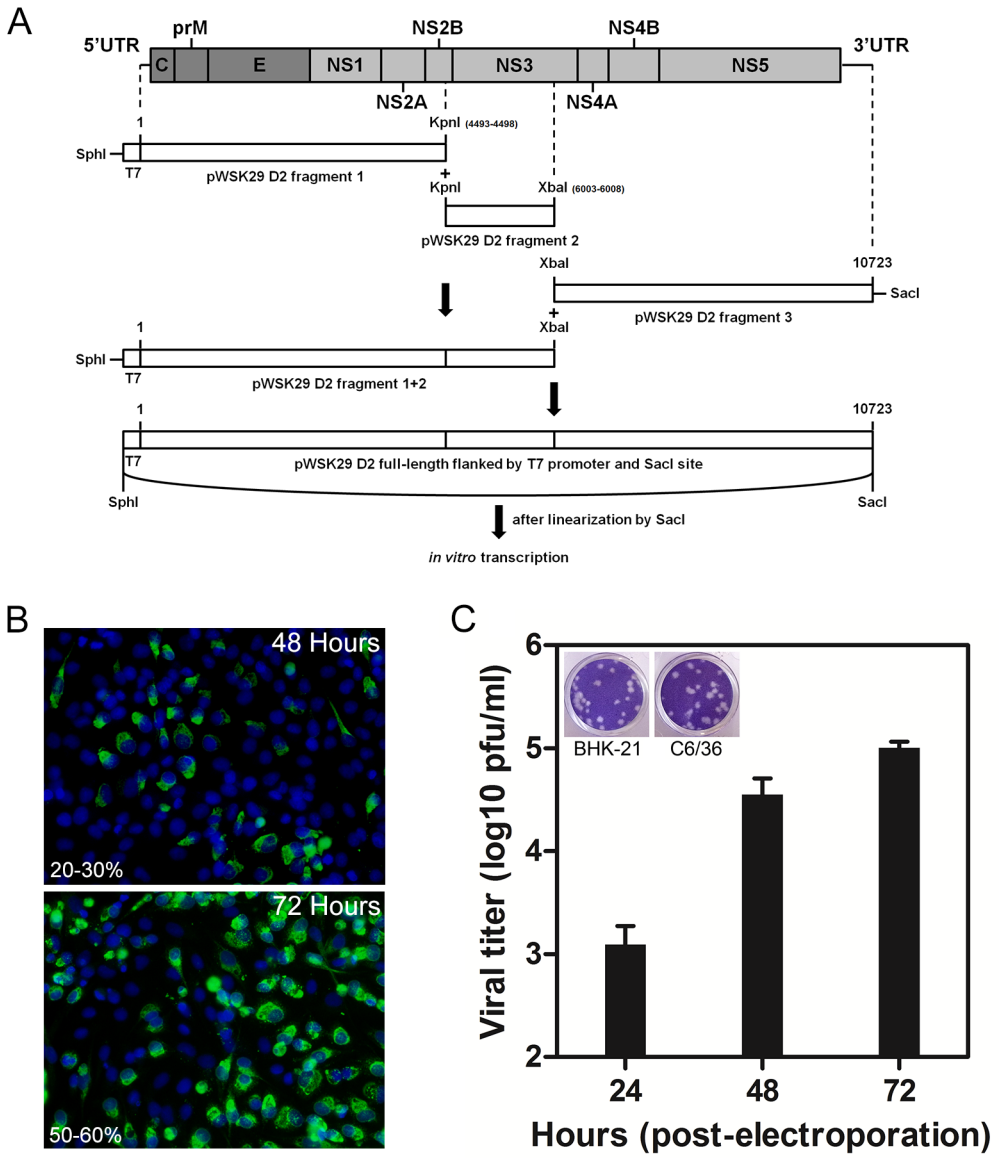

Figure 3-7: Characterization of DENV2 cDNA infectious clone. (A) Schematic representation of full-length DENV2 cDNA clone. The DENV2 genome (represented approximately to scale) contains a single open reading frame that encodes three structural proteins (C, prM and E) and seven NS proteins (NS1, NS2A, NS2B, NS3, NS4A, NS4B and NS5). The cDNA clone was subdivided into three fragments based on unique restriction sites that are present within the genome to facilitate the assembly of full-length clone. The complete DENV2 clone has T7 promoter at 5' end for *in vitro* transcription and *Sac*I site at 3' end for linearization of plasmid. (B and C) BHK-21 cells were electroporated with 10 µg of *in vitro* transcribed DENV2 RNA and samples were harvested daily, for 3 days. (B) Infected cells were analysed by IFA with mouse anti-E 4G2 antibody on 48 and 72 hours post-transfection for presence of E protein and percentage infection was determined. (C) Culture supernatants were used for plaque assay on BHK-21 cells to determine viral titer. The size of plaque on BHK-21 cells that was derived from the supernatant of either BHK-21 (left inset) or C6/36 (right inset) cells, which was transfected with DENV2 WT RNA was shown. This experiment was performed in collaboration with Kitti Chan from Duke-NUS Graduate Medical School.

After determining the growth kinetics of DENV2 WT virus that was derived from cDNA clone, DENV2 NS3:N570A cDNA mutant clone was constructed by SDM and its phenotype in viral protein synthesis and infectious virus production was examined over the course of 5-day post transfection. We also constructed DENV2 NS5:K330A mutant clone (Zou *et al.*, 2011), a known NS3-NS5 interaction defective mutant that failed to replicate by reverse genetics studies for bench-marking our studies. Similar to NS5:K330A mutant, no infectious virus particle was recovered from NS3:N570A mutant even when neat supernatant was used for titering (Figure 3-8B*)*. In agreement with the absence of infectious virus, extracellular viral RNA level for both mutants were at the limit of detection of viral RNA by real-time RT-PCR and did not change over the course of 5-day, suggesting that both mutants are inviable (Figure 3-8A). The viral RNA detection for WT increased over 72 hours when it reached maximal detection that stabilized until 120 hours. Next, to determine if polyprotein synthesis from the transfected RNA is occurring and that the lack of infectious virus may be due to absence of packaging and/or release of infectious virion, we checked the level of NS3 protein of transfected cells by both western blot and IFA. Surprisingly, for the cells that were transfected with NS3:N570A mutant transcript, we could detect NS3 protein with anti-NS3 3F8 IgG (Moreland *et al.*, 2012) in 24 and 48 hours samples (Figure 3-8C, red arrows) but not in 72 hour sample. The highest percentage of NS3-positive cells (5-10%) was observed at 48 hours post-transfection, which reduced to ≤ 5% of NS3-positive cells at 72 hours post-transfection (Figure 3-8D), and finally to an undetectable level at 96 and 120 hours post-transfection (data not shown). On the contrary, for NS5:K330A mutant, NS3 protein was almost undetectable by both western blot and IFA (≤ 1% of NS3-positive cells) at all time points post-transfection (Figure 3-8C and D). Taken together, the results imply that reduced NS3-NS5

interaction in NS3:N570A mutant reduces viral protein synthesis and infectious virus production.

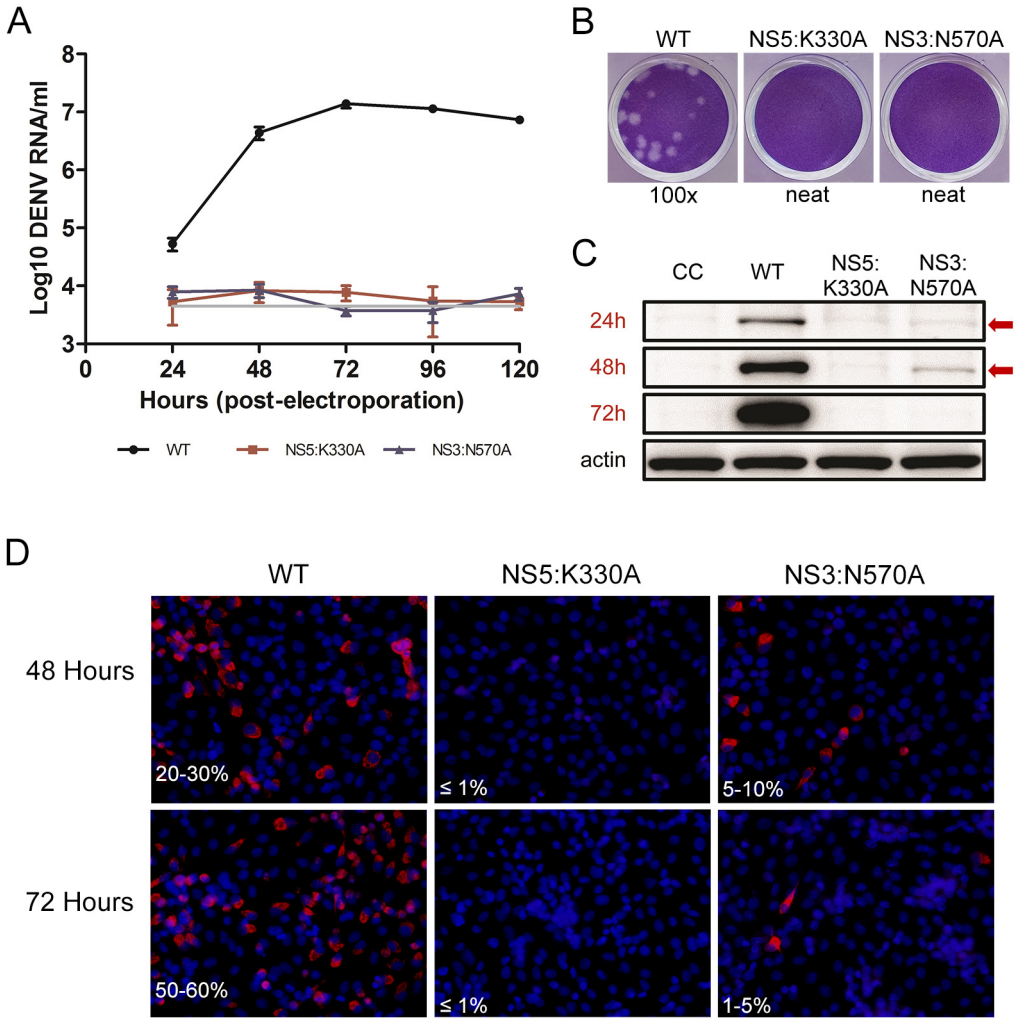

Figure 3-8: Growth kinetics of BHK-21 cells that were transfected with DENV2 WT, NS5:K330A or NS3:N570A RNAs were monitored over the course of 5-day. (A-C) BHK-21 cells were electroporated with 10 µg of WT and mutant (NS3:N570A and NS5:K330A as control) *in vitro* RNA transcripts and samples were harvested daily, for 5 days. Supernatants were used to (A) determine absolute copy numbers of extracellular viral RNA by real-time RT-PCR and to (B) check for plaque production on BHK-21 cells. Absolute copy numbers of viral RNA in log scale per ml of supernatant used for real-time RT-PCR were plotted; data are shown as the mean ± SD of duplicate from two independent experiments. The grey line indicates the detection limit of assay. (C) Western blot and (D) IFA against NS3 protein were performed with anti-NS3 3F8 IgG (Moreland *et al.*, 2012), and one representative experiment out of two independent studies was shown. This experiment was performed in collaboration with Kitti Chan from Duke-NUS Graduate Medical School.

3.1.7 NS3:N570A mutant has a defect in RNA replication

The reduction in viral protein synthesis for NS3:N570A mutant and lack of detectable infectious plaques suggests that attenuated RNA replication could occur at an early time point for this mutant. Hence, we examined the RNA replication kinetics by real-time RT-PCR and IFA for detection of dsRNA. The results showed that intracellular viral RNA can be detected for NS3:N570A and WT but intriguingly, not for NS5:K330A transfected cells (Figure 3-9A and B). The viral RNA copy number for WT increased from ~10^6 copies/μg at 6 hours post-transfection to 10^9 copies/μg at 120 hours, as detected by real-time RT-PCR. Although less than WT, a 10-fold increase in intracellular viral RNA copy number was observed from 24 to 48 hours post-transfection (p-value = 0.008) for NS3:N570A mutant and thereafter, the level declined till 120 hours. The viral RNA copy number for NS5:K330A mutant decreased from 6 to 48 hours post-transfection and remained relatively stable from 48 to 120 hours, implying that there was no active viral RNA replication and only the input RNA that was transfected by electroporation was being detected. Interestingly, the detection of peak intracellular RNA level for NS3:N570A mutant on at 48 hours correlated with the highest level of NS3 protein detected by western blotting (Figure 3-8C). Collectively, this result clearly shows that NS3:N570A mutant is defective in RNA replication.

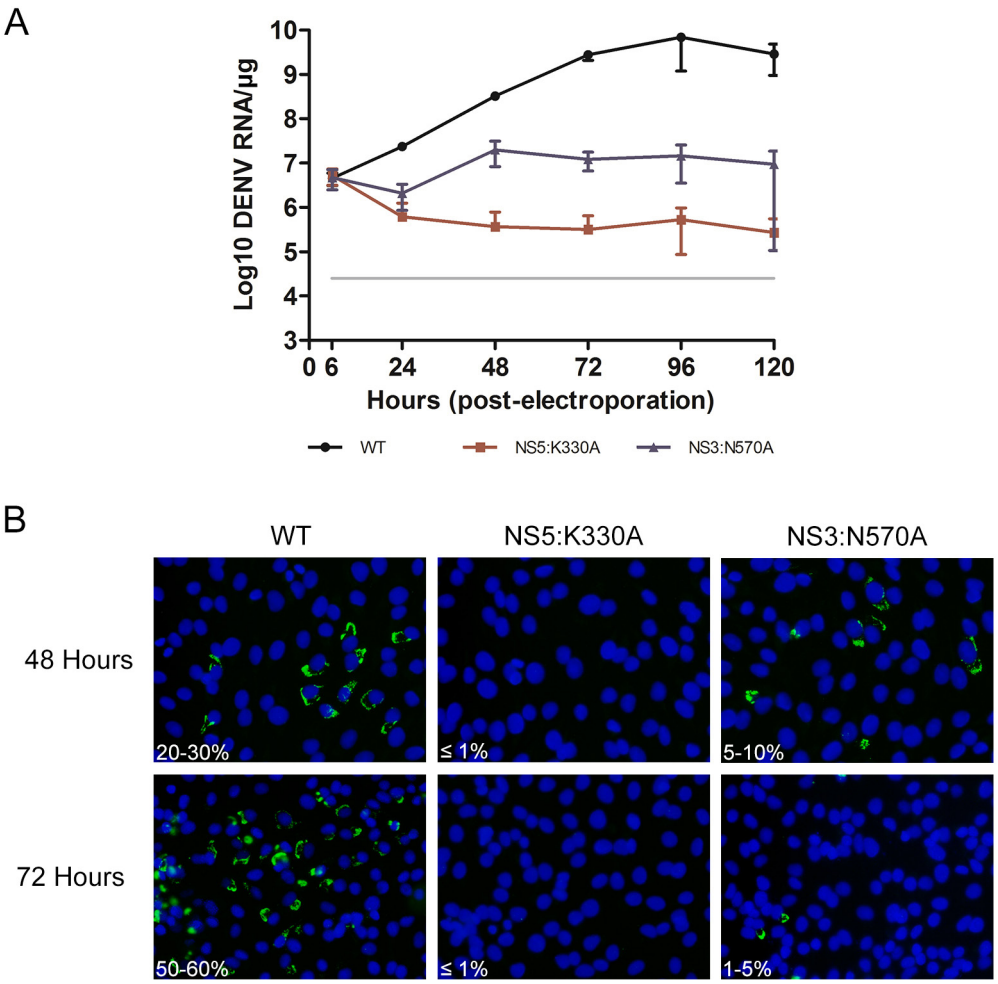

Figure 3-9: RNA replication kinetics of BHK-21 cells that were transfected with DENV2 WT, NS5:K330A or NS3:N570A RNAs were monitored over the course of 5-day. (A-B) Same experiment setup was performed as mentioned in Figure 3-8. (A) RNA was extracted from infected cells and absolute copy numbers of intracellular viral RNA were determined by real-time RT-PCR. (B) Infected cells were analysed by IFA for presence of dsRNA with mouse anti-dsRNA antibody on 48 and 72 hours post-transfection and percentage infection was determined. Data from one independent experiment are shown and it is a separate experiment from Fig 3-7B and 3-8D. The grey line in (A) indicates the amount of residual negative-strand from transfected RNA. This experiment was performed in collaboration with Kitti Chan from Duke-NUS Graduate Medical School.

3.1.8 Validation of strand-specific quantitative RT-PCR assay

To examine the dynamics of RNA synthesis of WT and both mutants further, we developed real-time RT-PCR assay that can accurately measure the level of intracellular negative- and positive-strand viral RNA with strand-specific tagged primers (Lim *et al.*, 2013a) (Lanford *et al.*, 1994). We adopted this approach because the phenomenon of self-priming by reverse transcriptase (RT) prevents accurate strand-specific detection as RT can initiate cDNA synthesis from the 3' end of RNA template in the absence of any primer (also known as endogenous priming) (Lanford *et al.*, 1995) and such cDNA product can contribute to significant amount of PCR product during RT-PCR assay (Tuiskunen *et al.*, 2010). However, the fusion of tag sequence to template complementary primer has been reported to prevent the amplification of self-primed cDNA during RT-PCR (Lanford *et al.*, 1994). In our study, the tag sequence (sequence not found in DENV genome, coloured in orange in Figure 3-10) that was described by (Plaskon *et al.*, 2009) was fused to the sequence that binds to DENV E gene (coloured in red in Figure 3-10) (Johnson *et al.*, 2005) to create a primer that can bind to either negative- or positive-strand during the cDNA synthesis step to generate cDNA strand of reverse polarity by exogenous priming (Figure 3-10) (Note: cDNA was also generated in the same reaction mix by endogenous priming). We chose to use primer pair directed against the E gene for fusion to tag sequence because we are familiar with this primer pair (Low *et al.*, 2014) and we wanted to avoid detecting sfRNA that is located at 3'UTR region (Pijlman *et al.*, 2008). Following cDNA synthesis, the reaction mix was used for strand-specific quantitative RT-PCR assay, where the tag and E specific primers were used to distinguish exogenous primed cDNAs that were transcribed from either negative- or positive-strand template from self-primed (endogenous primed) cDNAs (Tuiskunen *et*

al., 2010); the absolute viral RNA copy numbers were then determined by comparing the Ct values of samples to the Ct values from a standard curve made with dilutions of cDNA.

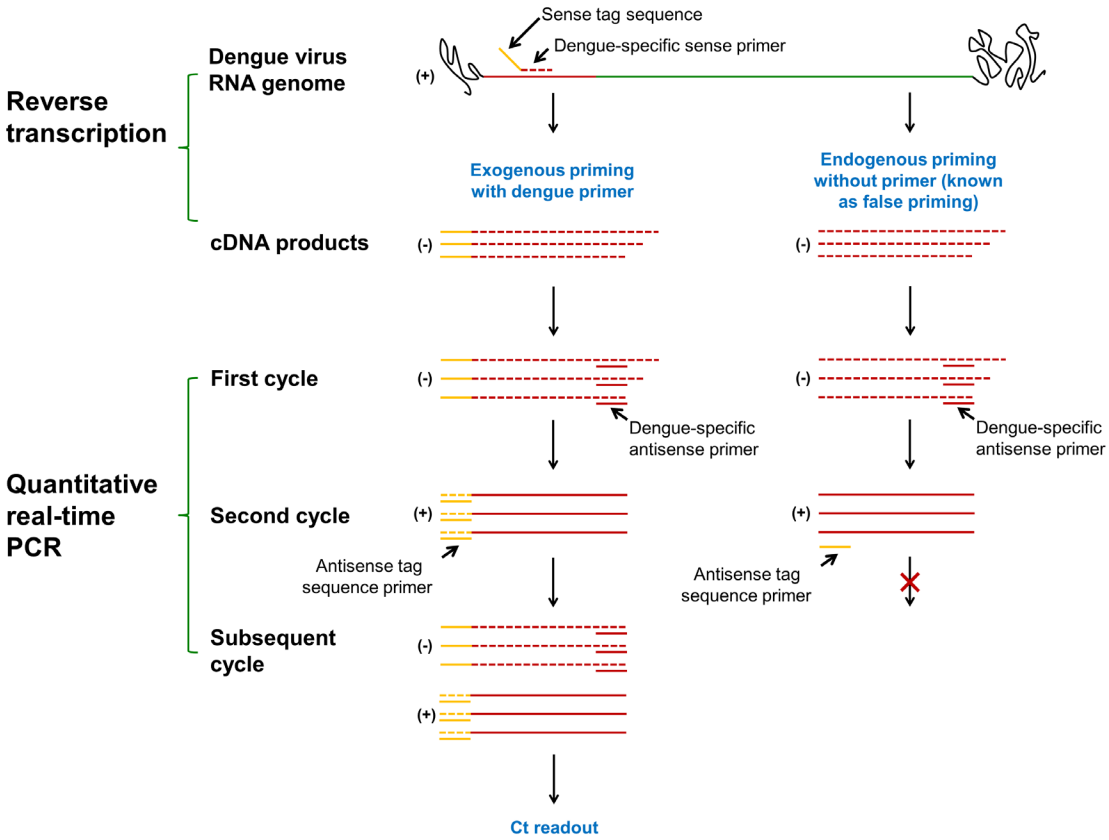

Figure 3-10: Schematic representation of strand-specific quantitative RT-PCR assay. Only the positive-strand detection is depicted here; the reverse also applies to negative-strand detection. During cDNA synthesis, dengue-specific sense primer that is fused to sense tag sequence (sequence not found in DENV genome) is used by RT to synthesize cDNA strand from template strand by exogenous priming. However, cDNA strand can also be synthesized by RT from template strand, in the absence of dengue-specific primer by endogenous priming. During RT-PCR, in the first cycle, both exogenous and endogenous primed cDNA products are used by Taq polymerase as template for amplification by dengue-specific anti-sense primer. However, in the second cycle, only the complementary strand from exogenous primed cDNA product can bind to antisense tag sequence primer for amplification whereas the complementary strand from endogenous primed cDNA product cannot bind to antisense tag sequence primer because it lacks the sense tag sequence. Therefore, exogenous primed cDNA product continues to contribute more PCR products that eventually gives a Ct value as readout.

We first evaluated the specificity of assay using tag and E primers with synthetic negative- and positive-strand cDNA transcripts. Both negative- and positive-strand specific primers were used to detect negative-strand (Figure 3-11A) and positive-strand (Figure 3-11B) cDNA standards that were serially diluted 10-fold, starting from 10^8 to 10^3 copies per reaction. As shown in Figure 3-11A and B, both negative- and positive-strand specific primers are highly specific because at 10^8 copies of negative-strand standard, negative-strand specific primer gave a Ct value of 6.96 whereas positive-strand specific primer gave a Ct value of 34.36 (difference of 27.4) and no Ct values were obtained for lower dilution. In agreement with that, at 10^8 copies of positive-strand standard, negative-strand specific primer gave a Ct value of 32.76 whereas positive-strand specific primer gave a Ct value of 8.33 (difference of 24.43) and no Ct values were obtained for lower dilution. This indicates that the primers are highly specific to its complementary template.

Next, we determined the sensitivity and reproducibility of the assay by mixing negative- and positive-strand cDNA standard with the opposite strand at various ratios or with the addition of BHK-21 cDNA to detect specific-strand with respective primers. Negative-strand standards that were serially diluted 10-fold (starting from 10^7 to 10^2 copies) were mixed with 10^7 copies of positive-strand standard (Figure 3-11C) or 40 ng of BHK-21 cDNA (Figure 3-11E). As shown in Figure 3-11C and E, the negative-strand detection assay was highly reproducible within the range of 10^3-10^7 dilution even when it was mixed with 10^7 copies of positive-strand standard or 40 ng of BHK-21 cDNA; therefore, we determined the minimum detection level for negative-strand to be 10^3 copies. The reverse experiment was also performed, where positive-strand standards that were serially diluted 10-fold (starting from 10^7 to 10^2

copies) were mixed with 10^7 copies of negative-strand standard (Figure 3-11D) or 40 ng of BHK-21 cDNA (Figure 3-11F). As shown in Figure 3-11D and F, the positive-strand detection assay was also highly reproducible within the range of 10^2-10^7 dilution even when it was mixed with 10^7 copies of negative-strand standard or 40 ng of BHK-21 cDNA; the minimum detection level for positive-strand was determined to be 10^2 copies and it was one log lower than the minimum detection limit for negative-strand. Taken together, the results suggest that the presence of opposite-sense cDNA transcript or cellular cDNA does not inhibit the accurate quantification of negative- and positive-strand of DENV.

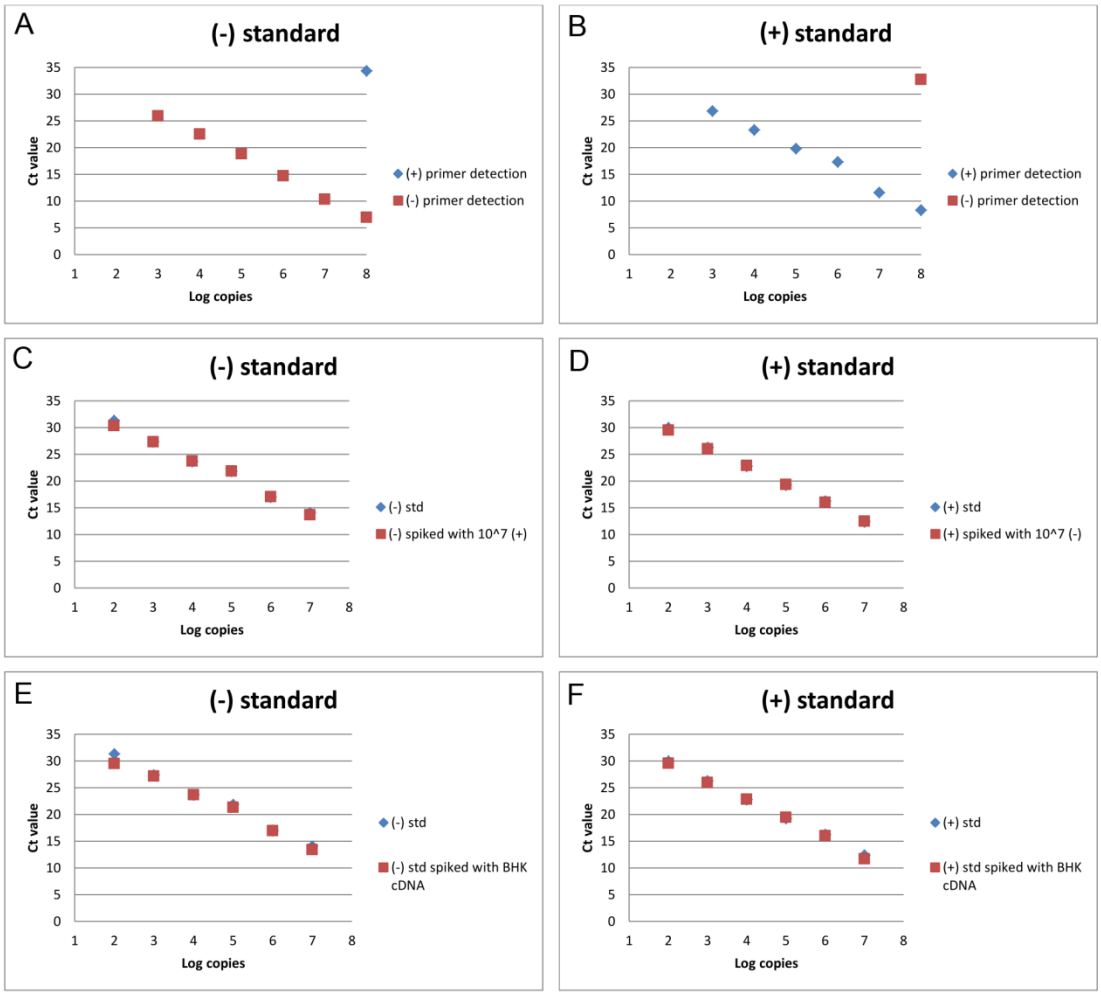

Figure 3-11: Validation of strand-specific quantitative RT-PCR assay. The strand-specific RT was carried out with a standard curve of 10^8 copies of negative- and positive-strand standards that were serially diluted 10-fold up to 10^2 copies. The log of the RNA copies is plotted against the cycle threshold (Ct). Data points are plotted for those that have Ct value ≤ 35. (A and B) The specificity of assay for detection of negative- and positive-strand RNA transcript using tag and E specific primers. Negative- and positive-strand specific primers were used to detect negative- and positive-strand RNA in (A) negative-strand standard samples (starting from 10^8 copies) and (B) positive-strand standard samples (starting from 10^8 copies). (C-F) Quantification of negative- and positive-strand RNA transcripts with the opposite strand at various ratios or with the addition of 40 ng of BHK-21 RNA. Negative-strand standards that were serially diluted 10-fold (starting from 10^7 copies) were mixed with (C) 10^7 copies of positive-strand standard or (E) 40 ng of BHK-21 RNA for detection of detection of negative-strand RNA transcript by negative-strand specific primers. Positive-strand standards that were serially diluted 10-fold (starting from 10^7 copies) were mixed with (D) 10^7 copies of negative-strand standard or (F) 40 ng of BHK-21 RNA for detection of detection of positive-strand RNA transcript by positive-strand specific primers.

To demonstrate the possibility of using this assay in both viral RNA transfected and infected systems, BHK-21 cells were either transfected with 10 μg of *in vitro* transcribed DENV2 WT RNAs or infected with DENV2 at MOI =1, and cells were harvested at indicated time points for RNA extraction, for a total of 24 hours. The extracted RNAs from all time points were subjected to the assay, as described above and absolute viral RNA copy numbers were determined with the use of standard curve. Intriguingly, we found that in transfected system, during 2 to 4 and 6 to 8 hours periods, the level of positive-strand decreased drastically, whereas its level remained relatively stable from 4 to 6 hours period (Fig 3-12A). Similar observation was also seen in infected system, where the positive-strand level also remained relatively stable from 4 to 6 hours period (Fig 3-12B). This suggests that during this period, positive-sense viral RNA from both systems may form a complex with ribosome and hence, prevent it from degradation, which may coincide with translation of DENV polyprotein. This is supported by the observation in both systems that during 8 to 10 hours period, a slight increase in negative-strand level was detected and its level continued to increase till 24 hours; this implies that following translation that occurs during 4 to 6 hours period, the polyprotein underwent processing to release individual viral proteins for replication, which can then act on positive-sense RNA template to synthesize negative-strand RNA during 8 to 10 hours period and continue all the way to the last timepoint (24 hours). Further work is required in this aspect to determine the correlation between dynamics of RNA synthesis and polyprotein translation. Nevertheless, we have demonstrated that the assay is a useful and reliable tool for evaluating the kinetics of positive- and negative-strand RNA synthesis in both infected and viral RNA-transfected cells.

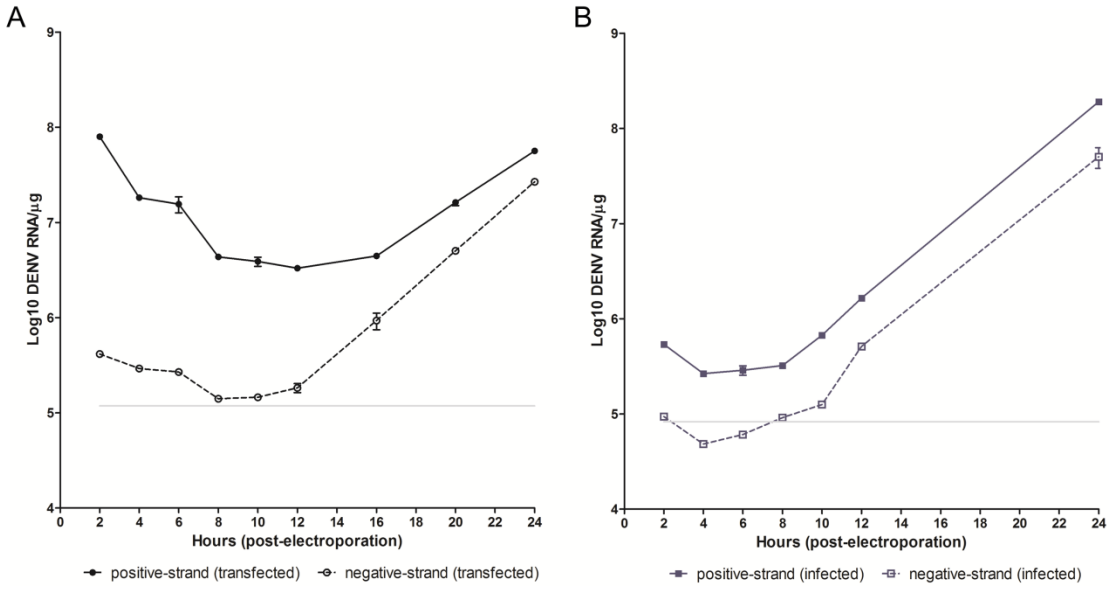

Figure 3-12: Viral RNA replication kinetics of BHK-21 cells that were either transfected with DENV2 WT RNAs or infected with DENV2 were monitored over the course of 24-hour. BHK-21 cells were either (A) electroporated with 10 µg of WT *in vitro* RNA transcripts or (B) infected with DENV2 at MOI=1 and samples were harvested at indicated time points, up to 24 hours. RNA was extracted from infected cells and was used to quantify the amount of negative and positive-strand synthesis by real-time RT-PCR. Absolute copy numbers of both strands in log scale per µg of RNA used for real-time RT-PCR were plotted; data are shown as the mean ± SD of duplicate from one independent experiment. The grey line in (A) indicates the amount of residual negative-strand from transfected RNA. The grey line in (B) indicates the amount of negative-strand that was present in virus stock. This data in B was kindly provided by Kitti Chan from Duke-NUS Graduate Medical School.

3.1.9 NS3:N570A mutant shows accumulation of negative-strand RNA

Following the evaluation of strand-specific quantitative RT-PCR assay, we employed this assay to study the dynamics of RNA synthesis for WT, and NS5:K330A and NS3:N570A mutant viruses. As expected, for WT RNA transfected cells, the level of both negative- and positive-strand RNAs increased over time until 72 hours and declined at slightly different rates after that until 120 hours (Figure 3-13). The quantification was consistent with previous data that an excess of positive- over negative-strand RNA can be detected in WT virus infected cells (Tomassini *et al.*, 2003). The RNA quantification for NS3:N570A mutant revealed a different trend to

WT and NS5:K330A mutant. Overall, the levels of negative- and positive-strand RNA for NS3:N570A were lower than WT. However, the rate of negative-strand RNA synthesis (rate = $2.06\times10^4 \pm 9.77\times10^2$ negative-strand/hour) for NS3:N570A appeared to increase faster than positive-strand RNA synthesis (rate = $-2.17\times10^5 \pm 5.82\times10^4$ positive-strand/hour) during 6 to 24 hours period, and at somewhat similar rate for both strands (rate = $3.55\times10^5 \pm 3.74\times10^3$ negative-strand/hour and $7.48\times10^5 \pm 1.28\times10^5$ positive-strand/hour) during 24 to 48 hours period, suggesting that the negative-strand RNA may be accumulating as double-stranded replicative form by base-pairing with the transfected positive-sense RNA. Interestingly, beyond 48 hours, the rates at which both strands accumulated for NS3:N570A mutant over time were almost identical. For NS5:K330A mutant, the level of detected negative- and positive-strand RNA corresponds to the amount of transfected negative- and positive-strand RNA that degraded over time (Note: T7 transcribed positive-sense RNA used for transfection contained ~0.1-0.3% negative-sense RNA that could be detected by the primers that bind to E gene and is the basis for the grey cutoff line for the residual negative-strand from transfected RNA in Figure 3-13). The NS3:N570A mutant probably results in either reduced or completely abolished NS3-NS5 interaction and hence, is unable to use the double-stranded replicative form as template to support further RNA synthesis (Chu & Westaway, 1985). This is consistent with the detection of highest percentage of dsRNA-positive cells at 48 hours (5-10%) by intracellular RNA staining that does not accumulate as seen in WT at the later time points (Fig 3-9B). Interestingly, our detailed analysis suggests that NS5:K330A mutant cannot synthesize negative-strand RNA although the mutation has been shown to have no effect on the *in vitro* enzymatic activities of NS5 protein (Zou *et al.*, 2011). These results suggest that the impairment of viral protein synthesis and infectious virus

production in NS3:N570A mutant may be due to the inability of the mutant NS3 to engage with NS5 and use the dsRNA template to produce more positive-strand genomic RNA for sustained replication.

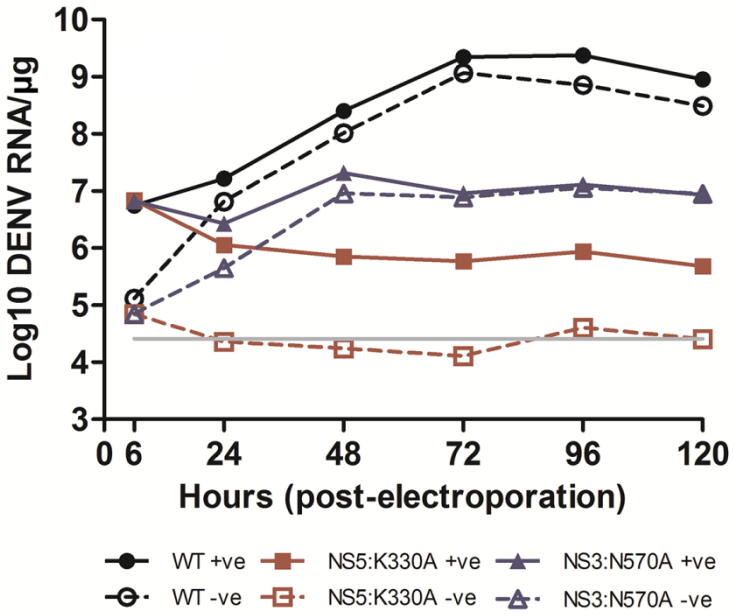

Figure 3-13: Dynamics of viral RNA replication of BHK-21 cells that were transfected with DENV2 WT, NS5:K330A or NS3:N570A RNAs were monitored over the course of 5-day. Same experiment setup was performed as mentioned in Figure 3-9. Extracted RNA was used to quantify the amount of negative and positive-strand synthesis by real-time RT-PCR. Absolute copy numbers of both strands in log scale per µg of RNA used for real-time RT-PCR were plotted; data are shown as the mean ± SD of duplicate from one independent experiment. The grey line in indicates the amount of residual negative-strand from transfected RNA. This experiment was performed in collaboration with Kitti Chan from Duke-NUS Graduate Medical School.

3.1.10 Peptides spanning NS3-NS5 interaction site reduce RNA replication

Since mutation in NS3-NS5 interaction site can impair viral replication, we next asked the question if synthetic peptides that span NS3-NS5 interaction site can also reduce RNA replication in viral inhibition assay. At 6 hours post-infection, Huh-7 cells were treated with either $NS3_{566-585}$ peptide, which formed non-convalent complex with penetrating peptide, penetratin (1:3 molar ratio, 7.5 μM of NS3 peptide) or $NS5_{320-341}$ peptide that was covalently linked to penetratin (7.5 μM of NS5 peptide) (Brugidou *et al.*, 1995; Derossi *et al.*, 1996; Keller *et al.*, 2013). At 24 hours post-infection, infected cells were harvested for RNA extraction and were subjected to real-time RT-PCR for viral RNA quantification. As indicated in Figure 3-14A and B, both peptides could reduce viral replication by ~33% (p-value for $NS3_{566-585}$ = 0.0195 and p-value for $NS5_{320-341}$ = 0.0043, Figure 3-14) when compared penetratin control. This implies that blocking interaction between NS3 and NS5 could be a potential therapeutic target.

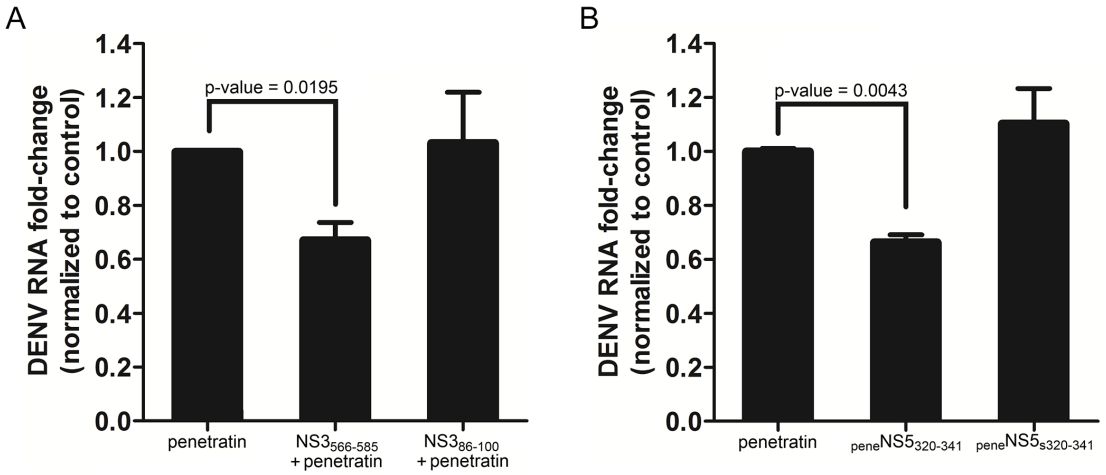

Figure 3-14: Viral inhibition assay was performed with NS3 or NS5 peptide that spanned NS3-NS5 interaction site. (A) For NS3 peptides, they formed non-convalent complex with penetratin peptide, which also enables NS3 peptide to be transported into the cells (1:3 molar ratio) (Keller *et al.*, 2013). (B) For NS5 peptides, they were synthesized as penetratin fusion peptide as penetratin has been shown to have cell-penetrating property (Brugidou *et al.*, 1995) and this enables NS5 peptide to be transported into the cells. (A and B) 6 hours post-infection, the cells were treated with 7.5 μM of each peptide. Infected cells were harvested at 24 hours post-infection for cellular viral RNA quantification by real-time RT-PCR analysis. Fold-change was normalized to 24 hours control (penetratin alone) was plotted and data are shown as the mean ± SD of duplicate from one independent experiment. The x-axis labels are as follows: penetratin, penetratin and $NS3_{566-585}$ complex ($NS3_{566-585}$+penetratin), and penetratin and $NS3_{86-100}$ complex ($NS3_{86-100}$+penetratin) for (A) and penetratin, penetratin fused to $NS5_{320-341}$ (peneNS5$_{320-341}$) and penetratin fused to scrambled $NS5_{320-341}$ (peneNS5$_{s320-341}$) for (B). This experiment was performed in collaboration with Kitti Chan from Duke-NUS Graduate Medical School.

3.2 Investigating the subcellular localization pattern of NS5 for DENV1-4 serotypes and its impact on virus replication

3.2.1 DENV1-4 NS5 of infected and transfected cells show differential subcellular localization

In order to detect DENV1-4 NS5 in infected cells, we first generated antibody against NS5 by biopanning of naïve human Fab-phage display library against NS5 MTase and RdRP proteins, while alternating between serotype 2 and 3 between each round of panning (Tay *et al.*, 2014a). After four rounds of panning and characterization, two Fabs, 5M1 and 5R3 were identified to bind to DENV1-4 MTase and RdRP proteins, respectively (Zhao *et al.*, 2014) and they were converted to IgG format as described previously to improve avidity (Moreland *et al.*, 2012). The specificity and avidity of IgG were tested in ELISA following conversion. As shown in Figure 3-15A and B, both IgGs have increase avidity as compared to their Fab counterparts to bind NS5 MTase and RdRP and the specificity of the IgGs are retained. Based on the ELISA results, 10 nM of 5M1 IgG and 30 nM of 5R3 IgG were used for IFA. Next, to ensure that 5R3 IgG can still recognise conformational epitope upon conversion (Zhao *et al.*, 2014), dot blot with both native and boiled NS5 full-length protein was done and as expected, 5R3 IgG still retains its ability to distinguish native folded NS5 from denatured/misfolded NS5 in IFA (Figure 3-15C).

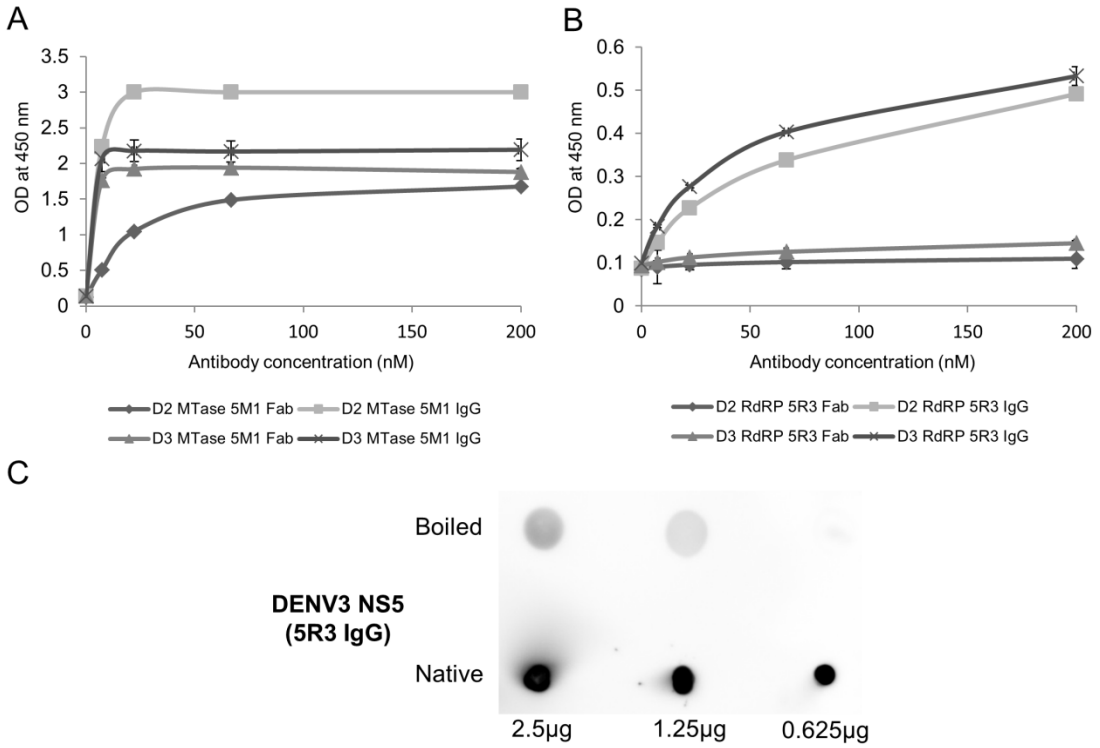

Figure 3-15: Conversion of cross-reactive anti-NS5 from Fab format to IgG format increases the avidity of anti-NS5. (A-C) Anti-NS5 IgGs were characterized by ELISA and dot blot. (A-B) ELISA with anti-NS5 of either Fab or IgG format (5M1 or 5R3, 2-fold serial dilution, starting from 200 nM) was performed against (A) DENV2 and 3 NS5 MTase and (B) DENV2 and 3 NS5 RdRP to determine antibody avidity and specificity. Data represent the mean ± SD (n=2) from a single experiment. (C) Dot blot was performed with either boiled or native DENV3 NS5 (2-fold serial dilution, starting from 2.5 µg) to determine the nature of epitope (linear or conformational) that 5R3 IgG recognises.

After the characterization of anti-NS5 IgGs, 5R3 was employed to detect NS5 of DENV1-4 Huh-7 infected cells (MOI=10) that were fixed at 24 hours post-infection by IFA and CLSM (Figure 3-16A). Nuclear to cytoplasmic fluorescence ratio ($F_{n/c}$) were determined from image analysis (Collins, 2007) of digitized CLSM images (such as those in (Figure 3-16B), confirmed that DENV3 NS5 was predominantly nuclear like DENV2 NS5 ($F_{n/c}$ = 11 and 12, respectively), whereas DENV1 NS5 was predominately cytoplasmic and it also exhibited localization in perinuclear region and possibly, in cytoskeleton region too ($F_{n/c}$ = 0.8) (similar phenomenon was able seen in another DENV1 strain Hawaii (Figure A-1), as well as with another anti-NS5 IgG

5M1 (Figure A-2). For DENV4 NS5, it was found in both cytoplasm and nucleus, with slightly more NS5 in nucleus ($F_{n/c}$ = 1.7). Similar results were also observed in DENV1-4 BHK-21 infected cells (data not shown). Therefore, although NS5 is clearly present in the nucleus of DENV1-4 infected cells, the amount of nuclear NS5 varies widely.

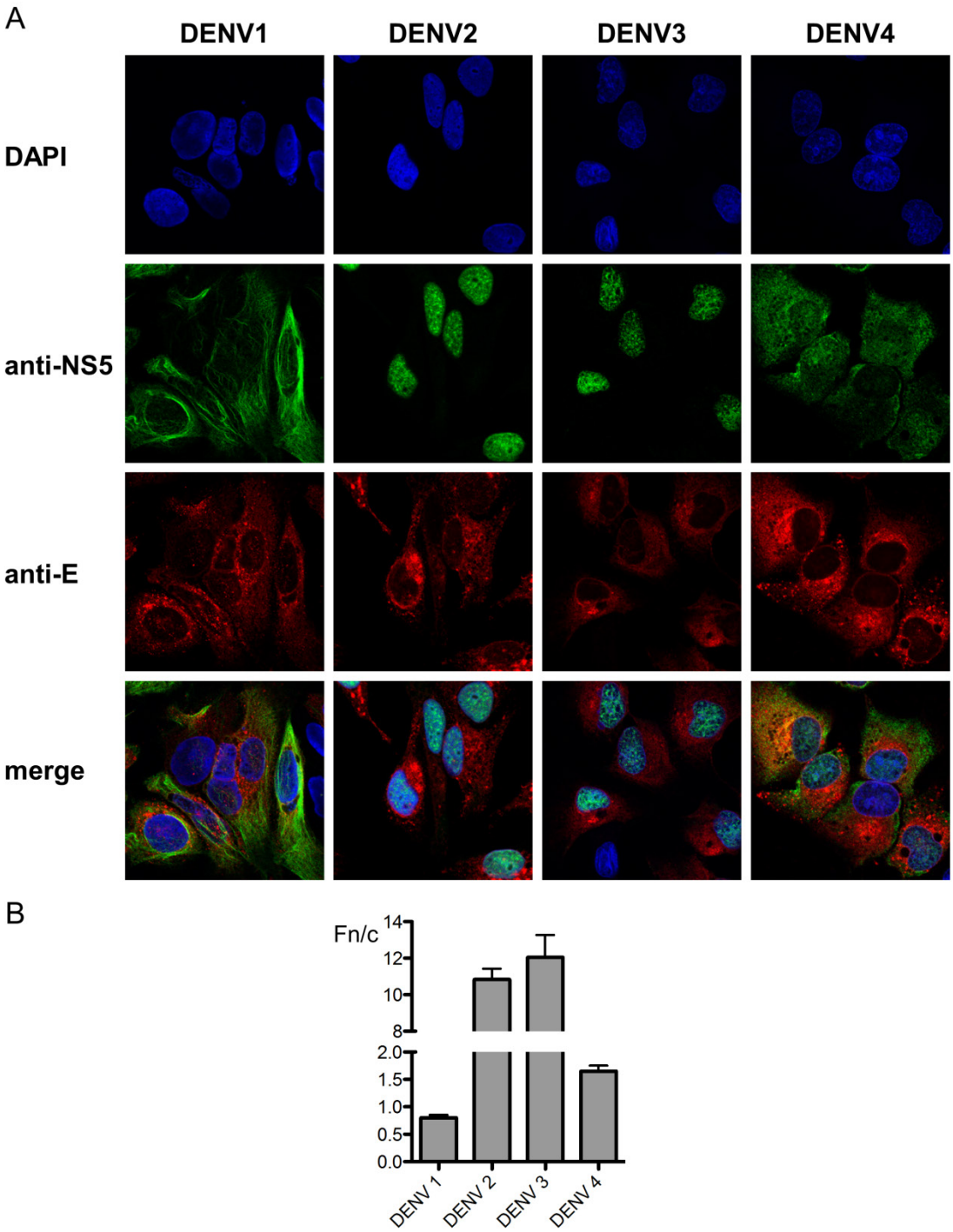

Figure 3-16: NS5 from DENV1-4 NS5 infected cells display nuclear localization, but to differing extents. Huh-7 cells were mock-infected or infected with DENV1-4 (known as EDEN isolates in this sutdy; GenBank accession numbers are: DENV1 (EU081230), DENV2 (EU081177), DENV3 (EU081190) and DENV4 (GQ398256)) at an MOI of 10 and fixed at 24h post-infection. (A) Anti-NS5 (5R3 IgG, 30 nM; green) and anti-E (4G2 IgG, 1:1000; red) antibodies were used for immunostaining. Images were captured by CLSM using a Zeiss LSM 710 upright confocal microscope by 63× oil immersion lens. (B) Image analysis was performed on digitized images that were based on anti-NS5 staining (green) to determine nuclear to cytoplasmic fluorescence ratio (Fn/c) with background fluorescence subtracted, for NS5 of each serotype using ImageJ software. Data represent the mean ± SEM (n > 25 cells) from a single experiment, representative of two independent experiments. (B) is adapted from (Tay et al., 2013). Image analysis was kindly performed by Dr Johanna Fraser from Monash University.

The nuclear targeting ability of DENV1-4 NS5 was further examined by fusing NS5 gene fragments to that of GFP and expressed GFP-NS5 fusion protein in Vero cells. The cells were fixed at 24 hours post-transfection, and cells were stained by both anti-GFP and anti-NS5 5R3. CLSM of transfected cells gave results that were similar to those NS5 from infected cells; all GFP-NS5 proteins showed nuclear localization, with DENV2 and 3 NS5 showing greater accumulation than DENV1 and 4 (Figure 3-17). Staining with anti-NS5 5R3 co-localize with the staining with anti-GFP indicates that GFP-NS5 proteins were properly folded and they resembled the native form of NS5 from infected cells because 5R3 recognizes conformational NS5 epitope. Collectively, these results demonstrate that the NS5 of DENV1-4 localize differently and the observed patter is similar in both transfected and infected cells.

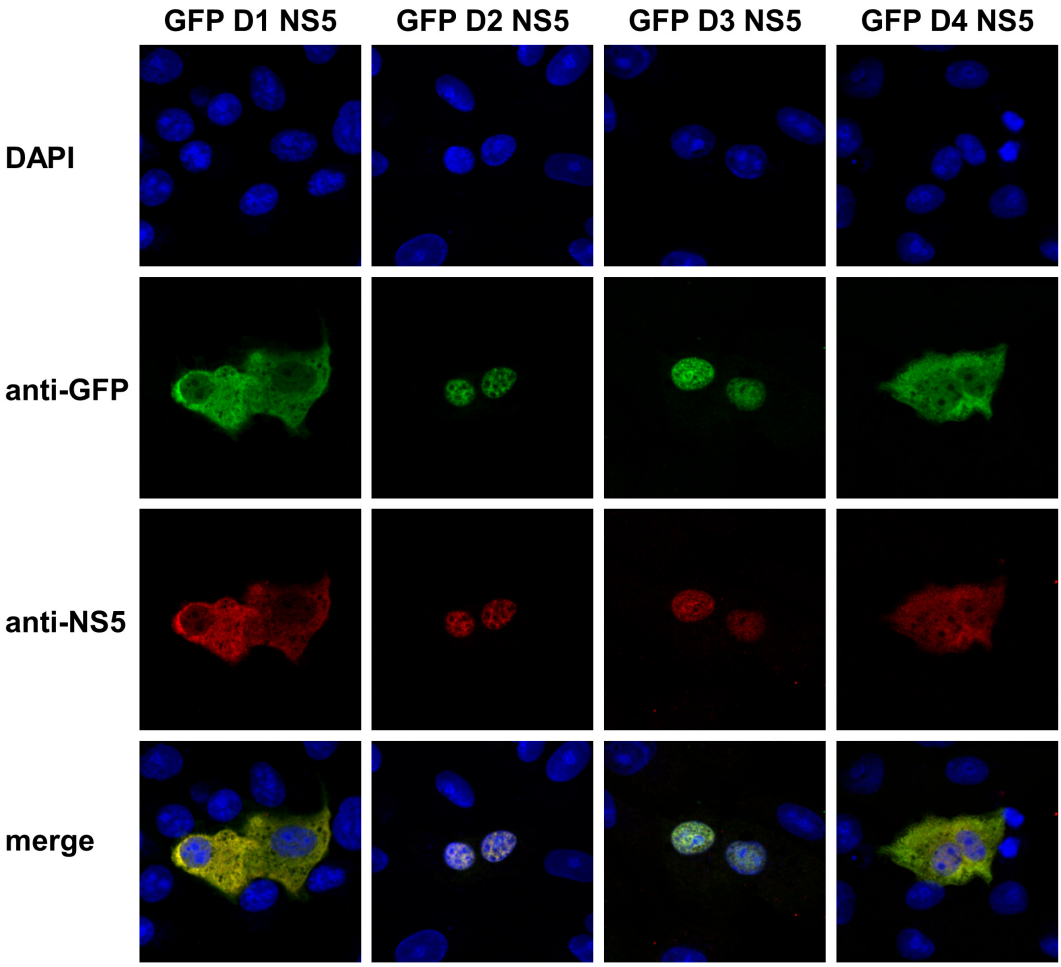

Figure 3-17: NS5 from DENV1-4 transfected cells show similar subcellular localization pattern as compared to NS5 from DENV1-4 infected cells. Vero cells were transfected with either GFP or GFP-NS5 from DENV1-4 (sequences as in Figure 3-16) and fixed at 24h post-transfection. Anti-GFP (ab6556 IgG, 1:1000; green) and anti-NS5 (5R3 IgG, 30 nM; red) antibodies were used for immunostaining. Images were captured as described in Figure 3-16A.

3.2.2 DENV1 NS5 has a functional α/βNLS

With the observation that DENV1 NS5 was predominately cytoplasmic, we focused on DENV1 and 2 NS5 as examples of protein that did not or did localize to the nucleus in subsequent experiments in order to explore any functional significance for our observation. A time course experiment where infected cells were fixed at various time points post-infection revealed more NS5 in the nucleus of DENV1 infected cells at later time points (ie. 36 hours onwards, Figure 3-18), which suggests that DENV1 NS5 may have a functional α/βNLS to allow its nuclear translocation, just like DENV2 NS5. This is further supported by AlphaScreen binding assay that detected binding between DENV1 and 2 NS5 with importin-α/β1 with similar apparent K_d (DENV1=0.2 nM and DENV2=0.4 nM), and also the treatment of DENV1 NS5 transfected cells with CRM1 specific inhibitor LMB that led to the accumulation of nuclear NS5 (data shown in (Tay *et al.*, 2013), both experiments did by Dr Johanna Fraser from Monash University). However, the α/βNLS of DENV1 NS5 did not allow it to nuclear-localise to the same extent as DENV2 NS5, which implies that it has a weaker NLS. In line with the hypothesis that DENV1 α/βNLS is probably weaker, the rational for focusing on DENV1 and 2 NS5 was also driven by the consistent observation in our laboratory that DENV1 produced more infectious virus particles than DENV2, (Figure 3-19A and B), despite similar MOI and infection rate as determined by anti-E 4G2 staining (data shown in (Tay *et al.*, 2013); similar observation was also seen by other group (Yohan *et al.*, 2014).

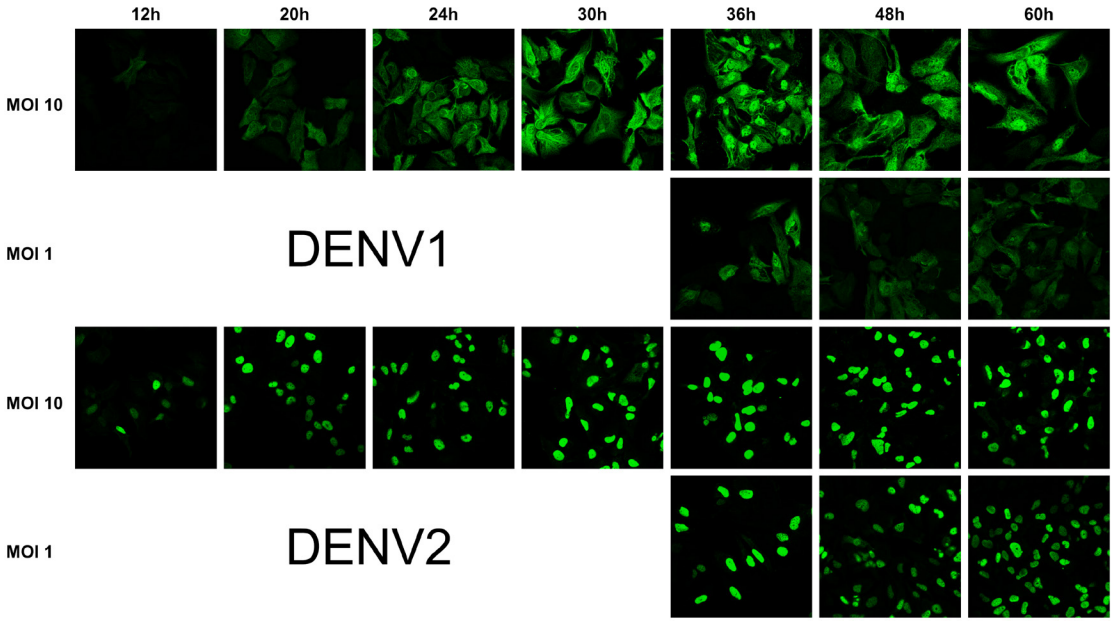

Figure 3-18: DENV1 NS5 shows increased nuclear localization over time in infected cells, but to a lower extent than DENV2 NS5 in infected cells. Huh-7 cells were mock-infected or infected with DENV1 or 2 (sequences as in Figure 3-16) at an MOI of 10 and fixed at various times post-infection. Images were captured by CLSM using a Zeiss LSM 710 upright confocal microscope by 63× oil immersion lens.

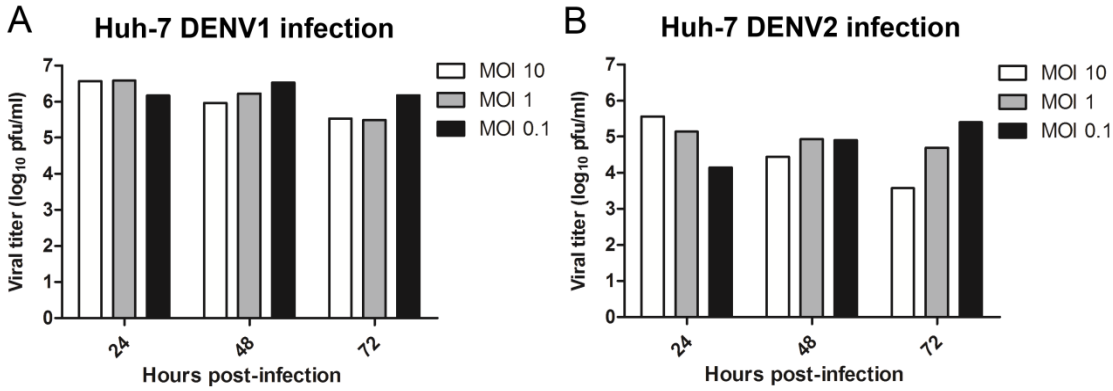

Figure 3-19: DENV1 produced more infectious virus particles than DENV2 despite similar MOI. Huh-7 cells were mock-infected or infected with DENV1 and 2 (refer to Figure 3-16 for GenBank accession numbers) at an MOI of 0.1, 1 and 10 and supernatants were collected at 24 hours, 48 hours and 72 hours post-infection. Viral titer was determined by plaque assay on BHK-21 cells and reported as $\log_{10}$ pfu/ml. This data was kindly provided by Kitti Chan from Duke-NUS Graduate Medical School.

Comparison of NES and α/βNLS sequence between DENV1 and 2 NS5 only revealed difference in the first basic cluster of α/βNLS; for DENV1, it is ^{371}AQ, whereas for DENV2, it is ^{371}KK. Therefore, we hypothesized that by mutating DENV2 ^{371}KK→AQ, we should be able to disrupt DENV2 NS5 nuclear localization because ^{371}KK→AA mutation was already shown by (Pryor *et al.*, 2007) to affect DENV2 NS5 localization in infected cells. Despite the change, DENV2 NS5 remains nuclear-localized (data not shown).

In order to characterize the α/βNLS of DENV1 NS5 more efficiently, we decided to exchange the corresponding gene segment that encodes α/βNLS sequence (residues 320-405) of DENV1 NS5 into DENV2 NS5 and vice versa. The experiment was done in a context of a full-length NS5 protein, in a transfected system to ensure that each chimeric GFP-NS5 protein is properly folded and the NLS sequence can function in the context of native NS5. Furthermore, the use of transfected system enables quicker molecular manipulation of gene fragment as compared to reverse genetics system and it can also produce similar results as infected system (as shown in Figure 3-16A and 3-17). During the study, anti-NS5 5R3 was employed to detect chimeric NS5 to ensure that the protein is properly folded (Note: a summary of anti-NS5 5R3 staining and western blot data for each chimeric protein was summarized in Table 3-8).

Through overlap extension PCR (Figure 2-1), the corresponding gene segments that encode α/βNLS sequence were successfully exchanged between the two serotypes of NS5. When DENV2 α/βNLS was replaced by DENV1 α/βNLS, the latter could target full-length DENV2 NS5 protein to the nucleus. On the contrary, when DENV1 α/βNLS was replaced by DENV2 α/βNLS, DENV2 α/βNLS could not target full-length DENV1 NS5 protein to the nucleus (Figure 3-20). These results suggest that DENV1 α/βNLS is functional; it can target protein greater than 45 kDa to the nucleus. However, despite a functional α/βNLS, there seems to be a greater signal (we named it CRS) outside the exchanged gene segment, which is either in residues 1-319 or 406-900 that is responsible for the cytoplasmic retention of DENV1 NS5.

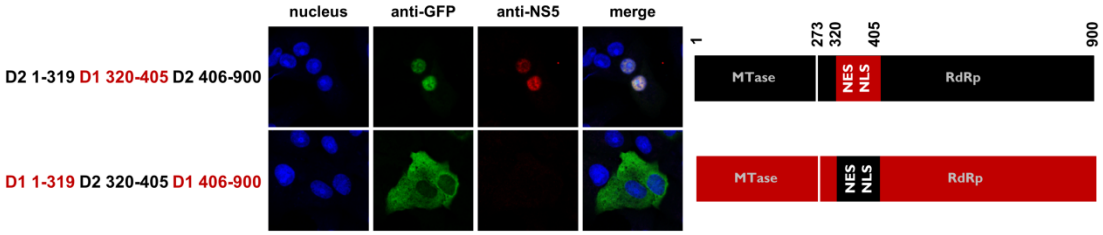

Figure 3-20: α/βNLS of DENV1 NS5 can target DENV2 NS5 to the nucleus. α/βNLS-swapping experiment between DENV1 and 2 GFP-NS5 was performed to determine if DENV1 α/βNLS is functional. Exchanges of gene segments (residues 320-405) that encode α/βNLS sequence between DENV1 and 2 GFP-NS5 were generated by overlap extension PCR. The plasmids were transfected into Vero cells and fixed 24 hours post-transfection. The cells were stained and images were captured as described in Figure 3-17. Red letters in construct name indicates gene segment from DENV1 NS5; black letters in construct name indicates gene segment from DENV2 NS5 (first column). Anti-GFP (ab6556 IgG, 1:1000; green) and anti-NS5 (5R3 IgG, 30 nM; red) antibodies were used for immunostaining. Anti-NS5 5R3 IgG recognises conformational epitope and was used to assess the folding of NS5 protein (second column). Schematic representation of the NS5 gene segments that were exchanged between DENV1 and 2 is showed in third column. NES indicates nuclear export signal and NLS indicates nuclear localization signal.

3.2.3 Small molecule inhibitor ivermectin can block interaction of DENV1 and 2 NS5 with importin-α/β1 *in vitro* and inhibit DENV1-4 viral replication

It was reported previously that ivermectin, a broad-spectrum anti-helminthic drug, can specifically block interaction between DENV2 NS5 and importin-α1/β1but not of importin-β1 alone in mid μM range (half-maximal inhibitory concentration (IC_{50}) = 17 μM, (Omura, 2008; Wagstaff *et al.*, 2012)). Since we have shown that α/βNLS of DENV1 NS5 is functional and it can bind to importin-α/β1 in AlphaScreen binding assay, we next determined if ivermectin can also block the interaction between DENV1 NS5 and importin-α/β1. AlphaScreen binding assay was carried out as described in (Tay *et al.*, 2013), in the presence of increasing concentrations of ivermectin and the IC_{50} for DENV1 and 2 NS5 to importin-α/β1 were 2.3 and 1.5 μM, respectively (experiment carried out by Dr Johanna Fraser from Monash University). This suggests that ivermectin specifically blocks NS5-importin-α/β1 interaction and this inhibition is supported by findings that ivermectin has no impact NS3-NS5 interaction and NS5 RdRP activity (data shown in (Tay *et al.*, 2013)).

To explore the implications of *in vitro* finding of ivermectin with respect to its antiviral potential in infected cell system, we tested its ability to protect against infection by DENV1-4 in Huh-7 and BHK-21 cells in cell-based infection assays that were established previously in our laboratory (Rathore *et al.*, 2011b; Tan *et al.*, 2014; Wang *et al.*, 2009b; Watanabe *et al.*, 2012). BHK-21 cells were either mock-infected or infected with DENV1-4 at an MOI of 0.3 in the absence or presence of increasing concentrations of ivermectin, followed by fixation and quantitation of IFA-positive

cells (based on anti-E 4G2 staining) at 48 h post-infection. The half-maximal effective concentration (EC_{50}) values were comparable for DENV1-4 (1.6-2.3 μM; see Table 3-1). In order to corroborate the observation that the inhibition is not cell-line dependent, we tested ivermectin's antiviral action in Huh-7 for DENV1 and 2 using established plaque assay and obtained similar EC_{50} values (Table 3-1).

With the observation that DENV1-4 NS5 nuclear-localize to different extents, it was not surprising to us that ivermectin could inhibit DENV1-4 with similar EC_{50} values because it was consistent with the idea that ivermectin specifically targets the host protein importin-α1 (Wagstaff *et al.*, 2011) and it does not inhibit NS5 RdRP activity and NS3-NS5 interaction (Tay *et al.*, 2013). However, it is also possible during DENV infection, ivermectin may exhibit its antiviral effect by blocking nuclear import of unidentified host protein(s) that is(are) important for viral replication. It should also be noted that ivermectin has also been reported to have inhibitory effect against helicase activity of NS3 and similar EC_{50} values were obtained (Mastrangelo *et al.*, 2012), meaning that it is not entirely possible to attribute the antiviral effect of ivermectin be solely due its action on NS5 nuclear import. Taken together, we have clearly shown that ivermectin has antiviral activity against all four serotypes of DENV and its main mode of inhibition remains to be determined.

Table 3-1. Summary of antiviral activities of ivermectin and other agents towards DENV1-4. Table is adapted from (Tay et al., 2013).

Serotypes	Agent	EC_{50} (μM)	
		BHK-21*	Huh-7^
DENV1	Ivermectin[@]	2.32 ± 1.06	2.97 ± 0.07
	Celgosivir[#]	0.26 ± 0.00	N.D.[+]
	NITD008[#]	1.37 ± 0.41	2.53 ± 0.08
DENV2	Ivermectin	2.08 ± 0.94	1.74 ± 0.15
	Celgosivir	0.32 ± 0.05	N.D.[+]
	NITD008	1.32 ± 0.56	0.22 ± 0.05
DENV3	Ivermectin	1.66 ± 0.66	N.D.[+]
	Celgosivir	0.09 ± 0.02	N.D.[+]
	NITD008	0.50 ± 0.19	N.D.[+]
DENV4	Ivermectin	1.90 ± 0.89	N.D.[+]
	Celgosivir	0.08 ± 0.01	N.D.[+]
	NITD008	0.65 ± 0.28	N.D.[+]

*Data are for the mean ± SD (2 independent experiments performed in triplicate) as determined by CFI assay on mock or DENV1-4 infected BHK-21 cells treated with 0-45 μM of the indicated agents.

^Data are for the mean ± SD (single experiment performed in duplicate), as determined by plaque assay on BHK-21 cells using media supernatant at 48h post-infection of mock-infected or DENV1 or 2 infected Huh-7 cells treated with 0.16-5 μM of the indicated agents.

[@]CC_{50} for BHK-21 and Huh-7 for ivermectin are 9.8 and 7.3 μM, respectively (48h treatment).

[#]Established inhibitors of DENV celgosivir (Rathore *et al.*, 2011a) and NITD008 (Yin et al., 2009) were included in the assays as controls; CC_{50} values of > 100 μM.

[+]N.D., Not determined

3.3 Identifying potential nuclear or cytoplasmic binding partners that are unique to DENV1 and 2 GFP-NS5 by co-immunoprecipitation coupled to mass spectrometry

3.3.1 Validation of DENV1 and 2 GFP-NS5 co-immunoprecipitation elutants prior to mass-spectrometry by silver staining and western blot

In order to better understand the nuclear role of DENV2 NS5, we set out to identify human host proteins that can bind to DENV1 and 2 GFP-NS5. The rationale for including DENV1 GFP-NS5 in this study was due to our finding that in both infected and transfected cells, DENV1 NS5 localizes to the cytoplasm, whereas DENV2 NS5 localizes to the nucleus. Based on this finding, we hypothesized that the physical compartmentation of these two proteins enabled them to interact with host proteins that are either unique to nucleus or cytoplasm, which in turn may help us to identify binding partners that are unique to either protein. For this study, we adopted the co-IP coupled with mass spectrometry approach for identifying protein-protein interactions between NS5 and host proteins because co-IP enables more interaction partners to be identified from purified NS5-host protein complexes as compared to Y2H that detects binary interaction. The co-IP experiments were carried out with lysates from GFP-NS5 (DENV1 and 2), GFP-NS3 (DENV1 and 2), GFP and mock-transfected cells. We included DENV1 and 2 GFP-NS3 in this study because we considered them to be a better control than GFP in term of size (GFP, ~25 kDa; GFP-NS3, ~100 kDa and GFP-NS5, ~125 kDa) and it may aid the identification of host proteins that are common to both NS3 and NS5.

We first transfected all the GFP plasmids into HEK293T cells (two 10-cm plates per construct). Prior to lysis at 24 hours post-transfection, the cells were checked under the fluorescence microscope to determine NS5 localization and transfection efficiency. The subcellular localization of DENV1 and 2 GFP-NS5 were similar to those in Vero cells (Figure 3-17 and 21). The transfection efficiency for GFP, GFP-NS3 and GFP-NS5 plasmids were ~80-90%, 50-60% and 40-50% respectively.

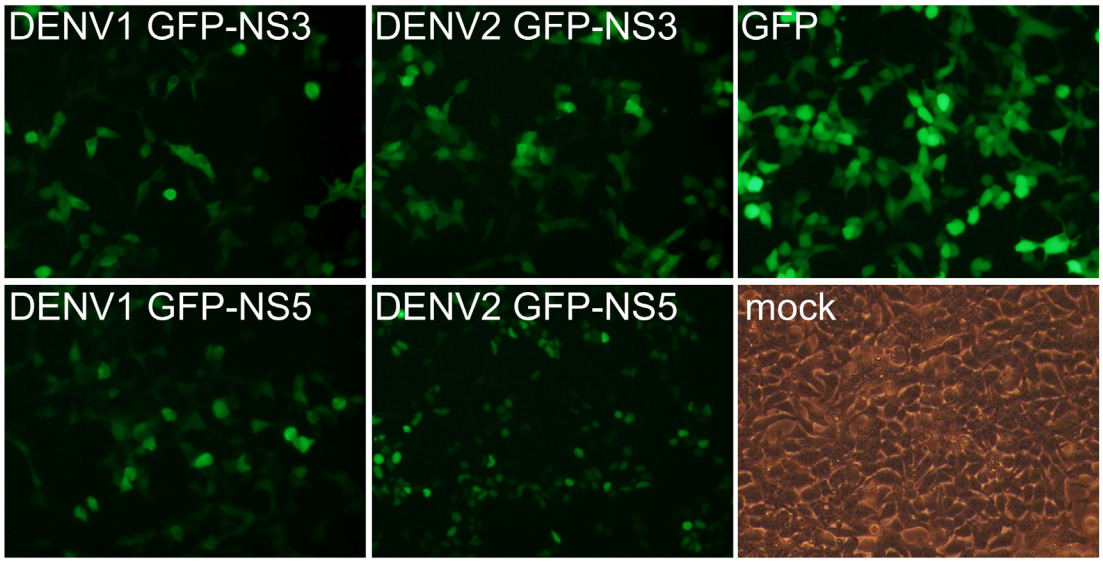

Figure 3-21: Subcellular localization patterns of DENV1 and 2 GFP-NS3 and GFP-NS5 in HEK293T cells. Plasmids encoding GFP-NS5 and GFP-NS3 of DENV1 and 2 were transfected into HEK293T cells. Fluorescent images of live transfected cells were taken at 24 hours post-transfection by Olympus fluorescence microscope to determine NS5 localization and transfection efficiency. Bright-field images of live mock-transfected cells were taken to determine cell confluency.

Following the lysis of these cells, the supernatants were subjected to IP overnight with GFP-Trap_A resin at 4°C. On the following day, the beads were washed three times and bound proteins were eluted from the beads first by vigorous vortexing for 5 minutes at RT, in the presence of 50 µl of 0.2% *Rapi*Gest SR surfactant reagent (termed as non-boiled elution here), followed by a second elution by boiling at 95°C for 5 minutes with 50 µl of 0.2% *Rapi*Gest SR surfactant reagent (termed as boiled elution here). The concentration of both types of elutants were determined by Nanodrop (amount of elutants listed in Table 3-2) and fixed amount of elutants were loaded onto two 8% SDS-PAGE gel for assessment by silver staining and western blot prior to sending them to the Duke University Protemics Facility (NC, USA) for LC-MS/MS protein identification (Figure 3-22).

Table 3-2: Total amount of elutants that were eluted from GFP-Trap_A resin and the amounts that were used for SDS-PAGE and LM-MS/MS. The amounts of elutants were determined by Nanodrop (*crude protein quantitation for SDS-PAGE gel loading) and BCA assay (#accurate protein quantification for LM-MS/MS carried out at Duke University Proteomics facility).

			GFP	D1 GFP-NS3	D2 GFP-NS3	D1 GFP-NS5	D2 GFP-NS5	mock
Protein quantification by Nanodrop	Non-boiled elutants	Total amount of elutant (µg) in 50 µl*	12.85	27.1	16.45	66.55	43.6	5.15
		Amount used for SDS-PAGE/gel (µg)*	1.29	2.71	1.65	4.03	4.03	0.52
		% of total elutant used for SDS-PAGE/gel*	10	10	10	6.06	9.24	10
	Boiled elutants	Total amount of elutant (µg) in 50 µl*	18.35	18.85	13.1	44.9	41.5	14.1
		Amount used for SDS-PAGE/gel (µg)*	1.84	1.89	1.31	2.79	2.79	1.41
		% of total elutant used for SDS-PAGE/gel*	10	10	10	6.22	6.72	10
Total amount of proteins eluted by both elution methods (µg)			31.2	45.95	29.55	111.45	85.1	19.25
Protein quantification by BCA assay	Non-boiled elutants	Total amount of elutant (µg) in 40 µl#	1.2	2	0.8	8.8	6.8	1.2
		Amount injected for MS (µg) #	0.14	0.91	0.36	1	0.77	0.14
		% of total elutant injected for MS#	11.36	45.44	45.44	11.36	11.36	11.36

The silver-stained gel from non-boiled elutants showed that the elution profiles of GFP-NS3 and GFP-NS5 were different, indicating that we were likely to identify unique binders to each protein from MS (Figure 3-22A). Closer inspection of silver-stained gels did not readily reveal any protein band that was unique to either DENV1 or 2 NS5, similarly for DENV1 or 2 NS3. Comparison of non-boiled elutants silver-stained gel (Figure 3-22A) against boiled elutants silver-stained gel boiled elutants silver-stained gel (Figure 3-22C) clearly demonstrated that there were less host proteins and more GFP-NS3 and GFP-NS5 proteins in boiled elutants, indicating that we had eluted most of the host proteins during the first elution. We could also determine the level of GFP protein expression from silver-stained gels; the order of GFP proteins in term of their expression levels (from the highest to the lowest) was as followed: DENV1 GFP-NS3 > DENV1 GFP-NS5 and DENV2 GFP-NS3 > DENV2 GFP-NS5.

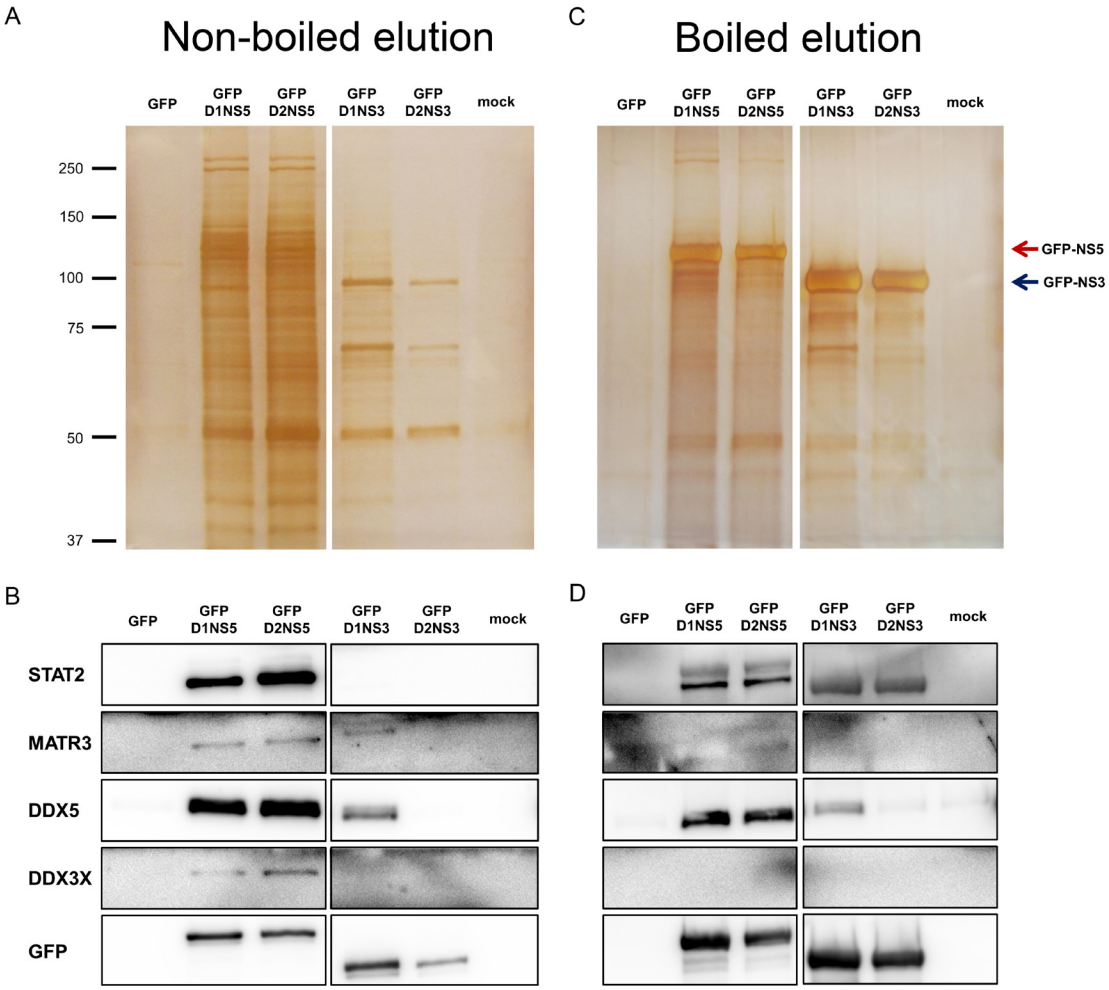

Figure 3-22: STAT2, MATR3, DDX5 and DDX3X are found in protein complex that are being pulled down with DENV1 and 2 GFP-NS5. Plasmids encoding GFP-NS5 and GFP-NS3 of DENV1 and 2 were transfected into HEK293T cells and were lysed at 24 hours post-transfection for co-IP. Co-IP was carried out overnight at 4°C with GFP-Trap_A resin. Bound proteins were eluted twice; first elution was by vortexing at RT for 5 minutes in 50 µl of 0.2% *Rapi*Gest SR surfactant reagent (termed as non-boiled elution here) and second elution was by boiling at 95°C for 5 minutes in 50 µl of 0.2% *Rapi*Gest SR surfactant reagent (termed as boiled elution here). Fixed amount of both types of elutants (indicate in Table 3-2) were loaded onto two 8% SDS-page (A-D). One set was subjected to (A and C) silver staining and the other one set was subjected to (B and D) western blotting with antibodies against STAT2, MATR3, DDX5, DDX3X and GFP. Lysates from GFP- and mock-transfected cells served as controls to exclude proteins that bound to either GFP or resins. No detection of GFP in GFP sample because the gels for both silver staining and western blot were overran.

Next, in order to verify that co-IP can pull down previously identified/characterized host proteins we did western blot for both types of elutants with antibodies against STAT2, MATR3, DDX5 and DDX3X (see Table 3-4 for the references of these proteins). As shown in Figure 3-22C for non-boiled elutant, STAT2 and MATR3 that were previously reported to interact with DENV2 NS5 via Y2H assays (Khadka *et al.*, 2011; Le Breton *et al.*, 2011) could also co-elute with DENV1 GFP-NS5. Interestingly, DDX5 that was previously reported to interact with both JEV NS3 and NS5 via pulldown assay (Li *et al.*, 2013) could also co-elute with DENV1 GFP-NS3, and DENV1 and 2 GFP-NS5. DDX3X was previously reported to bind to both JEV NS3 and NS5 via pulldown assay but in our study, we could only detect co-elution of DDX3X with DENV1 and 2 GFP-NS5, but not DENV1 and 2 NS3 (Li *et al.*, 2014a). No binding of STAT2 to NS3 implies that the binding of STAT2 to NS5 is unique to NS5. For boiled elutants (Figure 3-22D), we observed less STAT2 and DDX5 being detected and almost no detection of MATR3 and DDX3X, which further supported the presence of most of the relevant host proteins in samples by non-boiled elution. Collectively, the western blot data indicates data reliability of the co-IP experiment and LM-MS/MS of the non-boiled elutants were then used for protein identification.

3.3.2 Mapping DENV GFP-NS3- and GFP-NS5-human protein interaction network

Prior to MS analysis, the non-boiled elutants were quantified by BCA assay (Table 3-2). Based on BCA protein quantification, 11.36% of total elutant for DENV1 and 2 GFP-NS5, GFP and mock, and 44.54% of total elutant for DENV1 and 3 GFP-NS5 (maximum of 1 μg for each protein) were used for MS analysis.

Analysis of MS data by Scaffold Proteome software (version 4.3.4) (Searle, 2010) led to the identification of 405 human host proteins (refer to appendices Table A-1 for the whole list); each of these host proteins was represented by at least two unique peptide sequences and they were negative for GFP- and mock-transfected elutants. Through manual processing of protein dataset, 185 host proteins were identified to co-elute with DENV1/2 GFP-NS3, whereas 298 and 273 host proteins were identified to co-elute with DENV1 and 2 GFP-NS5, respectively (Note: DENV1 and 2 GFP-NS3 are considered as a single dataset because both proteins are cytoplasmic and DENV2 GFP-NS3 on its own has a small dataset (10 out 185 proteins). DENV1 and 2 GFP-NS5 are considered as two separate datasets because DENV1 NS5 is in cytoplasm whereas DENV2 NS5 is in nucleus) (Figure 3-23).

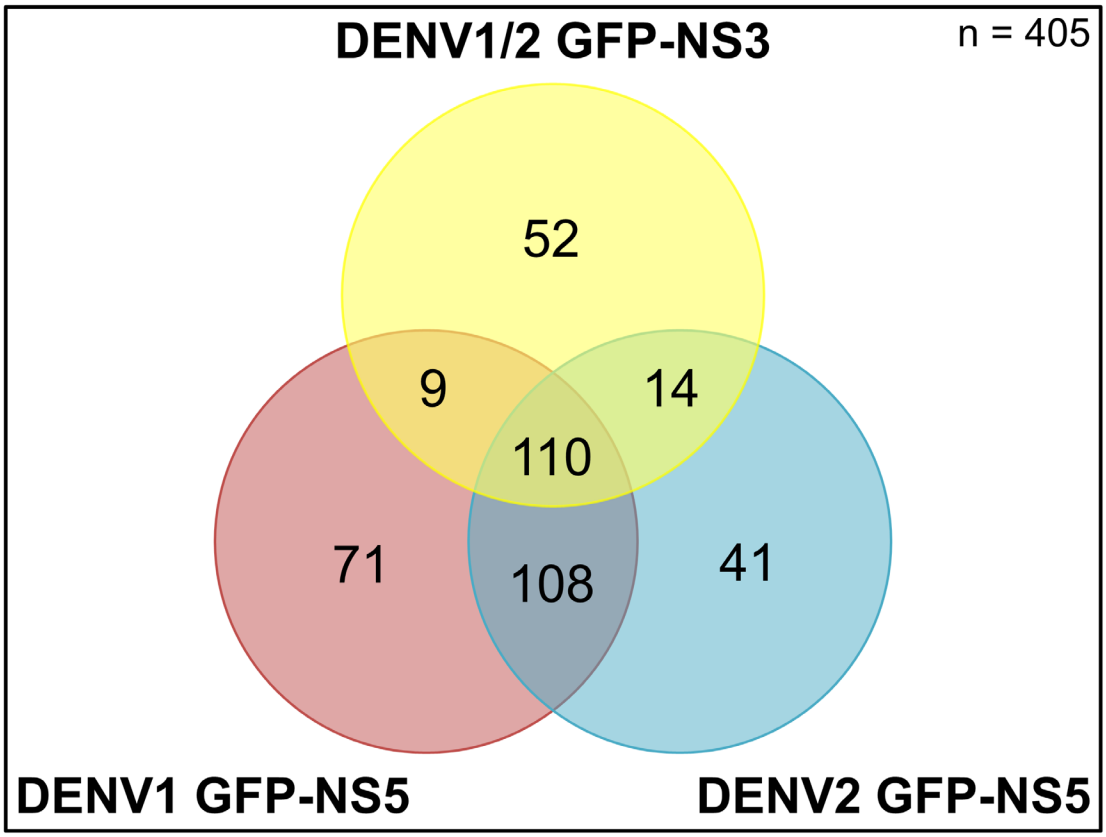

Figure 3-23: Venn diagram illustrating the overlap between the data sets of DENV1 and 2 GFP-NS3 and DENV1 and 2 GFP-NS5. DENV1 and 2 GFP-NS3 are considered as a single dataset because both proteins are cytoplasmic. DENV1 and 2 GFP-NS5 are considered as two separate datasets because DENV1 NS5 is in cytoplasm whereas DENV2 NS5 is in nucleus.

3.3.3 Validation of interactions through comparison to published dataset of viral proteomics screens

As of now, there have been several large-scale proteomics screens that have been done for DENV to look at human host proteins that physically interact with viral RNA, NS3 and NS5 proteins, either via RNA affinity chromatography (Ward *et al.*, 2011), Y2H (Chua *et al.*, 2004; Khadka *et al.*, 2011; Le Breton *et al.*, 2011; Mairiang *et al.*, 2013) or co-IP coupled to quantitative MS (Carpp *et al.*, 2014); comparison of our dataset to published dataset of host proteins that were identified by various proteomics screens enable us to identify meaningful hits for further study, as well as validating the reliability of our dataset through demonstrating the presence of expected/previously published host proteins in our dataset.

We first compared our dataset to existing set of human host proteins that was previously reported by Y2H, co-IP and pulldown studies to be interacting with flavivirus proteins through manual literature curation and this led to identification of 29 proteins that were listed in Table 3-3 and among these host proteins, HS90B was common to this study and all the other studies. In both this study and Y2H studies the matching hits are as follows: 8 proteins co-eluted with GFP-NS3 - GOGB1, HS90B, IKBA, NRBP, PTBP1, ILF3, PABP1 and RS20, 8 proteins co-eluted with GFP-NS5 - STAT2, MATR3, DDX3X, RB6I2, HNRPF, CGNL1, RIPL2 and SIAH2 and one protein bound to both GFP-NS3 and GFP-NS5 - DDX5 (Khadka *et al.*, 2011; Le Breton *et al.*, 2011; Mairiang *et al.*, 2013). Interestingly, we also identified LA protein that was previous identified to be interacting with DENV4 5' and 3' UTR, NS3 and NS5 to be also co-eluting with both GFP-NS3 and GFP-NS5 in this study (Garcia-

Montalvo *et al.*, 2004b). Our finding further supports the presence of LA protein in RC, even though its role in viral replication remains to be fully understood. LA protein is ubiquitous in eukaryotic cells and it binds to all nascent RNA transcripts to protect the 3' ends of these RNAs from exonucleases. The stabilization of RNA by La is needed for maturation of pre-tRNA, assembly of small RNAs into functional RNA-protein complexes, and nuclear retention of certain small RNAs (Wolin & Cedervall, 2002). It is likely that LA protein may be involved in either stabilization of RNA genome or translation of RNA genome since it can interact with both UTRs and major replicative enzymes (Alvarez *et al.*, 2005b; Paranjape & Harris, 2010; Wolin & Cedervall, 2002).

During the course of our study, Carpp and colleagues published their work on identifying viral-host protein interaction between human host proteins and NS3 or NS5. They also used supernatant from HEK293T that were either transfected by DENV2 GFP-NS3 or GFP-NS5 plasmid for co-IP, which was similar to our approach. However, following transfection, they infected the cells with DENV2 virus to identify viral-host interaction in the context of viral infection by quantitative MS and this enabled them to identify high confidence interactors of NS3 and NS5. They found 53 host proteins to be associated with NS5, 52 of which were novel and 41 host proteins to be associated with NS3, all of which were novel. Among them, 13 were common to GFP-NS3 and GFP-NS5 (Carpp *et al.*, 2014). Through comparison of our dataset to theirs, we have 4 common proteins that co-eluted with GFP-NS5 proteins - HS90A, TIM50, AIFM1 and DPM1, 9 common proteins that co-eluted with GFP-NS3 proteins - HS90B, HSP71, HSP7C, HSPB1, CH60, RCN2, RS27A, TBA1C and TBB6, and one common protein that bound to both GFP-NS3 and GFP-NS5 - S61A1 (also

known as transport protein Sec61 subunit alpha isoform A, will be discussed further in section 4.3). Interestingly, among the host proteins that were common to GFP-NS3 in this study and Carpp's study, some of the proteins were enriched in protein folding and unfolded protein response, which suggests that the unfolded protein response pathway plays an important role in viral replication (Fink *et al.*, 2007; Paradkar *et al.*, 2011b; Thepparit *et al.*, 2013; Umareddy *et al.*, 2007).

Table 3-3: List of human host proteins that were identified by us to co-elute with either DENV1 or 2 GFP-NS3 or GFP-NS5 proteins, and were also previously reported to be interacting with flavivirus NS3 and/or NS5 proteins. Host proteins were identified by Scaffold Proteome software (version 4.3.4) with the following parameters: peptide thresholds: 95.0% minimum, protein thresholds: 99.0% minimum and at least two exclusive unique peptide count. GFP and mock were excluded from the table as they were negative for any host protein. GN=Gene Name, PE=Protein Existence (the numerical value describing the evidence for the existence of the protein), SV=Sequence Version (the version number of the sequence). [1]from liver, brain, spleen and bronchial epithelia; [2]from peripheral blood leukocytes; [3]from liver; [4]from brain; *transfection of viral protein expression plasmid, followed by infection; ^transfection of viral protein expression plasmid.

Protein name	Uniprot ID (Human)	Peptide count of host protein that DENV protein bound in this study				Method	Cell type	Viral protein published	Reference
		GFP-NS3		GFP-NS5					
		D1	D2	D1	D2				
Heat shock protein HSP 90-alpha GN=HSP90AA1 PE=1 SV=5	HS90A	0	0	6	0	SILAC, co-IP and LC-MS/MS	HEK293T*	D2 NS5	(Carpp *et al.*, 2014)
Mitochondrial import inner membrane translocase subunit TIM50 GN=TIMM50 PE=1 SV=2	TIM50	0	0	2	0				
Apoptosis-inducing factor 1, mitochondrial GN=AIFM1 PE=1 SV=1	AIFM1	5	0	5	7				
Dolichol-phosphate mannosyltransferase GN=DPM1 PE=1 SV=1	DPM1	0	0	0	4				
Heat shock protein HSP 90-beta GN=HSP90AB1 PE=1 SV=4	HS90B	3	3	7	4	SILAC, co-IP and LC-MS/MS	HEK293T*	D2 NS3	(Carpp *et al.*, 2014)
						Y2H	Human cDNA library[1]	KUNV NS3 helicase	(Le Breton *et al.*, 2011)
							Human cDNA library[2]	D2 NS3	(Mairiang *et al.*, 2013)
Heat shock 70 kDa protein 1A/1B GN=HSPA1A PE=1 SV=5	HSP71	14	9	16	14	SILAC, co-IP and LC-MS/MS	HEK293T*	D2 NS3	(Carpp *et al.*, 2014)
						TAP and LC-MS/MS	HEK293T^	JEV NS5 RdRP aa406-905	(Ye *et al.*, 2013)
Heat shock cognate 71 kDa protein GN=HSPA8 PE=1 SV=1	HSP7C	16	9	18	17	SILAC, co-IP and LC-MS/MS	HEK293T*	D2 NS3	(Carpp *et al.*, 2014)
Heat shock protein beta-1 GN=HSPB1 PE=1 SV=2	HSPB1	2	0	0	3				
60 kDa heat shock protein, mitochondrial GN=HSPD1 PE=1 SV=2	CH60	10	0	4	9				
Reticulocalbin-2 GN=RCN2 PE=1 SV=1	RCN2	2	0	3	10				
Ubiquitin-40S ribosomal protein S27a GN=RPS27A PE=1 SV=2	RS27A	6	0	8	6				
Tubulin alpha-1C chain GN=TUBA1C PE=1 SV=1	TBA1C	3	0	3	3				
Tubulin beta-6 chain GN=TUBB6 PE=1 SV=1	TBB6	3	5	4	2				
Protein transport protein Sec61 subunit alpha isoform 1 GN=SEC61A1 PE=1 SV=2	S61A1	2	0	0	2	SILAC, co-IP and LC-MS/MS	HEK293T*	D2 NS3 and NS5	(Carpp *et al.*, 2014)
Interleukin enhancer-binding factor 3 GN=ILF3 PE=1 SV=3	ILF3	25	0	19	17	Y2H	Human cDNA library[1]	D2 NS3 helicase	(Le Breton *et al.*, 2011)

Lupus La protein GN=SSB PE=1 SV=2	LA	5	0	5	6	Co-IP and Western blot	U937 infected cell lysate	D4 NS3 and NS5	(Garcia-Montalvo *et al.*, 2004a)
40S ribosomal protein S20 GN=RPS20 PE=1 SV=1	RS20	5	0	4	0	Y2H	Human cDNA library[1]	JEV NS3 helicase	(Le Breton *et al.*, 2011)
Polypyrimidine tract-binding protein 1 GN=PTBP1 PE=1 SV=1	PTBP1	8	0	11	7	Y2H	Human cDNA library[3]	D2 NS3 helicase aa463-617	(Khadka *et al.*, 2011)
Matrin-3 GN=MATR3 PE=1 SV=2	MATR3	19	0	18	10	Y2H	Human cDNA library[1]	D1 NS5 RdRP	(Le Breton *et al.*, 2011)
							Human cDNA library[3]	D2 NS5 RdRP aa261-901	(Khadka *et al.*, 2011)
Signal transducer and activator of transcription 2 GN=STAT2 PE=1 SV=1	STAT2	0	0	8	9	Y2H	Human cDNA library[1]	D2 NS5	(Le Breton *et al.*, 2011)
							Human cDNA library[3]	D2 NS5 RdRP aa261-901	(Khadka *et al.*, 2011)
						Pulldown assay and western blot	K562 cells and HEK293T	D2 NS5	(Ashour *et al.*, 2009; Mazzon *et al.*, 2009)
ATP-dependent RNA helicase DDX3X GN=DDX3X PE=1 SV=3	DDX3X	12	0	21	21	Y2H	Human cDNA library[3]	D2 NS3 helicase aa463-617	(Khadka *et al.*, 2011)
						GST-pulldown assay	*E. coli*. recombinant protein	JEV NS3 and NS5	(Li *et al.*, 2014a)
Probable ATP-dependent RNA helicase DDX5 GN=DDX5 PE=1 SV=1	DDX5	15	0	18	22	GST-pulldown assay	*E. coli*. recombinant protein	JEV NS3 and NS5	(Li *et al.*, 2013)
ELKS/Rab6-interacting/CAST family member 1 GN=ERC1 PE=1 SV=1	RB6I2	0	0	26	33	Y2H	Human cDNA library[3]	D2 NS5 RdRP aa1-368	(Khadka *et al.*, 2011)
Heterogeneous nuclear ribonucleoprotein H3 GN=HNRNPH3 PE=1 SV=2	HNRH3	4	0	2	0	Y2H	Human cDNA library[1]	ALKV NS5 MTase	(Le Breton *et al.*, 2011)
Heterogeneous nuclear ribonucleoprotein F GN=HNRNPF PE=1 SV=3	HNRPF	6	0	8	8			TBEV NS5 MTase	
Nucleolar complex protein 2 homolog GN=NOC2L PE=1 SV=3	NOC2L	0	0	6	0			KUNV NS5 MTase	
Vimentin GN=VIM PE=1 SV=4	VIME	13	2	0	13	Y2H	Human cDNA libray[1]	ALKV and TBEV NS5 MTase	(Le Breton *et al.*, 2011)
						TAP and LC-MS/MS	Huh-7 stably expressing D2 NS4A-TAP protein	D2 NS4A	(Teo & Chu, 2014)
						co-IP, 2D-PAGE and LC-MS/MS	EA.hy926 (human umbilical vein cell line)	D2 NS1	(Kanlaya *et al.*, 2010)
Protein FAM192A GN=FAM192A PE=1 SV=1	F192A	0	0	2	0	Y2H	Human cDNA library[2]	D2 NS5	(Mairiang *et al.*, 2013)
DnaJ homolog subfamily A member 1 GN=DNAJA1 PE=1 SV=2	DNJA1	2	0	6	14	Y2H	Mouse cDNA library[4]	JEV NS5	(Wang *et al.*, 2011)

Lastly, when we compared our western blot data and MS data, we could demonstrate that STAT2, MATR3, DDX5 and DDX3X that were detected to bind to both DENV1 and 2 GFP-NS5 by western blot were also identified by MS with unique peptide count of more than 5 for each protein (Table 3-4). It is also surprising to note that STAT2 that was not detected by western blot to co-elute with GFP-NS3 was also not detected by MS, and this further confirmed that binding of STAT2 to NS5 is indeed unique to NS5. Taken together, through extensive (and not yet exhaustive) intra- and inter-comparisons of datasets, we were convinced that the dataset is of good quality for further studies.

Table 3-4: MS unique peptide count of proteins that co-eluted with DENV1 and 2 GFP-NS3 and GFP-NS5.

MS peptide count	GFP	GFP D1NS5	GFP D2NS5	GFP D1NS3	GFP D2NS3	mock
STAT2	0	8	9	0	0	0
MATR3	0	18	10	19	0	0
DDX5	0	18	22	15	0	0
DDX3X	0	21	21	12	0	0
GFP	12	10	8	15	13	0

3.3.4 Enriched features of GFP-NS3 and GFP-NS5 interaction networks

Due to lack of time to select and identify in detail unique host targets from our co-IP study, further bioinformatics characterization was carried out by generating GFP-NS3 and GFP-NS5 interaction networks with GeneMANIA (Warde-Farley *et al.*, 2010) to identify significantly enriched/over-represented Gene Ontology (GO) annotations (Table A-2 to A8). As expected, GFP-NS3 and GFP-NS5 interaction networks were enriched by features that were associated with [1] already known functions of NS3 and NS5 and [2] possible new/unknown functions of NS3 and NS5.

3.3.4.1 Enriched features of interactors that are common to both GFP-NS3 and GFP-NS5

Among 405 human host proteins, 110 proteins were identified to be interacting with both GFP-NS3 and GFP-NS5 proteins (Figure 3-23). Submission of these 110 proteins for GO analysis revealed enriched features that were associated with already known functions of NS3 and NS5, namely RNA binding, viral transcription and viral life cycle (Table A5). Therefore, it is likely that among these host proteins, some may be the key proteins that are needed for RNA replication. In order to provide evidence for this idea, we did manual literature curation and we managed to identify 13 out of 110 proteins that were previously reported to be interacting with flavivirus RNA (Table 3-5). Among the 10 proteins, 5 proteins, namely G3BP1, G3BP2, UBP10, CAPR1 and CNBP that were previously reported to bind to DENV2 5' and 3' UTRs (Ward *et al.*, 2011) were identified to co-elute with both GFP-NS3 and GFP-NS5 in our study. On top of that, PTBP1 that was identified to bind to DENV2 NS4A, and 5' and 3'UTR of DENV2 RNA for efficient virus particle production also co-eluted with

both GFP-NS3 and GFP-NS5 (Anwar *et al.*, 2009). Similarly, LA that was reported to NS3 and NS5, and also 5' and 3'UTR of DENV4 RNA also co-eluted with GFP-NS3 and GFP-NS5 is this study (Garcia-Montalvo *et al.*, 2004b). Taken together, these findings indicate that NS3 and NS5 interact with RNA-binding proteins or proteins that are involved in RNA-related processes in viral life cycle and hence, suggesting the potential involvement of these host proteins in RC, which is consistent with early studies in flavivirus replication that hypothesized the influence of host proteins in RC (Lindenbach & Rice, 2003; Westaway *et al.*, 2003).

Apart from the proteins that are associated with known functions of NS3 and NS5, we also identified some additional proteins that have not been reported to bind to NS3 or NS5 (Table A5) and thus, suggesting that these proteins may have important role in virus life cycle. Specifically, we observed proteins that are related RNA processing machinery, host translation pathway, and cytoplasm stress granule, which collectively suggests that NS3 and NS5 may recruit host RNA processing and translation machineries for viral RNA and protein synthesis (Pastorino *et al.*, 2009). The implication of these enriched functional features among the identified host proteins in virus life cycle will be discussed in sections 4-3.

Table 3-5: List of human host proteins that were identified by us to co-elute with either DENV1 or 2 GFP-NS3 or GFP-NS5 protein, and were also previously reported to be interacting with 5' or 3' end of flavivirus genome. Host proteins were identified by Scaffold Proteome software (version 4.3.4) with the following parameters: peptide thresholds: 95.0% minimum, protein thresholds: 99.0% minimum and at least two exclusive unique peptide count. GFP and mock were excluded from the table as they were negative for any host protein. GN=Gene Name, PE=Protein Existence (the numerical value describing the evidence for the existence of the protein), SV=Sequence Version (the version number of the sequence).

Protein name	Uniprot ID (Human)	Peptide count of host protein that DENV protein bound in this study				Method	Cell type	viral RNA sequence	Reference
		GFP-NS3		GFP-NS5					
		D1	D2	D1	D2				
Lupus La protein GN=SSB PE=1 SV=2	LA	5	0	5	6	UV-induced cross-linking and SDS-PAGE	C6/36 infected cell extracts	DENV4 genomic 3'UTR (384 nts)	(De Nova-Ocampo *et al.*, 2002)
							U937 (human monocytic cell line) infected cell extracts	DENV4 antigenomic 3'UTR (101 nts)	(Yocupicio-Monroy *et al.*, 2003)
								DENV4 genomic 5'UTR (101nts) and 3'UTR (384 nts)	(Garcia-Montalvo *et al.*, 2004b)
						UV-induced cross-linking and EMSA	*E. coli*. recombinant protein	JEV genomic 5'UTR (95 nt) and 3' SL	(Vashist *et al.*, 2009; Vashist *et al.*, 2011)
Polypyrimidine tract-binding protein 1 GN=PTBP1 PE=1 SV=1	PTBP1	8	0	11	7	UV-induced cross-linking and SDS-PAGE	C6/36 infected cell extracts	DENV4 genomic 3'UTR (384 nts)	(De Nova-Ocampo *et al.*, 2002)
						IP and real-time RT-PCR	Huh7 infected cell extracts	DENV2 5' and 3'UTR	(Anwar *et al.*, 2009)
Ras GTPase-activating protein-binding protein 1 GN=G3BP1 PE=1 SV=1	G3BP1	10	0	15	18	SILAC, RNA affinity chromatography and LC-MS/MS	HeLa cells	DENV2 genomic 5'UTR (172 nts) and 3'UTR (483 nts)	(Ward *et al.*, 2011)
Ras GTPase-activating protein-binding protein 2 GN=G3BP2 PE=1 SV=2	G3BP2	9	0	9	9				
Ubiquitin carboxyl-terminal hydrolase 10 GN=USP10 PE=1 SV=2	UBP10	6	0	6	13				
Caprin-1 GN=CAPRIN1 PE=1 SV=2	CAPR1	10	0	5	8				
Cellular nucleic acid-binding protein NBP PE=1 SV=1	CNBP	5	0	2	2				
Nuclease-sensitive element-binding protein 1 GN=YBX1 PE=1 SV=3	YBOX1	7	0	6	5	RNA affinity chromatography and LC-MS/MS	BHK-21	DENV2 genomic 3'UTR (482 nts)	(Paranjape & Harris, 2007)
Interleukin enhancer-binding factor 3 GN=ILF3 PE=1 SV=3	ILF3	25	0	19	17	RNA affinity chromatography and LC-MS/MS	K562	JEV 3'SL	(Gomila *et al.*, 2011)
Interleukin enhancer-binding factor 2 GN=ILF2 PE=1 SV=2	ILF2	11	0	11	11				
Polyadenylate-binding protein 1 GN=PABPC1 PE=1 SV=2	PABP1	11	0	3	6	Electrophoresis mobility shift assay	*E. coli*. recombinant protein	DENV2 genomic 3'UTR (451nts)	(Polacek *et al.*, 2009)
Polyadenylate-binding protein 3 GN=PABPC3 PE=1 SV=2	PABP3	0	0	2	4				
Polyadenylate-binding protein 4 GN=PABPC4 PE=1 SV=1	PABP4	18	0	10	11				

3.3.4.2 Enriched features of interactors that are unique to DENV1 and 2 GFP-NS5

As the purpose of the study at the outset was to identify any differences in the interaction of DENV1 and 2 GFP-NS5 with host factors to account for their differences in subcellular localization during the infection cycle, the host proteins that co-eluted with DENV1 and 2 GFP-NS5 were analysed separately by interaction networks (Table A3 and 4). Not surprisingly, the nucleocytoplasmic transport was one of the features that was significantly enriched (q-value $\leq 10^4$), which is consistent with our finding that DENV1 and 2 NS5 have the ability to recruit the host nuclear transport machinery for them to traffic into the nucleus; in contrast, this feature was not found in GFP-NS3 interaction network because NS3 is not known to be transported to the nucleus and only associated with replication that occurs in the cytoplasm, however, it is worth noting that we observed DENV1 GFP-NS3 binding to importin-α1 whereas in Carpp *et al*'s study, they observed DENV2 GFP-NS3 binding to importin-4 (gene name: IPO4, 119 kDa); the implication of this finding is unknown and remains to be determined.

From the dataset, we can see DENV1 and 2 GFP-NS5 binding to both importin-α1 and importin-α5 proteins (correspond to KPNA2 and KNPA1 genes, respectively, Table 3-6) which supports the AlphaScreen data in section 3.2.2 that both DENV1 and 2 NS5 can bind to importin-α1 despite the differences in nuclear localization. On the contrary, importin-α3 only bound to DENV1 GFP-NS5 whereas importin-α7 only bound to DENV2 GFP-NS5; it is unclear to us at the moment why DENV1 and 2 NS5 bind preferentially to certain importin-α isoform but it is possible that within the

context of a cell, different import cargoes may compete for a particular importin-α isoform that favor its entry into the nucleus (Kohler *et al.*, 1999) because of the specificity of NLS-importin-α interaction that is dependent on both the NLS and protein context (Gabriel *et al.*, 2011) and the differences in the binding strength of each importin-α isoform to different NLSs and the strength of auto-inhibitory activity on its NLS-binding pocket that is mediated by its importin-β1 binding domain (Pumroy & Cingolani, 2014; Pumroy *et al.*, 2015). It is worth mentioning that in recent years, importin-α3 and importin-α7 are found to be important in mediating the host tropism of avian and mammalian influenza A viruses (Gabriel *et al.*, 2011). The authors found out that for efficient influenza virus replication that occurs in the nucleus, avian influenza virus requires importin-α3 for its polymerase subunit (PB2) and nucleoprotein (NP) to traffic into the nucleus whereas mammalian influenza virus requires importin-α7. However, during avian-mammalian adaptation, the avian virus can switch to using importin-α7 to promote interspecies transmission and also, enhance pathogenicity (Gabriel *et al.*, 2011). Interestingly, mutation in PB2 was identified and may be implicated in promoting the switch to importin-α7 usage (Gabriel *et al.*, 2011). In the context of DENV, the virus is known to replicate in both mosquito and human, and it has also been demonstrated that the localization patterns for DENV1-4 NS5 are similar in both mosquito and human cells (Hannemann *et al.*, 2013) and hence, it will be interesting to study if particular importin-α isoform dependency is also observed in DENV NS5 protein in both mosquito and human and is there an interplay between viral, mosquito and human factors in this manner in mediating DENV pathogenesis.

Table 3-6: List of importin-α isoforms that bind to DENV1 and 2 GFP-NS3 and GFP-NS5. The peptide count reflects the number of unique peptides that is associated with the identified protein.

Protein	Gene name	Molecular Weight	Peptide count					
			GFP	GFP D1NS3	GFP D2NS3	GFP D1NS5	GFP D2NS5	mock
importin-α1	KNPA2	58 kDa	0	4	0	6	6	0
importin-α5	KPNA1	60 kDa	0	0	0	4	4	0
importin-α7	KNPA6	60 kDa	0	0	0	0	2	0
importin-α3	KNPA4	58 kDa	0	0	0	6	0	0

When we further dissected the dataset, we identified 71 proteins to be unique to DENV1 GFP-NS5 and 41 proteins to be unique to DENV2 GFP-NS5. Submission of these host proteins for GO analysis did not readily reveal any protein that was specifically associated with either the nucleus or cytoplasm and hence, we submitted the host proteins to GeneMANIA (Warde-Farley *et al.*, 2010) to construct interaction networks for DENV1 and 2 GFP-NS5 separately for identification of new potential roles for NS5 (Figure 3-24). To our surprise, no common GO feature was observed between the two interaction networks; the interaction network that was unique to DENV1 GFP-NS5 was enriched by biological processes that were related to RNA processing and splicing, which possibly occur in the nucleus (Figure 3-24A), whereas the one that was unique to DENV2 GFP-NS5 was enriched by component and biological process that were related to COPI vesicle coat and Golgi transport, which take place in the cytoplasm (denoted by red dot in Figure 3-24B). This seems to suggest that DENV1 and 2 NS5 may have slight differences in their roles in DENV life cycle, even though they share a huge group of proteins that are common to both in this study (218 host proteins, Figure 3-23) and this idea is indirectly supported by a recent study by Carpp and coworkers (Carpp *et al.*, 2014). They have demonstrated features like retrograde vesicle-mediated transport, Golgi to ER, COPI vesicle coat,

COPI-coated vesicle membrane, COPI-coated vesicle and etc. (denoted by red dot in Figure 3-24C) being enriched in their DENV2 GFP-NS5 interaction network and these features were also observed in our DENV2 GFP-NS5 interaction network but not in DENV1 GFP-NS5 interaction network. Furthermore, Carpp's DENV2 GFP-NS5 interaction network was established in the context of DENV2 infected cells, which further strengthened the possibility that the viral-host protein-protein interactions that we captured in our study were likely to be present in DENV infected cells. Taken together, we have demonstrated the reliability of the dataset and also provided additional evidence for previously identified interactions. The findings from this study will be used to identify new host factors and pathways/processes that are required for DENV replication and pathogenesis for further investigation.

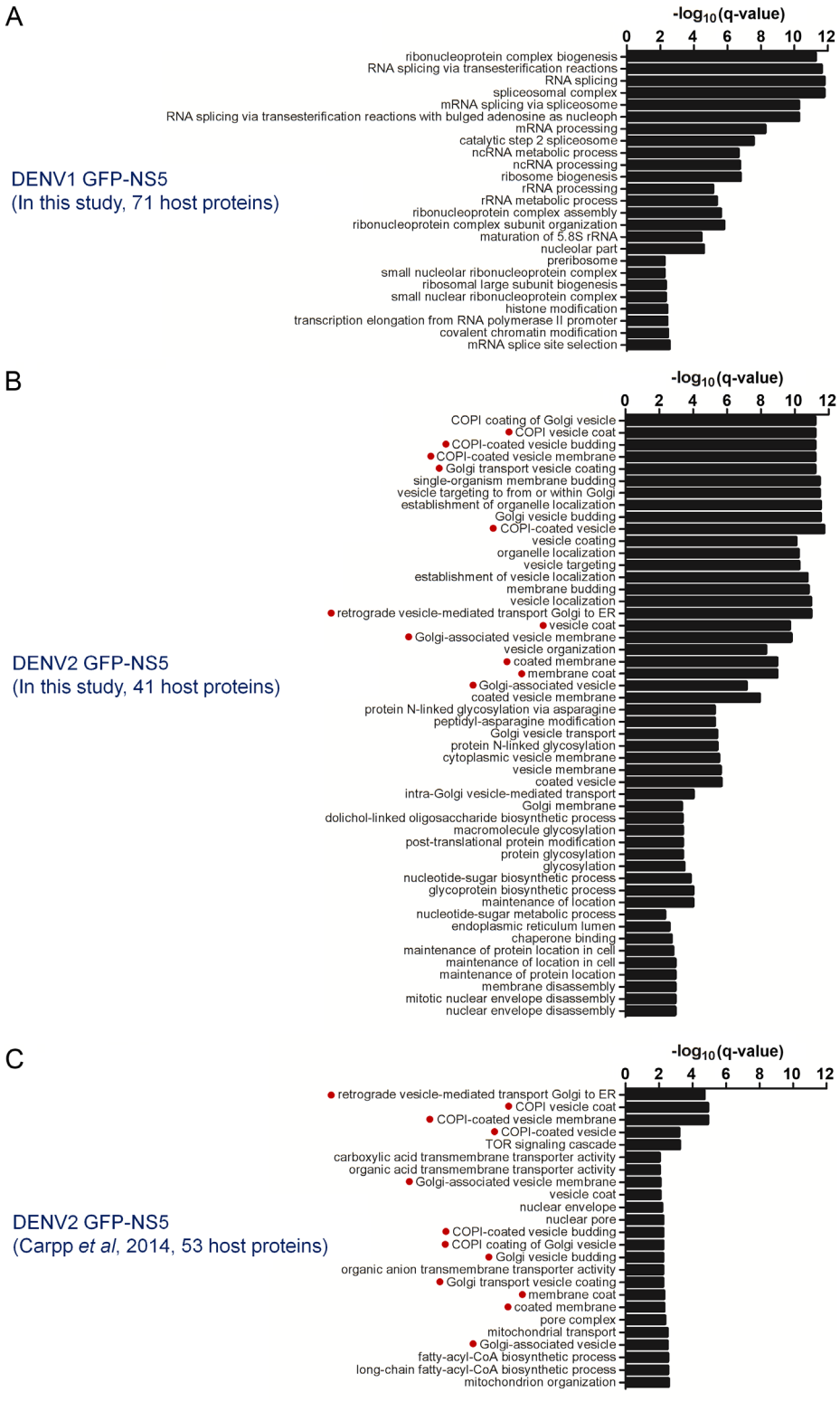

Figure 3-24: GO functional enrichment analysis of human host proteins that were identified to co-elute with either DENV1 or 2 GFP-NS5 by us and (Carpp *et al.*, 2014). GO terms that are associated with (A) DENV1 GFP-NS5 (71 proteins, in this study), (B) DENV2 GFP-NS5 (41 proteins, in this study) and (C) DENV2 GFP-NS5 (53 proteins, (Carpp *et al.*, 2014)) interaction networks are listed in graphs. GO terms that are common between groups are denoted by red dots. The Benjamini-Hochberg procedure was used to calculate the q-value (x-axis) of each enriched GO feature. For each enriched GO feature that is associated with the generated interaction network, the number of proteins in the interaction network listed in that group, as well as the number of total proteins in the Homo sapiens proteome associated with the same GO feature.

3.4 Characterizing a newly discovered C-terminal NLS of DENV2 NS5 and studying its importance in virus replication

3.4.1 DENV1 NS5 residues 709-900 contributes to its cytoplasmic retention

In section 3.2.2, we identified the CRS of DENV1 NS5 to reside either within residues 1-319 or 406-900 and therefore, in this study, we intended to further narrow down the region on DENV1 NS5 to identify the CRS sequence by adopting the same gene shuffling approach that we used in section 3.3.2. To do this, we exchanged gene fragment between DENV1 and 2 NS5 via overlap extension PCR based on the basis of functional domains that each gene fragment encodes; NS5 has two functional domains: MTase (residues 1-272) and RdRP (residues 273-900), and a previously classified NLS region (residues 320-405). Therefore, we exchanged gene segments that correspond to residues 1-272, 1-319 and 1-405 between DENV1 and 2 NS5 to generate GFP-NS5 plasmids that encode full-length NS5 protein for transfection (schematic representation of constructs in Figure 3-25).

The newly constructed plasmids were used to transfect Vero cells, and cells were fixed at 24 hours post-transfection for staining by anti-GFP (green) and anti-NS5 (5R3, red in Figure 3-25). The GFP-NS5 fusion constructs $D1_{1-272}D2_{273-900}$ and $D1_{1-319}D2_{320-900}$ were localized to the nucleus and this rules out the possibility that the DENV1 NS5 CRS is within the MTase domain. Similarly, GFP-NS5 fusion construct $D1_{1-405}D2_{406-900}$ was also localized to the nucleus and this implies that DENV1 NS5 CRS is not within the linker region (residues 320-405) and it is in agreement with Figure 3-20 that DENV1 α/βNLS is functional. On the contrary, the GFP-NS5 fusion

construct $D2_{1-272}D1_{273-900}$ was localized to the cytoplasm, suggesting that DENV1 NS5 CRS resides within the RdRP domain. Likewise, the GFP-NS5 fusion constructs $D2_{1-319}D1_{320-900}$ and $D2_{1-405}D1_{406-900}$ were also localized to the cytoplasm and this provided further support that DENV1 NS5 CRS is within the C-terminal end of RdRP domain, from residues 406-900.

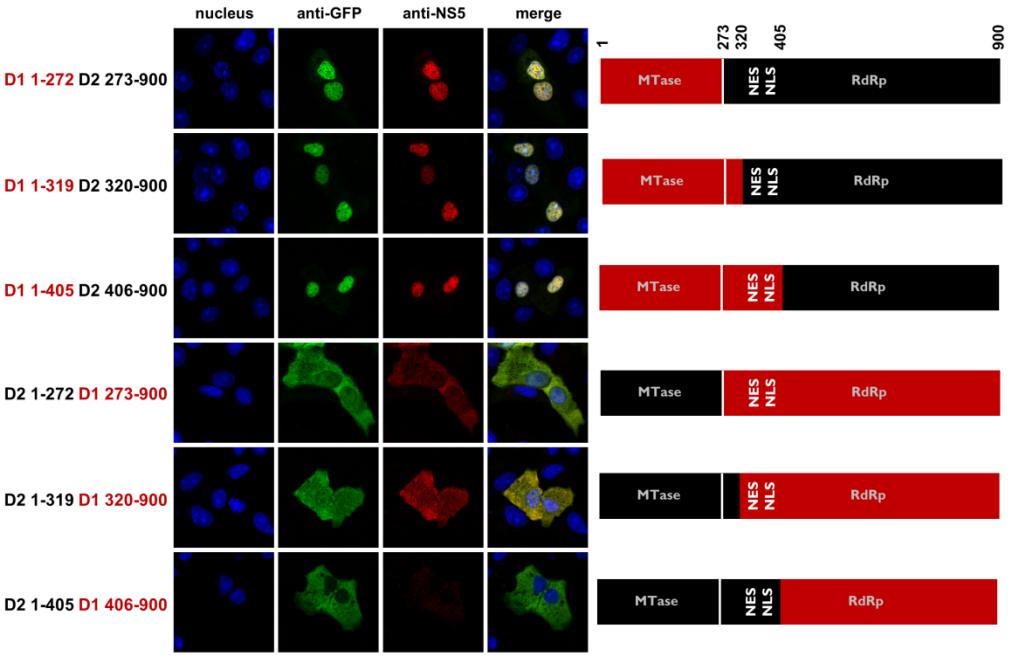

Figure 3-25: DENV1 NS5 residues 406-900 contributes to its cytoplasmic retention. Domain-swapping experiment between DENV1 and 2 GFP-NS5 was performed to identify region on DENV1 NS5 that is responsible for cytoplasmic retention. Exchanges of gene segments that encode functional domains (residues 1-272 is MTase domain, residues 273-900 is RdRP domain, and residues 320-405, which is previously known as the linker region, has been identified to an integral part of RdRP domain) between DENV1 and 2 NS5 were generated by overlap extension PCR. The plasmids were transfected into Vero cells and fixed 24 hours post-transfection. The cells were stained and images were captured as described in Figure 3-16. Figure legends were as described in Figure 3-20.

To further narrow down the region within residues 406-900 of DENV1 NS5 to identify the CRS, we replaced the corresponding gene fragment of DENV2 NS5 with DENV1 sequence via overlap extension PCR based on the structural motifs (ie. α-helices and β-strands) of the protein segment that is encoded by NS5. With DENV3 NS5 RdRP (PDB: 2J7U (Yap *et al.*, 2007) and JEV NS5 full-length 4K6M (Lu & Gong, 2013) crystal structures as templates, we defined the following regions of DENV2 NS5, namely residues 363-394, 395-497, 509-537, 543-576, 627-658, 627-900 and 709-900, for replacement (schematic representation of constructs in Figure 3-26). Transfection of these GFP-NS5 plasmids into Vero cells showed that $D2_{1-362}D1_{363-394}D2_{395-900}$, $D2_{1-394}D1_{395-497}D2_{498-900}$, $D2_{1-508}D1_{509-537}D2_{538-900}$, $D2_{1-542}D1_{543-576}D2_{577-900}$ and $D2_{1-626}D1_{627-658}D2_{659-900}$ were in nucleus and this implies that DENV1 NS5 CRS is not within the exchanged regions. On the other hand, the GFP-NS5 fusion constructs $D2_{1-626}D1_{627-900}$ and $D2_{1-708}D1_{709-900}$ were in the cytoplasm and this collectively suggested that DENV1 NS5 CRS probably resides within the last 190 amino acids of DENV1 NS5 (Figure 3-26).

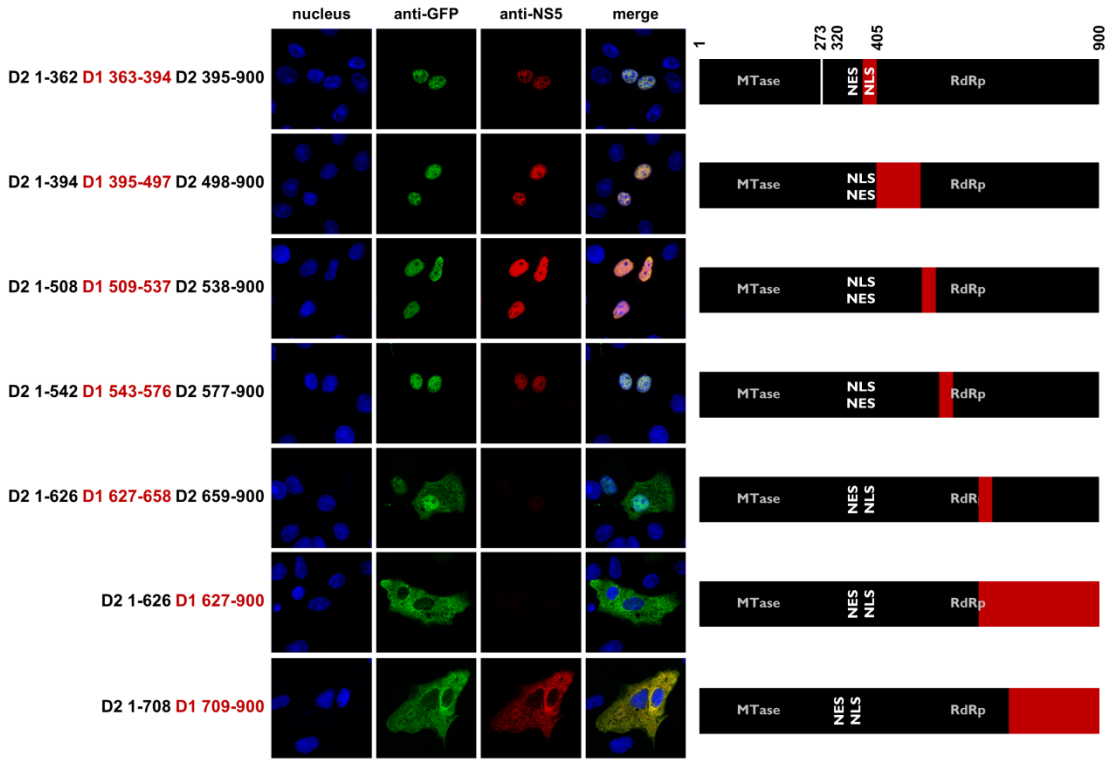

Figure 3-26: DENV1 NS5 residues 709-900 contributes to cytoplasmic retention. Motif-swapping experiment between DENV1 and 2 GFP-NS5 was performed to identify region on DENV1 NS5 that is responsible for cytoplasmic retention. Gene segments within residues 406-900 that encode protein segment of particular structural motif (ie. α-helices and β-strands) of DENV2 NS5 were replaced by corresponding DENV1 NS5 sequence by overlap extension PCR. The plasmids were transfected into Vero cells and fixed 24 hours post-transfection. The cells were stained and images were captured as described in Figure 3-16. Figure legends were as described in Figure 3-20.

3.4.2 DENV2 NS5 may have a monopartite NLS that resides at C-terminal end

Inspection of the last 190 amino acid residues of DENV1 and 2 NS5, revealed a striking sequence difference in the last 10 residues; in fact, this region is also very different for DENV3 and 4 NS5. Closer examination of this region of DENV2 and 3 NS5 revealed that the sequence is rich in glutamic acid (^{892}EEEE for DENV2 and ^{892}EEESE for DENV3). Therefore, we hypothesized that this region of the different serotypes of NS5 may interact with different unknown host proteins that eventually, fine tune the subcellular localization of the respective NS5's in both infected and

transfected cells. We replaced residues 890-900 of DENV2 NS5 with residues 890-900 of DENV1, 3 and 4 respectively via conventional PCR and transfected the plasmids into Vero cells (Figure 3-27). To our surprise, DENV2 NS5 with residues 890-900 of DENV1 and 3 was mostly nuclear-localized whereas DENV2 NS5 with residues 890-900 of DENV4 was predominantly in the cytoplasm. Upon analysis of this region in greater details, it turned out that replacing this region with DENV4 sequence might disrupt a potential NLS sequence that is in DENV2 NS5 and somehow, replacing this region with DENV1 sequence retained the minimum NLS sequence for DENV2 NS5 nuclear localization. Interestingly, replacing the region with DENV3 sequence retains DENV2 NS5 nuclear-localizing ability (see Figure 3-28A for sequence alignment).

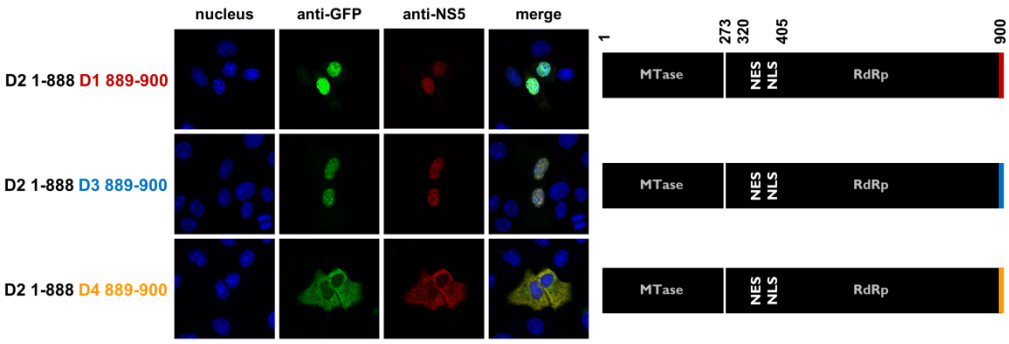

Figure 3-27: Residues 890-900 of DENV4 NS5, but not DENV1 NS5 affects nuclear localizing ability of DENV2 NS5. C-terminal-swapping experiment between DENV1-4 GFP-NS5 was performed to identify region on DENV1 NS5 that is responsible for cytoplasmic retention. Residues 890-900 of DENV2 NS5 were replaced with residues 890-900 of DENV1 (red), 3 (blue) and 4 (orange) respectively via conventional PCR. The plasmids were transfected into Vero cells and fixed 24 hours post-transfection. The cells were stained and images were captured as described in Figure 3-16.

3.4.3 DENV2 NS5 residues 883-900 can target an unrelated protein into the nucleus

To determine if the C-terminal end of DENV2 NS5 indeed contains a monopartite NLS sequence, we first did a sequence alignment of DENV1-4 NS5 residues 883-900 and compared it with the general consensus sequences of classical NLS (Figure 3-28A). This region of DENV1, 2 and 3 NS5 contains sequence of basic residues that resembles classical monopartite NLS. On the contrary, this region of DENV4 NS5 does not contain sequence that resembles classical monopartite NLS.

We next submitted NS5 protein sequences of DENV1-4 to online tool: cNLS Mapper (http://nls-mapper.iab.keio.ac.jp/cgi-bin/NLS_Mapper_form.cgi) that can be used to predict classical NLSs that are specific to importin-α/β pathway through a position-specific scoring matrix that was developed based on experimental data (Kosugi *et al.*, 2009a; Kosugi *et al.*, 2009b). Interestingly, cNLS Mapper supported the finding that a monopartite NLS is likely to be present at the C-terminal end of both DENV2 and 3 NS5; it also supported the finding that a monopartite NLS is unlikely to be present at the C-terminal end of DENV1 and 4 NS5 (Table 3-7).

Table 3-7: NLS search results from cNLS Mapper. The predicted monopartite and bipartite NLSs sequences, as well as their scores are listed in the table; the higher the score, the higher the NLS activity. The scoring is as follows: 1-2, localized to the cytoplasm; 3-5, localized to both nucleus and cytoplasm; 7-8, partially localized to the nucleus; 8-10, exclusively localized to nucleus (Kosugi *et al.*, 2009a; Kosugi *et al.*, 2009b). "-" indicates not found' "N.A." indicates not applicable. The basic residues are in red and bold.

Serotype of NS5	Predicted monopartite NLS	Score	Predicted bipartite NLS	Score
DENV1	^{385}S**R**N**KK**P**R**ICT**R**EEF	6	-	N.A.
DENV2	^{882}YMPSM**KR**F**RR**EEE	7.5	-	N.A.
DENV3	^{385}G**R**N**KR**P**R**LCT**R**EEF	8.5	^{382}**R**TLG**R**N**KR**P**R**LCT**R**EEFT**KK**V**R**TN	7.7
	^{882}YMPSM**KR**F**RK**EEE	6.5	-	N.A.
DENV4	-	N.A.	-	N.A.

To demonstrate experimentally that residues 883-900 of DENV2 NS5 indeed contains a monopartite NLS that can target an unrelated protein into the nucleus, we fused this region, as well as the corresponding region of DENV1 and 4 NS5, to the C-terminal of a tandem GFP gene construct (2×GFP), to encode a protein >45 kDa that could be transported into the nucleus actively by importin-α/β pathway, and not by passive diffusion (Figure 3-28A). We also fused SV40 NLS sequence to 2×GFP construct to act as positive control for monopartite NLS. These plasmids were transfected in Vero cells and cells were fixed and stained 24 hours post-transfection for CLSM. Results for nuclear to cytoplasmic fluorescence ratio ($F_{n/c}$) (Figure 3-28C) were determined from image analysis of digitized CLSM images (such as those in Figure 3-28B) by ImageJ software (Collins, 2007) demonstrated that DENV2 NS5 residues 883-900 ($F_{n/c}$ = 5.06 ± 0.22, refer to Table 3-8 for pooled data) was capable of driving an unrelated protein into the nucleus, just like the monopartite SV40 NLS ($F_{n/c}$ = 6.97 ± 0.37), whereas the corresponding region of DENV4 NS5 did not ($F_{n/c}$ = 0.63 ± 0.02), just like the negative control 2×GFP ($F_{n/c}$ = 0.81 ± 0.03). Interestingly, this corresponding region of DENV1 NS5 caused 2×GFP to be distributed equally in both nucleus and cytoplasm ($F_{n/c}$ = 1.03 ± 0.06), indicating that DENV1 NS5 residues 883-900 may have the ability to target an unrelated protein to the nucleus, albeit slower or less efficient that DENV2 NS5.

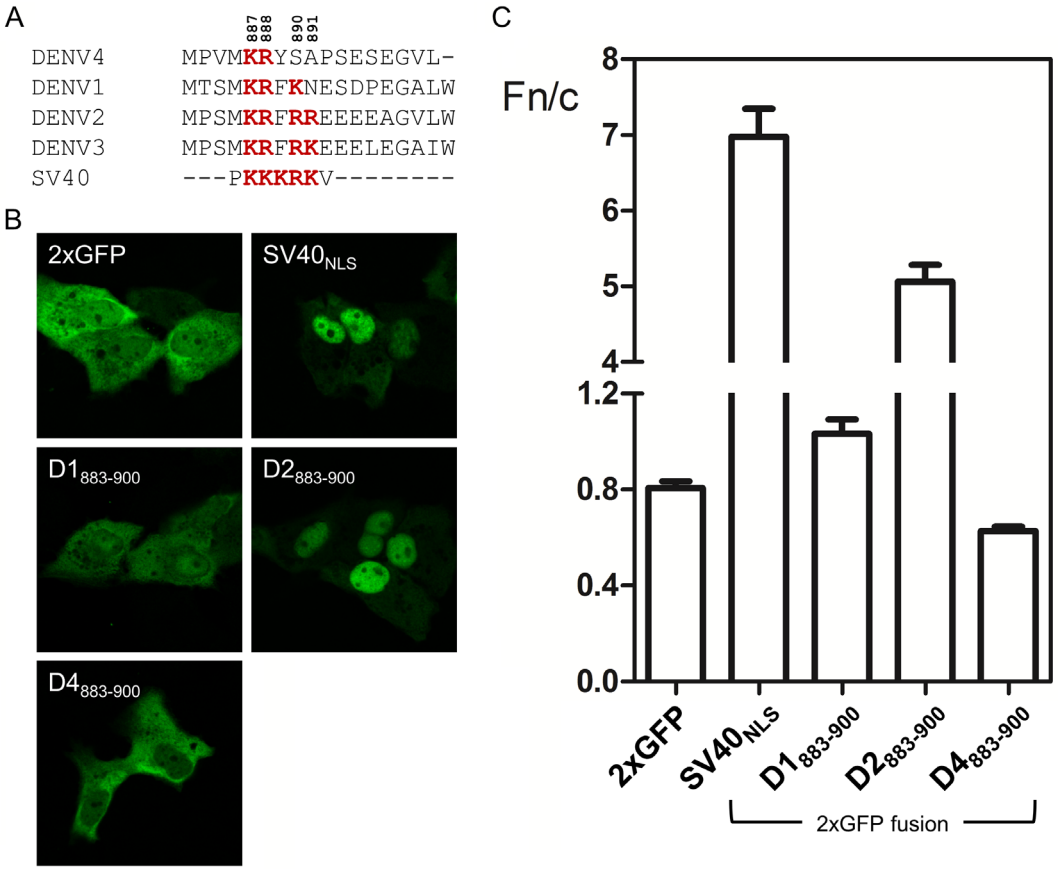

Figure 3-28: Fusion of residues 883-900 of DENV2 NS5 to 2×GFP targets 2×GFP to the nucleus. (A) Sequence alignment of residues 883-900 of DENV1-4 NS5 with SV40 NLS, which is a monopartite NLS. The virus sequences and their GenBank accession numbers are as described in Figure 3-4C. (B) Vero cells were transfected with either 2×GFP or 2×GFP-fusion plasmids encoding residues 883-900 of DENV1, 2 and 4 NS5, and fixed at 24h post-transfection. 2×GFP-fusion plasmid encoding SV40 NLS was included as a positive control for monopartite NLS. Anti-GFP (ab6556 IgG, 1:1000; green) antibody was used for immunostaining. Images were captured by CLSM using a Zeiss LSM 710 upright confocal microscope by 40× oil immersion lens. (C) Images, such as those shown in A were analysed to determine nuclear to cytoplasmic fluorescence ratio ($F_{n/c}$) as previously described (Kumar *et al.*, 2013; Pryor *et al.*, 2007; Rawlinson *et al.*, 2009; Tay *et al.*, 2013). Data are shown as mean $F_{n/c}$ ± SEM (error bars), n = 30 cells from a single assay, representative of two independent experiments.

We next asked if previously reported DENV2 NS5 α/βNLS that resides within residues 368-405 is able to target an unrelated protein to the nucleus, just like residues 883-900. Residues 368-405 of DENV2 NS5, as well as residues 320-405 that included previously reported NES and α/βNLS, was fused to 2×GFP construct (Figure 3-29A). In our hands both the 2×GFP-fusion constructs carrying the previously characterized internal NLS ($F_{n/c}$ = 0.88 ± 0.05 and 0.77 ± 0.02, respectively) could not be targeted to the nucleus, just like the negative control 2×GFP ($F_{n/c}$ = 0.81 ± 0.03, Figure 3-29B and C). 2×GFP-fusion constructs that spanned other regions that were within residues 320-405, namely residues 320-367, 368-389 and 387-405, also behaved similarly ($F_{n/c}$ ratio not determined). Taken together, our result suggests that residues 883-900 of DENV2 NS5 can mediate nuclear import just like classical monopartite SV40 NLS.

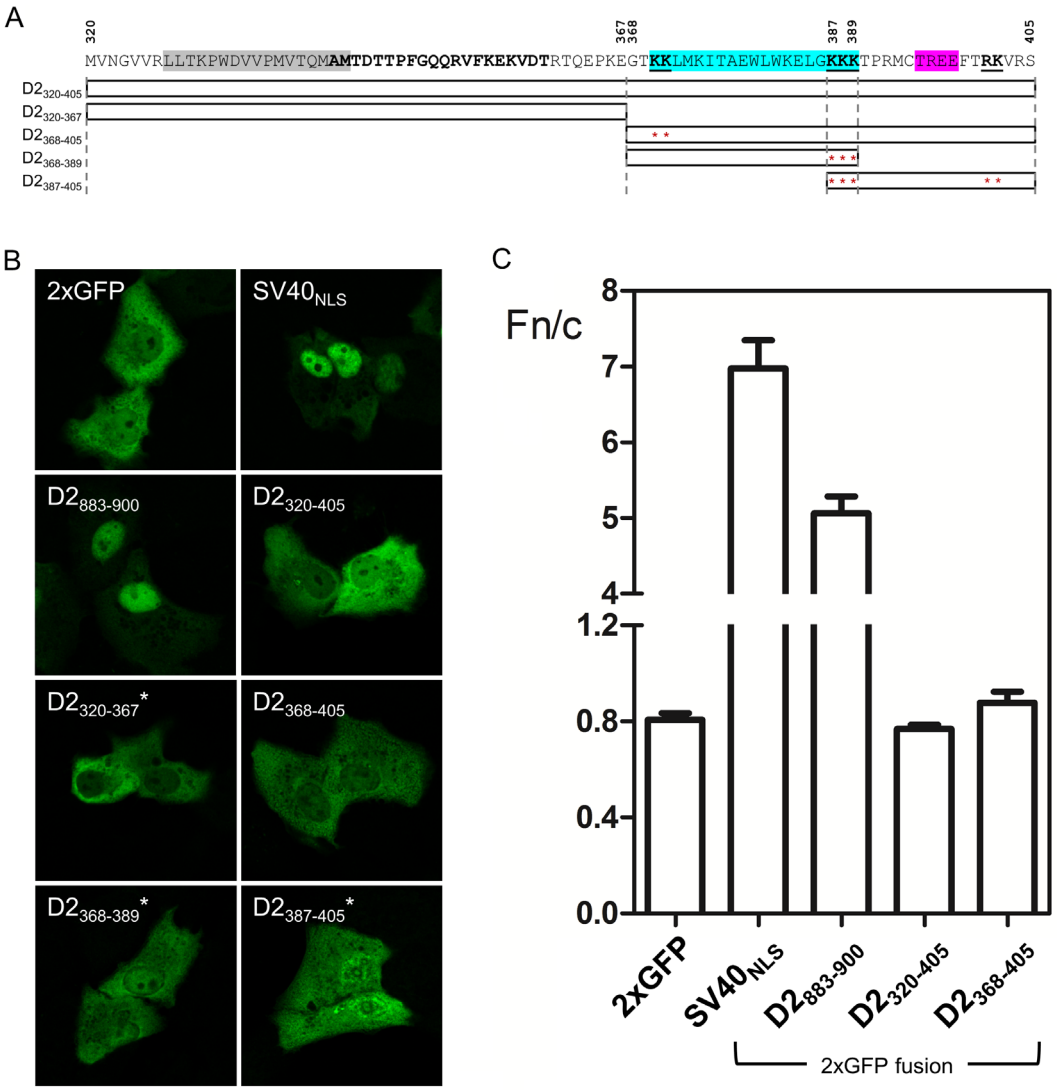

Figure 3-29: Fusion of residues 368-405 of DENV2 NS5 to 2×GFP does not target 2×GFP to the nucleus. (A) Schematic representation of transfected 2×GFP-fusion constructs. The displayed sequence is from residue 320-405 of DENV2 NS5. Regions are highlighted in grey, cyan and magenta denote NES, α/βNLS and CK2 site. The amino acids that are conserved among flavivirus NS5 are bold. The basic amino acid that constitutes the NLS is bold and underlined. The grey dotted line indicates the boundary of each construct. "*" indicates the position of basic amino acid. (B) Vero cells were transfected with either 2×GFP or 2×GFP-fusion plasmids encoding residues 320-405, 320-367, 368-405, 368-389, 387 and 405 and 883-900 of DENV2 NS5, and fixed at 24h post-transfection. 2×GFP-fusion plasmid encoding SV40 NLS was included as a positive control for monopartite NLS. The cells were stained and images were captured as described in Figure 3-28B. Images were analysed to calculate mean $F_{n/c}$ ± SEM (error bars), n = 30 cells from a single assay, representative of two independent experiments, as described in Figure 3-28C. "*" indicates that the $F_{n/c}$ ratio for these constructs were not quantified.

3.4.4 DENV2 NS5 residues 883-900 can target DENV1 NS5 into the nucleus

Since residues 883-900 of DENV2 NS5 can target 2×GFP into nucleus, we hypothesized that replacing this corresponding region on DENV1 NS5 can target DENV1 NS5 into nucleus (Figure 3-30A). As predicted, DENV1 NS5 with $DENV2_{883\text{-}900}$ could localize to the nucleus ($F_{n/c}$ = 4.57 ± 0.25) (Figure 3-30B and C) more efficiently than DENV1 NS5 WT ($F_{n/c}$ = 0.86 ± 0.02). On the other hand, replacing residues 883-900 of DENV2 NS5 with corresponding DENV1 sequence caused more NS5 protein to be in cytoplasm ($F_{n/c}$ = 1.01 ± 0.02) as compared to DENV2 NS5 WT ($F_{n/c}$ = 13.28 ± 1.08). Taken together, these results suggest that residues 883-900 of DENV2 NS5 indeed contains a functional monopartite NLS.

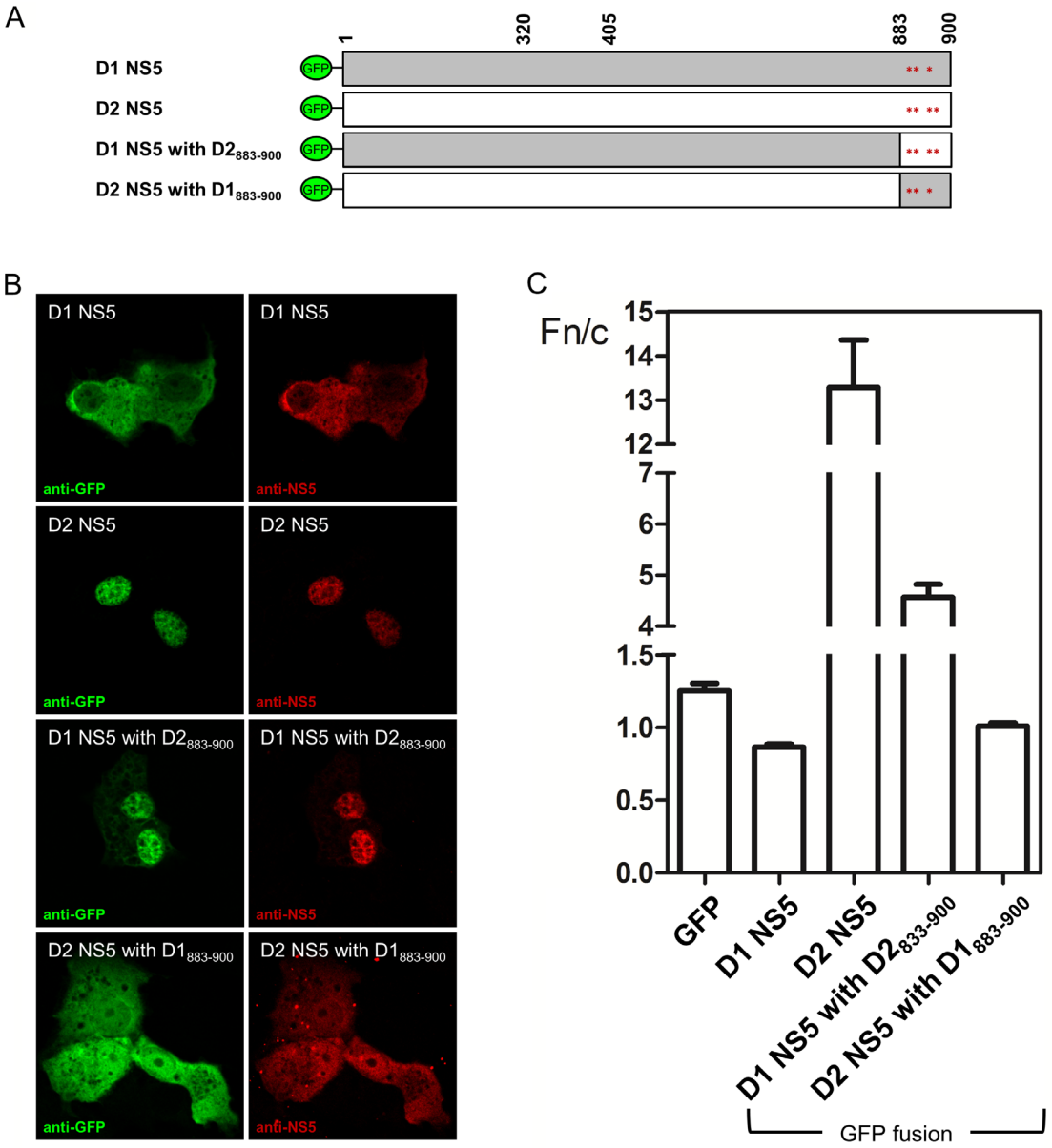

Figure 3-30: Replacement of residues 883-900 of DENV1 NS5 by corresponding sequence of DENV2 NS5 targets DENV1 NS5 to the nucleus. (A) Schematic representation of transfected GFP constructs. "*" indicates the position of basic amino acid. (B) Vero cells were transfected with the constructs showed in A and fixed at 24h post-transfection. Anti-GFP (ab6556 IgG, 1:1000; green) and anti-NS5 (5R3 IgG, 30 nM; red) antibodies were used for immunostaining and images were captured as described in Figure 3-16A. (C) Images taken from anti-GFP stained cells were analysed to calculate mean $F_{n/c}$ ± SEM (error bars), n = 30 cells from a single assay, representative of two independent experiments, as described in Figure 3-16B.

3.4.5 DENV2 NS5 residues 887-888 and 890-891 are needed for nuclear localization of DENV2 NS5

To further test if monopartite NLS is indeed present in residues 883-900 of DENV2 NS5, we made DENV2 NS5 GFP constructs that expressed NS5 residues 1-882 protein, which terminated before the putative monopartite NLS sequence, as well as NS5 residues 1-891 protein, which stopped right after the basic cluster of the putative monopartite NLS sequence (refer to Figure 3-31A). Both proteins gave expected results; DENV2 $NS5_{1-882}$ protein was predominantly localized to the cytoplasm ($F_{n/c}$ = 0.73 ± 0.04), whereas DENV2 $NS5_{1-891}$ protein was mostly nuclear-localized ($F_{n/c}$ = 5.85 ± 0.33), albeit much less efficiently than DENV2 NS5 full-length protein ($F_{n/c}$ = 13.28 ± 1.08) (Figure 3-31B and C). On the other hand, DENV1 $NS5_{1-882}$ protein still remained mainly in the cytoplasm ($F_{n/c}$ = 0.92 ± 0.03), just like DENV1 NS5 full-length protein ($F_{n/c}$ = 0.86 ± 0.02).

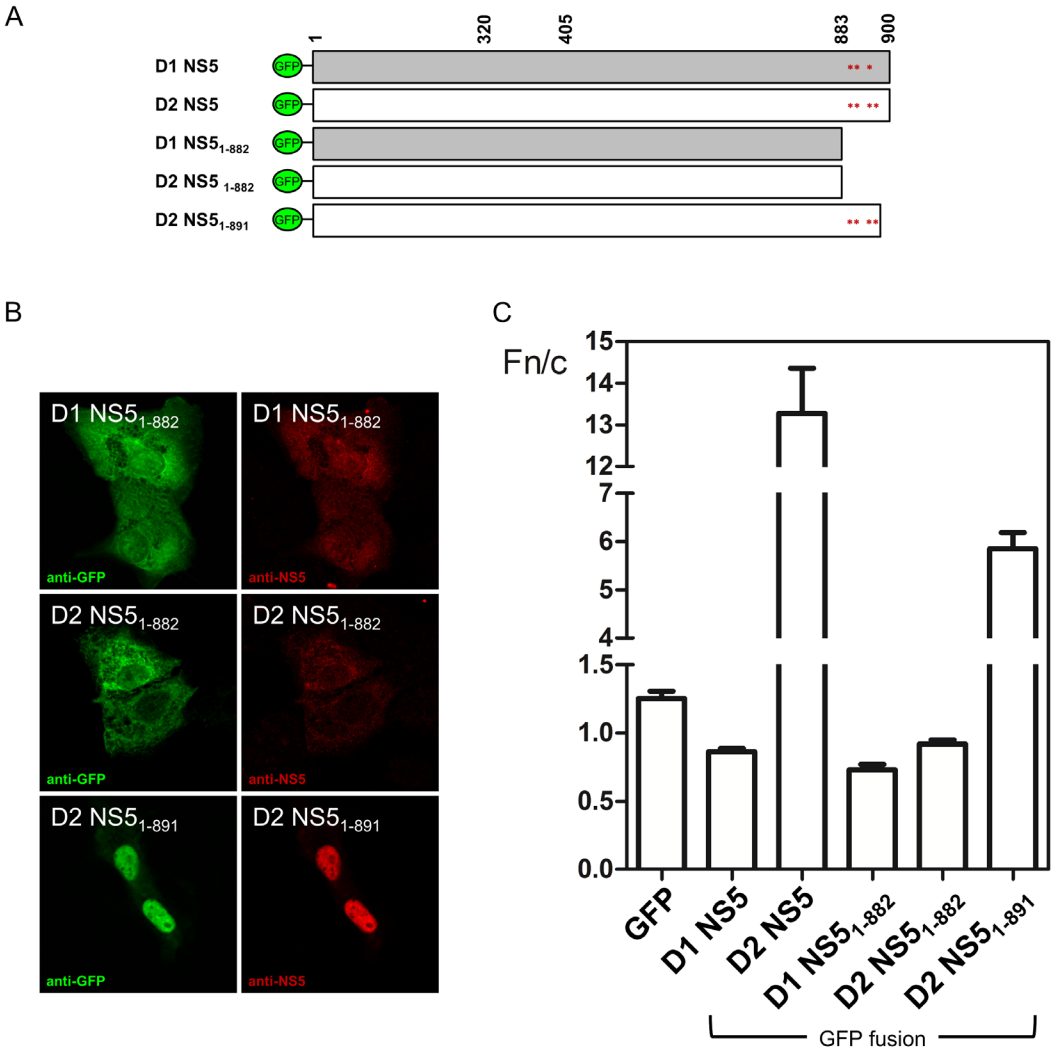

Figure 3-31: Truncation of residues 883-900 from DENV2 NS5 reduces its nuclear localization. (A) Schematic representation of transfected constructs. "*" indicates the position of basic amino acid. (B) Vero cells were transfected with the constructs showed in A and fixed at 24h post-transfection. The cells were stained and images were captured as described in Figure 3-16A. (C) Images taken from anti-GFP stained cells were analysed to calculate mean $F_{n/c}$ ± SEM (error bars), n = 30 cells from a single assay, representative of two independent experiments, as described in Figure 3-16B.

Next, we disrupted the NLS sequence by mutating the basic residues that constitute the monopartite NLS sequence (hereafter defines as C-terminal NLS, short form; C-term NLS) to alanine to generate DENV2 C-term A1 (^{887}KR→AA), A2 (^{890}RR→AA) and A1+A2 (^{887}KR→AA+^{890}RR→AA) DENV2 NS5 GFP constructs (refer to Figure 3-32A). We also included previously published α/βNLS mutants, namely DENV2 α/βNLS A2 (^{387}KKK→AAA) and A1+A2 (^{371}KK→AA+^{387}KKK→AAA) DENV2 NS5 GFP constructs for comparison. As expected, by disrupting the NLS sequence through alanine mutation reduced the ability of DENV2 NS5 to nuclear-localize; alanine mutation to either basic cluster of C-terminal NLS gave comparable $F_{n/c}$ ratios (The $F_{n/c}$ ratios for C-term A1, C-term A2 and C-term A1+A2 mutants were 0.50 ± 0.01, 0.22 ± 0.01 and 0.56 ± 0.03, respectively) (Figure 3-32B and C). Through $F_{n/c}$ ratio comparison, C-terminal NLS mutants seemed to have more cytoplasmic NS5 than α/βNLS A1+A2 mutant ($F_{n/c}$ = 0.77 ± 0.02). Taken together, these results supported the idea that the C-terminal end of DENV2 NS5 resides a functional monopartite NLS.

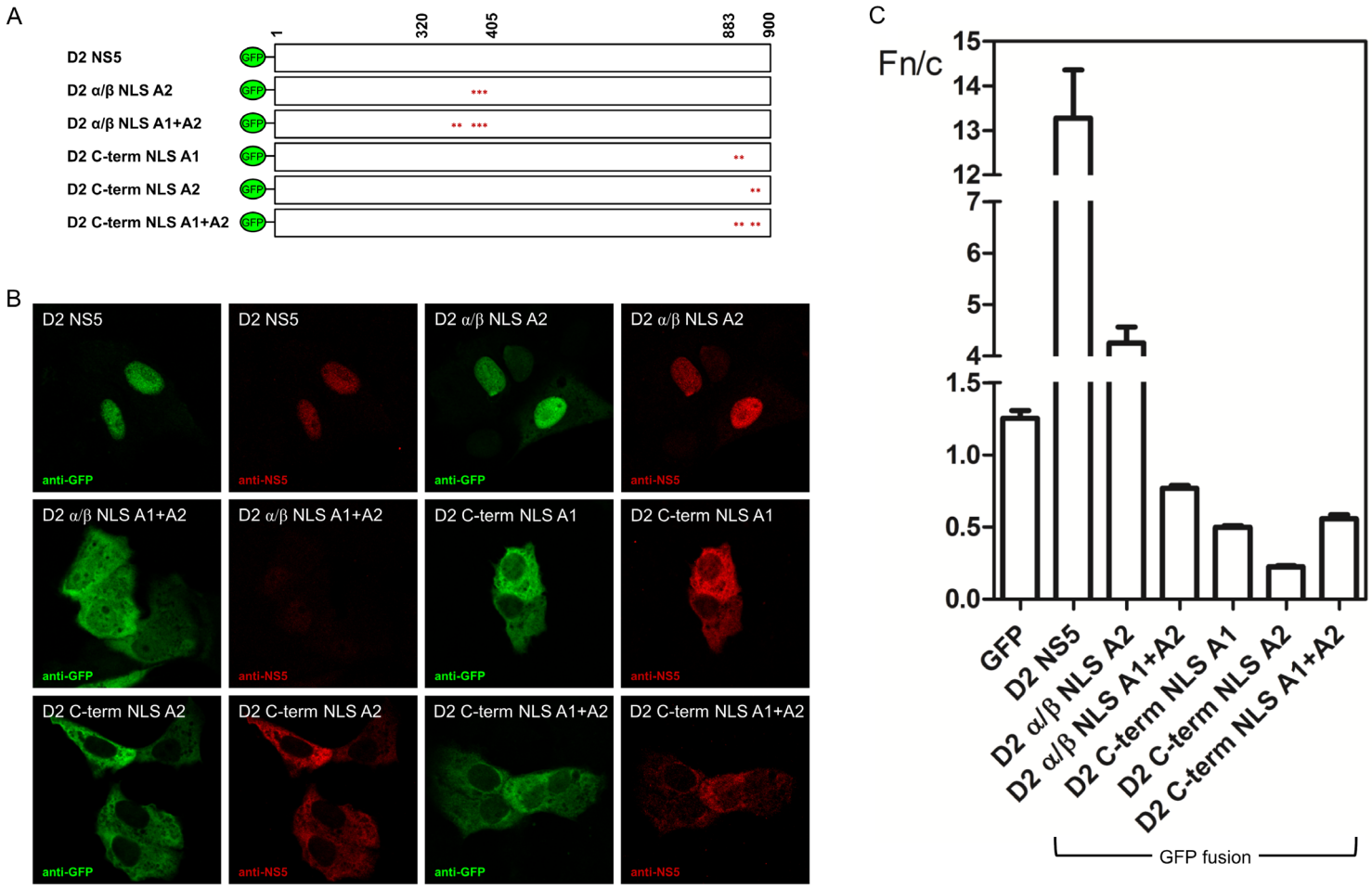

Figure 3-32: Mutating basic residues that constitute C-terminal NLS of DENV2 NS5 to alanine disrupts DENV2 NS5 nuclear-localization. (A) Schematic representation of transfected constructs. "*" indicates the position of basic amino acid. (B) Vero cells were transfected with the constructs showed in A and fixed at 24h post-transfection. The cells were stained and images were captured as described in Figure 3-16A. (C) Images taken from anti-GFP stained cells were analysed to calculate mean $F_{n/c}$ ± SEM (error bars), n = 30 cells from a single assay, representative of two independent experiments, as described in Figure 3-16B.

3.4.6 C-terminal NLS mutant virus affects viral replication and disrupts DENV2 NS5 nuclear localization

To corroborate these results in the context of virus infection, NS5 C-terminal alanine mutations were introduced into DENV2 cDNA clone. We also included another DENV2 cDNA clone that had its NS5 RdRP sequence (residues 273-900) being replaced by corresponding DENV1 sequence for comparison (defined as DENV2/1) because its chimeric NS5 protein also has less nuclear targeting ability (Figure 3-25). *In vitro* RNA transcripts that were produced from these clones were used to transfect BHK-21 cells and samples were harvested over the course of a 5-day experiment. The harvested supernatants were used to determine viral titres and extracellular viral RNA copy numbers, whereas the infected cells were used to determine intracellular viral RNA copy numbers and for IFA.

No infectious virus was recovered from the supernatant of DENV2 C-terminal A1 and A1+A2 mutant viruses, and DENV2/1 chimeric virus, whereas the number of infectious virus that was produced by DENV2 C-terminal A2 mutant virus was 100× lower than WT virus for day 2 and 3 post-trasfection, and smaller plaque was seen (Figure 3-33A and B). To confirm that no infectious virus was indeed present in supernatant, we employed real-time RT-PCR to measure absolute copy numbers of extracellular viral RNA. Interestingly, though no visible plaque was seen for DENV2/1 chimeric virus, we could detect similar level of extracellular viral RNA for both DENV2 C-terminal A2 mutant virus and DENV2/1 chimeric virus (Figure 3-33C). On the contrary, in agreement with plaque assay data, the extracellular viral RNA level for both DENV2 C-terminal A1 and A1+A2 mutant viruses remained

consistent throughout the 5-day experiment, indicating no infectious virus particles were being produced for these mutant viruses. Next, we also measured the absolute copy numbers of intracellular viral RNA and showed that DENV2 C-terminal A2 mutant virus and DENV2/1 chimeric virus replicated at similar rate and their viral RNA copy numbers were at least 10× lower than DENV2 WT for days 1-4 post-transfection (Figure 3-33D). On the other hand, viral RNA copy numbers for DENV2 C-terminal A1 and A1+A2 mutant viruses remained fairly consistent throughout the 5-day experiment, implying that no active RNA replication was taking place and both mutations were lethal to virus.

To confirm that the lower replication rates of DENV2 C-terminal A2 mutant virus and DENV2/1 chimeric virus were linked to reduced nuclear targeting of NS5, we examined the localization pattern of dsRNA and NS5 protein of transfected cells by IFA. We observed co-localization of NS5 (red) and cytoplasmic dsRNA (green) on day 3 post-transfection for DENV2 C-terminal A2 mutant virus and DENV2/1 chimeric virus but not for DENV2 WT virus (Figure 3-33E). This data further supported the finding that ^{890}RR of DENV2 NS5 is important for NS5 nuclear localization (Figure 3-32) and there may be a correlation between lower virus replication rate and reduced nuclear targeting ability of NS5. We did not detect any NS5 and dsRNA staining for DENV2 C-terminal A1 and A1+A2 mutant viruses, which was in agreement with real-time RT-PCR data and this further supported the finding that these viruses are unable to synthesize viral RNA (Figure 3-33D).

In conclusion, we have shown a possible correlation between reduced DENV2 NS5 nuclear localization and lower virus replication. It also appears that ^{887}KR has a more severe effect on virus replication than ^{890}RR. However, this effect may not be fully attributed to just nuclear localization defect because basic amino acids (either KR or RR) at residues 887-888 are highly conserved among flaviviruses and the extent of NS5 nuclear localization is not a conserved feature among flaviviruses (Figure 3-34); the implication of this finding will be further discussed in section 4-4. Nevertheless, based on these findings, further studies have been initiated to gain a more comprehensive understanding on the C-terminal region DENV2 NS5, as well as other serotypes of NS5, on its binding to importin-α via biochemical and structural methods, and the implication of the two NLSs on DENV2 NS5 nuclear localization in infected cells.

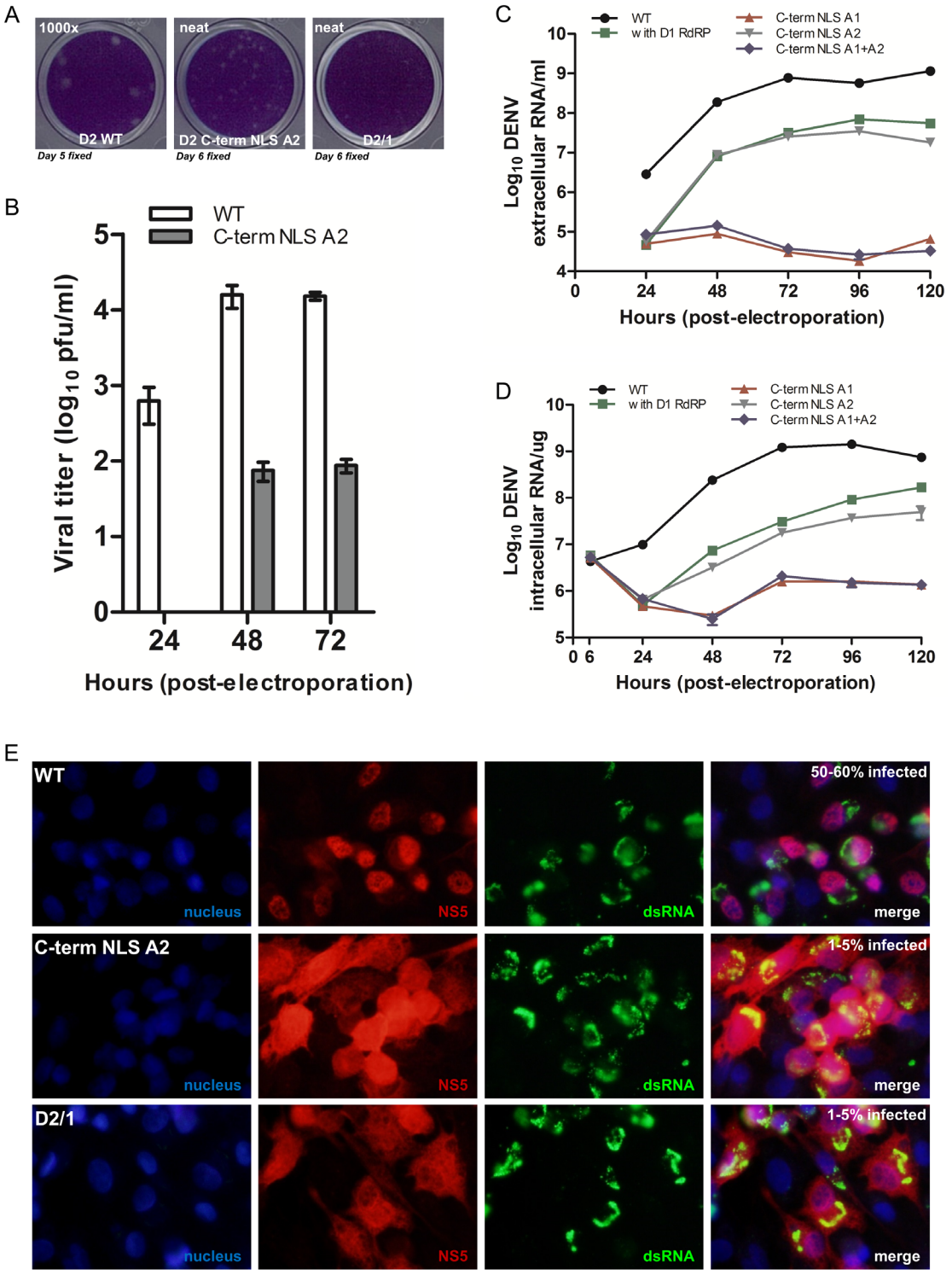

Figure 3-33: DENV2 NS5 C-term NLS A2 mutant virus and DENV2/1 chimeric virus have reduced nuclear accumulation of NS5 protein and viral replication. (A-E) BHK-21 cells were electroporated with 10 µg of genomic-length RNA of WT and mutants; supernatants and infected cells were harvested daily, for 5 days. Supernatants were used to (A-B) check for plaque production on BHK-21 cells and to (C) determine absolute copy numbers of extracellular viral RNA by real-time RT-PCR. Absolute copy numbers of viral RNA in log scale per ml of supernatant used for real-time RT-PCR was plotted; data are shown as the mean ± SD from one experiment. (D) RNA was extracted from infected cells and absolute copy numbers of intracellular viral RNA was determined by real-time RT-PCR. Absolute copy numbers of viral RNA per µg of RNA used for real-time RT-PCR was plotted; data are shown as the mean ± SD from one experiment. (E) Infected cells were analysed for presence of NS5 (red) and dsRNA (green) by IFA on day 3 post-transfection. Data from one experiment are shown.

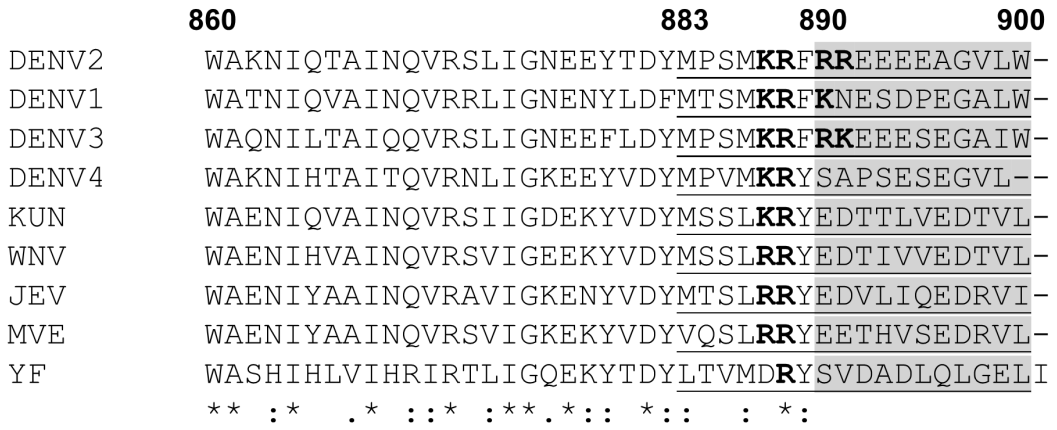

Figure 3-34: Sequence alignment of NS5 residues 860-900 of DENV2 with other DENV serotypes and representative members of the Flavivirus genus. In this study, residues 883-900 is defined as C-terminal NLS and the basic residues that important are important for binding to importin-α are bold. Residues 890-900 that are exchanged between serotypes in Figure 3-27 are highlighted in grey. The alignment was performed using ClustalW (Thompson *et al.*, 1994). The numbering is based on DENV2 sequence. The virus sequences and their GenBank accession numbers are as described in Figure 3-4C.

Table 3-8: Summary of $F_{n/c}$ ratio, western blot and IFA data of WT and chimeric NS5 of DENV1-4. The $F_{n/c}$ ratios were computed from images that had NS5 being stained by in transfected vero cells by anti-GFP; anti-NS5 (5R3) was included to check the folding of WT and chimeric NS5 proteins. GFP-NS5 and 2×GPF constructs were also transfected into HEK293T cells to check the expression of these proteins by western blot with anti-NS5. Under construct name, D1 = DENV1 and D2 = DENV2. The number of "*" denotes the intensity of western blot band; "*****" indicates the highest intensity, "*" indicates the lowest intensity. "Y" denotes yes, "N" denotes no. N.D. indicates not determined. $F_{n/c}$ = nuclear to cytoplasmic fluorescence ratio, $F_{n/c} < 1$, predominantly cytoplasmic, $F_{n/c} > 1$, predominantly nucleus.

Construct name	Vero			HEK293T
	anti-GFP	anti-NS5 (5R3)	$F_{n/c}$ ± SEM	Western blot with anti-GFP
GFP-NS5 constructs				
D1	Y	Y	0.86 ± 0.02	***
D2	Y	Y	13.28 ± 1.08	**
D1 1-319 D2 320-405 D1 406-900	Y	Y	N.D.	*
D2 1-319 D1 320-405 D2 406-900	Y	N	N.D.	***
D1 1-272 D2 273-900	Y	Y	N.D.	**
D1 1-319 D2 320-900	Y	Y	N.D.	*****
D1 1-405 D2 406-900	Y	Y	N.D.	***
D2 1-272 D1 273-900	Y	Y	N.D.	*****
D2 1-319 D1 320-900	Y	Y	N.D.	*
D2 1-405 D1 406-900	Y	N	N.D.	*
D2 1-362 D1 363-394 D2 395-900	Y	Y	N.D.	N.D.
D2 1-394 D1 395-497 D2 498-900	Y	Y	N.D.	N.D.
D2 1-508 D1 509-537 D2 538-900	Y	Y	N.D.	N.D.
D2 1-542 D1 543-576 D2 577-900	Y	Y	N.D.	N.D.
D2 1-626 D1 627-658 D2 659-900	Y	N	N.D.	*
D2 1-626 D1 627-900	Y	N	N.D.	N.D.
D2 1-708 D1 709-900	Y	Y	N.D.	**
D2 1-888 D1 889-900	Y	Y	N.D.	N.D.
D2 1-888 D3 889-900	Y	Y	N.D.	**
D2 1-888 D4 889-900	Y	Y	N.D.	****
D1 with D2 883-900	Y	Y	4.57 ± 0.25	**
D2 with D1 883-900	Y	Y	1.01 ± 0.02	**
D1 1-882	Y	Y	0.92 ± 0.03	N.D.
D2 1-882	Y	Y	0.73 ± 0.04	N.D.
D2 1-891	Y	Y	5.85 ± 0.33	N.D.
D2 α/βNLS A2	Y	Y	4.25 ± 0.31	**
D2 α/βNLS A1+A2	Y	N	0.77 ± 0.02	*
D2 C-term A1	Y	Y	0.50 ± 0.01	**
D2 C-term A2	Y	Y	0.22 ± 0.01	*
D2 C-term A1+A2	Y	Y	0.56 ± 0.03	***
2×GFP fusion constructs				
D1 883-900	Y	N.A.	1.03 ± 0.06	****
D2 883-900	Y	N.A.	5.06 ± 0.22	****
D4 883-900	Y	N.A.	0.63 ± 0.02	****
D2 320-405	Y	N.A.	0.77 ± 0.02	***
D2 320-267	Y	N.A.	N.D.	****
D2 368-405	Y	N.A.	0.88 ± 0.05	****
D2 368-389	Y	N.A.	N.D.	****
D2 387-405	Y	N.A.	N.D.	****

Chapter 4: Discussion

4.1 Preface

This work aimed to understand in detail the viral factors that modulate the replication cycle of DENV and test the hypothesis that such knowledge can lead to validation of potential targets for antiviral therapy. In infected cells, protein-protein interactions among viral proteins and between viral and host proteins are key players in mediating virus replication and disease pathogenesis. Considerable amount of effort has been put into characterizing the largest and most highly conserved NS5 protein in term of its enzymatic roles and potential as a directly acting antiviral target. However, molecular studies on the impact of its interaction with other viral proteins, as well as with host proteins on virus replication and diseases pathogenesis is still lacking and also often restricted to the study of DENV2 NS5.

DENV2 NS5 exists in two different forms in infected cells: cytoplasmic NS5 and nuclear NS5. Cytoplasmic NS5 interacts with NS3 in the perinuclear region to participate in viral RNA replication (Cui *et al.*, 1998; Kapoor *et al.*, 1995; Welsch *et al.*, 2009; Yon *et al.*, 2005; Yu *et al.*, 2013) whereas nuclear NS5 interacts with importin-α/β1 in the cytoplasm to translocate into nucleus, where it may mediate infectious virus production and IL-8 secretion (Brooks *et al.*, 2002; Forwood *et al.*, 1999; Johansson *et al.*, 2001a; Kumar *et al.*, 2013; Pryor *et al.*, 2007). Previous studies have identified NS3-NS5 and NS5-importin-α/β1 interaction sites to reside within previously identified interdomain linker region, residues 320-405 of NS5 (Figure 1-16) through Y2H studies (Brooks *et al.*, 2002; Forwood *et al.*, 1999; Johansson *et al.*, 2001a). Mutations in NS5 $^{330}K \rightarrow A$ and

^{371}KK→AA+^{387}KKK→AAA disrupt NS3-NS5 and NS5-importin-α interactions, respectively and mutagenesis studies with DENV2 infectious cDNA clone showed that these mutations are lethal (Pryor *et al.*, 2007; Zou *et al.*, 2011).

4.2 NS3-NS5 interaction is required for coordinated positive- and negative-strand RNA synthesis

With the availability of structural information for domains or full-length proteins of DENV NS3 & NS5 (Erbel *et al.*, 2006; Luo *et al.*, 2010; Luo *et al.*, 2008a; Xu *et al.*, 2005b; Yap *et al.*, 2007), the information on the interaction sites can be used to facilitate structure-guided drug design. In this study, we have fine mapped the interaction region on NS3 that is involved in NS3-NS5 interaction to residues 566-585 by competitive NS3-NS5 interaction ELISA, peptide-phage ELISA and SPR (in collaboration with Profs Luo Dahai and Julien Lescar (NTU)). Although obtaining crystal structures of the complex has been challenging and not yet available, this study obtained a solution structure by SAXS in collaboration with Prof Gerhard Gruber and Miss Saw Wuan Geok (NTU) that supports physical interaction between $NS3_{172-618}$ and $NS5_{320-341}$ is a significant contribution towards the reconstruction of the RC.

Electrostatic potential surface analysis of $NS3_{566-585}$ and $NS5_{320-341}$ shows a negatively-charge contiguous surface on NS3 and a positively-charged contiguous surface on NS5 that are charge-complementary to each other and this further supports the data that the two regions can indeed interact with one another via charge interaction (Figure 4-1A). This study demonstrates that NS3 residue N570 is important for NS3-NS5 interaction and its mutation to alanine disrupted *in vitro* NS3-NS5 interaction (Figure 3-4B). When the same mutation was introduced into DENV2 cDNA infectious clone, it abolished infectious virus production (Figure 3-8A and B), similar to NS5:K330A mutant, which is a known NS3-NS5 interaction defective mutant (Zou *et al.*, 2011). However, unlike NS5:K330A mutant, NS3:N570A mutant

was able to synthesize low but unsustainable amount of viral RNA and proteins (Figure 3-8C and D and Figure 3-9). Comparison of the pattern of negative- and positive-strand RNA synthesis between WT, NS3:N570A and NS5:K330A confirmed that the NS5:K330A mutant is completely inactive since transfected positive-strand RNA degraded over time and the negative-strand RNA detected corresponded to background (Figure 3-13). The WT RNA transfected cells showed synchronized synthesis of negative- and positive-strand RNA, which is in agreement with previous studies that have shown an excess of positive- to negative-strand RNA in DENV infected cells (Tomassini *et al.*, 2003). However, it is possible that the long term coordinated synthesis of negative- and positive-strand RNA requires a functional RC with optimum protein interaction affinities between NS3 and NS5 (Figure 4-1B). This is supported by NS3:N570A mutant that showed fairly robust negative-strand synthesis using the transfected RNA as a template, and is probably analogous to the situation at the early stages of viral replication in an infected cell. The weakened or abolished interaction between NS3 and NS5 in NS3:N570A mutant does not support the replication of new positive-strand RNA from 6 to 24 hour when compared to WT virus, which fits rather well with the carefully conducted real-time RT-PCR quantifications. Surprisingly, the NS5:K330A mutant that has been shown to be enzymatically active *in vitro* and demonstrated to have no interaction with NS3 did not show a similar increase in negative-strand RNA as compared to NS3:N570A mutant. There may be two possible reasons for - the inactivity of NS5:K330A mutant in making negative-strand RNA. First, it may be due to impaired intramolecular signalling between the two NS5 domains that probably coordinates the two functional activities of NS5 (Li *et al.*, 2014b; Lu & Gong, 2013; Wu *et al.*, 2015) required for *in vivo* polymerase activity, or second, that its weak/abolished interaction with NS3 may

affect the unwinding of secondary structures in the transfected positive-sense RNA that is needed for negative-strand synthesis. Taken together, the results from this study imply that different NS3-NS5 interaction defective mutants can impair viral protein synthesis, infectious virus production and viral RNA replication to varying degree, which is likely to be dependent on the importance of the amino acids that are involved in NS3-NS5 interaction (ie. it is possible that other residues within the conserved region that we mapped are also important), and also possibly, intramolecular interactions in NS5. It is interesting to note that the coordinated synthesis of negative- and positive-strand RNA at the early stages of replication can be further explored by studying NS3-NS5 interaction mutants displaying varying strength/degree of binding and also, the contribution of intramolecular cross-talk between domains of NS5 in strand-specific RNA synthesis in the RC. Importantly, we also note that although NS3 residue N570 is conserved amongst the four DENV serotypes and several members of flavivirus genus, it is not conserved in YFV NS3 which has a histidine in place of asparagine at this position in NS3 and, tyrosine instead of lysine at position 330 of NS5 (refer to Figure 3-4C and Figure 3-5A for sequence alignment). This suggests that protein interaction sites of different flaviviruses could co-evolve with the different host proteins.

The fine tuning of NS3-NS5 interaction site in this study, together with the available 3D structural data can be used in conjunction with ab initio modelling and in silico drug discovery efforts to discover novel inhibitors against DENV. As a starting point the validation that peptide sequences in the interaction region can function as inhibitors in cellular infection studies (Figure 3-14) also opens the way to examine stapled-peptides approach (Verdine & Hilinski, 2012) to inhibit protein-protein

interaction. Another attractive proposition from this study is that mutant such as NS3:N570 may serve as potential RNA-mediated vaccine since our study shows that low level translation of viral proteins can be achieved with residues that are selected on the basis of structure and function. However, for developing RNA-based vaccines new technologies need to be developed in the area of stabilization and delivery.

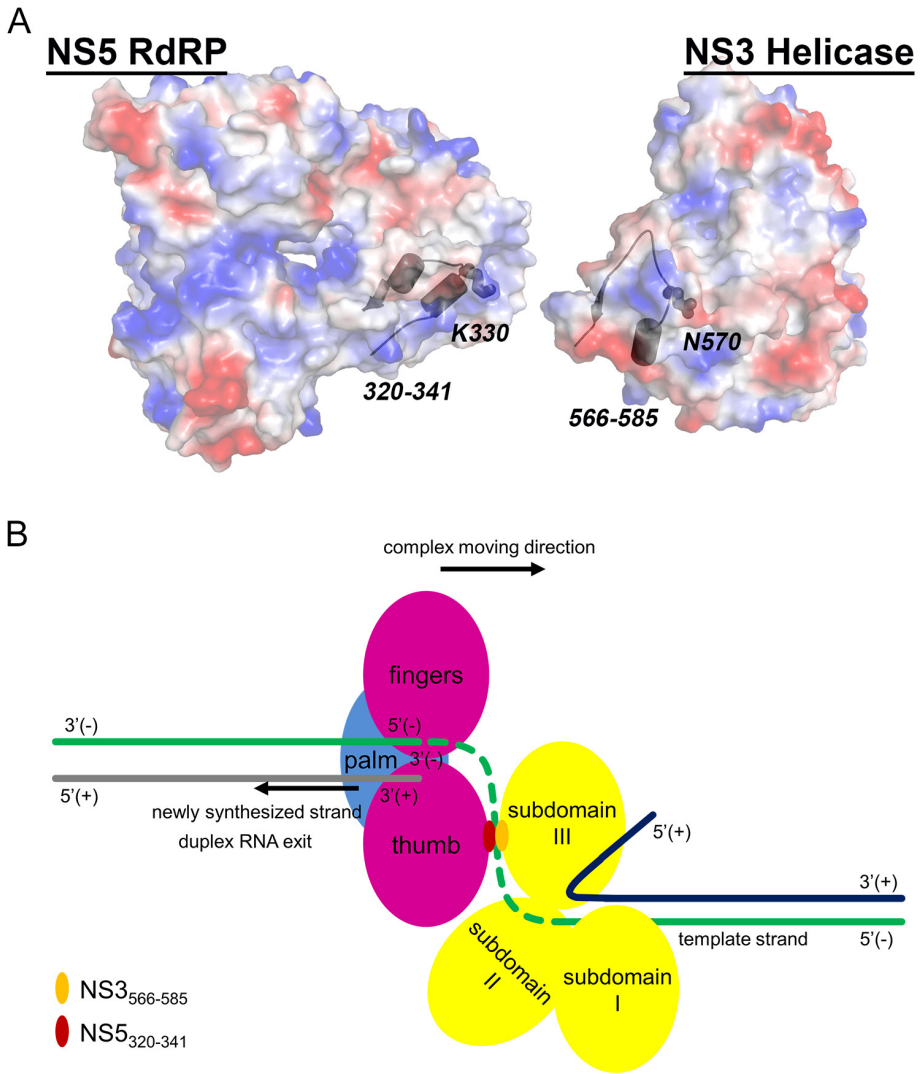

Figure 4-1: Schematic representation of NS3-NS5-RNA interaction. (A) Surface electrostatic potential presentation of $NS5_{273-900}$ (RdRP) and $NS3_{172-618}$ (Helicase). The protein backbones of $NS5_{320-341}$ and $NS3_{566-585}$ are shown in ribbon presentation. The side-chains of NS5 K330 and NS3 N570 are displayed. (B) Simplified schematic model of NS3-NS5 interaction complex with RNA. The orange and red solid ovals represent residues 566-585 of NS3 and residues 320-341 of NS5, respectively. Dotted line (green) is used to denote that the uncertain path that exiting template RNA from NS3 takes to enter NS5 for complementary daughter strand synthesis. Dark blue line denotes the unwound parental strand; green line denotes the parental strand that serves as template; grey line denotes the newly synthesized daughter strand.

4.3 GFP-NS3 and GFP-NS5 interaction networks reveal novel host factors that interact with NS3 and NS5 for DENV replication and pathogenesis

Even though DENV2 NS5 nuclear localization has been known for twenty years (Kapoor *et al.*, 1995), its precise role in nucleus remains elusive. Furthermore, both our finding (Tay *et al.*, 2013) and that of the Dr Davidson's group (Hannemann *et al.*, 2013) that variations in DENV1-4 NS5 subcellular localization can be observed, throws some doubt if nuclear NS5 has any critical functions. However, the most powerful case in favor of its important role in nucleus comes from the drug discovery approach used in the laboratory of Prof David Jans, where the AlphaScreen technology has been used to identify compounds that inhibit the interaction between DENV NS5 and mouse importin-α/β1 (Fraser *et al.*, 2014; Tay *et al.*, 2013; Wagstaff *et al.*, 2011; Wagstaff *et al.*, 2012). One possible hypothesis is that an important host protein that is required for viral RNA replication in the RC may be recruited through the nuclear-cytoplasmic shuttling of NS5. For this purpose, a detailed proteomics, genomics and interactomics based approach that characterize host protein interaction network is important and this will be greatly facilitated by the wealth of knowledge accumulated in recent years from genome-wide siRNA screens (Krishnan *et al.*, 2008; Le Sommer *et al.*, 2012; Sessions *et al.*, 2009), microarray (Becerra *et al.*, 2009; Conceicao *et al.*, 2010; Fink *et al.*, 2007; Loke *et al.*, 2010; Nasirudeen & Liu, 2009; Sessions *et al.*, 2013; Villas-Boas *et al.*, 2009), proteomics (Chiu *et al.*, 2014; Pando-Robles *et al.*, 2014) and interactomics (Carpp *et al.*, 2014; Khadka *et al.*, 2011; Le Breton *et al.*, 2011; Mairiang *et al.*, 2013) studies (see (Acosta *et al.*, 2014) and (Krishnan & Garcia-Blanco, 2014) for a complete review). The task to integrate this

fragmented information will be challenging but it will be rewarding in identifying critical host factors and new/novel therapeutic targets (Huang & Fraenkel, 2009).

In this study, the co-IP coupled to MS approach was used to address the potential roles of nuclear NS5 on dengue pathogenesis. A total of 405 human proteins were identified, of which 185, 298 and 273 co-eluted with DENV1/2 GFP-NS3, DENV1 GFP-NS5 and DENV2 GFP-NS5, respectively. Out of 405 human proteins, around 10% of the hits have already been reported (most of them are not characterized in term of their importance in virus replication and pathogenesis) by various studies (Y2H, pulldown assay, co-IP coupled to quantitative MS and RNA affinity chromatography) to be interacting with NS3, NS5 or viral RNA (Table 3-3 and 3-5). Comparison of our dataset to four dataset of published viral-host protein interaction screens that involved the same viral proteins, NS3 and NS5 (three Y2H datasets (Khadka *et al.*, 2011; Le Breton *et al.*, 2011; Mairiang *et al.*, 2013) and one co-IP dataset (Carpp *et al.*, 2014)) yielded a small overlap in datasets (Figure 4-2, circle in blue). Similarly, comparison among these 5 datasets also generated a small overlap in datasets. Taken together, this implies that dataset from each screen is unlikely to be exhaustive and complementary proteomic approaches that capture direct and indirect interactions are required to generate a comprehensive virus-host interaction network (Bailer & Haas, 2009; Le Breton *et al.*, 2011).

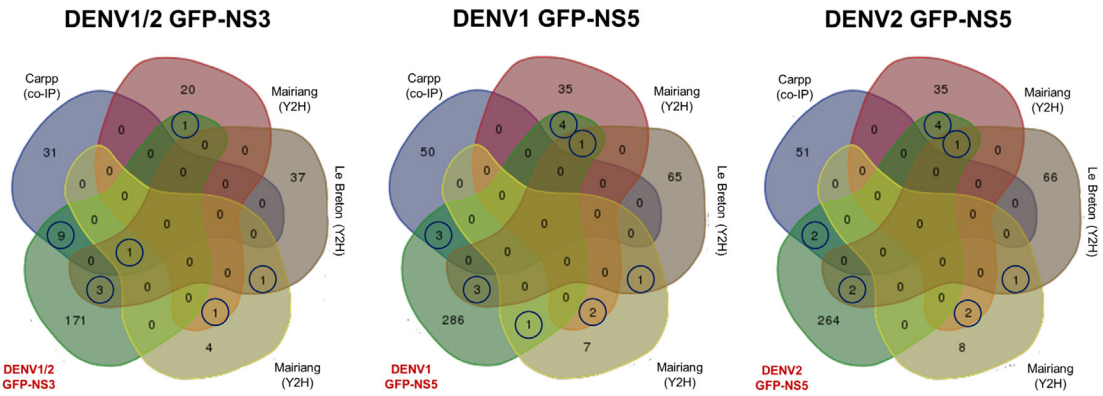

Figure 4-2: Comparisons of dataset overlap between published Y2H screens, co-IP study and our co-IP work. Each dataset is labelled according to the first name of the author. The datasets that we generated in our study are labelled according to the GFP-proteins (in red) that they co-eluted with. The description in bracket describes the method (either Y2H or co-IP) that was used in each study. The region that overlaps is circled in blue.

As mentioned in results, both Carpp *et al* and this work used GFP-tagged NS3 and NS5 proteins for co-IP. However, they did co-IP in the context of DENV2 infected cells to identify bona fide high confidence viral-host protein interactions. Out of 41 and 53 host proteins that Carpp and colleagues have reported to be interacting with GFP-NS3 and GFP-NS5, respectively, we observed an overlap of 5 and 10 with our GFP-NS3 and GFP-NS5 interaction networks. One protein, Sec61α1 (protein transport protein Sec61 subunit alpha isoform 1) is common to both GFP-NS3 and GFP-NS5 of Carpp *et al* and our screen. Sec61α1 is a component of the heterotrimeric Sec61 complex (composed of three subunits: α, β and γ) that forms a transmembrane channel in the ER membrane to mediate the translocation of newly synthesized unfolded proteins into ER, and it is a component of ER-associated protein degradation pathway (ERAD), which targets misfolded protein from ER to proteasome for ubiquitin-mediated degradation (Meusser *et al.*, 2005). Surprisingly, Sec61α1, β and γ have been collectively shown to be proviral host factors for DENV2, WNV and YFV in human and mosquito genome-wide siRNA screens (Krishnan *et al.*, 2008; Le

Sommer *et al.*, 2012; Sessions *et al.*, 2009). In the work by Krishnan and colleagues, the knockdown of Sec61α1 and γ in human HeLa cells led to the reduction of WNV and DENV2 positive cells by ~50 and ~85%, respectively. Through further functional studies in WNV infected cells, the authors have shown a ~10% reduction in infectious virus production when ERAD components were knockdown and ruled out the involvement of ERAD in virus internalization, endosomal transport, or RNA translation in mediating the reduction (Krishnan *et al.*, 2008). In another study the knockdown of Sec61β in *Drosophila* Mel-2 cells led to the reduction of DENV2 positive cells by ~75%; an ~90% reduction in infectious virus production by Huh-7 DENV2 infected cells was observed with Sec61β knockdown (Sessions *et al.*, 2009). Taken together, these findings highlight the possible importance of Sec61 complex in DENV life cycle, and NS3 and NS5 may be involved in biological processes that are associated with the function of Sec61 complex in ERAD pathway.

Although our primary goal to identify nuclear host factors for NS5 with our experiment setup has not readily revealed any hits, we have however, managed to identify new potential roles for NS3 and NS5 in DENV replication and pathogenesis for further study by performing GO enrichment analysis on the co-eluted host proteins. Specifically, cellular processes related to RNA processing, translation machinery and cytoplasm stress granule components appear to be significantly enriched and their implications in DENV life cycles are discussed in the following section.

RNA processing machinery and host translation pathway - GO terms for 110 proteins that co-eluted with both GPF-NS3 and GFP-NS5 were associated with RNA processing and splicing, viral transcription, viral gene expression, translation, ribosome, eukaryotic translation initiation factor 3 complex and protein targeting to ER and membrane. Collectively, this suggests the potential involvement of both NS3 and NS5 in biological processes or molecular functions that are related to RNA processing machinery and host translation pathway (Table A-5) which fits with the known functions of NS3 and NS5 in DENV replication cycle because DENV is a positive-sense RNA virus that replicates in cytoplasm and therefore it has to recruit/exploit components of host RNA processing or translation machinery for its synthesis of viral genome and proteins (Li *et al.*, 1999a; Pastorino *et al.*, 2009). In fact, Pando-Robles and colleagues have recently published a novel set of human proteins that is involved in protein biogenesis during DENV2 infection (Pando-Robles *et al.*, 2014), which supports the importance of targeting the host translation machinery by DENV during infection. Coincidentally, among this novel set of human proteins, hnRNPC (heterogeneous nuclear ribonucleoproteins C1/C2), EIF2α (eukaryotic initiation factor 2 subunit 1 alpha), PABPC1 (polyadenylate-binding protein 1) and YB-1 (nuclease-sensitive element-binding protein 1) were found to co-elute with both GFP-NS3 and GFP-NS5 in our study. Previous studies have already reported that hnRNPC interacted with DENV2 NS1 and vimentin (Kanlaya *et al.*, 2010; Noisakran *et al.*, 2008b), whereas PABPC1 (Polacek *et al.*, 2009) and YB-1 (Paranjape & Harris, 2007) were found to bind DENV2 3'UTR (also see result Table 3-5). Interestingly, YB-1 was also identified to interact with HCV NS3/4A to influence the equilibrium between viral RNA replication and infectious virus production at different stages of HCV life cycle (Chatel-Chaix *et al.*, 2011), whereas

in DENV2, it binds 3'UTR to repress synthesis of viral RNA and protein (Paranjape & Harris, 2007). Therefore, it appears that NS3 and NS5, together with their RNA-binding ability, may bind viral RNA and proteins of RNA processing machinery/host translation pathway to regulate the switch between translation and replication.

Cytoplasm stress granule - Stress granules are cytoplasmic RNA granules that serve as site for mRNA degradation; they are typically formed during cellular stress (eg. viral infection, heat shock, oxidative stress and ischemia) to accompany global translational shutdown as part of an integrated stress response (Anderson & Kedersha, 2008; Kedersha *et al.*, 2013). In recent years, stress granule formation during viral infection has been proposed to play an important role in host antiviral defence because of increasing reports on inhibition of stress granule formation by several viruses (reviewed by (Beckham & Parker, 2008) and (Bidet & Garcia-Blanco, 2014)). For example, among flaviviruses, viral components like WNV NS3 and JEV capsid proteins can interact with stress granule proteins like TIA1/TIAR (T cell intracellular antigen-1/TIA-1-related protein) (Emara & Brinton, 2007) and Caprin-1 (Katoh *et al.*, 2013), respectively, to inhibit stress granule formation. Similar phenomenon was observed in other positive-sense RNA viruses, like poliovirus, where its viral proteinase 3C cleaved G3BP1 (Ras GTPase-activating protein-binding protein 1) to trigger the disassembly of stress granules (White *et al.*, 2007). In both instances, the inhibition of stress granule formation favors virus propagation in general, either by recruiting stress granule proteins to replication site to aid genome synthesis in perinuclear region (Emara & Brinton, 2007) or possibly restore host translation machinery for viral protein translation (White *et al.*, 2007). Of the 110 proteins that co-eluted with GFP-NS3 and GFP-NS5, we found 16 common proteins to be among

the up- and down-regulated protein lists (Table A-10) of Pando-Robles *et al*'s study that looked at changes in the proteome of DENV2 infected Huh-7 cells at 24 hours post-infection by LC-MS/MS. Coincidentally, GO analysis of down-regulated proteins (12 out of 16) revealed the cellular component - cytoplasm stress granule to be significantly enriched (q-value=9.41×10^{-6}, Table A-11). This implies that DENV may interfere with stress granule formation through down-regulation of stress granule proteins and both NS3 and NS5 both play a role in mediating that.

The proteomic approach to identifying novel factors is still work-in-progress but the increased interest in this area and the comparison with published works suggest that hits from this study can be further characterized experimentally to identify significant host protein partners that are important for DENV replication and pathogenesis. Integrating our dataset with published datasets from siRNA screens (see above), viral-host protein interaction screens, whole genome proteomics and gene expression studies can be used to build a comprehensive and highly confident virus-host interaction network for further study.

4.4 The search for cytoplasmic retention factor reveals surprising complexity of nucleocytoplasmic transport of DENV NS5

Although the nuclear-localizing ability of DENV2 NS5 in infected and transfected cells has been the subject of study by several groups, the ability of NS5 of other serotypes to do the same had not been explored previously (Brooks *et al.*, 2002; Kumar *et al.*, 2013; Pryor *et al.*, 2007; Rawlinson *et al.*, 2009). Based on the similarities in NS5 α/βNLS sequence that is contained within residues 320-405 (Figure 1-11), it has been long hypothesized that DENV1, 3 and 4 NS5 should nuclear-localize to similar extent as DENV2 NS5. Therefore, we tested this hypothesis, by first generating a cross-reactive anti-NS5 antibody for this study. Using the Fab-phage display technology, we generated two anti-NS5 IgG antibodies, 5M1 and 5R3 that can bind to NS5 of all serotypes (Figure 3-15). 5M1 epitope was mapped to residues 6-20 of NS5 MTase domain, whereas 5R3 epitope was mapped to a conformational epitope on NS5 RdRP domain, within residues 786-800 (residues 786-800 is found within NS5 priming loop). Using 5R3 antibody, we were able to show for the first time that DENV1-4 NS5 displayed differential localization patterns in both infected and transfected cells, with DENV2 and 3 NS5 being predominately nuclear, while DENV1 and 4 NS5 were more cytoplasmic (Tay *et al.*, 2013).

DENV1 NS5 α/βNLS is functional - Because of the higher sequence identity between DENV1 and 2 NS5 (79%) than between DENV4 and 2 NS5 (75%) we focused on DENV1 and 2 NS5, as examples of NS5 protein that remained predominantly cytoplasmic or nuclear for further study. By exchanging gene fragments (DNA shuffling) between the two serotypes, we demonstrated DENV1 α/βNLS to be functional when it was inserted into the corresponding DENV2 NS5 sequence even though in the context of its own sequence it is more cytoplasmic. Two scenarios are possible: one is that the DENV1 NS5 may require some additional post-translational modification (phosphorylation or dephosphorylation) to retain the protein in the cytoplasm (Jans & Hubner, 1996) or alternatively, a host factor that binds to a specific CRS on DENV 1 NS5 may mediate the observed subcellular localization (Moseley *et al.*, 2009).

Functional NLS sequences in NS5 - Based on functional and structural motifs, extensive swapping of gene fragments and functional analysis was carried out in this work to ultimately make a serendipitous discovery that a sequence that resembles a monopartite NLS is located at the C-terminal end of DENV2 NS5, within residues 883-900 (C-terminal NLS). We have supported this finding by demonstrating that (i) first, by fusing C-terminal NLS sequence of DENV2 NS5 to a tandem GFP gene construct (2×GFP), targets the predominantly cytoplasmic 2×GFP ($F_{n/c}$ = 0.81 ± 0.03), into the nucleus ($F_{n/c}$ = 5.06 ± 0.22), similar to the classical monopartite SV40 NLS ($F_{n/c}$ = 6.97 ± 0.37); (ii) second, by replacing the C-terminal NLS sequence of DENV1 NS5 with corresponding region of DENV2 NS5, we showed that predominantly cytoplasmic DENV1 NS5 ($F_{n/c}$ = 0.86 ± 0.02) could be trafficked into the nucleus ($F_{n/c}$ = 4.57 ± 0.25); (iii) third, by truncating the C-terminal end from

DENV2 NS5, its nuclear targeting ability was also greatly reduced (from $F_{n/c}$ = 13.28 ± 1.08 for DENV2 full-length NS5 to $F_{n/c}$ = 0.73 ± 0.04 for DENV2 NS5 residues 1-882) despite an intact importin-α/β1 NLS within the previously identified interdomain linker region, residues 320-405 of NS5 and (iv) forth, by disrupting the C-terminal NLS sequence in DENV2 NS5 protein through alanine mutation resulted in a predominantly cytoplasmic NS5 protein ($F_{n/c}$ = 0.50 ± 0.01, 0.22 ± 0.01 and 0.56 ± 0.03 for ^{887}KR→AA, ^{890}RR→AA and ^{887}KR→AA+^{890}RR→AA, respectively). Taken together, these results suggest that the rapid nuclear localization observed for DENV2 NS5 in the context of infection appears to be largely due to C-terminal NLS within residues 883-900 of DENV2 NS5. This is in agreement with the observation that classical NLS is usually found at either at N- or C-terminal end of nuclear cargo proteins so that they are accessible to nuclear transport factors (Marfori *et al.*, 2012). Intriguingly, there is a lack of structural information of this region of NS5, especially residues 890-900 in various flavivirus NS5 crystal structures (Lim *et al.*, 2013b; Lu & Gong, 2013; Malet *et al.*, 2007; Yap *et al.*, 2007; Zhao *et al.*, 2015). This suggests that the C-terminal sequence of NS5 is highly flexible and disordered, which also fits with the finding that truncation of the last 5 amino acids of DENV3 NS5 formed high quality crystals that resulted in the resolution of the first full-length structure of DENV3 NS5 (Zhao *et al.*, 2015), Furthermore, the disordered C-terminal region containing an NLS is also consistent with other studies that have found that peptide sequences that contain the NLS are usually disordered/unfolded until importin-α is bound (Marfori *et al.*, 2012).

The discovery of the C-terminal NLS cannot entirely exclude the existence of an internal α/βNLS because of the availability of extensive supportive published data with both recombinant proteins and infectious clones (Kumar *et al.*, 2013; Pryor *et al.*, 2007; Rawlinson *et al.*, 2009). Mutations in NS5 α/βNLS in the context of DENV2 infectious cDNA clone, namely ^{387}KKK→AAA ("A2") and ^{371}KK→AA+^{387}KKK→AAA ("A1+A2") were previously shown to reduce both infectious virus production and NS5 nuclear accumulation (Kumar *et al.*, 2013; Pryor *et al.*, 2007). Furthermore, it was argued recently that there is no strict correlation between efficient viral RNA replication and DENV2 NS5 nuclear localization because mutation of negatively charged residues (^{397}EE→AA) that are outside the minimal α/βNLS sequence could also affect NS5 nuclear localization drastically in mutant virus ($F_{n/c}$ =~13 for WT and $F_{n/c}$ =~1.5 for ^{397}EE→AA) and yet, it could replicate like WT with an intact *in vivo* NS5 activity (Kumar *et al.*, 2013). Nevertheless, in this study when C-terminal NLS mutations were introduced into DENV2 infectious cDNA clone, namely ^{887}KR→AA ("C-term NLS A1"), ^{890}RR→AA ("C-term NLS A2"), and ^{887}KR→AA+^{890}RR→AA ("C-term NLS A1+A2"), lower viral RNA replication and reduced NS5 nuclear localization was observed for C-term NLS A2 mutant virus, whereas C-term NLS A1 and A1+A2 mutations were lethal (Figure 3-33). Taken together, it is unclear at this stage if α/βNLS and C-terminal NLS play a synergistic or mutually exclusive role in mediating NS5 nuclear localization.

A thorough evaluation of α/βNLS and C-terminal NLS data and their implications is in progress (Jans, Forewood and Vasudevan, personal communication). It is the report that hyperphosphorylated DENV2 NS5 accumulated in the nucleus of infected cells by (Kapoor *et al.*, 1995) resulted in the identification of the putative bipartite α/βNLS between residues 369-405 (Forwood *et al.*, 1999). However, the initial identification was based on the sequence resemblance of this region to bipartite NLS sequence of nucleoplasm (Vancurova *et al.*, 1995), and the fusion of DENV 2 NS5 residues 369-405 to normally cytoplasmic β-galactosidase could be targeted to the nucleus in both *in vivo* and *in vitro* confocal microscopy-based assay. Subsequently, yeast two-hybrid technique coupled with site-directed mutagenesis provided further support for the finding and also additionally found out that NS3 residues 313-608 interacted with NS5 residues 320-368. The NS3 interaction site was predicted to contain a 20 amino acid sequence (residues 342-361) that is completely conserved in all flaviviruses (Brooks *et al.*, 2002; Johansson *et al.*, 2001a; Khromykh *et al.*, 1999). At that stage, since there were no available crystal structures for NS5 MTase or RdRP domains, the NLS region was thought to be a potential interdomain linker; the initial idea was suggested by (Egloff *et al.*, 2002) when they observed a compact MTase domain within residues 7-267 in a DENV NS5 truncated protein (residues 1-296) and the remaining unstructured/disordered region (residues 268-296) was thought to be the interdomain linker region for interaction with NS3, importins and other host proteins.

The discovery of the C-terminal NLS in this work was driven by the search for CRS within DENV1 NS5. Despite the confounding issues with DENV NS5 nuclear localization, the inhibitors that have been identified by *in vitro* AlphaScreen-based NS5-importin-α/β1 binding assay function *in vitro* and one of them, 4-HPR (N-(4-hydroxyphenyl) retinamide) is even active *in vivo* in a mouse model and human PBMC infection assay (Fraser *et al.*, 2014). Therefore, taken together, NS5 nuclear localization is important for DENV replication.

4.5 The thumb subdomain of NS5 may be a hotspot for viral-viral and viral-host protein interactions

The DENV3 NS5 RdRP structure threw a surprise when it showed that NS5 residues 320-405 (coloured in yellow in Figure 4-3) are an integral part of the RdRP domain, and were distributed with α2-α7 helices (βNLS in α2-α5 and α/βNLS in α6-α7 (circled in purple)) (Yap *et al.*, 2007). The α2-α4 helices (residues 323-341) are part of the thumb subdomain (coloured in red); α5 and α7 helices (residues 349-355 and 397-405) are found at the finger tips, between the fingers (coloured in blue) and thumb subdomains and α6 helix (residues 367-386) is close to the palm subdomain (coloured in green). Given the involvement and/or close proximity of these helices to the three subdomains, it may not be surprising if mutations (Iglesias *et al.*, 2011; Kumar *et al.*, 2013; Pryor *et al.*, 2007) or truncations (Rawlinson *et al.*, 2009; Yap *et al.*, 2007) in residues 320-405 destabilize NS5 protein structure. This can conceivably result in a pleiotropic effect on NS5 activity, nuclear localization and RNA replication. On the other hand, the newly discovered C-terminal NLS is at the C-terminal end of NS5 protein (not visible in the structure, resides within the thumb subdomain, circled in green) that is far from the RNA template tunnel (indicated by arrow), priming loop (circled in grey) and palm subdomain (coloured in green) and hence, mutations or truncations at the C-terminal end of NS5 are less likely to impact on protein structure and affect NS5 activity.

With the recently solved crystal structure of full-length DENV3 NS5, the MTase is placed above the fingers subdomian, and the MTase and RdRP domains interact at two contact areas via residues from the MTase domain (residues 63-69, 95-96 and 252-256), the linker region (residues 262-273) and the fingers subdomain from the RdRP domain to create an interaction interface that is unique to DENV. Intriguingly, analysis of the solution structure of NS5 by hydrogen/deuterium exchange mass spectrometry demonstrated that the thumb subdomain has a higher deuterium exchange dynamics than its fingers and palm subdomains (circled in orange in Figure 4-3). This suggests that the thumb subdomain is more flexible and may be able to adopt different conformations to interact with different viral proteins and host proteins. Indeed, this idea is supported by findings from this thesis that both the NS3 binding site (residues 320-341, within α3 helix, circled in blue) and the newly discovered importin-α binding site (residues 883-900, circled in green, missing in structure) reside within the thumb subdomain. Moreover, as discussed in section 4.4, ^{887}KR may have the ability to RNA, and possibly viral RNA and therefore, it is tempting to speculate the ^{87}KR residues may help to facilitate the newly unwound template strand that is exiting from the helicase to enter RdRP (Figure 4-1, green line) via the template tunnel (Figure 4-3) because (1) ^{87}KR are conserved among the flaviviruses (Figure 3-34), (2) residues 890-900 is flexible and (3) it is close to NS3-NS5 interaction site and hence, the inability for viral RNA to enter the template tunnel properly may prevent the synthesis of complementary strand, which results in the inability for sustained RNA replication to occur in ^{887}KR→AA and ^{887}KR→AA+^{890}RR→AA mutant viruses (Figure 3-33). Indeed, elegant mutational study on basic residues of NS5 have led to the identification of dibasic residue on thumb subdomain, namely ^{840}KR (located within helix α26) that were lethal to virus

when mutated to alanine, despite an intact polymerase activity, which used viral RNA as template (Iglesias *et al.*, 2011) and therefore, this further supports the importance involvement of basic residues in RNA binding activity that is not directly related to NS5 polymerase activity. Interestingly, several viral proteins have been reported to have their functional NLS sequence overlapping with RNA binding domain (Donnelly *et al.*, 2007; Elster *et al.*, 1997; Yik *et al.*, 2004). Based on the importance of the ^{87}KR in this study and its location in thumb subdomain, it is tempting to hypothesize that ^{887}KR may be involved in binding to both RNA and importin-α/β1 and it is likely that the loss of binding to RNA resulted in absence of virus replication. Further work examine this aspect is currently ongoing.

Taken together, the thumb subdomain may hold the key to controlling the localization of NS5 through interacting with either NS3 and/or viral RNA, and possibly host factors to stay in the cytoplasm for viral RNA replication or importin-α/β1 to enter the nucleus for it elusive and yet intriguing role.

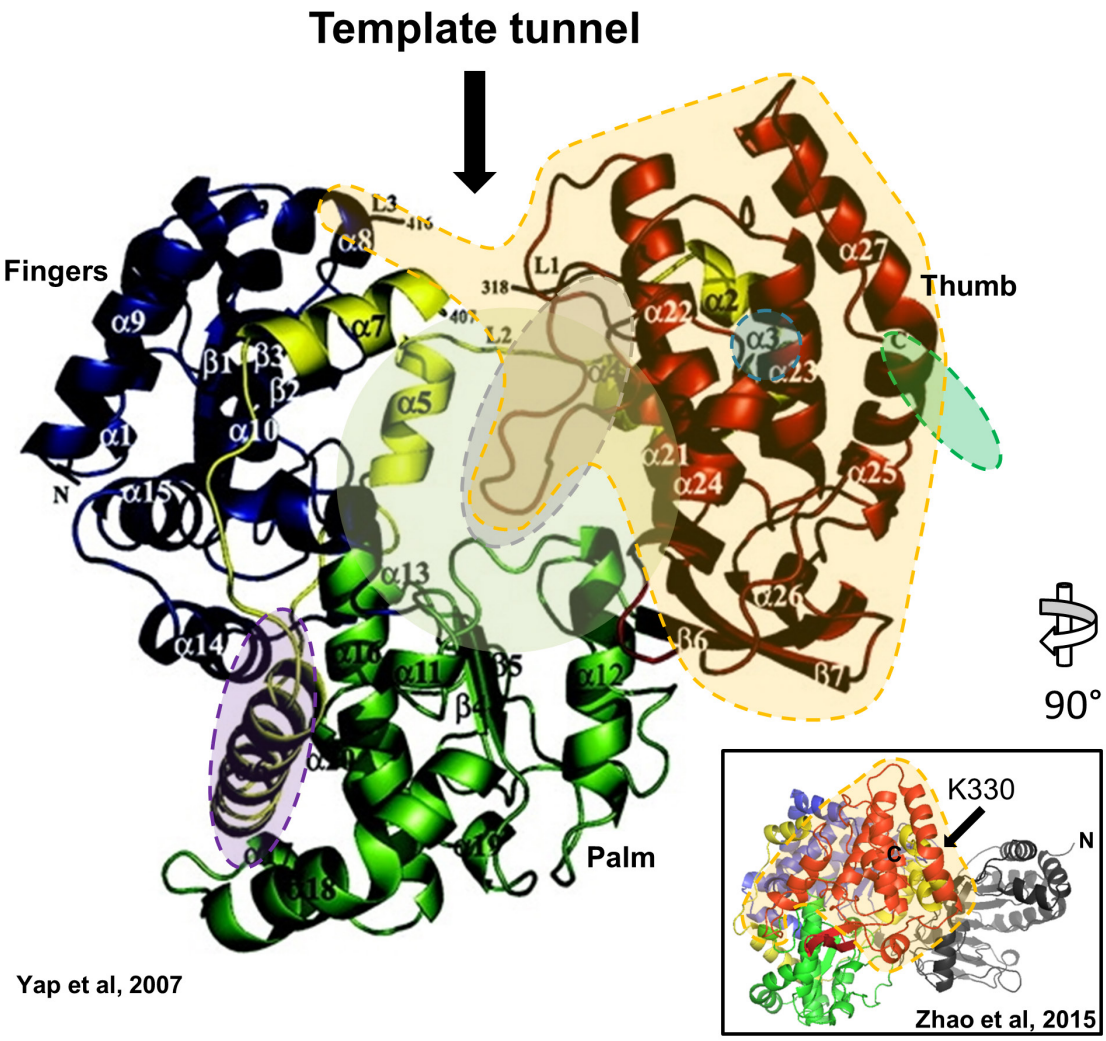

Figure 4-3: Dynamics of DENV3 NS5 in solution. Ribbon representation of DENV3 NS5 RdRP (residues 273 to 900, PDB: 2J7U, (Yap *et al.*, 2007)) and full-length (in inset, residues 6-895, PDB: 4V0Q (Zhao *et al.*, 2015)) structures. The fingers, palm and thumb subdomains and residues 320-405 are colored blue, yellow, green and red, respectively. The MTase is shaded in light green. The secondary structures (α-helix and β-strand) and protein termini (N and C) are labeled as described in (Yap *et al.*, 2007)). The region that is missing in the structure is also defined by the boundary numbers. The template entry tunnel is arrowed. The priming looing is circled in grey. The α/βNLS and C-terminal NLS are circled in purple and green, respectively; C-terminal NLS is missing in the structure and the position is to denote its location in the structure, should it be resolved. NS5 K330 that is important for NS3-NS5 interaction reside in α3 and it is circled in blue. The regions on NS5 RdRP that were shown (Zhao *et al.*, 2015) by Hydrogen/Deuterium Exchange Mass Spectrometry to be of higher dynamics as compared to other parts of the protein are circled in orange, which include residues 735-748, 781-809, 812-850 and 853-895 from thumb subdomain and residues 311-340 from fingers subdomain. *Inset*: The different regions are coloured as per described above, with the following exception: the MTase is coloured in grey and an arrow is used to indicate the position of K330. Figure is adapted from (Yap *et al.*, 2007) and (Zhao *et al.*, 2015).

4.6 Future directions

This thesis has collectively studied the two aspects of NS5 - its interaction with it viral replication partner NS3, and its interaction with host proteins, namely importin-α and human proteins that were identified by our co-IP study. The future work will ultimately converge to help us understand the role of NS5 in DENV replication and pathogenesis and they include the following:

- Since we have demonstrated for the first time that NS3-NS5 interaction play an important role in coordinating the balanced synthesis of positive- and negative-strand, further analysis with different NS3-NS5 interaction mutants may be useful to elucidate the underlying mechanism of NS3-NS5 interaction in coordinating the synthesis of plus- and minus-strand. The studies could provide some insights on how this interaction can influence the dynamics of circular and linear forms of genomic RNA needed for initiation of negative-strand synthesis (Alvarez *et al.*, 2005b), since perturbing the transition between circular and linear forms may upset the 1:10-100 ratio of negative- versus positive-strand RNA in infected cells (Cleaves *et al.*, 1981; Tomassini *et al.*, 2003; Villordo *et al.*, 2010).

- With the dissection of co-IP data in section 3.3, another future work emanating from this study will include the validation of some of the host proteins including Sec61α1 and proteins that are unique to DENV1 and 2 NS5.

- The role of the C-terminal NLS in dengue pathogenesis will form a very productive future study given the recent finding that Sanofi tetravalent vaccine was least effective against DENV serotype 2. It is tempting to speculate that the rapid localization of NS5 to the nucleus may have contributed to the reduced efficacy against this serotype and studies could be carried out to evaluate this finding using the recombinant viruses generated in this study.

References

Acosta, E. G., Kumar, A. & Bartenschlager, R. (2014). Revisiting dengue virus-host cell interaction: new insights into molecular and cellular virology. *Adv Virus Res* **88**, 1-109.

Akey, D. L., Brown, W. C., Dutta, S., Konwerski, J., Jose, J., Jurkiw, T. J., DelProposto, J., Ogata, C. M., Skiniotis, G., Kuhn, R. J. & Smith, J. L. (2014). Flavivirus NS1 structures reveal surfaces for associations with membranes and the immune system. *Science* **343**, 881-885.

Alen, M. M., Dallmeier, K., Balzarini, J., Neyts, J. & Schols, D. (2012). Crucial role of the N-glycans on the viral E-envelope glycoprotein in DC-SIGN-mediated dengue virus infection. *Antiviral Res* **96**, 280-287.

Aleshin, A. E., Shiryaev, S. A., Strongin, A. Y. & Liddington, R. C. (2007). Structural evidence for regulation and specificity of flaviviral proteases and evolution of the Flaviviridae fold. *Protein Sci* **16**, 795-806.

Alvarez, D. E., De Lella Ezcurra, A. L., Fucito, S. & Gamarnik, A. V. (2005a). Role of RNA structures present at the 3'UTR of dengue virus on translation, RNA synthesis, and viral replication. *Virology* **339**, 200-212.

Alvarez, D. E., Lodeiro, M. F., Luduena, S. J., Pietrasanta, L. I. & Gamarnik, A. V. (2005b). Long-range RNA-RNA interactions circularize the dengue virus genome. *J Virol* **79**, 6631-6643.

Anderson, P. & Kedersha, N. (2008). Stress granules: the Tao of RNA triage. *Trends Biochem Sci* **33**, 141-150.

Anwar, A., Leong, K. M., Ng, M. L., Chu, J. J. & Garcia-Blanco, M. A. (2009). The polypyrimidine tract-binding protein is required for efficient dengue virus propagation and associates with the viral replication machinery. *J Biol Chem* **284**, 17021-17029.

Arnold, M., Nath, A., Wohlwend, D. & Kehlenbach, R. H. (2006). Transportin is a major nuclear import receptor for c-Fos: a novel mode of cargo interaction. *J Biol Chem* **281**, 5492-5499.

Ashour, J., Laurent-Rolle, M., Shi, P. Y. & Garcia-Sastre, A. (2009). NS5 of dengue virus mediates STAT2 binding and degradation. *J Virol* **83**, 5408-5418.

Ausubel, F. M. (2010). *Current Protocols in Molecular Biology*: John Wiley & Sons.

Avirutnan, P., Fuchs, A., Hauhart, R. E., Somnuke, P., Youn, S., Diamond, M. S. & Atkinson, J. P. (2010). Antagonism of the complement component C4 by flavivirus nonstructural protein NS1. *J Exp Med* **207**, 793-806.

Avirutnan, P., Punyadee, N., Noisakran, S., Komoltri, C., Thiemmeca, S., Auethavornanan, K., Jairungsri, A., Kanlaya, R., Tangthawornchaikul, N., Puttikhunt, C., Pattanakitsakul, S. N., Yenchitsomanus, P. T., Mongkolsapaya, J., Kasinrerk, W., Sittisombut, N., Husmann, M., Blettner, M., Vasanawathana, S., Bhakdi, S. & Malasit, P. (2006). Vascular leakage in severe dengue virus infections: a potential role for the nonstructural viral protein NS1 and complement. *J Infect Dis* **193**, 1078-1088.

Bailer, S. M. & Haas, J. (2009). Connecting viral with cellular interactomes. *Curr Opin Microbiol* **12**, 453-459.

Bartelma, G. & Padmanabhan, R. (2002). Expression, purification, and characterization of the RNA 5 '-triphosphatase activity of dengue virus type 2 nonstructural protein 3. *Virology* **299**, 122-132.

Bartholomeusz, A. I. & Wright, P. J. (1993). Synthesis of dengue virus RNA in vitro: initiation and the involvement of proteins NS3 and NS5. *Arch Virol* **128**, 111-121.

Becerra, A., Warke, R. V., Martin, K., Xhaja, K., de Bosch, N., Rothman, A. L. & Bosch, I. (2009). Gene expression profiling of dengue infected human primary cells identifies secreted mediators in vivo. *J Med Virol* **81**, 1403-1411.

Beckham, C. J. & Parker, R. (2008). P bodies, stress granules, and viral life cycles. *Cell Host Microbe* **3**, 206-212.

Benarroch, D., Selisko, B., Locatelli, G. A., Maga, G., Romette, J. L. & Canard, B. (2004). The RNA helicase, nucleotide 5 '-triphosphatase, and RNA 5 '-triphosphatase activities of Dengue virus protein NS3 are Mg2+-dependent and require a functional Walker B motif in the helicase catalytic core. *Virology* **328**, 208-218.

Bernado, P., Mylonas, E., Petoukhov, M. V., Blackledge, M. & Svergun, D. I. (2007). Structural characterization of flexible proteins using small-angle X-ray scattering. *J Am Chem Soc* **129**, 5656-5664.

Bhatt, S., Gething, P. W., Brady, O. J., Messina, J. P., Farlow, A. W., Moyes, C. L., Drake, J. M., Brownstein, J. S., Hoen, A. G., Sankoh, O., Myers, M. F., George, D. B., Jaenisch, T., Wint, G. R., Simmons, C. P., Scott, T. W., Farrar, J. J. & Hay, S. I. (2013). The global distribution and burden of dengue. *Nature* **496**, 504-507.

Bhuvanakantham, R., Li, J., Tan, T. T. & Ng, M. L. (2010). Human Sec3 protein is a novel transcriptional and translational repressor of flavivirus. *Cell Microbiol* **12**, 453-472.

Bhuvanakantham, R. & Ng, M. L. (2013). West Nile virus and dengue virus capsid protein negates the antiviral activity of human Sec3 protein through the proteasome pathway. *Cell Microbiol* **15**, 1688-1706.

Bidet, K., Dadlani, D. & Garcia-Blanco, M. A. (2014). G3BP1, G3BP2 and CAPRIN1 are required for translation of interferon stimulated mRNAs and are targeted by a dengue virus non-coding RNA. *PLoS Pathog* **10**, e1004242.

Bidet, K. & Garcia-Blanco, M. A. (2014). Flaviviral RNAs: weapons and targets in the war between virus and host. *Biochem J* **462**, 215-230.

Brault, J. B., Kudelko, M., Vidalain, P. O., Tangy, F., Despres, P. & Pardigon, N. (2011). The interaction of flavivirus M protein with light chain Tctex-1 of human dynein plays a role in late stages of virus replication. *Virology* **417**, 369-378.

Brooks, A. J., Johansson, M., John, A. V., Xu, Y. B., Jans, D. A. & Vasudevan, S. G. (2002). The interdomain region of dengue NS5 protein that binds to the viral helicase NS3 contains independently functional importin beta 1 and importin alpha/beta-recognized nuclear localization signals. *J Biol Chem* **277**, 36399-36407.

Brugidou, J., Legrand, C., Mery, J. & Rabie, A. (1995). The retro-inverso form of a homeobox-derived short peptide is rapidly internalised by cultured neurones: a new basis for an efficient intracellular delivery system. *Biochem Biophys Res Commun* **214**, 685-693.

Bryant, J. E., Calvert, A. E., Mesesan, K., Crabtree, M. B., Volpe, K. E., Silengo, S., Kinney, R. M., Huang, C. Y., Miller, B. R. & Roehrig, J. T. (2007). Glycosylation of the dengue 2 virus E protein at N67 is critical for virus growth in vitro but not for growth in intrathoracically inoculated Aedes aegypti mosquitoes. *Virology* **366**, 415-423.

Caly, L., Wagstaff, K. M. & Jans, D. A. (2012a). Nuclear trafficking of proteins from RNA viruses: potential target for antivirals? *Antiviral Res* **95**, 202-206.

Caly, L., Wagstaff, K. M. & Jans, D. A. (2012b). Nuclear trafficking of proteins from RNA viruses: potential target for antivirals? *Antiviral Res* **95**, 202-206.

Carpp, L. N., Rogers, R. S., Moritz, R. L. & Aitchison, J. D. (2014). Quantitative Proteomic Analysis of Host-virus Interactions Reveals a Role for Golgi Brefeldin

A Resistance Factor 1 (GBF1) in Dengue Infection. *Mol Cell Proteomics* **13**, 2836-2854.

Chakravarti, A. & Kumaria, R. (2006). Circulating levels of tumour necrosis factor-alpha & interferon-gamma in patients with dengue & dengue haemorrhagic fever during an outbreak. *Indian J Med Res* **123**, 25-30.

Chapman, E. G., Moon, S. L., Wilusz, J. & Kieft, J. S. (2014). RNA structures that resist degradation by Xrn1 produce a pathogenic Dengue virus RNA. *Elife* **3**, e01892.

Chatel-Chaix, L., Melancon, P., Racine, M. E., Baril, M. & Lamarre, D. (2011). Y-box-binding protein 1 interacts with hepatitis C virus NS3/4A and influences the equilibrium between viral RNA replication and infectious particle production. *J Virol* **85**, 11022-11037.

Chau, T. N., Quyen, N. T., Thuy, T. T., Tuan, N. M., Hoang, D. M., Dung, N. T., Lien le, B., Quy, N. T., Hieu, N. T., Hieu, L. T., Hien, T. T., Hung, N. T., Farrar, J. & Simmons, C. P. (2008). Dengue in Vietnamese infants--results of infection-enhancement assays correlate with age-related disease epidemiology, and cellular immune responses correlate with disease severity. *J Infect Dis* **198**, 516-524.

Chen, C. J., Kuo, M. D., Chien, L. J., Hsu, S. L., Wang, Y. M. & Lin, J. H. (1997). RNA-protein interactions: Involvement of NS3, NS5, and 3' noncoding regions of Japanese encephalitis virus genomic RNA. *J Virol* **71**, 3466-3473.

Chiu, H. C., Hannemann, H., Heesom, K. J., Matthews, D. A. & Davidson, A. D. (2014). High-throughput quantitative proteomic analysis of dengue virus type 2 infected A549 cells. *PLoS One* **9**, e93305.

Christenbury, J. G., Aw, P. P., Ong, S. H., Schreiber, M. J., Chow, A., Gubler, D. J., Vasudevan, S. G., Ooi, E. E. & Hibberd, M. L. (2010). A method for full genome sequencing of all four serotypes of the dengue virus. *J Virol Methods* **169**, 202-206.

Chu, P. W. & Westaway, E. G. (1985). Replication strategy of Kunjin virus: evidence for recycling role of replicative form RNA as template in semiconservative and asymmetric replication. *Virology* **140**, 68-79.

Chua, J. J., Ng, M. M. & Chow, V. T. (2004). The non-structural 3 (NS3) protein of dengue virus type 2 interacts with human nuclear receptor binding protein and is associated with alterations in membrane structure. *Virus Res* **102**, 151-163.

Chung, K. M., Liszewski, M. K., Nybakken, G., Davis, A. E., Townsend, R. R., Fremont, D. H., Atkinson, J. P. & Diamond, M. S. (2006). West Nile virus nonstructural protein NS1 inhibits complement activation by binding the regulatory protein factor H. *Proc Natl Acad Sci U S A* **103**, 19111-19116.

Cleaves, G. R., Ryan, T. E. & Schlesinger, R. W. (1981). Identification and characterization of type 2 dengue virus replicative intermediate and replicative form RNAs. *Virology* **111**, 73-83.

Clum, S., Ebner, K. E. & Padmanabhan, R. (1997). Cotranslational membrane insertion of the serine proteinase precursor NS2B-NS3(Pro) of dengue virus type 2 is required for efficient in vitro processing and is mediated through the hydrophobic regions of NS2B. *J Biol Chem* **272**, 30715-30723.

Clyde, K., Barrera, J. & Harris, E. (2008). The capsid-coding region hairpin element (cHP) is a critical determinant of dengue virus and West Nile virus RNA synthesis. *Virology* **379**, 314-323.

Clyde, K. & Harris, E. (2006). RNA secondary structure in the coding region of dengue virus type 2 directs translation start codon selection and is required for viral replication. *J Virol* **80**, 2170-2182.

Collins, T. J. (2007). ImageJ for microscopy. *Biotechniques* **43**, 25-30.

Colpitts, T. M., Barthel, S., Wang, P. & Fikrig, E. (2011a). Dengue virus capsid protein binds core histones and inhibits nucleosome formation in human liver cells. *PLoS One* **6**, e24365.

Colpitts, T. M., Cox, J., Nguyen, A., Feitosa, F., Krishnan, M. N. & Fikrig, E. (2011b). Use of a tandem affinity purification assay to detect interactions between West Nile and dengue viral proteins and proteins of the mosquito vector. *Virology* **417**, 179-187.

Conceicao, T. M., El-Bacha, T., Villas-Boas, C. S., Coello, G., Ramirez, J., Montero-Lomeli, M. & Da Poian, A. T. (2010). Gene expression analysis during dengue virus infection in HepG2 cells reveals virus control of innate immune response. *J Infect* **60**, 65-75.

Cui, T., Sugrue, R. J., Xu, Q., Lee, A. K., Chan, Y. C. & Fu, J. (1998). Recombinant dengue virus type 1 NS3 protein exhibits specific viral RNA binding and NTPase activity regulated by the NS5 protein. *Virology* **246**, 409-417.

De Nova-Ocampo, M., Villegas-Sepulveda, N. & del Angel, R. M. (2002). Translation elongation factor-1alpha, La, and PTB interact with the 3' untranslated region of dengue 4 virus RNA. *Virology* **295**, 337-347.

Dejnirattisai, W., Jumnainsong, A., Onsirisakul, N., Fitton, P., Vasanawathana, S., Limpitikul, W., Puttikhunt, C., Edwards, C., Duangchinda, T., Supasa, S., Chawansuntati, K., Malasit, P., Mongkolsapaya, J. & Screaton, G. (2010). Cross-reacting antibodies enhance dengue virus infection in humans. *Science* **328**, 745-748.

Derossi, D., Calvet, S., Trembleau, A., Brunissen, A., Chassaing, G. & Prochiantz, A. (1996). Cell internalization of the third helix of the Antennapedia homeodomain is receptor-independent. *J Biol Chem* **271**, 18188-18193.

Deubel, V., Bordier, M., Megret, F., Gentry, M. K., Schlesinger, J. J. & Girard, M. (1991). Processing, secretion, and immunoreactivity of carboxy terminally truncated dengue-2 virus envelope proteins expressed in insect cells by recombinant baculoviruses. *Virology* **180**, 442-447.

Dingwall, C. & Laskey, R. A. (1991). Nuclear targeting sequences--a consensus? *Trends Biochem Sci* **16**, 478-481.

Dong, H., Fink, K., Zust, R., Lim, S. P., Qin, C. F. & Shi, P. Y. (2014). Flavivirus RNA methylation. *J Gen Virol* **95**, 763-778.

Donnelly, M., Verhagen, J. & Elliott, G. (2007). RNA binding by the herpes simplex virus type 1 nucleocytoplasmic shuttling protein UL47 is mediated by an N-terminal arginine-rich domain that also functions as its nuclear localization signal. *J Virol* **81**, 2283-2296.

Duan, X., Lu, X., Li, J. & Liu, Y. (2008). Novel binding between pre-membrane protein and vacuolar ATPase is required for efficient dengue virus secretion. *Biochem Biophys Res Commun* **373**, 319-324.

Duyen, H. T., Ngoc, T. V., Ha do, T., Hang, V. T., Kieu, N. T., Young, P. R., Farrar, J. J., Simmons, C. P., Wolbers, M. & Wills, B. A. (2011). Kinetics of plasma viremia and soluble nonstructural protein 1 concentrations in dengue: differential effects according to serotype and immune status. *J Infect Dis* **203**, 1292-1300.

Egloff, M. P., Benarroch, D., Selisko, B., Romette, J. L. & Canard, B. (2002). An RNA cap (nucleoside-2'-O-)-methyltransferase in the flavivirus RNA polymerase NS5: crystal structure and functional characterization. *EMBO J* **21**, 2757-2768.

Egloff, M. P., Decroly, E., Malet, H., Selisko, B., Benarroch, D., Ferron, F. & Canard, B. (2007). Structural and functional analysis of methylation and 5'-RNA sequence requirements of short capped RNAs by the methyltransferase domain of dengue virus NS5. *J Mol Biol* **372**, 723-736.

Elster, C., Larsen, K., Gagnon, J., Ruigrok, R. W. & Baudin, F. (1997). Influenza virus M1 protein binds to RNA through its nuclear localization signal. *J Gen Virol* **78 (Pt 7)**, 1589-1596.

Emara, M. M. & Brinton, M. A. (2007). Interaction of TIA-1/TIAR with West Nile and dengue virus products in infected cells interferes with stress granule formation and processing body assembly. *Proc Natl Acad Sci U S A* **104**, 9041-9046.

Erbel, P., Schiering, N., D'Arcy, A., Renatus, M., Kroemer, M., Lim, S. P., Yin, Z., Keller, T. H., Vasudevan, S. G. & Hommel, U. (2006). Structural basis for the activation of flaviviral NS3 proteases from Dengue and West Nile virus. *Nat Struct Mol Biol* **13**, 372-373.

Falgout, B., Pethel, M., Zhang, Y. M. & Lai, C. J. (1991). Both nonstructural proteins NS2B and NS3 are required for the proteolytic processing of dengue virus nonstructural proteins. *J Virol* **65**, 2467-2475.

Filomatori, C. V., Lodeiro, M. F., Alvarez, D. E., Samsa, M. M., Pietrasanta, L. & Gamarnik, A. V. (2006). A 5' RNA element promotes dengue virus RNA synthesis on a circular genome. *Genes Dev* **20**, 2238-2249.

Fink, J., Gu, F., Ling, L., Tolfvenstam, T., Olfat, F., Chin, K. C., Aw, P., George, J., Kuznetsov, V. A., Schreiber, M., Vasudevan, S. G. & Hibberd, M. L. (2007). Host gene expression profiling of dengue virus infection in cell lines and patients. *PLoS Negl Trop Dis* **1**, e86.

Flamand, M., Megret, F., Mathieu, M., Lepault, J., Rey, F. A. & Deubel, V. (1999). Dengue virus type 1 nonstructural glycoprotein NS1 is secreted from mammalian cells as a soluble hexamer in a glycosylation-dependent fashion. *J Virol* **73**, 6104-6110.

Folly, B. B., Weffort-Santos, A. M., Fathman, C. G. & Soares, L. R. (2011). Dengue-2 structural proteins associate with human proteins to produce a coagulation and innate immune response biased interactome. *BMC Infect Dis* **11**, 34.

Fornerod, M. & Ohno, M. (2002). Exportin-mediated nuclear export of proteins and ribonucleoproteins. *Results Probl Cell Differ* **35**, 67-91.

Forwood, J. K., Brooks, A., Briggs, L. J., Xiao, C. Y., Jans, D. A. & Vasudevan, S. G. (1999). The 37-amino-acid interdomain of dengue virus NS5 protein contains a functional NLS and inhibitory CK2 site. *Biochem Biophys Res Commun* **257**, 731-737.

Fraser, J. E., Watanabe, S., Wang, C., Chan, W. K., Maher, B., Lopez-Denman, A., Hick, C., Wagstaff, K. M., Mackenzie, J. M., Sexton, P. M., Vasudevan, S. G. & Jans, D. A. (2014). A nuclear transport inhibitor that modulates the unfolded protein response and provides in vivo protection against lethal dengue virus infection. *J Infect Dis* **210**, 1780-1791.

Fraser, K. B. & Gharpure, M. (1962). Immunoofluorescent tracing of polyoma virus in transformation experiments with BHK 21 cells. *Virology* **18**, 505-507.

Friebe, P., Pena, J., Pohl, M. O. & Harris, E. (2012). Composition of the sequence downstream of the dengue virus 5' cyclization sequence (dCS) affects viral RNA replication. *Virology* **422**, 346-356.

Fried, J. R., Gibbons, R. V., Kalayanarooj, S., Thomas, S. J., Srikiatkhachorn, A., Yoon, I. K., Jarman, R. G., Green, S., Rothman, A. L. & Cummings, D. A. (2010). Serotype-specific differences in the risk of dengue hemorrhagic fever: an analysis of data collected in Bangkok, Thailand from 1994 to 2006. *PLoS Negl Trop Dis* **4**, e617.

Gabriel, G., Klingel, K., Otte, A., Thiele, S., Hudjetz, B., Arman-Kalcek, G., Sauter, M., Shmidt, T., Rother, F., Baumgarte, S., Keiner, B., Hartmann, E., Bader, M., Brownlee, G. G., Fodor, E. & Klenk, H. D. (2011). Differential use of

importin-alpha isoforms governs cell tropism and host adaptation of influenza virus. *Nat Commun* **2**, 156.

Gao, F., Duan, X., Lu, X., Liu, Y., Zheng, L., Ding, Z. & Li, J. (2010). Novel binding between pre-membrane protein and claudin-1 is required for efficient dengue virus entry. *Biochem Biophys Res Commun* **391**, 952-957.

Garcia-Montalvo, B. M., Medina, F. & del Angel, R. M. (2004a). La protein binds to NS5 and NS3 and to the 5' and 3' ends of Dengue 4 virus RNA. *Virus Res* **102**, 141-150.

Garcia-Montalvo, B. M., Medina, F. & del Angel, R. M. (2004b). La protein binds to NS5 and NS3 and to the 5 ' and 3 ' ends of Dengue 4 virus RNA. *Virus Res* **102**, 141-150.

Geiss, B. J., Stahla, H., Hannah, A. M., Gari, A. M. & Keenan, S. M. (2009). Focus on flaviviruses: current and future drug targets. *Future Med Chem* **1**, 327-344.

Gollins, S. W. & Porterfield, J. S. (1986). A new mechanism for the neutralization of enveloped viruses by antiviral antibody. *Nature* **321**, 244-246.

Gomila, R. C., Martin, G. W. & Gehrke, L. (2011). NF90 binds the dengue virus RNA 3' terminus and is a positive regulator of dengue virus replication. *PLoS One* **6**, e16687.

Gorbalenya, A. E., Donchenko, A. P., Koonin, E. V. & Blinov, V. M. (1989). N-terminal domains of putative helicases of flavi- and pestiviruses may be serine proteases. *Nucleic Acids Res* **17**, 3889-3897.

Graham, F. L., Smiley, J., Russell, W. C. & Nairn, R. (1977). Characteristics of a human cell line transformed by DNA from human adenovirus type 5. *J Gen Virol* **36**, 59-74.

Grant, D., Tan, G. K., Qing, M., Ng, J. K., Yip, A., Zou, G., Xie, X., Yuan, Z., Schreiber, M. J., Schul, W., Shi, P. Y. & Alonso, S. (2011). A single amino acid in nonstructural protein NS4B confers virulence to dengue virus in AG129 mice through enhancement of viral RNA synthesis. *J Virol* **85**, 7775-7787.

Gubler, D., Kuno, G. & Markoff, L. (2007). Flaviviruses. In *Fields virology*, 5th edn, pp. 1153 -1253. Philadelphia: Wolters kluwer/Lippincott Williams & Wilkins.

Gubler, D. J. (1998). Dengue and dengue hemorrhagic fever. *Clin Microbiol Rev* **11**, 480-496.

Gubler, D. J. (2012). The economic burden of dengue. *Am J Trop Med Hyg* **86**, 743-744.

Gutsche, I., Coulibaly, F., Voss, J. E., Salmon, J., d'Alayer, J., Ermonval, M., Larquet, E., Charneau, P., Krey, T., Megret, F., Guittet, E., Rey, F. A. & Flamand, M. (2011). Secreted dengue virus nonstructural protein NS1 is an atypical barrel-shaped high-density lipoprotein. *Proc Natl Acad Sci U S A* **108**, 8003-8008.

Guzman, M. G. & Kouri, G. (2002). Dengue: an update. *Lancet Infect Dis* **2**, 33-42.

Halstead, S. B. (1988). Pathogenesis of Dengue: challenges to molecular biology. *Science* **239**, 476-481.

Halstead, S. B. (1997). Epidemiology of dengue and dengue hemorrhagic fever. In *Dengue and Dengue Hemorrhagic Fever*, pp. 23-44. Edited by D. J. Gubler & G. Kuno. Wallingford: CAB International.

Halstead, S. B. (2007). Dengue. *Lancet* **370**, 1644-1652.

Hancock, P. A., Sinkins, S. P. & Godfray, H. C. (2011). Strategies for introducing Wolbachia to reduce transmission of mosquito-borne diseases. *PLoS Negl Trop Dis* **5**, e1024.

Hannemann, H., Sung, P. Y., Chiu, H. C., Yousuf, A., Bird, J., Lim, S. P. & Davidson, A. D. (2013). Serotype-specific differences in dengue virus non-structural protein 5 nuclear localization. *J Biol Chem* **288**, 22621-22635.

Heaton, N. S., Perera, R., Berger, K. L., Khadka, S., Lacount, D. J., Kuhn, R. J. & Randall, G. (2010). Dengue virus nonstructural protein 3 redistributes fatty acid synthase to sites of viral replication and increases cellular fatty acid synthesis. *Proc Natl Acad Sci U S A* **107**, 17345-17350.

Heinz, F. X., Collett, M. S., Purcell, R. H., Gould, E. A., Howard, C. R., Houghton, M., Moormann, R. J. M., Rice, C. M. & Thiel, H. J. (2000). Family Flaviviridae. In *Virus Taxonomy: Seventh Report of the International Committee on Taxonomy of Viruses* pp. 859–878. Edited by M. H. V. v. Regenmortel, C. M. Fauquet, D. H. L. Bishop, E. B. Carstens, M. K. Estes, S. M. Lemon, J. Maniloff, M. A. Mayo, D. J. McGeoch, C. R. Pringle & R. B. Wickner. San Diego: Academic Press.

Hidari, K. I. & Suzuki, T. (2011). Dengue virus receptor. *Trop Med Health* **39**, 37-43.

Holden, K. L., Stein, D. A., Pierson, T. C., Ahmed, A. A., Clyde, K., Iversen, P. L. & Harris, E. (2006). Inhibition of dengue virus translation and RNA synthesis by a morpholino oligomer targeted to the top of the terminal 3' stem-loop structure. *Virology* **344**, 439-452.

Hsieh, S. C., Zou, G., Tsai, W. Y., Qing, M., Chang, G. J., Shi, P. Y. & Wang, W. K. (2011). The C-terminal helical domain of dengue virus precursor membrane protein is involved in virus assembly and entry. *Virology* **410**, 170-180.

Huang, S. S. & Fraenkel, E. (2009). Integrating proteomic, transcriptional, and interactome data reveals hidden components of signaling and regulatory networks. *Sci Signal* **2**, ra40.

Hulo, C., de Castro, E., Masson, P., Bougueleret, L., Bairoch, A., Xenarios, I. & Le Mercier, P. (2011). ViralZone: a knowledge resource to understand virus diversity. *Nucleic Acids Res* **39**, D576-582.

Hutten, S. & Kehlenbach, R. H. (2007). CRM1-mediated nuclear export: to the pore and beyond. *Trends Cell Biol* **17**, 193-201.

Igarashi, A. (1978). Isolation of a Singh's Aedes albopictus cell clone sensitive to Dengue and Chikungunya viruses. *J Gen Virol* **40**, 531-544.

Iglesias, N. G., Filomatori, C. V. & Gamarnik, A. V. (2011). The F1 motif of dengue virus polymerase NS5 is involved in promoter-dependent RNA synthesis. *J Virol* **85**, 5745-5756.

Issur, M., Geiss, B. J., Bougie, I., Picard-Jean, F., Despins, S., Mayette, J., Hobdey, S. E. & Bisaillon, M. (2009). The flavivirus NS5 protein is a true RNA guanylyltransferase that catalyzes a two-step reaction to form the RNA cap structure. *RNA* **15**, 2340-2350.

Jacobs, M. G., Robinson, P. J., Bletchly, C., Mackenzie, J. M. & Young, P. R. (2000). Dengue virus nonstructural protein 1 is expressed in a glycosyl-phosphatidylinositol-linked form that is capable of signal transduction. *FASEB J* **14**, 1603-1610.

Jans, D. A. & Hubner, S. (1996). Regulation of protein transport to the nucleus: central role of phosphorylation. *Physiol Rev* **76**, 651-685.

Jiang, L., Yao, H., Duan, X., Lu, X. & Liu, Y. (2009). Polypyrimidine tract-binding protein influences negative strand RNA synthesis of dengue virus. *Biochem Biophys Res Commun* **385**, 187-192.

Johansson, M., Brooks, A. J., Jans, D. A. & Vasudevan, S. G. (2001a). A small region of the dengue virus-encoded RNA-dependent RNA polymerase, NS5, confers interaction with both the nuclear transport receptor importin-beta and the viral helicase, NS3. *J Gen Virol* **82**, 735-745.

Johansson, M., Brooks, A. J., Jans, D. A. & Vasudevan, S. G. (2001b). A small region of the dengue virus-encoded RNA-dependent RNA polymerase, NS5, confers

interaction with both the nuclear transport receptor importin-ss and the viral helicase, NS3. *J Gen Virol* **82**, 735-745.

Johnson, B. W., Russell, B. J. & Lanciotti, R. S. (2005). Serotype-specific detection of dengue viruses in a fourplex real-time reverse transcriptase PCR assay. *J Clin Microbiol* **43**, 4977-4983.

Jones, C. T., Ma, L., Burgner, J. W., Groesch, T. D., Post, C. B. & Kuhn, R. J. (2003). Flavivirus capsid is a dimeric alpha-helical protein. *J Virol* **77**, 7143-7149.

Juffrie, M., Meer, G. M., Hack, C. E., Haasnoot, K., Sutaryo, Veerman, A. J. & Thijs, L. G. (2001). Inflammatory mediators in dengue virus infection in children: interleukin-6 and its relation to C-reactive protein and secretory phospholipase A2. *Am J Trop Med Hyg* **65**, 70-75.

Kanakaratne, N., Wahala, W. M., Messer, W. B., Tissera, H. A., Shahani, A., Abeysinghe, N., de-Silva, A. M. & Gunasekera, M. (2009). Severe dengue epidemics in Sri Lanka, 2003-2006. *Emerg Infect Dis* **15**, 192-199.

Kanlaya, R., Pattanakitsakul, S. N., Sinchaikul, S., Chen, S. T. & Thongboonkerd, V. (2010). Vimentin interacts with heterogeneous nuclear ribonucleoproteins and dengue nonstructural protein 1 and is important for viral replication and release. *Mol Biosyst* **6**, 795-806.

Kapoor, A., Simmonds, P., Cullen, J. M., Scheel, T. K., Medina, J. L., Giannitti, F., Nishiuchi, E., Brock, K. V., Burbelo, P. D., Rice, C. M. & Lipkin, W. I. (2013). Identification of a pegivirus (GB virus-like virus) that infects horses. *J Virol* **87**, 7185-7190.

Kapoor, M., Zhang, L. W., Ramachandra, M., Kusukawa, J., Ebner, K. E. & Padmanabhan, R. (1995). Association between NS3 and NS5 proteins of dengue virus type 2 in the putative RNA replicase is linked to differential phosphorylation of NS5. *J Biol Chem* **270**, 19100-19106.

Katoh, H., Okamoto, T., Fukuhara, T., Kambara, H., Morita, E., Mori, Y., Kamitani, W. & Matsuura, Y. (2013). Japanese encephalitis virus core protein inhibits stress granule formation through an interaction with Caprin-1 and facilitates viral propagation. *J Virol* **87**, 489-502.

Kedersha, N., Ivanov, P. & Anderson, P. (2013). Stress granules and cell signaling: more than just a passing phase? *Trends Biochem Sci* **38**, 494-506.

Keelapang, P., Sriburi, R., Supasa, S., Panyadee, N., Songjaeng, A., Jairungsri, A., Puttikhunt, C., Kasinrerk, W., Malasit, P. & Sittisombut, N. (2004). Alterations of pr-M cleavage and virus export in pr-M junction chimeric dengue viruses. *J Virol* **78**, 2367-2381.

Keller, A. A., Mussbach, F., Breitling, R., Hemmerich, P., Schaefer, B., Lorkowski, S. & Reissmann, S. (2013). Relationships between Cargo, Cell Penetrating Peptides and Cell Type for Uptake of Non-Covalent Complexes into Live Cells. *Pharmaceuticals (Basel)* **6**, 184-203.

Kelley, J. F., Kaufusi, P. H., Volper, E. M. & Nerurkar, V. R. (2011). Maturation of dengue virus nonstructural protein 4B in monocytes enhances production of dengue hemorrhagic fever-associated chemokines and cytokines. *Virology* **418**, 27-39.

Kelly, E. P., Puri, B., Sun, W. & Falgout, B. (2010). Identification of mutations in a candidate dengue 4 vaccine strain 341750 PDK20 and construction of a full-length cDNA clone of the PDK20 vaccine candidate. *Vaccine* **28**, 3030-3037.

Khadka, S., Vangeloff, A. D., Zhang, C., Siddavatam, P., Heaton, N. S., Wang, L., Sengupta, R., Sahasrabudhe, S., Randall, G., Gribskov, M., Kuhn, R. J., Perera, R. & LaCount, D. J. (2011). A physical interaction network of dengue virus and human proteins. *Mol Cell Proteomics* **10**, M111 012187.

Khromykh, A. A., Harvey, T. J., Abedinia, M. & Westaway, E. G. (1996). Expression and purification of the seven nonstructural proteins of the flavivirus Kunjin in the E. coli and the baculovirus expression systems. *J Virol Methods* **61**, 47-58.

Khromykh, A. A., Sedlak, P. L. & Westaway, E. G. (1999). trans-Complementation analysis of the flavivirus Kunjin ns5 gene reveals an essential role for translation of its N-terminal half in RNA replication. *J Virol* **73**, 9247-9255.

Khunchai, S., Junking, M., Suttitheptumrong, A., Yasamut, U., Sawasdee, N., Netsawang, J., Morchang, A., Chaowalit, P., Noisakran, S., Yenchitsomanus, P. T. & Limjindaporn, T. (2012). Interaction of dengue virus nonstructural protein 5 with Daxx modulates RANTES production. *Biochem Biophys Res Commun* **423**, 398-403.

Kohler, M., Speck, C., Christiansen, M., Bischoff, F. R., Prehn, S., Haller, H., Gorlich, D. & Hartmann, E. (1999). Evidence for distinct substrate specificities of importin alpha family members in nuclear protein import. *Mol Cell Biol* **19**, 7782-7791.

Kosugi, S., Hasebe, M., Matsumura, N., Takashima, H., Miyamoto-Sato, E., Tomita, M. & Yanagawa, H. (2009a). Six classes of nuclear localization signals specific to different binding grooves of importin alpha. *J Biol Chem* **284**, 478-485.

Kosugi, S., Hasebe, M., Tomita, M. & Yanagawa, H. (2009b). Systematic identification of cell cycle-dependent yeast nucleocytoplasmic shuttling proteins by prediction of composite motifs. *Proc Natl Acad Sci U S A* **106**, 10171-10176.

Kozin, M. B. & Svergun, D. I. (2001). Automated matching of high- and low-resolution structural models. *J Appl Crystallogr* **34**, 33-41.

Krishnan, M. N. & Garcia-Blanco, M. A. (2014). Targeting host factors to treat West Nile and dengue viral infections. *Viruses* **6**, 683-708.

Krishnan, M. N., Ng, A., Sukumaran, B., Gilfoy, F. D., Uchil, P. D., Sultana, H., Brass, A. L., Adametz, R., Tsui, M., Qian, F., Montgomery, R. R., Lev, S., Mason, P. W., Koski, R. A., Elledge, S. J., Xavier, R. J., Agaisse, H. & Fikrig, E. (2008). RNA interference screen for human genes associated with West Nile virus infection. *Nature* **455**, 242-245.

Kroschewski, H., Lim, S. P., Butcher, R. E., Yap, T. L., Lescar, J., Wright, P. J., Vasudevan, S. G. & Davidson, A. D. (2008). Mutagenesis of the dengue virus type 2 NS5 methyltransferase domain. *J Biol Chem* **283**, 19410-19421.

Kuhn, R. J., Zhang, W., Rossmann, M. G., Pletnev, S. V., Corver, J., Lenches, E., Jones, C. T., Mukhopadhyay, S., Chipman, P. R., Strauss, E. G., Baker, T. S. & Strauss, J. H. (2002). Structure of dengue virus: implications for flavivirus organization, maturation, and fusion. *Cell* **108**, 717-725.

Kumar, A., Buhler, S., Selisko, B., Davidson, A., Mulder, K., Canard, B., Miller, S. & Bartenschlager, R. (2013). Nuclear localization of dengue virus nonstructural protein 5 does not strictly correlate with efficient viral RNA replication and inhibition of type I interferon signaling. *J Virol* **87**, 4545-4557.

Kurosu, T., Chaichana, P., Yamate, M., Anantapreecha, S. & Ikuta, K. (2007). Secreted complement regulatory protein clusterin interacts with dengue virus nonstructural protein 1. *Biochem Biophys Res Commun* **362**, 1051-1056.

Kutay, U., Bischoff, F. R., Kostka, S., Kraft, R. & Gorlich, D. (1997). Export of importin alpha from the nucleus is mediated by a specific nuclear transport factor. *Cell* **90**, 1061-1071.

Kutay, U. & Guttinger, S. (2005). Leucine-rich nuclear-export signals: born to be weak. *Trends Cell Biol* **15**, 121-124.

Kyle, J. L. & Harris, E. (2008). Global spread and persistence of dengue. *Annu Rev Microbiol* **62**, 71-92.

la Cour, T., Kiemer, L., Molgaard, A., Gupta, R., Skriver, K. & Brunak, S. (2004). Analysis and prediction of leucine-rich nuclear export signals. *Protein Eng Des Sel* **17**, 527-536.

Lanford, R. E., Chavez, D., Chisari, F. V. & Sureau, C. (1995). Lack of detection of negative-strand hepatitis C virus RNA in peripheral blood mononuclear cells and other extrahepatic tissues by the highly strand-specific rTth reverse transcriptase PCR. *J Virol* **69**, 8079-8083.

Lanford, R. E., Sureau, C., Jacob, J. R., White, R. & Fuerst, T. R. (1994). Demonstration of in vitro infection of chimpanzee hepatocytes with hepatitis C virus using strand-specific RT/PCR. *Virology* **202**, 606-614.

Le Breton, M., Meyniel-Schicklin, L., Deloire, A., Coutard, B., Canard, B., de Lamballerie, X., Andre, P., Rabourdin-Combe, C., Lotteau, V. & Davoust, N. (2011). Flavivirus NS3 and NS5 proteins interaction network: a high-throughput yeast two-hybrid screen. *BMC Microbiol* **11**, 234.

Le Sommer, C., Barrows, N. J., Bradrick, S. S., Pearson, J. L. & Garcia-Blanco, M. A. (2012). G protein-coupled receptor kinase 2 promotes flaviviridae entry and replication. *PLoS Negl Trop Dis* **6**, e1820.

Lee, E., Leang, S. K., Davidson, A. & Lobigs, M. (2010a). Both E protein glycans adversely affect dengue virus infectivity but are beneficial for virion release. *J Virol* **84**, 5171-5180.

Lee, K. S., Lai, Y. L., Lo, S., Barkham, T., Aw, P., Ooi, P. L., Tai, J. C., Hibberd, M., Johansson, P., Khoo, S. P. & Ng, L. C. (2010b). Dengue virus surveillance for early warning, Singapore. *Emerg Infect Dis* **16**, 847-849.

Ler, T. S., Ang, L. W., Yap, G. S., Ng, L. C., Tai, J. C., James, L. & Goh, K. T. (2011). Epidemiological characteristics of the 2005 and 2007 dengue epidemics in Singapore - similarities and distinctions. *Western Pac Surveill Response J* **2**, 24-29.

Leung, D., Schroder, K., White, H., Fang, N. X., Stoermer, M. J., Abbenante, G., Martin, J. L., Young, P. R. & Fairlie, D. P. (2001). Activity of recombinant dengue 2 virus NS3 protease in the presence of a truncated NS2B co-factor, small peptide substrates, and inhibitors. *J Biol Chem* **276**, 45762-45771.

Leyssen, P., De Clercq, E. & Neyts, J. (2000). Perspectives for the treatment of infections with Flaviviridae. *Clin Microbiol Rev* **13**, 67-82, table of contents.

Li, C., Ge, L. L., Li, P. P., Wang, Y., Dai, J. J., Sun, M. X., Huang, L., Shen, Z. Q., Hu, X. C., Ishag, H. & Mao, X. (2014a). Cellular DDX3 regulates Japanese encephalitis virus replication by interacting with viral un-translated regions. *Virology* **449**, 70-81.

Li, C., Ge, L. L., Li, P. P., Wang, Y., Sun, M. X., Huang, L., Ishag, H., Di, D. D., Shen, Z. Q., Fan, W. X. & Mao, X. (2013). The DEAD-box RNA helicase DDX5 acts as a positive regulator of Japanese encephalitis virus replication by binding to viral 3' UTR. *Antiviral Res* **100**, 487-499.

Li, H. P., Huang, P., Park, S. & Lai, M. M. (1999a). Polypyrimidine tract-binding protein binds to the leader RNA of mouse hepatitis virus and serves as a regulator of viral transcription. *J Virol* **73**, 772-777.

Li, H. T., Clum, S., You, S. H., Ebner, K. E. & Padmanabhan, R. (1999b). The serine protease and RNA-stimulated nucleoside triphosphatase and RNA helicase functional domains of Dengue virus type 2 NS3 converge within a region of 20 amino acids. *J Virol* **73**, 3108-3116.

Li, J., Huang, R., Liao, W., Chen, Z. & Zhang, S. (2012). Dengue virus utilizes calcium modulating cyclophilin-binding ligand to subvert apoptosis. *Biochem Biophys Res Commun* **418**, 622-627.

Li, J., Lim, S. P., Beer, D., Patel, V., Wen, D., Tumanut, C., Tully, D. C., Williams, J. A., Jiricek, J., Priestle, J. P., Harris, J. L. & Vasudevan, S. G. (2005). Functional profiling of recombinant NS3 proteases from all four serotypes of dengue virus using tetrapeptide and octapeptide substrate libraries. *J Biol Chem* **280**, 28766-28774.

Li, L., Lok, S. M., Yu, I. M., Zhang, Y., Kuhn, R. J., Chen, J. & Rossmann, M. G. (2008). The flavivirus precursor membrane-envelope protein complex: structure and maturation. *Science* **319**, 1830-1834.

Li, X. D., Shan, C., Deng, C. L., Ye, H. Q., Shi, P. Y., Yuan, Z. M., Gong, P. & Zhang, B. (2014b). The interface between methyltransferase and polymerase of NS5 is essential for flavivirus replication. *PLoS Negl Trop Dis* **8**, e2891.

Libraty, D. H., Endy, T. P., Houng, H. S., Green, S., Kalayanarooj, S., Suntayakorn, S., Chansiriwongs, W., Vaughn, D. W., Nisalak, A., Ennis, F. A. & Rothman, A. L. (2002a). Differing influences of virus burden and immune activation on disease severity in secondary dengue-3 virus infections. *J Infect Dis* **185**, 1213-1221.

Libraty, D. H., Young, P. R., Pickering, D., Endy, T. P., Kalayanarooj, S., Green, S., Vaughn, D. W., Nisalak, A., Ennis, F. A. & Rothman, A. L. (2002b). High circulating levels of the dengue virus nonstructural protein NS1 early in dengue illness correlate with the development of dengue hemorrhagic fever. *J Infect Dis* **186**, 1165-1168.

Lim, A. P., Chan, C. E., Wong, S. K., Chan, A. H., Ooi, E. E. & Hanson, B. J. (2008). Neutralizing human monoclonal antibody against H5N1 influenza HA selected from a Fab-phage display library. *Virol J* **5**, 130.

Lim, S. M., Koraka, P., Osterhaus, A. D. & Martina, B. E. (2013a). Development of a strand-specific real-time qRT-PCR for the accurate detection and quantitation of West Nile virus RNA. *J Virol Methods* **194**, 146-153.

Lim, S. P., Koh, J. H., Seh, C. C., Liew, C. W., Davidson, A. D., Chua, L. S., Chandrasekaran, R., Cornvik, T. C., Shi, P. Y. & Lescar, J. (2013b). A crystal structure of the dengue virus non-structural protein 5 (NS5) polymerase delineates interdomain amino acid residues that enhance its thermostability and de novo initiation activities. *J Biol Chem* **288**, 31105-31114.

Lim, S. P., Wang, Q. Y., Noble, C. G., Chen, Y. L., Dong, H., Zou, B., Yokokawa, F., Nilar, S., Smith, P., Beer, D., Lescar, J. & Shi, P. Y. (2013c). Ten years of dengue drug discovery: progress and prospects. *Antiviral Res* **100**, 500-519.

Limjindaporn, T., Netsawang, J., Noisakran, S., Thiemmeca, S., Wongwiwat, W., Sudsaward, S., Avirutnan, P., Puttikhunt, C., Kasinrerk, W., Sriburi, R., Sittisombut, N., Yenchitsomanus, P. T. & Malasit, P. (2007). Sensitization to Fas-mediated apoptosis by dengue virus capsid protein. *Biochem Biophys Res Commun* **362**, 334-339.

Limjindaporn, T., Wongwiwat, W., Noisakran, S., Srisawat, C., Netsawang, J., Puttikhunt, C., Kasinrerk, W., Avirutnan, P., Thiemmeca, S., Sriburi, R., Sittisombut, N., Malasit, P. & Yenchitsomanus, P. T. (2009). Interaction of dengue virus envelope protein with endoplasmic reticulum-resident chaperones facilitates dengue virus production. *Biochem Biophys Res Commun* **379**, 196-200.

Lin, S. R., Zou, G., Hsieh, S. C., Qing, M., Tsai, W. Y., Shi, P. Y. & Wang, W. K. (2011). The helical domains of the stem region of dengue virus envelope protein are involved in both virus assembly and entry. *J Virol* **85**, 5159-5171.

Lindenbach, B. D. & Rice, C. M. (1999). Genetic interaction of flavivirus nonstructural proteins NS1 and NS4A as a determinant of replicase function. *J Virol* **73**, 4611-4621.

Lindenbach, B. D. & Rice, C. M. (2003). Molecular biology of flaviviruses. *Adv Virus Res* **59**, 23-61.

Lindenbach, B. D., Thiel, H. & Rice, C. M. (2007). Flaviviridae: The Viruses and Their Replication. In *Fields virology*, 5 edn, pp. 1101 - 1152. Philadelphia: Wolters kluwer/Lippincott Williams & Wilkins.

Lipson, H. (1956). Small-Angle Scattering of X-rays by A. Guinier and G. Fournet. *Acta Crystallogr* **9**, 839.

Loke, P., Hammond, S. N., Leung, J. M., Kim, C. C., Batra, S., Rocha, C., Balmaseda, A. & Harris, E. (2010). Gene expression patterns of dengue virus-infected children from nicaragua reveal a distinct signature of increased metabolism. *PLoS Negl Trop Dis* **4**, e710.

Low, J. G., Sung, C., Wijaya, L., Wei, Y., Rathore, A. P., Watanabe, S., Tan, B. H., Toh, L., Chua, L. T., Hou, Y., Chow, A., Howe, S., Chan, W. K., Tan, K. H., Chung, J. S., Cherng, B. P., Lye, D. C., Tambayah, P. A., Ng, L. C., Connolly, J., Hibberd, M. L., Leo, Y. S., Cheung, Y. B., Ooi, E. E. & Vasudevan, S. G. (2014). Efficacy and safety of celgosivir in patients with dengue fever (CELADEN): a phase 1b, randomised, double-blind, placebo-controlled, proof-of-concept trial. *Lancet Infect Dis* **14**, 706-715.

Lu, G. & Gong, P. (2013). Crystal Structure of the full-length Japanese encephalitis virus NS5 reveals a conserved methyltransferase-polymerase interface. *PLoS Pathog* **9**, e1003549.

Luo, D., Wei, N., Doan, D. N., Paradkar, P. N., Chong, Y., Davidson, A. D., Kotaka, M., Lescar, J. & Vasudevan, S. G. (2010). Flexibility between the protease and helicase domains of the dengue virus NS3 protein conferred by the linker region and its functional implications. *J Biol Chem* **285**, 18817-18827.

Luo, D., Xu, T., Hunke, C., Grüber, G., Vasudevan, S. G. & Lescar, J. (2008a). Crystal structure of the NS3 protease-helicase from dengue virus. *J Virol* **82**, 173-183.

Luo, D. H., Xu, T., Watson, R. P., Scherer-Becker, D., Sampath, A., Jahnke, W., Yeong, S. S., Wang, C. H., Lim, S. P., Strongin, A., Vasudevan, S. G. & Lescar, J. (2008b). Insights into RNA unwinding and ATP hydrolysis by the flavivirus NS3 protein. *EMBO J* **27**, 3209-3219.

Ma, L., Jones, C. T., Groesch, T. D., Kuhn, R. J. & Post, C. B. (2004). Solution structure of dengue virus capsid protein reveals another fold. *Proc Natl Acad Sci U S A* **101**, 3414-3419.

Mackenzie, J. M., Jones, M. K. & Young, P. R. (1996). Immunolocalization of the dengue virus nonstructural glycoprotein NS1 suggests a role in viral RNA replication. *Virology* **220**, 232-240.

Mackenzie, J. M., Khromykh, A. A., Jones, M. K. & Westaway, E. G. (1998). Subcellular localization and some biochemical properties of the flavivirus Kunjin nonstructural proteins NS2A and NS4A. *Virology* **245**, 203-215.

Mackenzie, J. S., Gubler, D. J. & Petersen, L. R. (2004). Emerging flaviviruses: the spread and resurgence of Japanese encephalitis, West Nile and dengue viruses. *Nat Med* **10**, S98-109.

Mahoney, R., Chocarro, L., Southern, J., Francis, D. P., Vose, J. & Margolis, H. (2011). Dengue vaccines regulatory pathways: a report on two meetings with regulators of developing countries. *PLoS Med* **8**, e1000418.

Mairiang, D., Zhang, H., Sodja, A., Murali, T., Suriyaphol, P., Malasit, P., Limjindaporn, T. & Finley, R. L., Jr. (2013). Identification of new protein interactions between dengue fever virus and its hosts, human and mosquito. *PLoS One* **8**, e53535.

Makino, Y., Tadano, M., Anzai, T., Ma, S. P., Yasuda, S. & Fukunaga, T. (1989). Detection of dengue 4 virus core protein in the nucleus. II. Antibody against dengue 4 core protein produced by a recombinant baculovirus reacts with the antigen in the nucleus. *J Gen Virol* **70 (Pt 6)**, 1417-1425.

Malet, H., Egloff, M. P., Selisko, B., Butcher, R. E., Wright, P. J., Roberts, M., Gruez, A., Sulzenbacher, G., Vonrhein, C., Bricogne, G., Mackenzie, J. M., Khromykh, A. A., Davidson, A. D. & Canard, B. (2007). Crystal structure of the RNA polymerase domain of the West Nile virus non-structural protein 5. *J Biol Chem* **282**, 10678-10689.

Marfori, M., Lonhienne, T. G., Forwood, J. K. & Kobe, B. (2012). Structural basis of high-affinity nuclear localization signal interactions with importin-alpha. *Traffic* **13**, 532-548.

Mastrangelo, E., Pezzullo, M., De Burghgraeve, T., Kaptein, S., Pastorino, B., Dallmeier, K., de Lamballerie, X., Neyts, J., Hanson, A. M., Frick, D. N., Bolognesi, M. & Milani, M. (2012). Ivermectin is a potent inhibitor of flavivirus replication specifically targeting NS3 helicase activity: new prospects for an old drug. *J Antimicrob Chemother* **67**, 1884-1894.

Matsuura, Y., Lange, A., Harreman, M. T., Corbett, A. H. & Stewart, M. (2003). Structural basis for Nup2p function in cargo release and karyopherin recycling in nuclear import. *EMBO J* **22**, 5358-5369.

Mazzon, M., Jones, M., Davidson, A., Chain, B. & Jacobs, M. (2009). Dengue virus NS5 inhibits interferon-alpha signaling by blocking signal transducer and activator of transcription 2 phosphorylation. *J Infect Dis* **200**, 1261-1270.

Medin, C. L., Fitzgerald, K. A. & Rothman, A. L. (2005). Dengue virus nonstructural protein NS5 induces interleukin-8 transcription and secretion. *J Virol* **79**, 11053-11061.

Melchior, F. & Gerace, L. (1998). Two-way trafficking with Ran. *Trends Cell Biol* **8**, 175-179.

Men, R. H., Bray, M. & Lai, C. J. (1991). Carboxy-terminally truncated dengue virus envelope glycoproteins expressed on the cell surface and secreted extracellularly exhibit increased immunogenicity in mice. *J Virol* **65**, 1400-1407.

Meusser, B., Hirsch, C., Jarosch, E. & Sommer, T. (2005). ERAD: the long road to destruction. *Nat Cell Biol* **7**, 766-772.

Miller, S., Kastner, S., Krijnse-Locker, J., Buhler, S. & Bartenschlager, R. (2007). The non-structural protein 4A of dengue virus is an integral membrane protein inducing membrane alterations in a 2K-regulated manner. *J Biol Chem* **282**, 8873-8882.

Modis, Y., Ogata, S., Clements, D. & Harrison, S. C. (2004). Structure of the dengue virus envelope protein after membrane fusion. *Nature* **427**, 313-319.

Modis, Y., Ogata, S., Clements, D. & Harrison, S. C. (2005). Variable surface epitopes in the crystal structure of dengue virus type 3 envelope glycoprotein. *J Virol* **79**, 1223-1231.

Mondotte, J. A., Lozach, P. Y., Amara, A. & Gamarnik, A. V. (2007). Essential role of dengue virus envelope protein N glycosylation at asparagine-67 during viral propagation. *J Virol* **81**, 7136-7148.

Mongkolsapaya, J., Dejnirattisai, W., Xu, X. N., Vasanawathana, S., Tangthawornchaikul, N., Chairunsri, A., Sawasdivorn, S., Duangchinda, T., Dong, T., Rowland-Jones, S., Yenchitsomanus, P. T., McMichael, A., Malasit, P. & Screaton, G. (2003). Original antigenic sin and apoptosis in the pathogenesis of dengue hemorrhagic fever. *Nat Med* **9**, 921-927.

Moon, S. L., Anderson, J. R., Kumagai, Y., Wilusz, C. J., Akira, S., Khromykh, A. A. & Wilusz, J. (2012). A noncoding RNA produced by arthropod-borne

flaviviruses inhibits the cellular exoribonuclease XRN1 and alters host mRNA stability. *RNA* **18**, 2029-2040.

Moore, M. S. & Blobel, G. (1993). The GTP-binding protein Ran/TC4 is required for protein import into the nucleus. *Nature* **365**, 661-663.

Moreland, N. J., Tay, M. Y., Lim, E., Paradkar, P. N., Doan, D. N., Yau, Y. H., Geifman Shochat, S. & Vasudevan, S. G. (2010). High affinity human antibody fragments to dengue virus non-structural protein 3. *PLoS Negl Trop Dis* **4**, e881.

Moreland, N. J., Tay, M. Y., Lim, E., Rathore, A. P., Lim, A. P., Hanson, B. J. & Vasudevan, S. G. (2012). Monoclonal antibodies against dengue NS2B and NS3 proteins for the study of protein interactions in the flaviviral replication complex. *J Virol Methods* **179**, 97-103.

Morrison, J., Laurent-Rolle, M., Maestre, A. M., Rajsbaum, R., Pisanelli, G., Simon, V., Mulder, L. C., Fernandez-Sesma, A. & Garcia-Sastre, A. (2013). Dengue virus co-opts UBR4 to degrade STAT2 and antagonize type I interferon signaling. *PLoS Pathog* **9**, e1003265.

Mosca, J. D. & Pitha, P. M. (1986). Transcriptional and posttranscriptional regulation of exogenous human beta interferon gene in simian cells defective in interferon synthesis. *Mol Cell Biol* **6**, 2279-2283.

Moseley, G. W., Lahaye, X., Roth, D. M., Oksayan, S., Filmer, R. P., Rowe, C. L., Blondel, D. & Jans, D. A. (2009). Dual modes of rabies P-protein association with microtubules: a novel strategy to suppress the antiviral response. *J Cell Sci* **122**, 3652-3662.

Muller, D. A., Landsberg, M. J., Bletchly, C., Rothnagel, R., Waddington, L., Hankamer, B. & Young, P. R. (2012). Structure of the dengue virus glycoprotein non-structural protein 1 by electron microscopy and single-particle analysis. *J Gen Virol* **93**, 771-779.

Muller, D. A. & Young, P. R. (2013). The flavivirus NS1 protein: molecular and structural biology, immunology, role in pathogenesis and application as a diagnostic biomarker. *Antiviral Res* **98**, 192-208.

Murrell, S., Wu, S. C. & Butler, M. (2011). Review of dengue virus and the development of a vaccine. *Biotechnol Adv* **29**, 239-247.

Nakabayashi, H., Taketa, K., Miyano, K., Yamane, T. & Sato, J. (1982). Growth of human hepatoma cells lines with differentiated functions in chemically defined medium. *Cancer Res* **42**, 3858-3863.

Nasirudeen, A. M. & Liu, D. X. (2009). Gene expression profiling by microarray analysis reveals an important role for caspase-1 in dengue virus-induced p53-mediated apoptosis. *J Med Virol* **81**, 1069-1081.

NEA (2014). Factsheet on managing Singapore's dengue outbreak. Singapore: National Environmental Agency.

NEA (2015). Overview of vector control in Singapore.

Netsawang, J., Noisakran, S., Puttikhunt, C., Kasinrerk, W., Wongwiwat, W., Malasit, P., Yenchitsomanus, P. T. & Limjindaporn, T. (2010). Nuclear localization of dengue virus capsid protein is required for DAXX interaction and apoptosis. *Virus Res* **147**, 275-283.

Ng, L. C. & Ho, D. (2013). Challenges of dengue control. *Ann Acad Med Singapore* **42**, 696-697.

Nguyen, N. M., Tran, C. N., Phung, L. K., Duong, K. T., Huynh Hle, A., Farrar, J., Nguyen, Q. T., Tran, H. T., Nguyen, C. V., Merson, L., Hoang, L. T., Hibberd, M. L., Aw, P. P., Wilm, A., Nagarajan, N., Nguyen, D. T., Pham, M. P., Nguyen, T. T., Javanbakht, H., Klumpp, K., Hammond, J., Petric, R., Wolbers, M., Nguyen, C. T. & Simmons, C. P. (2013a). A randomized, double-

blind placebo controlled trial of balapiravir, a polymerase inhibitor, in adult dengue patients. *J Infect Dis* **207**, 1442-1450.

Nguyen, T. H., Nguyen, T. L., Lei, H. Y., Lin, Y. S., Le, B. L., Huang, K. J., Lin, C. F., Do, Q. H., Vu, T. Q., Lam, T. M., Yeh, T. M., Huang, J. H., Liu, C. C. & Halstead, S. B. (2005). Association between sex, nutritional status, severity of dengue hemorrhagic fever, and immune status in infants with dengue hemorrhagic fever. *Am J Trop Med Hyg* **72**, 370-374.

Nguyen, T. H., Vu, T. T., Farrar, J., Hoang, T. L., Dong, T. H., Ngoc Tran, V., Phung, K. L., Wolbers, M., Whitehead, S. S., Hibberd, M. L., Wills, B. & Simmons, C. P. (2013b). Corticosteroids for dengue - why don't they work? *PLoS Negl Trop Dis* **7**, e2592.

Noble, C. G., Chen, Y. L., Dong, H., Gu, F., Lim, S. P., Schul, W., Wang, Q. Y. & Shi, P. Y. (2010). Strategies for development of Dengue virus inhibitors. *Antiviral Res* **85**, 450-462.

Noble, C. G., Seh, C. C., Chao, A. T. & Shi, P. Y. (2012). Ligand-bound structures of the dengue virus protease reveal the active conformation. *J Virol* **86**, 438-446.

Noisakran, S., Dechtawewat, T., Avirutnan, P., Kinoshita, T., Siripanyaphinyo, U., Puttikhunt, C., Kasinrerk, W., Malasit, P. & Sittisombut, N. (2008a). Association of dengue virus NS1 protein with lipid rafts. *J Gen Virol* **89**, 2492-2500.

Noisakran, S., Dechtawewat, T., Rinkaewkan, P., Puttikhunt, C., Kanjanahaluethai, A., Kasinrerk, W., Sittisombut, N. & Malasit, P. (2007). Characterization of dengue virus NS1 stably expressed in 293T cell lines. *J Virol Methods* **142**, 67-80.

Noisakran, S., Sengsai, S., Thongboonkerd, V., Kanlaya, R., Sinchaikul, S., Chen, S. T., Puttikhunt, C., Kasinrerk, W., Limjindaporn, T., Wongwiwat, W., Malasit, P. & Yenchitsomanus, P. T. (2008b). Identification of human hnRNP C1/C2 as a dengue virus NS1-interacting protein. *Biochem Biophys Res Commun* **372**, 67-72.

Normile, D. (2013). Tropical medicine. Surprising new dengue virus throws a spanner in disease control efforts. *Science* **342**, 415.

Omura, S. (2008). Ivermectin: 25 years and still going strong. *Int J Antimicrob Agents* **31**, 91-98.

Ooi, E. E., Goh, K. T. & Gubler, D. J. (2006). Dengue prevention and 35 years of vector control in Singapore. *Emerg Infect Dis* **12**, 887-893.

Orozco, S., Schmid, M. A., Parameswaran, P., Lachica, R., Henn, M. R., Beatty, R. & Harris, E. (2012). Characterization of a model of lethal dengue virus 2 infection in C57BL/6 mice deficient in the alpha/beta interferon receptor. *J Gen Virol* **93**, 2152-2157.

Pando-Robles, V., Oses-Prieto, J. A., Rodriguez-Gandarilla, M., Meneses-Romero, E., Burlingame, A. L. & Batista, C. V. (2014). Quantitative proteomic analysis of Huh-7 cells infected with Dengue virus by label-free LC-MS. *J Proteomics* **111**, 16-29.

Pang, T., Cardosa, M. J. & Guzman, M. G. (2007). Of cascades and perfect storms: the immunopathogenesis of dengue haemorrhagic fever-dengue shock syndrome (DHF/DSS). *Immunol Cell Biol* **85**, 43-45.

Paradkar, P. N., Ooi, E. E., Hanson, B. J., Gubler, D. J. & Vasudevan, S. G. (2011a). Unfolded protein response (UPR) gene expression during antibody-dependent enhanced infection of cultured monocytes correlates with dengue disease severity. *Biosci Rep* **31**, 221-230.

Paradkar, P. N., Ooi, E. E., Hanson, B. J., Gubler, D. J. & Vasudevan, S. G. (2011b). Unfolded protein response (UPR) gene expression during antibody-dependent

enhanced infection of cultured monocytes correlates with dengue disease severity. *Biosci Rep* **31**, 221-230.

Paranjape, S. M. & Harris, E. (2007). Y box-binding protein-1 binds to the dengue virus 3'-untranslated region and mediates antiviral effects. *J Biol Chem* **282**, 30497-30508.

Paranjape, S. M. & Harris, E. (2010). Control of dengue virus translation and replication. *Curr Top Microbiol Immunol* **338**, 15-34.

Pastorino, B., Boucomont-Chapeaublanc, E., Peyrefitte, C. N., Belghazi, M., Fusai, T., Rogier, C., Tolou, H. J. & Almeras, L. (2009). Identification of cellular proteome modifications in response to West Nile virus infection. *Mol Cell Proteomics* **8**, 1623-1637.

Perez, A. B., Garcia, G., Sierra, B., Alvarez, M., Vazquez, S., Cabrera, M. V., Rodriguez, R., Rosario, D., Martinez, E., Denny, T. & Guzman, M. G. (2004). IL-10 levels in Dengue patients: some findings from the exceptional epidemiological conditions in Cuba. *J Med Virol* **73**, 230-234.

Petoukhov, M. V., Franke, D., Shkumatov, A. V., Tria, G., Kikhney, A. G., Gajda, M., Gorba, C., Mertens, H. D. T., Konarev, P. V. & Svergun, D. I. (2012). New developments in the ATSAS program package for small-angle scattering data analysis. *J Appl Crystallogr* **45**, 342-350.

Phong, W. Y., Moreland, N. J., Lim, S. P., Wen, D., Paradkar, P. N. & Vasudevan, S. G. (2011). Dengue protease activity: the structural integrity and interaction of NS2B with NS3 protease and its potential as a drug target. *Biosci Rep* **31**, 399-409.

Pijlman, G. P., Funk, A., Kondratieva, N., Leung, J., Torres, S., van der Aa, L., Liu, W. J., Palmenberg, A. C., Shi, P. Y., Hall, R. A. & Khromykh, A. A. (2008). A highly structured, nuclease-resistant, noncoding RNA produced by flaviviruses is required for pathogenicity. *Cell Host Microbe* **4**, 579-591.

Plaskon, N. E., Adelman, Z. N. & Myles, K. M. (2009). Accurate strand-specific quantification of viral RNA. *PLoS One* **4**, e7468.

Polacek, C., Friebe, P. & Harris, E. (2009). Poly(A)-binding protein binds to the non-polyadenylated 3' untranslated region of dengue virus and modulates translation efficiency. *J Gen Virol* **90**, 687-692.

Pong, W. L., Huang, Z. S., Teoh, P. G., Wang, C. C. & Wu, H. N. (2011). RNA binding property and RNA chaperone activity of dengue virus core protein and other viral RNA-interacting proteins. *FEBS Lett* **585**, 2575-2581.

Preugschat, F., Yao, C. W. & Strauss, J. H. (1990). In vitro processing of dengue virus type 2 nonstructural proteins NS2A, NS2B, and NS3. *J Virol* **64**, 4364-4374.

Pryor, M. J., Rawlinson, S. M., Butcher, R. E., Barton, C. L., Waterhouse, T. A., Vasudevan, S. G., Bardin, P. G., Wright, P. J., Jans, D. A. & Davidson, A. D. (2007). Nuclear localization of dengue virus nonstructural protein 5 through its importin alpha/beta-recognized nuclear localization sequences is integral to viral infection. *Traffic* **8**, 795-807.

Pumroy, R. & Cingolani, G. (2014). Molecular basis for import cargo discrimination by importin α isoforms (793.2). *The FASEB Journal* **28**.

Pumroy, R. A., Ke, S., Hart, D. J., Zachariae, U. & Cingolani, G. (2015). Molecular Determinants for Nuclear Import of Influenza A PB2 by Importin alpha Isoforms 3 and 7. *Structure*.

Pyhtila, B. & Rexach, M. (2003). A gradient of affinity for the karyopherin Kap95p along the yeast nuclear pore complex. *J Biol Chem* **278**, 42699-42709.

Quan, P. L., Firth, C., Conte, J. M., Williams, S. H., Zambrana-Torrelio, C. M., Anthony, S. J., Ellison, J. A., Gilbert, A. T., Kuzmin, I. V., Niezgoda, M., Osinubi, M. O., Recuenco, S., Markotter, W., Breiman, R. F., Kalemba, L.,

Malekani, J., Lindblade, K. A., Rostal, M. K., Ojeda-Flores, R., Suzan, G., Davis, L. B., Blau, D. M., Ogunkoya, A. B., Alvarez Castillo, D. A., Moran, D., Ngam, S., Akaibe, D., Agwanda, B., Briese, T., Epstein, J. H., Daszak, P., Rupprecht, C. E., Holmes, E. C. & Lipkin, W. I. (2013). Bats are a major natural reservoir for hepaciviruses and pegiviruses. *Proc Natl Acad Sci U S A* **110**, 8194-8199.

Rabaa, M. A., Ty Hang, V. T., Wills, B., Farrar, J., Simmons, C. P. & Holmes, E. C. (2010). Phylogeography of recently emerged DENV-2 in southern Viet Nam. *PLoS Negl Trop Dis* **4**, e766.

Raghupathy, R., Chaturvedi, U. C., Al-Sayer, H., Elbishbishi, E. A., Agarwal, R., Nagar, R., Kapoor, S., Misra, A., Mathur, A., Nusrat, H., Azizieh, F., Khan, M. A. & Mustafa, A. S. (1998). Elevated levels of IL-8 in dengue hemorrhagic fever. *J Med Virol* **56**, 280-285.

Rathore, A. P., Paradkar, P. N., Watanabe, S., Tan, K. H., Sung, C., Connolly, J. E., Low, J., Ooi, E. E. & Vasudevan, S. G. (2011a). Celgosivir treatment misfolds dengue virus NS1 protein, induces cellular pro-survival genes and protects against lethal challenge mouse model. *Antiviral research* **92**, 453-460.

Rathore, A. P., Paradkar, P. N., Watanabe, S., Tan, K. H., Sung, C., Connolly, J. E., Low, J., Ooi, E. E. & Vasudevan, S. G. (2011b). Celgosivir treatment misfolds dengue virus NS1 protein, induces cellular pro-survival genes and protects against lethal challenge mouse model. *Antiviral Res* **92**, 453-460.

Rawlinson, S. M., Pryor, M. J., Wright, P. J. & Jans, D. A. (2009). CRM1-mediated nuclear export of dengue virus RNA polymerase NS5 modulates interleukin-8 induction and virus production. *J Biol Chem* **284**, 15589-15597.

Richter, M. K., da Silva Voorham, J. M., Torres Pedraza, S., Hoornweg, T. E., van de Pol, D. P., Rodenhuis-Zybert, I. A., Wilschut, J. & Smit, J. M. (2014). Immature dengue virus is infectious in human immature dendritic cells via interaction with the receptor molecule DC-SIGN. *PLoS One* **9**, e98785.

Rico-Hesse, R. (1990). Molecular evolution and distribution of dengue viruses type 1 and 2 in nature. *Virology* **174**, 479-493.

Rivino, L., Kumaran, E. A., Jovanovic, V., Nadua, K., Teo, E. W., Pang, S. W., Teo, G. H., Gan, V. C., Lye, D. C., Leo, Y. S., Hanson, B. J., Smith, K. G., Bertoletti, A., Kemeny, D. M. & MacAry, P. A. (2013). Differential targeting of viral components by CD4+ versus CD8+ T lymphocytes in dengue virus infection. *J Virol* **87**, 2693-2706.

Rodenhuis-Zybert, I. A., van der Schaar, H. M., da Silva Voorham, J. M., van der Ende-Metselaar, H., Lei, H. Y., Wilschut, J. & Smit, J. M. (2010). Immature dengue virus: a veiled pathogen? *PLoS Pathog* **6**, e1000718.

Sambrook, J. (2001). Molecular cloning : a laboratory manual, 3rd ed. edn. Edited by D. W. Russell. Cold Spring Harbor, N.Y. :: Cold Spring Harbor Laboratory Press.

Sampath, A. & Padmanabhan, R. (2009). Molecular targets for flavivirus drug discovery. *Antiviral Res* **81**, 6-15.

Samsa, M. M., Mondotte, J. A., Iglesias, N. G., Assuncao-Miranda, I., Barbosa-Lima, G., Da Poian, A. T., Bozza, P. T. & Gamarnik, A. V. (2009). Dengue virus capsid protein usurps lipid droplets for viral particle formation. *PLoS Pathog* **5**, e1000632.

Schreiber, M. J., Holmes, E. C., Ong, S. H., Soh, H. S., Liu, W., Tanner, L., Aw, P. P., Tan, H. C., Ng, L. C., Leo, Y. S., Low, J. G., Ong, A., Ooi, E. E., Vasudevan, S. G. & Hibberd, M. L. (2009a). Genomic epidemiology of a dengue virus epidemic in urban Singapore. *J Virol* **83**, 4163-4173.

Schreiber, M. J., Holmes, E. C., Ong, S. H., Soh, H. S., Liu, W., Tanner, L., Aw, P. P., Tan, H. C., Ng, L. C., Leo, Y. S., Low, J. G., Ong, A., Ooi, E. E.,

Vasudevan, S. G. & Hibberd, M. L. (2009b). Genomic epidemiology of a dengue virus epidemic in urban Singapore. *J Virol* **83**, 4163-4173.

Searle, B. C. (2010). Scaffold: a bioinformatic tool for validating MS/MS-based proteomic studies. *Proteomics* **10**, 1265-1269.

Sekimoto, T. & Yoneda, Y. (2012). Intrinsic and extrinsic negative regulators of nuclear protein transport processes. *Genes Cells* **17**, 525-535.

Selisko, B., Peyrane, F. F., Canard, B., Alvarez, K. & Decroly, E. (2010). Biochemical characterization of the (nucleoside-2'O)-methyltransferase activity of dengue virus protein NS5 using purified capped RNA oligonucleotides (7Me)GpppAC(n) and GpppAC(n). *J Gen Virol* **91**, 112-121.

Selisko, B., Wang, C., Harris, E. & Canard, B. (2014). Regulation of Flavivirus RNA synthesis and replication. *Curr Opin Virol* **9C**, 74-83.

Sessions, O. M., Barrows, N. J., Souza-Neto, J. A., Robinson, T. J., Hershey, C. L., Rodgers, M. A., Ramirez, J. L., Dimopoulos, G., Yang, P. L., Pearson, J. L. & Garcia-Blanco, M. A. (2009). Discovery of insect and human dengue virus host factors. *Nature* **458**, 1047-1050.

Sessions, O. M., Tan, Y., Goh, K. C., Liu, Y., Tan, P., Rozen, S. & Ooi, E. E. (2013). Host cell transcriptome profile during wild-type and attenuated dengue virus infection. *PLoS Negl Trop Dis* **7**, e2107.

Shi, P. Y. (2014). Structural biology. Unraveling a flavivirus enigma. *Science* **343**, 849-850.

Shiryaev, S. A., Chernov, A. V., Aleshin, A. E., Shiryaeva, T. N. & Strongin, A. Y. (2009). NS4A regulates the ATPase activity of the NS3 helicase: a novel cofactor role of the non-structural protein NS4A from West Nile virus. *J Gen Virol* **90**, 2081-2085.

Silva, E. M., Conde, J. N., Allonso, D., Nogueira, M. L. & Mohana-Borges, R. (2013). Mapping the interactions of dengue virus NS1 protein with human liver proteins using a yeast two-hybrid system: identification of C1q as an interacting partner. *PLoS One* **8**, e57514.

Simmons, C. P., Chau, T. N., Thuy, T. T., Tuan, N. M., Hoang, D. M., Thien, N. T., Lien le, B., Quy, N. T., Hieu, N. T., Hien, T. T., McElnea, C., Young, P., Whitehead, S., Hung, N. T. & Farrar, J. (2007). Maternal antibody and viral factors in the pathogenesis of dengue virus in infants. *J Infect Dis* **196**, 416-424.

Smothers, J. F., Henikoff, S. & Carter, P. (2002). Tech.Sight. Phage display. Affinity selection from biological libraries. *Science* **298**, 621-622.

Snow, G. E., Haaland, B., Ooi, E. E. & Gubler, D. J. (2014). Review article: Research on dengue during World War II revisited. *Am J Trop Med Hyg* **91**, 1203-1217.

Somnuke, P., Hauhart, R. E., Atkinson, J. P., Diamond, M. S. & Avirutnan, P. (2011). N-linked glycosylation of dengue virus NS1 protein modulates secretion, cell-surface expression, hexamer stability, and interactions with human complement. *Virology* **413**, 253-264.

Stapleton, J. T., Foung, S., Muerhoff, A. S., Bukh, J. & Simmonds, P. (2011). The GB viruses: a review and proposed classification of GBV-A, GBV-C (HGV), and GBV-D in genus Pegivirus within the family Flaviviridae. *J Gen Virol* **92**, 233-246.

Stern, O., Hung, Y. F., Valdau, O., Yaffe, Y., Harris, E., Hoffmann, S., Willbold, D. & Sklan, E. H. (2013). An N-terminal amphipathic helix in dengue virus nonstructural protein 4A mediates oligomerization and is essential for replication. *J Virol* **87**, 4080-4085.

Stoker, M. (1962). Characteristics of normal and transformed clones arising from BHK21 cells exposed to polyoma virus. *Virology* **18**, 649-651.

Svergun, D. (1992). Determination of the regularization parameter in indirect-transform methods using perceptual criteria. *J Appl Crystallogr* **25**, 495-503.

Svergun, D. (1993). A direct indirect method of small-angle scattering data treatment. *J Appl Crystallogr* **26**, 258-267.

Svergun, D. I., Koch, M. H., Timmins, P. A. & May, R. P. (2013). *Small Angle X-Ray and Neutron Scattering from Solutions of Biological Macromolecules*: Oxford University Press.

Svergun, D. I., Petoukhov, M. V. & Koch, M. H. (2001). Determination of domain structure of proteins from X-ray solution scattering. *Biophys J* **80**, 2946-2953.

Tajima, S., Takasaki, T. & Kurane, I. (2011). Restoration of replication-defective dengue type 1 virus bearing mutations in the N-terminal cytoplasmic portion of NS4A by additional mutations in NS4B. *Arch Virol* **156**, 63-69.

Takahashi, H., Takahashi, C., Moreland, N. J., Chang, Y. T., Sawasaki, T., Ryo, A., Vasudevan, S. G., Suzuki, Y. & Yamamoto, N. (2012). Establishment of a robust dengue virus NS3-NS5 binding assay for identification of protein-protein interaction inhibitors. *Antiviral Res* **96**, 305-314.

Tam, D. T., Ngoc, T. V., Tien, N. T., Kieu, N. T., Thuy, T. T., Thanh, L. T., Tam, C. T., Truong, N. T., Dung, N. T., Qui, P. T., Hien, T. T., Farrar, J. J., Simmons, C. P., Wolbers, M. & Wills, B. A. (2012). Effects of short-course oral corticosteroid therapy in early dengue infection in Vietnamese patients: a randomized, placebo-controlled trial. *Clin Infect Dis* **55**, 1216-1224.

Tan, K. H., Ki, K. C., Watanabe, S., Vasudevan, S. G. & Krishnan, M. (2014). Cell-based flavivirus infection (CFI) assay for the evaluation of dengue antiviral candidates using high-content imaging. *Methods Mol Biol* **1138**, 99-109.

Tay, M. Y., Fraser, J. E., Chan, W. K., Moreland, N. J., Rathore, A. P., Wang, C., Vasudevan, S. G. & Jans, D. A. (2013). Nuclear localization of dengue virus (DENV) 1-4 non-structural protein 5; protection against all 4 DENV serotypes by the inhibitor Ivermectin. *Antiviral Res* **99**, 301-306.

Tay, M. Y., Lee, C. C., Vasudevan, S. G. & Moreland, N. J. (2014a). Identification of dengue-specific human antibody fragments using phage display. *Methods Mol Biol* **1138**, 161-173.

Tay, M. Y., Saw, W. G., Zhao, Y., Chan, K. W., Singh, D., Chong, Y., Forwood, J. K., Ooi, E. E., Gruber, G., Lescar, J., Luo, D. & Vasudevan, S. G. (2014b). The C-terminal 50 amino acid residues of Dengue NS3 protein are important for NS3-NS5 interaction and viral replication. *J Biol Chem*.

Teo, C. S. & Chu, J. J. (2014). Cellular vimentin regulates construction of dengue virus replication complexes through interaction with NS4A protein. *J Virol* **88**, 1897-1913.

Thepparit, C., Khakpoor, A., Khongwichit, S., Wikan, N., Fongsaran, C., Chingsuwanrote, P., Panraksa, P. & Smith, D. R. (2013). Dengue 2 infection of HepG2 liver cells results in endoplasmic reticulum stress and induction of multiple pathways of cell death. *BMC Res Notes* **6**, 372.

Thisyakorn, U. & Thisyakorn, C. (2014). Latest developments and future directions in dengue vaccines. *Ther Adv Vaccines* **2**, 3-9.

Thomas, L., Verlaeten, O., Cabie, A., Kaidomar, S., Moravie, V., Martial, J., Najioullah, F., Plumelle, Y., Fonteau, C., Dussart, P. & Cesaire, R. (2008). Influence of the dengue serotype, previous dengue infection, and plasma viral load on clinical presentation and outcome during a dengue-2 and dengue-4 co-epidemic. *Am J Trop Med Hyg* **78**, 990-998.

Thompson, J. D., Higgins, D. G. & Gibson, T. J. (1994). CLUSTAL W: improving the sensitivity of progressive multiple sequence alignment through sequence

weighting, position-specific gap penalties and weight matrix choice. *Nucleic Acids Res* **22**, 4673-4680.

Tilgner, M., Deas, T. S. & Shi, P. Y. (2005). The flavivirus-conserved penta-nucleotide in the 3' stem-loop of the West Nile virus genome requires a specific sequence and structure for RNA synthesis, but not for viral translation. *Virology* **331**, 375-386.

Tomassini, J. E., Boots, E., Gan, L., Graham, P., Munshi, V., Wolanski, B., Fay, J. F., Getty, K. & LaFemina, R. (2003). An in vitro Flaviviridae replicase system capable of authentic RNA replication. *Virology* **313**, 274-285.

Tricou, V., Minh, N. N., Farrar, J., Tran, H. T. & Simmons, C. P. (2011). Kinetics of viremia and NS1 antigenemia are shaped by immune status and virus serotype in adults with dengue. *PLoS Negl Trop Dis* **5**, e1309.

Tricou, V., Minh, N. N., Van, T. P., Lee, S. J., Farrar, J., Wills, B., Tran, H. T. & Simmons, C. P. (2010). A randomized controlled trial of chloroquine for the treatment of dengue in Vietnamese adults. *PLoS Negl Trop Dis* **4**, e785.

Tuiskunen, A., Leparc-Goffart, I., Boubis, L., Monteil, V., Klingstrom, J., Tolou, H. J., Lundkvist, A. & Plumet, S. (2010). Self-priming of reverse transcriptase impairs strand-specific detection of dengue virus RNA. *J Gen Virol* **91**, 1019-1027.

Uchil, P. D., Kumar, A. V. A. & Satchidanandam, V. (2006). Nuclear localization of flavivirus RNA synthesis in infected cells. *J Virol* **80**, 5451-5464.

Uchil, P. D. & Satchidanandam, V. (2003). Architecture of the flaviviral replication complex. Protease, nuclease, and detergents reveal encasement within double-layered membrane compartments. *J Biol Chem* **278**, 24388-24398.

Umareddy, I., Chao, A., Sampath, A., Gu, F. & Vasudevan, S. G. (2006a). Dengue virus NS4B interacts with NS3 and dissociates it from single-stranded RNA. *J Gen Virol* **87**, 2605-2614.

Umareddy, I., Chao, A., Sampath, A., Gu, F. & Vasudevan, S. G. (2006b). Dengue virus NS4B interacts with NS3 and dissociates it from single-stranded RNA. *J Gen Virol* **87**, 2605-2614.

Umareddy, I., Pluquet, O., Wang, Q. Y., Vasudevan, S. G., Chevet, E. & Gu, F. (2007). Dengue virus serotype infection specifies the activation of the unfolded protein response. *Virol J* **4**, 91.

Vancurova, I., Paine, T. M., Lou, W. & Paine, P. L. (1995). Nucleoplasmin associates with and is phosphorylated by casein kinase II. *J Cell Sci* **108 (Pt 2)**, 779-787.

Vashist, S., Anantpadma, M., Sharma, H. & Vrati, S. (2009). La protein binds the predicted loop structures in the 3' non-coding region of Japanese encephalitis virus genome: role in virus replication. *J Gen Virol* **90**, 1343-1352.

Vashist, S., Bhullar, D. & Vrati, S. (2011). La protein can simultaneously bind to both 3'- and 5'-noncoding regions of Japanese encephalitis virus genome. *DNA Cell Biol* **30**, 339-346.

Vasilakis, N. & Weaver, S. C. (2008a). The history and evolution of human dengue emergence. *Adv Virus Res* **72**, 1-76.

Vasilakis, N. & Weaver, S. C. (2008b). The history and evolution of human dengue emergence. *Adv Virus Res* **72**, 1-76.

Vasudevan, S. G., Johansson, M., Brooks, A. J., Llewellyn, L. E. & Jans, D. A. (2001). Characterisation of inter- and intra-molecular interactions of the dengue virus RNA dependent RNA polymerase as potential drug targets. *Farmaco* **56**, 33-36.

Verdine, G. L. & Hilinski, G. J. (2012). Stapled peptides for intracellular drug targets. *Methods Enzymol* **503**, 3-33.

Villas-Boas, C. S., Conceicao, T. M., Ramirez, J., Santoro, A. B., Da Poian, A. T. & Montero-Lomeli, M. (2009). Dengue virus-induced regulation of the host cell translational machinery. *Braz J Med Biol Res* **42**, 1020-1026.

Villordo, S. M., Alvarez, D. E. & Gamarnik, A. V. (2010). A balance between circular and linear forms of the dengue virus genome is crucial for viral replication. *RNA* **16**, 2325-2335.

Villordo, S. M. & Gamarnik, A. V. (2009). Genome cyclization as strategy for flavivirus RNA replication. *Virus Res* **139**, 230-239.

Viruses, I. C. o. T. o. (2014).

Wagstaff, K. M., Rawlinson, S. M., Hearps, A. C. & Jans, D. A. (2011). An AlphaScreen(R)-based assay for high-throughput screening for specific inhibitors of nuclear import. *J Biomol Screen* **16**, 192-200.

Wagstaff, K. M., Sivakumaran, H., Heaton, S. M., Harrich, D. & Jans, D. A. (2012). Ivermectin is a specific inhibitor of importin alpha/beta-mediated nuclear import able to inhibit replication of HIV-1 and dengue virus. *Biochem J* **443**, 851-856.

Waldmann, I., Walde, S. & Kehlenbach, R. H. (2007). Nuclear import of c-Jun is mediated by multiple transport receptors. *J Biol Chem* **282**, 27685-27692.

Wang, C. C., Huang, Z. S., Chiang, P. L., Chen, C. T. & Wu, H. N. (2009a). Analysis of the nucleoside triphosphatase, RNA triphosphatase, and unwinding activities of the helicase domain of dengue virus NS3 protein. *FEBS Lett* **583**, 691-696.

Wang, Q. Y., Patel, S. J., Vangrevelinghe, E., Xu, H. Y., Rao, R., Jaber, D., Schul, W., Gu, F., Heudi, O., Ma, N. L., Poh, M. K., Phong, W. Y., Keller, T. H., Jacoby, E. & Vasudevan, S. G. (2009b). A small-molecule dengue virus entry inhibitor. *Antimicrob Agents Chemother* **53**, 1823-1831.

Wang, R. F. & Kushner, S. R. (1991). Construction of versatile low-copy-number vectors for cloning, sequencing and gene expression in Escherichia coli. *Gene* **100**, 195-199.

Wang, R. Y., Huang, Y. R., Chong, K. M., Hung, C. Y., Ke, Z. L. & Chang, R. Y. (2011). DnaJ homolog Hdj2 facilitates Japanese encephalitis virus replication. *Virol J* **8**, 471.

Wang, S. H., Syu, W. J., Huang, K. J., Lei, H. Y., Yao, C. W., King, C. C. & Hu, S. T. (2002). Intracellular localization and determination of a nuclear localization signal of the core protein of dengue virus. *J Gen Virol* **83**, 3093-3102.

Wang, W. K., Chao, D. Y., Kao, C. L., Wu, H. C., Liu, Y. C., Li, C. M., Lin, S. C., Ho, S. T., Huang, J. H. & King, C. C. (2003). High levels of plasma dengue viral load during defervescence in patients with dengue hemorrhagic fever: implications for pathogenesis. *Virology* **305**, 330-338.

Wang, W. K., Chen, H. L., Yang, C. F., Hsieh, S. C., Juan, C. C., Chang, S. M., Yu, C. C., Lin, L. H., Huang, J. H. & King, C. C. (2006). Slower rates of clearance of viral load and virus-containing immune complexes in patients with dengue hemorrhagic fever. *Clin Infect Dis* **43**, 1023-1030.

Ward, A. M., Bidet, K., Yinglin, A., Ler, S. G., Hogue, K., Blackstock, W., Gunaratne, J. & Garcia-Blanco, M. A. (2011). Quantitative mass spectrometry of DENV-2 RNA-interacting proteins reveals that the DEAD-box RNA helicase DDX6 binds the DB1 and DB2 3' UTR structures. *RNA Biol* **8**, 1173-1186.

Warde-Farley, D., Donaldson, S. L., Comes, O., Zuberi, K., Badrawi, R., Chao, P., Franz, M., Grouios, C., Kazi, F., Lopes, C. T., Maitland, A., Mostafavi, S., Montojo, J., Shao, Q., Wright, G., Bader, G. D. & Morris, Q. (2010). The GeneMANIA prediction server: biological network integration for gene prioritization and predicting gene function. *Nucleic Acids Res* **38**, W214-220.

Watanabe, S., Tan, K. H., Rathore, A. P., Rozen-Gagnon, K., Shuai, W., Ruedl, C. & Vasudevan, S. G. (2012). The magnitude of dengue virus NS1 protein secretion

is strain dependent and does not correlate with severe pathologies in the mouse infection model. *J Virol* **86**, 5508-5514.

Weiskopf, D. & Sette, A. (2014). T-cell immunity to infection with dengue virus in humans. *Front Immunol* **5**, 93.

Welsch, S., Miller, S., Romero-Brey, I., Merz, A., Bleck, C. K., Walther, P., Fuller, S. D., Antony, C., Krijnse-Locker, J. & Bartenschlager, R. (2009). Composition and three-dimensional architecture of the dengue virus replication and assembly sites. *Cell Host Microbe* **5**, 365-375.

Wengler, G. (1993). The NS 3 nonstructural protein of flaviviruses contains an RNA triphosphatase activity. *Virology* **197**, 265-273.

Westaway, E. G. & Blok, J. (1997). Taxonomy and evolutionary relationships of flaviviruses. In *In Dengue and Dengue Hemorrhagic Fever*, pp. 147-173. Edited by G. DJ & K. G. Cambridge: CAB International.

Westaway, E. G., Mackenzie, J. M., Kenney, M. T., Jones, M. K. & Khromykh, A. A. (1997). Ultrastructure of Kunjin virus-infected cells: colocalization of NS1 and NS3 with double-stranded RNA, and of NS2B with NS3, in virus-induced membrane structures. *J Virol* **71**, 6650-6661.

Westaway, E. G., Mackenzie, J. M. & Khromykh, A. A. (2003). Kunjin RNA replication and applications of Kunjin replicons. *Adv Virus Res* **59**, 99-140.

White, J. P., Cardenas, A. M., Marissen, W. E. & Lloyd, R. E. (2007). Inhibition of cytoplasmic mRNA stress granule formation by a viral proteinase. *Cell Host Microbe* **2**, 295-305.

Whitehead, S. S., Blaney, J. E., Durbin, A. P. & Murphy, B. R. (2007). Prospects for a dengue virus vaccine. *Nat Rev Microbiol* **5**, 518-528.

Whitehorn, J. & Simmons, C. P. (2011). The pathogenesis of dengue. *Vaccine* **29**, 7221-7228.

Whitehorn, J., Van Vinh Chau, N., Truong, N. T., Tai, L. T., Van Hao, N., Hien, T. T., Wolbers, M., Merson, L., Dung, N. T., Peeling, R., Simmons, C., Wills, B. & Farrar, J. (2012). Lovastatin for adult patients with dengue: protocol for a randomised controlled trial. *Trials* **13**, 203.

WHO (2009). Dengue: guidelines for diagnosis, treatment, prevention and control. Geneva: WHO.

WHO (2012). Global Strategy for Dengue Prevention and Control 2012-2020. Geneva: WHO.

WHO (2014). Dengue, countries or areas at risk, 2013. Geneva: WHO.

Winkler, G., Maxwell, S. E., Ruemmler, C. & Stollar, V. (1989). Newly synthesized dengue-2 virus nonstructural protein NS1 is a soluble protein but becomes partially hydrophobic and membrane-associated after dimerization. *Virology* **171**, 302-305.

Winkler, G., Randolph, V. B., Cleaves, G. R., Ryan, T. E. & Stollar, V. (1988). Evidence that the mature form of the flavivirus nonstructural protein NS1 is a dimer. *Virology* **162**, 187-196.

Wolin, S. L. & Cedervall, T. (2002). The La protein. *Annu Rev Biochem* **71**, 375-403.

Wu, J., Lu, G., Zhang, B. & Gong, P. (2015). Perturbation in the Conserved Methyltransferase-Polymerase Interface of Flavivirus NS5 Differentially Affects Polymerase Initiation and Elongation. *J Virol* **89**, 249-261.

Wu, J. H., Bera, A. K., Kuhn, R. J. & Smith, J. L. (2005). Structure of the flavivirus helicase: Implications for catalytic activity, protein interactions, and proteolytic processing. *J Virol* **79**, 10268-10277.

Xie, X., Gayen, S., Kang, C., Yuan, Z. & Shi, P. Y. (2013). Membrane topology and function of dengue virus NS2A protein. *J Virol* **87**, 4609-4622.

Xie, X., Zou, J., Puttikhunt, C., Yuan, Z. & Shi, P. Y. (2015). Two Distinct Sets of NS2A Molecules Are Responsible for Dengue Virus RNA Synthesis and Virion Assembly. *J Virol* **89**, 1298-1313.

Xu, T., Sampath, A., Chao, A., Wen, D., Nanao, M., Chene, P., Vasudevan, S. G. & Lescar, J. (2005a). Structure of the Dengue virus helicase/nucleoside triphosphatase catalytic domain at a resolution of 2.4 A. *J Virol* **79**, 10278-10288.

Xu, T., Sampath, A., Chao, A., Wen, D., Nanao, M., Chene, P., Vasudevan, S. G. & Lescar, J. (2005b). Structure of the Dengue virus helicase/nucleoside triphosphatase catalytic domain at a resolution of 2.4 A. *J Virol* **79**, 10278-10288.

Yacoub, S., Wertheim, H., Simmons, C. P., Screaton, G. & Wills, B. (2014). Cardiovascular manifestations of the emerging dengue pandemic. *Nat Rev Cardiol* **11**, 335-345.

Yap, T. L., Xu, T., Chen, Y. L., Malet, H., Egloff, M. P., Canard, B., Vasudevan, S. G. & Lescar, J. (2007). Crystal structure of the dengue virus RNA-dependent RNA polymerase catalytic domain at 1.85-angstrom resolution. *J Virol* **81**, 4753-4765.

Ye, J., Chen, Z., Zhang, B., Miao, H., Zohaib, A., Xu, Q., Chen, H. & Cao, S. (2013). Heat shock protein 70 is associated with replicase complex of Japanese encephalitis virus and positively regulates viral genome replication. *PLoS One* **8**, e75188.

Yik, J. H., Chen, R., Pezda, A. C., Samford, C. S. & Zhou, Q. (2004). A human immunodeficiency virus type 1 Tat-like arginine-rich RNA-binding domain is essential for HEXIM1 to inhibit RNA polymerase II transcription through 7SK snRNA-mediated inactivation of P-TEFb. *Mol Cell Biol* **24**, 5094-5105.

Yin, Z., Chen, Y. L., Schul, W., Wang, Q. Y., Gu, F., Duraiswamy, J., Kondreddi, R. R., Niyomrattanakit, P., Lakshminarayana, S. B., Goh, A., Xu, H. Y., Liu, W., Liu, B., Lim, J. Y., Ng, C. Y., Qing, M., Lim, C. C., Yip, A., Wang, G., Chan, W. L., Tan, H. P., Lin, K., Zhang, B., Zou, G., Bernard, K. A., Garrett, C., Beltz, K., Dong, M., Weaver, M., He, H., Pichota, A., Dartois, V., Keller, T. H. & Shi, P. Y. (2009). An adenosine nucleoside inhibitor of dengue virus. *Proceedings of the National Academy of Sciences of the United States of America* **106**, 20435-20439.

Yocupicio-Monroy, R. M., Medina, F., Reyes-del Valle, J. & del Angel, R. M. (2003). Cellular proteins from human monocytes bind to dengue 4 virus minus-strand 3' untranslated region RNA. *J Virol* **77**, 3067-3076.

Yohan, B., Kendarsari, R. I., Mutia, K., Bowolaksono, A., Harahap, A. R. & Sasmono, R. T. (2014). Growth characteristics and cytokine/chemokine induction profiles of dengue viruses in various cell lines. *Acta Virol* **58**, 20-27.

Yon, C., Teramoto, T., Mueller, N., Phelan, J., Ganesh, V. K., Murthy, K. H. & Padmanabhan, R. (2005). Modulation of the nucleoside triphosphatase/RNA helicase and 5'-RNA triphosphatase activities of Dengue virus type 2 nonstructural protein 3 (NS3) by interaction with NS5, the RNA-dependent RNA polymerase. *J Biol Chem* **280**, 27412-27419.

You, S., Falgout, B., Markoff, L. & Padmanabhan, R. (2001). In vitro RNA synthesis from exogenous dengue viral RNA templates requires long range interactions between 5'- and 3'-terminal regions that influence RNA structure. *J Biol Chem* **276**, 15581-15591.

Yu, L., Takeda, K. & Markoff, L. (2013). Protein-protein interactions among West Nile non-structural proteins and transmembrane complex formation in mammalian cells. *Virology* **446**, 365-377.

Zeng, L., Falgout, B. & Markoff, L. (1998). Identification of specific nucleotide sequences within the conserved 3'-SL in the dengue type 2 virus genome required for replication. *J Virol* **72**, 7510-7522.

Zhang, W., Chipman, P. R., Corver, J., Johnson, P. R., Zhang, Y., Mukhopadhyay, S., Baker, T. S., Strauss, J. H., Rossmann, M. G. & Kuhn, R. J. (2003). Visualization of membrane protein domains by cryo-electron microscopy of dengue virus. *Nat Struct Biol* **10**, 907-912.

Zhang, Y., Kostyuchenko, V. A. & Rossmann, M. G. (2007). Structural analysis of viral nucleocapsids by subtraction of partial projections. *J Struct Biol* **157**, 356-364.

Zhao, Y., Moreland, N. J., Tay, M. Y., Lee, C. C., Swaminathan, K. & Vasudevan, S. G. (2014). Identification and molecular characterization of human antibody fragments specific for dengue NS5 protein. *Virus Res* **179**, 225-230.

Zhao, Y., Soh, T. S., Zheng, J., Chan, K. W., Phoo, W. W., Lee, C. C., Tay, M. Y., Swaminathan, K., Cornvik, T. C., Lim, S. P., Shi, P. Y., Lescar, J., Vasudevan, S. G. & Luo, D. (2015). A Crystal Structure of the Dengue Virus NS5 Protein Reveals a Novel Inter-domain Interface Essential for Protein Flexibility and Virus Replication. *PLoS Pathog* **11**, e1004682.

Zhou, Y., Ray, D., Zhao, Y., Dong, H., Ren, S., Li, Z., Guo, Y., Bernard, K. A., Shi, P. Y. & Li, H. (2007). Structure and function of flavivirus NS5 methyltransferase. *J Virol* **81**, 3891-3903.

Zou, G., Chen, Y. L., Dong, H., Lim, C. C., Yap, L. J., Yau, Y. H., Shochat, S. G., Lescar, J. & Shi, P. Y. (2011). Functional analysis of two cavities in flavivirus NS5 polymerase. *J Biol Chem* **286**, 14362-14372.

Zou, J., Lee, L. T., Wang, Q. Y., Xie, X., Lu, S., Yau, Y. H., Yuan, Z., Geifman Shochat, S., Kang, C., Lescar, J. & Shi, P. Y. (2015a). Mapping the interactions between the NS4B and NS3 proteins of dengue virus. *J Virol*.

Zou, J., Xie, X., Lee le, T., Chandrasekaran, R., Reynaud, A., Yap, L., Wang, Q. Y., Dong, H., Kang, C., Yuan, Z., Lescar, J. & Shi, P. Y. (2014). Dimerization of flavivirus NS4B protein. *J Virol* **88**, 3379-3391.

Zou, J., Xie, X., Wang, Q. Y., Dong, H., Lee, M. Y., Kang, C., Yuan, Z. & Shi, P. Y. (2015b). Characterization of dengue virus NS4A and NS4B protein interaction. *J Virol*.

Zuo, Z., Liew, O. W., Chen, G., Chong, P. C., Lee, S. H., Chen, K., Jiang, H., Puah, C. M. & Zhu, W. (2009). Mechanism of NS2B-mediated activation of NS3pro in dengue virus: molecular dynamics simulations and bioassays. *J Virol* **83**, 1060-1070.

Zust, R., Dong, H., Li, X. F., Chang, D. C., Zhang, B., Balakrishnan, T., Toh, Y. X., Jiang, T., Li, S. H., Deng, Y. Q., Ellis, B. R., Ellis, E. M., Poidinger, M., Zolezzi, F., Qin, C. F., Shi, P. Y. & Fink, K. (2013). Rational design of a live attenuated dengue vaccine: 2'-o-methyltransferase mutants are highly attenuated and immunogenic in mice and macaques. *PLoS Pathog* **9**, e1003521.

Zybert, I. A., van der Ende-Metselaar, H., Wilschut, J. & Smit, J. M. (2008). Functional importance of dengue virus maturation: infectious properties of immature virions. *J Gen Virol* **89**, 3047-3051.

Appendix

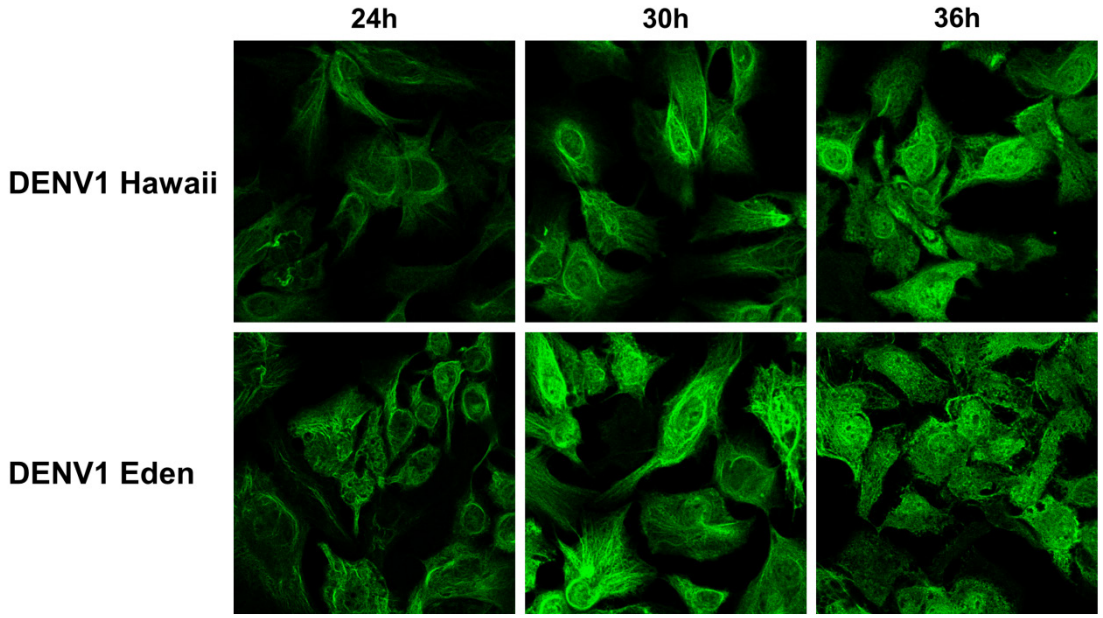

Figure A-1: Subcellular localization pattern of DENV1 NS5 in infected cells is not strain-dependent, and it is a common observation seen in DENV1. Huh-7 cells were mock-infected or infected with DENV1 or 2 (sequences as in Figure 3-16) at an MOI of 10 and fixed at 24h, 30h and 36h post-infection. DENV1 of Hawaii strain (GenBank accession number: EU848545) was also done for comparison. Cells were stained and images were captured as described in Figure 3-16A.

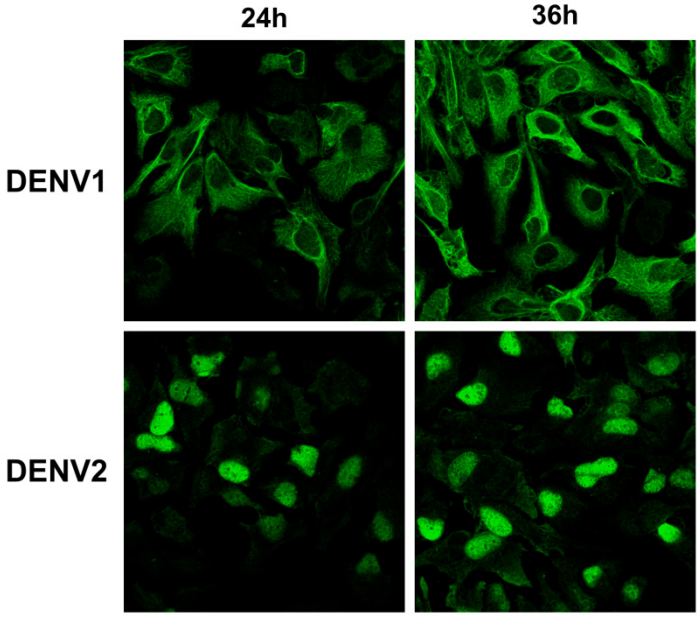

Figure A-2: Subcellular localization of DENV1 NS5 in infected cells remains the same, despite the use of a different cross-reactive anti-NS5 IgG. Huh-7 cells were mock-infected or infected with DENV1 or 2 (sequences as in Figure 3-16) at an MOI of 10 and fixed at 24h and 36h post-infection. Anti-NS5 (5M1 IgG, 20 nM; green) and anti-E (4G2 IgG, 1:1000; red, not shown here) antibodies were used for immunostaining. Images were captured as described in Figure 3-16B.

Table A-1: Human host proteins that were identified in this study to co-elute with DENV1/2 GFP-NS3, DENV1 or 2 GFP-NS5. Host proteins were identified by Scaffold Proteome software (version 4.3.4) with the following parameters: peptide thresholds: 95.0% minimum, protein thresholds: 99.0% minimum and at least two exclusive unique peptide count (the number of different amino acid sequences, regardless of any modification that are associated with a single protein group). GN=Gene Name, PE=Protein Existence (the numerical value describing the evidence for the existence of the protein), SV=Sequence Version (the version number of the sequence). The table is arranged in alphabetical order of protein name.

No	Identified Proteins (405)	Accession Number	Molecular Weight	GFP	GFP D1NS3	GFP D2NS3	GFP D1NS5	GFP D2NS5	mock
1	116 kDa U5 small nuclear ribonucleoprotein component GN=EFTUD2 PE=1 SV=1	U5S1_HUMAN	109 kDa	0	0	0	8	4	0
2	14-3-3 protein beta/alpha GN=YWHAB PE=1 SV=3	1433B_HUMAN	28 kDa	0	2	0	0	0	0
3	14-3-3 protein epsilon GN=YWHAE PE=1 SV=1	1433E_HUMAN	29 kDa	0	4	0	7	7	0
4	14-3-3 protein zeta/delta GN=YWHAZ PE=1 SV=1	1433Z_HUMAN	28 kDa	0	0	0	0	3	0
5	28S ribosomal protein S22, mitochondrial GN=MRPS22 PE=1 SV=1	RT22_HUMAN	41 kDa	0	8	0	6	5	0
6	28S ribosomal protein S23, mitochondrial GN=MRPS23 PE=1 SV=2	RT23_HUMAN	22 kDa	0	3	0	2	0	0
7	28S ribosomal protein S27, mitochondrial GN=MRPS27 PE=1 SV=3	RT27_HUMAN	48 kDa	0	0	0	4	0	0
8	28S ribosomal protein S29, mitochondrial GN=DAP3 PE=1 SV=1	RT29_HUMAN	46 kDa	0	0	0	4	0	0
9	28S ribosomal protein S7, mitochondrial GN=MRPS7 PE=1 SV=2	RT07_HUMAN	28 kDa	0	9	0	0	4	0
10	40S ribosomal protein S16 GN=RPS16 PE=1 SV=2	RS16_HUMAN	16 kDa	0	3	0	2	0	0
11	40S ribosomal protein S17 GN=RPS17 PE=1 SV=2	RS17_HUMAN	16 kDa	0	7	0	9	8	0
12	40S ribosomal protein S18 GN=RPS18 PE=1 SV=3	RS18_HUMAN	18 kDa	0	4	0	0	0	0
13	40S ribosomal protein S19 GN=RPS19 PE=1 SV=2	RS19_HUMAN	16 kDa	0	3	0	0	0	0
14	40S ribosomal protein S20 GN=RPS20 PE=1 SV=1	RS20_HUMAN	13 kDa	0	5	0	4	0	0
15	40S ribosomal protein S21 GN=RPS21 PE=1 SV=1	RS21_HUMAN	9 kDa	0	2	0	0	0	0
16	40S ribosomal protein S23 GN=RPS23 PE=1 SV=3	RS23_HUMAN	16 kDa	0	2	0	0	0	0
17	40S ribosomal protein S27 GN=RPS27 PE=1 SV=3	RS27_HUMAN	9 kDa	0	2	2	0	0	0
18	40S ribosomal protein S3a GN=RPS3A PE=1 SV=2	RS3A_HUMAN	30 kDa	0	7	0	4	0	0
19	40S ribosomal protein S4, X isoform GN=RPS4X PE=1 SV=2	RS4X_HUMAN	30 kDa	0	2	0	0	0	0
20	5'-3' exoribonuclease 2 GN=XRN2 PE=1 SV=1	XRN2_HUMAN	109 kDa	0	6	0	16	15	0
21	60 kDa heat shock protein, mitochondrial GN=HSPD1 PE=1 SV=2	CH60_HUMAN	61 kDa	0	10	0	4	9	0
22	60S ribosomal protein L12 GN=RPL12 PE=1 SV=1	RL12_HUMAN	18 kDa	0	3	0	0	0	0
23	60S ribosomal protein L13a GN=RPL13A PE=1 SV=2	RL13A_HUMAN	24 kDa	0	0	0	5	4	0
24	60S ribosomal protein L22 GN=RPL22 PE=1 SV=2	RL22_HUMAN	15 kDa	0	2	0	0	0	0
25	60S ribosomal protein L26-like 1 GN=RPL26L1 PE=1 SV=1	RL26L_HUMAN	17 kDa	0	0	0	2	2	0
26	60S ribosomal protein L27 GN=RPL27 PE=1 SV=2	RL27_HUMAN	16 kDa	0	5	0	7	6	0
27	60S ribosomal protein L32 GN=RPL32 PE=1 SV=2	RL32_HUMAN	16 kDa	0	3	0	9	8	0
28	60S ribosomal protein L34 GN=RPL34 PE=1 SV=3	RL34_HUMAN	13 kDa	0	2	0	2	2	0
29	60S ribosomal protein L35 GN=RPL35 PE=1 SV=2	RL35_HUMAN	15 kDa	0	2	0	0	0	0
30	60S ribosomal protein L37a GN=RPL37A PE=1 SV=2	RL37A_HUMAN	10 kDa	0	5	0	3	4	0

31	60S ribosomal protein L38 GN=RPL38 PE=1 SV=2	RL38_HUMAN	8 kDa	0	2	0	0	3	0
32	78 kDa glucose-regulated protein GN=HSPA5 PE=1 SV=2	GRP78_HUMAN	72 kDa	0	10	0	2	2	0
33	Acidic leucine-rich nuclear phosphoprotein 32 family member A GN=ANP32A PE=1 SV=1	AN32A_HUMAN	29 kDa	0	0	0	6	7	0
34	Acidic leucine-rich nuclear phosphoprotein 32 family member B GN=ANP32B PE=1 SV=1	AN32B_HUMAN	29 kDa	0	0	0	7	4	0
35	Acidic leucine-rich nuclear phosphoprotein 32 family member E GN=ANP32E PE=1 SV=1	AN32E_HUMAN	31 kDa	0	0	0	4	2	0
36	Actin, alpha cardiac muscle 1 GN=ACTC1 PE=1 SV=1	ACTC_HUMAN	42 kDa	0	2	0	0	0	0
37	Actin, cytoplasmic 2 GN=ACTG1 PE=1 SV=1	ACTG_HUMAN	42 kDa	0	0	0	0	2	0
38	Activator of 90 kDa heat shock protein ATPase homolog 1 GN=AHSA1 PE=1 SV=1	AHSA1_HUMAN	38 kDa	0	0	0	0	3	0
39	A-kinase anchor protein 8-like GN=AKAP8L PE=1 SV=3	AKP8L_HUMAN	72 kDa	0	0	0	0	2	0
40	Angio-associated migratory cell protein GN=AAMP PE=1 SV=2	AAMP_HUMAN	47 kDa	0	9	0	0	0	0
41	AP-3 complex subunit beta-1 GN=AP3B1 PE=1 SV=3	AP3B1_HUMAN	121 kDa	0	0	0	0	6	0
42	Apoptosis-inducing factor 1, mitochondrial GN=AIFM1 PE=1 SV=1	AIFM1_HUMAN	67 kDa	0	5	0	5	7	0
43	Arginyl-tRNA synthetase, cytoplasmic GN=RARS PE=1 SV=2	SYRC_HUMAN	75 kDa	0	2	0	0	0	0
44	Aspartyl/asparaginyl beta-hydroxylase GN=ASPH PE=1 SV=3	ASPH_HUMAN	86 kDa	0	0	0	0	8	0
45	Aspartyl-tRNA synthetase, cytoplasmic GN=DARS PE=1 SV=2	SYDC_HUMAN	57 kDa	0	9	0	3	3	0
46	Ataxin-2-like protein GN=ATXN2L PE=1 SV=2	ATX2L_HUMAN	113 kDa	0	8	0	0	6	0
47	ATP synthase subunit alpha, mitochondrial GN=ATP5A1 PE=1 SV=1	ATPA_HUMAN	60 kDa	0	2	0	2	7	0
48	ATP-binding cassette sub-family F member 1 GN=ABCF1 PE=1 SV=2	ABCF1_HUMAN	96 kDa	0	0	0	8	3	0
49	ATP-binding cassette sub-family F member 2 GN=ABCF2 PE=1 SV=2	ABCF2_HUMAN	71 kDa	0	7	0	8	4	0
50	ATP-dependent RNA helicase DDX18 GN=DDX18 PE=1 SV=2	DDX18_HUMAN	75 kDa	0	0	0	10	3	0
51	ATP-dependent RNA helicase DDX39 GN=DDX39 PE=1 SV=2	DDX39_HUMAN	49 kDa	0	3	0	0	3	0
52	ATP-dependent RNA helicase DDX3X GN=DDX3X PE=1 SV=3	DDX3X_HUMAN	73 kDa	0	12	0	21	21	0
53	ATP-dependent RNA helicase DDX50 GN=DDX50 PE=1 SV=1	DDX50_HUMAN	83 kDa	0	0	0	8	6	0
54	ATP-dependent RNA helicase DDX54 GN=DDX54 PE=1 SV=2	DDX54_HUMAN	99 kDa	0	0	0	6	5	0
55	Bcl-2-associated transcription factor 1 GN=BCLAF1 PE=1 SV=2	BCLF1_HUMAN	106 kDa	0	0	0	11	7	0
56	Bifunctional aminoacyl-tRNA synthetase GN=EPRS PE=1 SV=5	SYEP_HUMAN	171 kDa	0	2	0	0	3	0
57	Breakpoint cluster region protein GN=BCR PE=1 SV=2	BCR_HUMAN	143 kDa	0	0	0	0	5	0
58	BRISC complex subunit Abro1 GN=FAM175B PE=1 SV=2	F175B_HUMAN	47 kDa	0	0	0	6	0	0
59	Bystin GN=BYSL PE=1 SV=3	BYST_HUMAN	50 kDa	0	3	0	11	10	0
60	Calcium homeostasis endoplasmic reticulum protein GN=CHERP PE=1 SV=3	CHERP_HUMAN	104 kDa	0	0	0	6	0	0
61	Caprin-1 GN=CAPRIN1 PE=1 SV=2	CAPR1_HUMAN	78 kDa	0	10	0	5	8	0
62	Casein kinase I isoform alpha GN=CSNK1A1 PE=1 SV=2	KC1A_HUMAN	39 kDa	0	0	0	5	2	0
63	Casein kinase I isoform epsilon GN=CSNK1E PE=1 SV=1	KC1E_HUMAN	47 kDa	0	0	0	4	0	0
64	Casein kinase II subunit alpha' GN=CSNK2A2 PE=1 SV=1	CSK22_HUMAN	41 kDa	0	0	0	3	0	0
65	Casein kinase II subunit beta GN=CSNK2B PE=1 SV=1	CSK2B_HUMAN	25 kDa	0	0	0	5	3	0

66	Caseinolytic peptidase B protein homolog GN=CLPB PE=1 SV=1	CLPB_HUMAN	79 kDa	0	0	0	0	4	0
67	CD2 antigen cytoplasmic tail-binding protein 2 GN=CD2BP2 PE=1 SV=1	CD2B2_HUMAN	38 kDa	0	0	0	9	6	0
68	Cell division cycle 5-like protein GN=CDC5L PE=1 SV=2	CDC5L_HUMAN	92 kDa	0	0	0	18	13	0
69	Cell division protein kinase 1 GN=CDK1 PE=1 SV=2	CDK1_HUMAN	34 kDa	0	0	0	0	2	0
70	Cell growth-regulating nucleolar protein GN=LYAR PE=1 SV=2	LYAR_HUMAN	44 kDa	0	0	0	6	0	0
71	Cellular nucleic acid-binding protein GN=CNBP PE=1 SV=1	CNBP_HUMAN	19 kDa	0	5	0	2	2	0
72	Cellular tumor antigen p53 GN=TP53 PE=1 SV=4	P53_HUMAN	44 kDa	0	3	0	9	7	0
73	Cleavage and polyadenylation specificity factor subunit 6 GN=CPSF6 PE=1 SV=2	CPSF6_HUMAN	59 kDa	0	10	0	5	3	0
74	Cleavage and polyadenylation specificity factor subunit 7 GN=CPSF7 PE=1 SV=1	CPSF7_HUMAN	52 kDa	0	4	0	5	2	0
75	Coatomer subunit alpha GN=COPA PE=1 SV=2	COPA_HUMAN	138 kDa	0	0	0	0	3	0
76	Coatomer subunit beta' GN=COPB2 PE=1 SV=2	COPB2_HUMAN	102 kDa	0	0	0	0	3	0
77	Coiled-coil domain-containing protein 124 GN=CCDC124 PE=1 SV=1	CC124_HUMAN	26 kDa	0	0	0	6	4	0
78	Cold-inducible RNA-binding protein GN=CIRBP PE=1 SV=1	CIRBP_HUMAN	19 kDa	0	4	0	4	3	0
79	Complement component 1 Q subcomponent-binding protein, mitochondrial GN=C1QBP PE=1 SV=1	C1QBP_HUMAN	31 kDa	0	3	0	7	6	0
80	Constitutive coactivator of PPAR-gamma-like protein 1 GN=FAM120A PE=1 SV=2	F120A_HUMAN	122 kDa	0	20	0	0	0	0
81	Creatine kinase U-type, mitochondrial GN=CKMT1A PE=1 SV=1	KCRU_HUMAN	47 kDa	0	0	0	4	0	0
82	Cystathionine beta-synthase GN=CBS PE=1 SV=2	CBS_HUMAN	61 kDa	0	2	0	0	0	0
83	Developmentally-regulated GTP-binding protein 1 GN=DRG1 PE=1 SV=1	DRG1_HUMAN	41 kDa	0	8	0	9	8	0
84	DNA damage-binding protein 1 GN=DDB1 PE=1 SV=1	DDB1_HUMAN	127 kDa	0	0	0	19	15	0
85	DNA replication complex GINS protein PSF3 GN=GINS3 PE=1 SV=1	PSF3_HUMAN	25 kDa	0	8	0	0	0	0
86	DNA replication complex GINS protein SLD5 GN=GINS4 PE=1 SV=1	SLD5_HUMAN	26 kDa	0	6	0	0	0	0
87	DNA replication licensing factor MCM3 GN=MCM3 PE=1 SV=3	MCM3_HUMAN	91 kDa	0	2	0	0	0	0
88	DNA replication licensing factor MCM7 GN=MCM7 PE=1 SV=4	MCM7_HUMAN	81 kDa	0	2	0	2	2	0
89	DNA topoisomerase 1 GN=TOP1 PE=1 SV=2	TOP1_HUMAN	91 kDa	0	0	0	4	2	0
90	DNA topoisomerase 3-beta-1 GN=TOP3B PE=1 SV=1	TOP3B_HUMAN	97 kDa	0	20	0	0	0	0
91	DNA-binding protein A GN=CSDA PE=1 SV=4	DBPA_HUMAN	40 kDa	0	7	0	4	4	0
92	DnaJ homolog subfamily A member 1 GN=DNAJA1 PE=1 SV=2	DNJA1_HUMAN	45 kDa	0	2	0	6	14	0
93	DnaJ homolog subfamily A member 2 GN=DNAJA2 PE=1 SV=1	DNJA2_HUMAN	46 kDa	0	4	0	5	10	0
94	DnaJ homolog subfamily A member 3, mitochondrial GN=DNAJA3 PE=1 SV=1	DNJA3_HUMAN	53 kDa	0	3	0	8	7	0
95	DnaJ homolog subfamily B member 6 GN=DNAJB6 PE=1 SV=2	DNJB6_HUMAN	36 kDa	0	0	0	3	4	0
96	Dolichol-phosphate mannosyltransferase GN=DPM1 PE=1 SV=1	DPM1_HUMAN	30 kDa	0	0	0	0	4	0
97	Double-stranded RNA-binding protein Staufen homolog 1 GN=STAU1 PE=1 SV=2	STAU1_HUMAN	63 kDa	0	11	0	20	19	0
98	E2F-associated phosphoprotein GN=EAPP PE=1 SV=4	EAPP_HUMAN	33 kDa	0	0	0	8	4	0
99	E3 ubiquitin/ISG15 ligase TRIM25 GN=TRIM25 PE=1 SV=1	TRI25_HUMAN	71 kDa	0	0	0	0	5	0
100	E3 ubiquitin-protein ligase HERC2 GN=HERC2 PE=1 SV=2	HERC2_HUMAN	527 kDa	0	67	0	0	0	0
101	E3 ubiquitin-protein ligase Praja-2 GN=PJA2 PE=1 SV=4	PJA2_HUMAN	78 kDa	0	0	0	3	6	0
102	E3 ubiquitin-protein ligase UBR5 GN=UBR5 PE=1 SV=2	UBR5_HUMAN	309 kDa	0	0	0	5	0	0

103	ELAV-like protein 1 GN=ELAVL1 PE=1 SV=2	ELAV1_HUMAN	36 kDa	0	10	0	5	4	0
104	ELKS/Rab6-interacting/CAST family member 1 GN=ERC1 PE=1 SV=1	RB6I2_HUMAN	128 kDa	0	0	0	26	33	0
105	Emerin GN=EMD PE=1 SV=1	EMD_HUMAN	29 kDa	0	0	0	9	10	0
106	Eukaryotic initiation factor 4A-III GN=EIF4A3 PE=1 SV=4	IF4A3_HUMAN	47 kDa	0	0	0	5	0	0
107	Eukaryotic translation initiation factor 2 subunit 1 GN=EIF2S1 PE=1 SV=3	IF2A_HUMAN	36 kDa	0	2	0	11	10	0
108	Eukaryotic translation initiation factor 2 subunit 2 GN=EIF2S2 PE=1 SV=2	IF2B_HUMAN	38 kDa	0	3	0	0	0	0
109	Eukaryotic translation initiation factor 2 subunit 2-like protein PE=1 SV=1	IF2BL_HUMAN	38 kDa	0	0	0	4	2	0
110	Eukaryotic translation initiation factor 2 subunit 3 GN=EIF2S3 PE=1 SV=3	IF2G_HUMAN	51 kDa	0	8	0	13	15	0
111	Eukaryotic translation initiation factor 2A GN=EIF2A PE=1 SV=3	EIF2A_HUMAN	65 kDa	0	3	0	3	6	0
112	Eukaryotic translation initiation factor 3 subunit A GN=EIF3A PE=1 SV=1	EIF3A_HUMAN	167 kDa	0	0	0	15	13	0
113	Eukaryotic translation initiation factor 3 subunit B GN=EIF3B PE=1 SV=3	EIF3B_HUMAN	92 kDa	0	8	0	14	14	0
114	Eukaryotic translation initiation factor 3 subunit C GN=EIF3C PE=1 SV=1	EIF3C_HUMAN	105 kDa	0	4	0	14	13	0
115	Eukaryotic translation initiation factor 3 subunit D GN=EIF3D PE=1 SV=1	EIF3D_HUMAN	64 kDa	0	0	0	12	9	0
116	Eukaryotic translation initiation factor 3 subunit E GN=EIF3E PE=1 SV=1	EIF3E_HUMAN	52 kDa	0	0	0	9	4	0
117	Eukaryotic translation initiation factor 3 subunit F GN=EIF3F PE=1 SV=1	EIF3F_HUMAN	38 kDa	0	2	0	7	5	0
118	Eukaryotic translation initiation factor 3 subunit G GN=EIF3G PE=1 SV=2	EIF3G_HUMAN	36 kDa	0	3	0	3	5	0
119	Eukaryotic translation initiation factor 3 subunit H GN=EIF3H PE=1 SV=1	EIF3H_HUMAN	40 kDa	0	0	0	5	0	0
120	Eukaryotic translation initiation factor 3 subunit I GN=EIF3I PE=1 SV=1	EIF3I_HUMAN	37 kDa	0	7	0	10	7	0
121	Eukaryotic translation initiation factor 3 subunit L GN=EIF3L PE=1 SV=1	EIF3L_HUMAN	67 kDa	0	0	0	8	8	0
122	Eukaryotic translation initiation factor 3 subunit M GN=EIF3M PE=1 SV=1	EIF3M_HUMAN	43 kDa	0	0	0	0	4	0
123	Eukaryotic translation initiation factor 4 gamma 1 GN=EIF4G1 PE=1 SV=4	IF4G1_HUMAN	175 kDa	0	4	0	0	0	0
124	Eukaryotic translation initiation factor 6 GN=EIF6 PE=1 SV=1	IF6_HUMAN	27 kDa	0	0	0	6	2	0
125	Exosome complex exonuclease RRP4 GN=EXOSC2 PE=1 SV=2	EXOS2_HUMAN	33 kDa	0	0	0	0	3	0
126	Exosome complex exonuclease RRP45 GN=EXOSC9 PE=1 SV=3	EXOS9_HUMAN	49 kDa	0	0	0	3	2	0
127	Exosome component 10 GN=EXOSC10 PE=1 SV=2	EXOSX_HUMAN	101 kDa	0	0	0	2	0	0
128	FACT complex subunit SSRP1 GN=SSRP1 PE=1 SV=1	SSRP1_HUMAN	81 kDa	0	0	0	5	0	0
129	Far upstream element-binding protein 3 GN=FUBP3 PE=1 SV=2	FUBP3_HUMAN	62 kDa	0	10	0	0	0	0
130	Far upstream element-binding protein 3 GN=FUBP3 PE=1 SV=2	RS15_HUMAN	17 kDa	0	7	0	4	4	0
131	Fermitin family homolog 2 GN=FERMT2 PE=1 SV=1	FERM2_HUMAN	78 kDa	0	19	0	0	0	0
132	Four and a half LIM domains protein 1 GN=FHL1 PE=1 SV=4	FHL1_HUMAN	36 kDa	0	6	0	5	5	0
133	Fragile X mental retardation syndrome-related protein 1 GN=FXR1 PE=1 SV=3	FXR1_HUMAN	70 kDa	0	2	0	2	2	0
134	Fragile X mental retardation syndrome-related protein 2 GN=FXR2 PE=1 SV=2	FXR2_HUMAN	74 kDa	0	4	0	7	7	0
135	G patch domain and KOW motifs-containing protein GN=GPKOW PE=1 SV=2	GPKOW_HUMAN	52 kDa	0	0	0	11	0	0
136	Galactokinase GN=GALK1 PE=1 SV=1	GALK1_HUMAN	42 kDa	0	2	0	2	5	0
137	General transcription factor IIE subunit 1 GN=GTF2E1 PE=1 SV=2	T2EA_HUMAN	49 kDa	0	0	0	8	0	0
138	Glutamate-rich WD repeat-containing protein 1 GN=GRWD1 PE=1 SV=1	GRWD1_HUMAN	49 kDa	0	5	0	11	10	0
139	G-rich sequence factor 1 GN=GRSF1 PE=1 SV=3	GRSF1_HUMAN	53 kDa	0	3	0	7	0	0
140	GTP-binding protein 1 GN=GTPBP1 PE=1 SV=3	GTPB1_HUMAN	72 kDa	0	3	0	9	4	0

141	Guanine nucleotide-binding protein-like 3 GN=GNL3 PE=1 SV=2	GNL3_HUMAN	62 kDa	0	0	0	5	8	0
142	Heat shock 70 kDa protein 1A/1B GN=HSPA1A PE=1 SV=5	HSP71_HUMAN	70 kDa	0	14	9	16	14	0
143	Heat shock 70 kDa protein 4 GN=HSPA4 PE=1 SV=4	HSP74_HUMAN	94 kDa	0	6	0	0	0	0
144	Heat shock cognate 71 kDa protein GN=HSPA8 PE=1 SV=1	HSP7C_HUMAN	71 kDa	0	16	9	18	17	0
145	Heat shock protein 105 kDa GN=HSPH1 PE=1 SV=1	HS105_HUMAN	97 kDa	0	3	0	0	0	0
146	Heat shock protein beta-1 GN=HSPB1 PE=1 SV=2	HSPB1_HUMAN	23 kDa	0	2	0	0	3	0
147	Heat shock protein HSP 90-alpha GN=HSP90AA1 PE=1 SV=5	HS90A_HUMAN	85 kDa	0	0	0	6	0	0
148	Heat shock protein HSP 90-beta GN=HSP90AB1 PE=1 SV=4	HS90B_HUMAN	83 kDa	0	3	3	7	4	0
149	Heterogeneous nuclear ribonucleoprotein A/B GN=HNRNPAB PE=1 SV=2	ROAA_HUMAN	36 kDa	0	8	0	2	0	0
150	Heterogeneous nuclear ribonucleoprotein D0 GN=HNRNPD PE=1 SV=1	HNRPD_HUMAN	38 kDa	0	10	0	8	11	0
151	Heterogeneous nuclear ribonucleoprotein D-like GN=HNRPDL PE=1 SV=3	HNRDL_HUMAN	46 kDa	0	6	0	5	7	0
152	Heterogeneous nuclear ribonucleoprotein F GN=HNRNPF PE=1 SV=3	HNRPF_HUMAN	46 kDa	0	6	0	8	8	0
153	Heterogeneous nuclear ribonucleoprotein H2 GN=HNRNPH2 PE=1 SV=1	HNRH2_HUMAN	49 kDa	0	7	0	6	4	0
154	Heterogeneous nuclear ribonucleoprotein H3 GN=HNRNPH3 PE=1 SV=2	HNRH3_HUMAN	37 kDa	0	4	0	2	0	0
155	Heterogeneous nuclear ribonucleoprotein M GN=HNRNPM PE=1 SV=3	HNRPM_HUMAN	78 kDa	0	17	0	32	23	0
156	Heterogeneous nuclear ribonucleoprotein U-like protein 1 GN=HNRNPUL1 PE=1 SV=2	HNRL1_HUMAN	96 kDa	0	15	0	15	12	0
157	Heterogeneous nuclear ribonucleoproteins C1/C2 GN=HNRNPC PE=1 SV=4	HNRPC_HUMAN	34 kDa	0	6	0	5	3	0
158	Hexokinase-1 GN=HK1 PE=1 SV=3	HXK1_HUMAN	102 kDa	0	0	0	0	5	0
159	Histone deacetylase 1 GN=HDAC1 PE=1 SV=1	HDAC1_HUMAN	55 kDa	0	0	0	2	0	0
160	Histone H2B type 1-D GN=HIST1H2BD PE=1 SV=2	H2B1D_HUMAN	14 kDa	0	3	0	0	0	0
161	Histone lysine demethylase PHF8 GN=PHF8 PE=1 SV=3	PHF8_HUMAN	118 kDa	0	0	0	3	0	0
162	HIV Tat-specific factor 1 GN=HTATSF1 PE=1 SV=1	HTSF1_HUMAN	86 kDa	0	0	0	25	6	0
163	Importin subunit alpha-1 GN=KPNA1 PE=1 SV=3	IMA1_HUMAN	60 kDa	0	0	0	4	4	0
164	Importin subunit alpha-2 GN=KPNA2 PE=1 SV=1	IMA2_HUMAN	58 kDa	0	4	0	6	6	0
165	Importin subunit alpha-3 GN=KPNA3 PE=1 SV=2	IMA3_HUMAN	58 kDa	0	0	0	6	0	0
166	Importin subunit alpha-7 GN=KPNA6 PE=1 SV=1	IMA7_HUMAN	60 kDa	0	0	0	0	2	0
167	Insulin receptor substrate 4 GN=IRS4 PE=1 SV=1	IRS4_HUMAN	134 kDa	0	0	0	4	11	0
168	Insulin-like growth factor 2 mRNA-binding protein 2 GN=IGF2BP2 PE=1 SV=2	IF2B2_HUMAN	66 kDa	0	11	0	6	7	0
169	Insulin-like growth factor 2 mRNA-binding protein 3 GN=IGF2BP3 PE=1 SV=2	IF2B3_HUMAN	64 kDa	0	18	0	4	11	0
170	Integrator complex subunit 9 GN=INTS9 PE=1 SV=2	INT9_HUMAN	74 kDa	0	0	0	3	0	0
171	Interleukin enhancer-binding factor 2 GN=ILF2 PE=1 SV=2	ILF2_HUMAN	43 kDa	0	11	0	11	11	0
172	Interleukin enhancer-binding factor 3 GN=ILF3 PE=1 SV=3	ILF3_HUMAN	95 kDa	0	25	0	19	17	0
173	Intraflagellar transport protein 172 homolog GN=IFT172 PE=1 SV=2	IF172_HUMAN	198 kDa	0	0	0	10	0	0
174	Intraflagellar transport protein 20 homolog GN=IFT20 PE=1 SV=1	IFT20_HUMAN	15 kDa	0	0	0	5	0	0
175	Intraflagellar transport protein 27 homolog GN=IFT27 PE=1 SV=1	IFT27_HUMAN	20 kDa	0	0	0	6	0	0
176	Intraflagellar transport protein 46 homolog GN=IFT46 PE=2 SV=1	IFT46_HUMAN	34 kDa	0	0	0	5	0	0
177	Intraflagellar transport protein 52 homolog GN=IFT52 PE=2 SV=3	IFT52_HUMAN	50 kDa	0	0	0	5	0	0

178	Intraflagellar transport protein 57 homolog GN=IFT57 PE=1 SV=1	IFT57_HUMAN	49 kDa	0	0	0	5	0	0
179	Intraflagellar transport protein 80 homolog GN=IFT80 PE=1 SV=3	IFT80_HUMAN	88 kDa	0	0	0	6	0	0
180	Kanadaptin GN=SLC4A1AP PE=1 SV=1	NADAP_HUMAN	89 kDa	0	0	0	19	0	0
181	Kinesin-like protein KIF2A GN=KIF2A PE=1 SV=3	KIF2A_HUMAN	80 kDa	0	0	0	6	8	0
182	Lamina-associated polypeptide 2, isoform alpha GN=TMPO PE=1 SV=2	LAP2A_HUMAN	75 kDa	0	5	0	6	0	0
183	Lamina-associated polypeptide 2, isoforms beta/gamma GN=TMPO PE=1 SV=2	LAP2B_HUMAN	51 kDa	0	4	0	0	0	0
184	La-related protein 1 GN=LARP1 PE=1 SV=2	LARP1_HUMAN	124 kDa	0	27	0	12	9	0
185	Leucine-rich repeat-containing protein 59 GN=LRRC59 PE=1 SV=1	LRC59_HUMAN	35 kDa	0	0	0	9	9	0
186	Liprin-alpha-1 GN=PPFIA1 PE=1 SV=1	LIPA1_HUMAN	136 kDa	0	2	0	2	5	0
187	Lupus La protein GN=SSB PE=1 SV=2	LA_HUMAN	47 kDa	0	5	0	5	6	0
188	Lysyl-tRNA synthetase GN=KARS PE=1 SV=3	SYK_HUMAN	68 kDa	0	0	0	2	0	0
189	Mannose-1-phosphate guanyltransferase alpha GN=GMPPA PE=1 SV=1	GMPPA_HUMAN	46 kDa	0	0	0	0	2	0
190	Mannose-1-phosphate guanyltransferase beta GN=GMPPB PE=1 SV=2	GMPPB_HUMAN	40 kDa	0	0	0	0	3	0
191	Mannosyl-oligosaccharide glucosidase GN=MOGS PE=1 SV=5	MOGS_HUMAN	92 kDa	0	0	0	0	2	0
192	Matrin-3 GN=MATR3 PE=1 SV=2	MATR3_HUMAN	95 kDa	0	19	0	18	10	0
193	Medium-chain specific acyl-CoA dehydrogenase, mitochondrial GN=ACADM PE=1 SV=1	ACADM_HUMAN	47 kDa	0	2	0	0	4	0
194	Membrane-associated progesterone receptor component 1 GN=PGRMC1 PE=1 SV=3	PGRC1_HUMAN	22 kDa	0	0	0	0	2	0
195	Methylosome protein 50 GN=WDR77 PE=1 SV=1	MEP50_HUMAN	37 kDa	0	0	0	2	0	0
196	Microfibrillar-associated protein 1 GN=MFAP1 PE=1 SV=2	MFAP1_HUMAN	52 kDa	0	0	0	10	8	0
197	Midline-1 GN=MID1 PE=1 SV=1	TRI18_HUMAN	75 kDa	0	0	0	0	6	0
198	Mitochondrial import inner membrane translocase subunit TIM44 GN=TIMM44 PE=1 SV=2	TIM44_HUMAN	51 kDa	0	0	0	0	3	0
199	Mitochondrial import inner membrane translocase subunit TIM50 GN=TIMM50 PE=1 SV=2	TIM50_HUMAN	40 kDa	0	0	0	2	0	0
200	Mitochondrial ribonuclease P protein 1 GN=RG9MTD1 PE=1 SV=2	MRRP1_HUMAN	47 kDa	0	0	0	5	3	0
201	Mitogen-activated protein kinase kinase kinase kinase 4 GN=MAP4K4 PE=1 SV=2	M4K4_HUMAN	142 kDa	0	0	0	2	0	0
202	mRNA export factor GN=RAE1 PE=1 SV=1	RAE1L_HUMAN	41 kDa	0	0	0	5	0	0
203	mRNA turnover protein 4 homolog GN=MRTO4 PE=1 SV=2	MRT4_HUMAN	28 kDa	0	0	0	5	5	0
204	N-acetyltransferase 10 GN=NAT10 PE=1 SV=1	NAT10_HUMAN	116 kDa	0	0	0	14	7	0
205	NAD-dependent deacetylase sirtuin-1 GN=SIRT1 PE=1 SV=2	SIRT1_HUMAN	82 kDa	0	0	0	16	0	0
206	NADH dehydrogenase [ubiquinone] 1 alpha subcomplex subunit 4 GN=NDUFA4 PE=1 SV=1	NDUA4_HUMAN	9 kDa	0	2	0	2	4	0
207	Neuralized-like protein 4 GN=NEURL4 PE=1 SV=2	NEUL4_HUMAN	167 kDa	0	33	0	0	0	0
208	NF-kappa-B-repressing factor GN=NKRF PE=1 SV=2	NKRF_HUMAN	78 kDa	0	4	0	6	11	0
209	Nicotinamide phosphoribosyltransferase GN=NAMPT PE=1 SV=1	NAMPT_HUMAN	56 kDa	0	0	0	2	3	0
210	Nuclear cap-binding protein subunit 1 GN=NCBP1 PE=1 SV=1	NCBP1_HUMAN	92 kDa	0	7	0	0	0	0

211	Nuclease-sensitive element-binding protein 1 GN=YBX1 PE=1 SV=3	YBOX1_HUMAN	36 kDa	0	7	0	6	5	0
212	Nucleolar complex protein 2 homolog GN=NOC2L PE=1 SV=3	NOC2L_HUMAN	85 kDa	0	0	0	6	0	0
213	Nucleolar GTP-binding protein 1 GN=GTPBP4 PE=1 SV=3	NOG1_HUMAN	74 kDa	0	0	0	12	9	0
214	Nucleolar protein 10 GN=NOL10 PE=1 SV=1	NOL10_HUMAN	80 kDa	0	0	0	4	0	0
215	Nucleolar protein 14 GN=NOP14 PE=1 SV=3	NOP14_HUMAN	98 kDa	0	0	0	3	5	0
216	Nucleolar protein 58 GN=NOP58 PE=1 SV=1	NOP58_HUMAN	60 kDa	0	0	0	7	4	0
217	Nucleolar RNA helicase 2 GN=DDX21 PE=1 SV=5	DDX21_HUMAN	87 kDa	0	6	0	26	22	0
218	Nucleolin GN=NCL PE=1 SV=3	NUCL_HUMAN	77 kDa	0	7	0	16	16	0
219	Nucleoplasmin-3 GN=NPM3 PE=1 SV=3	NPM3_HUMAN	19 kDa	0	0	0	5	2	0
220	Nucleoporin SEH1 GN=SEH1L PE=1 SV=3	SEH1_HUMAN	40 kDa	0	0	0	0	11	0
221	Nucleoside-triphosphatase C1orf57 GN=C1orf57 PE=1 SV=1	CA057_HUMAN	21 kDa	0	0	0	2	5	0
222	Nucleosome assembly protein 1-like 1 GN=NAP1L1 PE=1 SV=1	NP1L1_HUMAN	45 kDa	0	2	0	4	4	0
223	Ornithine aminotransferase, mitochondrial GN=OAT PE=1 SV=1	OAT_HUMAN	49 kDa	0	3	0	0	0	0
224	Parafibromin GN=CDC73 PE=1 SV=1	CDC73_HUMAN	61 kDa	0	0	0	9	5	0
225	Partitioning defective 3 homolog GN=PARD3 PE=1 SV=2	PARD3_HUMAN	151 kDa	0	0	0	2	2	0
226	Partner of Y14 and mago GN=WIBG PE=1 SV=1	WIBG_HUMAN	23 kDa	0	4	0	0	5	0
227	PDZ and LIM domain protein 5 GN=PDLIM5 PE=1 SV=4	PDLI5_HUMAN	64 kDa	0	0	0	0	3	0
228	Pleckstrin homology-like domain family B member 2 GN=PHLDB2 PE=1 SV=2	PHLB2_HUMAN	142 kDa	0	0	0	0	3	0
229	Pleiotropic regulator 1 GN=PLRG1 PE=1 SV=1	PLRG1_HUMAN	57 kDa	0	0	0	4	2	0
230	Poly(U)-binding-splicing factor PUF60 GN=PUF60 PE=1 SV=1	PUF60_HUMAN	60 kDa	0	4	0	4	4	0
231	Polyadenylate-binding protein 1 GN=PABPC1 PE=1 SV=2	PABP1_HUMAN	71 kDa	0	11	0	3	6	0
232	Polyadenylate-binding protein 3 GN=PABPC3 PE=1 SV=2	PABP3_HUMAN	70 kDa	0	0	0	2	4	0
233	Polyadenylate-binding protein 4 GN=PABPC4 PE=1 SV=1	PABP4_HUMAN	71 kDa	0	18	0	10	11	0
234	Polyglutamine-binding protein 1 GN=PQBP1 PE=1 SV=1	PQBP1_HUMAN	30 kDa	0	0	0	9	5	0
235	Polypyrimidine tract-binding protein 1 GN=PTBP1 PE=1 SV=1	PTBP1_HUMAN	57 kDa	0	8	0	11	7	0
236	Polyribonucleotide nucleotidyltransferase 1, mitochondrial GN=PNPT1 PE=1 SV=2	PNPT1_HUMAN	86 kDa	0	22	0	0	0	0
237	Pre-mRNA 3'-end-processing factor FIP1 GN=FIP1L1 PE=1 SV=1	FIP1_HUMAN	67 kDa	0	0	0	9	8	0
238	Pre-mRNA-processing factor 19 GN=PRPF19 PE=1 SV=1	PRP19_HUMAN	55 kDa	0	3	0	16	10	0
239	Pre-mRNA-processing factor 6 GN=PRPF6 PE=1 SV=1	PRP6_HUMAN	107 kDa	0	0	0	28	20	0
240	Pre-mRNA-processing-splicing factor 8 GN=PRPF8 PE=1 SV=2	PRP8_HUMAN	274 kDa	0	0	0	80	62	0
241	Pre-mRNA-splicing factor 38A GN=PRPF38A PE=1 SV=1	PR38A_HUMAN	37 kDa	0	0	0	7	7	0
242	Pre-mRNA-splicing factor SPF27 GN=BCAS2 PE=1 SV=1	SPF27_HUMAN	26 kDa	0	0	0	8	0	0
243	Pre-rRNA-processing protein TSR1 homolog GN=TSR1 PE=1 SV=1	TSR1_HUMAN	92 kDa	0	7	0	13	14	0
244	Probable ATP-dependent RNA helicase DDX10 GN=DDX10 PE=1 SV=2	DDX10_HUMAN	101 kDa	0	0	0	10	4	0
245	Probable ATP-dependent RNA helicase DDX17 GN=DDX17 PE=1 SV=1	DDX17_HUMAN	72 kDa	0	14	0	17	20	0
246	Probable ATP-dependent RNA helicase DDX23 GN=DDX23 PE=1 SV=3	DDX23_HUMAN	96 kDa	0	0	0	23	18	0
247	Probable ATP-dependent RNA helicase DDX46 GN=DDX46 PE=1 SV=2	DDX46_HUMAN	117 kDa	0	0	0	24	0	0
248	Probable ATP-dependent RNA helicase DDX47 GN=DDX47 PE=1 SV=1	DDX47_HUMAN	51 kDa	0	0	0	4	6	0

249	Probable ATP-dependent RNA helicase DDX5 GN=DDX5 PE=1 SV=1	DDX5_HUMAN	69 kDa	0	15	0	18	22	0
250	Probable ATP-dependent RNA helicase DHX36 GN=DHX36 PE=1 SV=1	DHX36_HUMAN	115 kDa	0	16	0	0	4	0
251	Prolyl 4-hydroxylase subunit alpha-1 GN=P4HA1 PE=1 SV=2	P4HA1_HUMAN	61 kDa	0	15	0	0	0	0
252	Protein arginine N-methyltransferase 1 GN=PRMT1 PE=1 SV=2	ANM1_HUMAN	42 kDa	0	7	0	8	2	0
253	Protein arginine N-methyltransferase 5 GN=PRMT5 PE=1 SV=4	ANM5_HUMAN	73 kDa	0	0	0	6	0	0
254	Protein argonaute-1 GN=EIF2C1 PE=1 SV=3	AGO1_HUMAN	97 kDa	0	3	0	0	0	0
255	Protein argonaute-2 GN=EIF2C2 PE=1 SV=3	AGO2_HUMAN	97 kDa	0	9	0	0	0	0
256	Protein diaphanous homolog 3 GN=DIAPH3 PE=1 SV=4	DIAP3_HUMAN	137 kDa	0	14	0	0	0	0
257	Protein disulfide-isomerase GN=P4HB PE=1 SV=3	PDIA1_HUMAN	57 kDa	0	13	0	0	0	0
258	Protein FAM192A GN=FAM192A PE=1 SV=1	F192A_HUMAN	29 kDa	0	0	0	2	0	0
259	Protein FAM98A GN=FAM98A PE=1 SV=1	FA98A_HUMAN	55 kDa	0	2	0	0	0	0
260	Protein HEXIM1 GN=HEXIM1 PE=1 SV=1	HEXI1_HUMAN	41 kDa	0	0	0	5	4	0
261	Protein IWS1 homolog GN=IWS1 PE=1 SV=2	IWS1_HUMAN	92 kDa	0	0	0	8	4	0
262	Protein KIAA1967 GN=KIAA1967 PE=1 SV=2	K1967_HUMAN	103 kDa	0	9	0	0	0	0
263	Protein kinase C iota type GN=PRKCI PE=1 SV=2	KPCI_HUMAN	68 kDa	0	0	0	5	2	0
264	Protein KRI1 homolog GN=KRI1 PE=1 SV=2	KRI1_HUMAN	83 kDa	0	0	0	5	8	0
265	Protein LTV1 homolog GN=LTV1 PE=1 SV=1	LTV1_HUMAN	55 kDa	0	0	0	6	3	0
266	Protein LYRIC GN=MTDH PE=1 SV=2	LYRIC_HUMAN	64 kDa	0	0	0	7	8	0
267	Protein pelota homolog GN=PELO PE=1 SV=1	PELO_HUMAN	43 kDa	0	0	0	13	14	0
268	Protein phosphatase 1G GN=PPM1G PE=1 SV=1	PPM1G_HUMAN	59 kDa	0	0	0	13	0	0
269	Protein SEC13 homolog GN=SEC13 PE=1 SV=3	SEC13_HUMAN	36 kDa	0	4	0	8	5	0
270	Protein SET GN=SET PE=1 SV=3	SET_HUMAN	33 kDa	0	0	0	10	10	0
271	Protein strawberry notch homolog 1 GN=SBNO1 PE=1 SV=1	SBNO1_HUMAN	154 kDa	0	4	0	0	0	0
272	Protein transport protein Sec16A GN=SEC16A PE=1 SV=3	SC16A_HUMAN	234 kDa	0	12	0	15	11	0
273	Protein transport protein Sec23A GN=SEC23A PE=1 SV=2	SC23A_HUMAN	86 kDa	0	0	0	5	0	0
274	Protein transport protein Sec23B GN=SEC23B PE=1 SV=2	SC23B_HUMAN	86 kDa	0	0	0	5	0	0
275	Protein transport protein Sec61 subunit alpha isoform 1 GN=SEC61A1 PE=1 SV=2	S61A1_HUMAN	52 kDa	0	2	0	0	2	0
276	Protein TSSC4 GN=TSSC4 PE=1 SV=3	TSSC4_HUMAN	34 kDa	0	0	0	10	0	0
277	Protein VPRBP GN=VPRBP PE=1 SV=3	VPRBP_HUMAN	169 kDa	0	0	0	3	0	0
278	Putative adenosylhomocysteinase 2 GN=AHCYL1 PE=1 SV=2	SAHH2_HUMAN	59 kDa	0	0	0	9	0	0
279	Putative ATP-dependent RNA helicase DHX30 GN=DHX30 PE=1 SV=1	DHX30_HUMAN	134 kDa	0	23	0	33	27	0
280	Putative heat shock 70 kDa protein 7 GN=HSPA7 PE=5 SV=2	HSP77_HUMAN	40 kDa	0	0	2	0	0	0
281	Putative heat shock protein HSP 90-beta-3 GN=HSP90AB3P PE=5 SV=1	H90B3_HUMAN	68 kDa	0	2	0	0	0	0
282	Putative pre-mRNA-splicing factor ATP-dependent RNA helicase DHX15 GN=DHX15 PE=1 SV=2	DHX15_HUMAN	91 kDa	0	12	0	18	15	0
283	Putative pre-mRNA-splicing factor ATP-dependent RNA helicase DHX16 GN=DHX16 PE=1 SV=2	DHX16_HUMAN	119 kDa	0	0	0	14	0	0
284	Putative ribosomal RNA methyltransferase NOP2 GN=NOP2 PE=1 SV=2	NOP2_HUMAN	89 kDa	0	0	0	9	4	0

285	Putative RNA-binding protein 3 GN=RBM3 PE=1 SV=1	RBM3_HUMAN	17 kDa	0	4	0	3	5	0
286	Putative RNA-binding protein Luc7-like 1 GN=LUC7L PE=1 SV=1	LUC7L_HUMAN	44 kDa	0	0	0	5	0	0
287	Putative RNA-binding protein Luc7-like 2 GN=LUC7L2 PE=1 SV=2	LC7L2_HUMAN	47 kDa	0	0	0	8	10	0
288	Putative rRNA methyltransferase 3 GN=FTSJ3 PE=1 SV=2	RRMJ3_HUMAN	97 kDa	0	0	0	10	7	0
289	Pyruvate dehydrogenase E1 component subunit alpha, somatic form, mitochondrial GN=PDHA1 PE=1 SV=3	ODPA_HUMAN	43 kDa	0	0	0	0	3	0
290	Pyruvate dehydrogenase E1 component subunit beta, mitochondrial GN=PDHB PE=1 SV=3	ODPB_HUMAN	39 kDa	0	3	0	6	8	0
291	Ras GTPase-activating protein-binding protein 1 GN=G3BP1 PE=1 SV=1	G3BP1_HUMAN	52 kDa	0	10	0	15	18	0
292	Ras GTPase-activating protein-binding protein 2 GN=G3BP2 PE=1 SV=2	G3BP2_HUMAN	54 kDa	0	9	0	9	9	0
293	Regulator of nonsense transcripts 1 GN=UPF1 PE=1 SV=2	RENT1_HUMAN	124 kDa	0	9	0	0	0	0
294	Replication factor C subunit 4 GN=RFC4 PE=1 SV=2	RFC4_HUMAN	40 kDa	0	2	0	0	3	0
295	Replication factor C subunit 5 GN=RFC5 PE=1 SV=1	RFC5_HUMAN	38 kDa	0	0	0	3	2	0
296	Reticulocalbin-1 GN=RCN1 PE=1 SV=1	RCN1_HUMAN	39 kDa	0	0	0	0	7	0
297	Reticulocalbin-2 GN=RCN2 PE=1 SV=1	RCN2_HUMAN	37 kDa	0	2	0	3	10	0
298	Rho guanine nucleotide exchange factor 2 GN=ARHGEF2 PE=1 SV=4	ARHG2_HUMAN	112 kDa	0	0	0	5	0	0
299	Ribonuclease inhibitor GN=RNH1 PE=1 SV=2	RINI_HUMAN	50 kDa	0	10	0	5	7	0
300	Ribonucleases P/MRP protein subunit POP1 GN=POP1 PE=1 SV=2	POP1_HUMAN	115 kDa	0	0	0	8	6	0
301	Ribosome biogenesis protein BMS1 homolog GN=BMS1 PE=1 SV=1	BMS1_HUMAN	146 kDa	0	0	0	10	0	0
302	Ribosome biogenesis protein BOP1 GN=BOP1 PE=1 SV=2	BOP1_HUMAN	84 kDa	0	0	0	5	0	0
303	Ribosome biogenesis protein BRX1 homolog GN=BRIX1 PE=1 SV=2	BRX1_HUMAN	41 kDa	0	0	0	7	0	0
304	Ribosome biogenesis protein WDR12 GN=WDR12 PE=1 SV=2	WDR12_HUMAN	48 kDa	0	0	0	6	0	0
305	Ribosome biogenesis regulatory protein homolog GN=RRS1 PE=1 SV=2	RRS1_HUMAN	41 kDa	0	0	0	3	5	0
306	Ribosome production factor 2 homolog GN=RPF2 PE=1 SV=2	RPF2_HUMAN	36 kDa	0	0	0	6	4	0
307	RING finger protein 114 GN=RNF114 PE=1 SV=1	RN114_HUMAN	26 kDa	0	3	0	0	0	0
308	RNA polymerase II-associated factor 1 homolog GN=PAF1 PE=1 SV=2	PAF1_HUMAN	60 kDa	0	0	0	0	2	0
309	RNA polymerase-associated protein CTR9 homolog GN=CTR9 PE=1 SV=1	CTR9_HUMAN	134 kDa	0	0	0	2	2	0
310	RNA-binding motif protein, X-linked-like-3 GN=RBMXL3 PE=2 SV=2	RMXL3_HUMAN	115 kDa	0	4	0	0	2	0
311	RNA-binding protein 10 GN=RBM10 PE=1 SV=3	RBM10_HUMAN	104 kDa	0	0	0	18	15	0
312	RNA-binding protein 14 GN=RBM14 PE=1 SV=2	RBM14_HUMAN	69 kDa	0	6	0	10	5	0
313	RNA-binding protein 25 GN=RBM25 PE=1 SV=3	RBM25_HUMAN	100 kDa	0	0	0	4	0	0
314	RNA-binding protein 39 GN=RBM39 PE=1 SV=2	RBM39_HUMAN	59 kDa	0	0	0	11	6	0
315	RNA-binding protein 4 GN=RBM4 PE=1 SV=1	RBM4_HUMAN	40 kDa	0	0	0	4	5	0
316	RNA-binding protein NOB1 GN=NOB1 PE=1 SV=1	NOB1_HUMAN	47 kDa	0	0	0	5	3	0
317	rRNA 2'-O-methyltransferase fibrillarin GN=FBL PE=1 SV=2	FBRL_HUMAN	34 kDa	0	3	0	6	5	0
318	RuvB-like 2 GN=RUVBL2 PE=1 SV=3	RUVB2_HUMAN	51 kDa	0	12	2	10	9	0
319	SAM domain and HD domain-containing protein 1 GN=SAMHD1 PE=1 SV=2	SAMH1_HUMAN	72 kDa	0	0	0	0	3	0
320	Serine/arginine-rich splicing factor 5 GN=SRSF5 PE=1 SV=1	SRSF5_HUMAN	31 kDa	0	0	0	4	3	0

321	Serine/threonine-protein kinase SRPK1 GN=SRPK1 PE=1 SV=2	SRPK1_HUMAN	74 kDa	0	0	0	7	4	0
322	Serine/threonine-protein phosphatase 2A 65 kDa regulatory subunit A alpha isoform GN=PPP2R1A PE=1 SV=4	2AAA_HUMAN	65 kDa	0	0	0	3	9	0
323	Serine/threonine-protein phosphatase 6 catalytic subunit GN=PPP6C PE=1 SV=1	PPP6_HUMAN	35 kDa	0	0	0	11	6	0
324	Serine/threonine-protein phosphatase 6 regulatory ankyrin repeat subunit A GN=ANKRD28 PE=1 SV=4	ANR28_HUMAN	117 kDa	0	0	0	9	0	0
325	Serine/threonine-protein phosphatase 6 regulatory ankyrin repeat subunit C GN=ANKRD52 PE=1 SV=3	ANR52_HUMAN	115 kDa	0	0	0	8	0	0
326	Serine/threonine-protein phosphatase 6 regulatory subunit 3 GN=PPP6R3 PE=1 SV=2	PP6R3_HUMAN	98 kDa	0	0	0	13	4	0
327	Serine/threonine-protein phosphatase PGAM5, mitochondrial GN=PGAM5 PE=1 SV=2	PGAM5_HUMAN	32 kDa	0	0	0	0	2	0
328	Signal recognition particle 9 kDa protein GN=SRP9 PE=1 SV=2	SRP09_HUMAN	10 kDa	0	5	0	3	3	0
329	Signal recognition particle receptor subunit beta GN=SRPRB PE=1 SV=3	SRPRB_HUMAN	30 kDa	0	2	0	0	0	0
330	Signal transducer and activator of transcription 2 GN=STAT2 PE=1 SV=1	STAT2_HUMAN	98 kDa	0	0	0	8	9	0
331	Single-stranded DNA-binding protein, mitochondrial GN=SSBP1 PE=1 SV=1	SSBP_HUMAN	17 kDa	0	7	0	0	0	0
332	Small nuclear ribonucleoprotein Sm D1 GN=SNRPD1 PE=1 SV=1	SMD1_HUMAN	13 kDa	0	2	0	6	4	0
333	Small nuclear ribonucleoprotein Sm D2 GN=SNRPD2 PE=1 SV=1	SMD2_HUMAN	14 kDa	0	4	0	7	5	0
334	Sodium/potassium-transporting ATPase subunit alpha-1 GN=ATP1A1 PE=1 SV=1	AT1A1_HUMAN	113 kDa	0	0	0	0	3	0
335	Spermatid perinuclear RNA-binding protein GN=STRBP PE=1 SV=1	STRBP_HUMAN	74 kDa	0	0	0	0	2	0
336	Spermatogenesis-associated protein 5 GN=SPATA5 PE=1 SV=3	SPAT5_HUMAN	98 kDa	0	0	0	0	2	0
337	Spermidine synthase GN=SRM PE=1 SV=1	SPEE_HUMAN	34 kDa	0	0	0	0	3	0
338	Splicing factor 3A subunit 1 GN=SF3A1 PE=1 SV=1	SF3A1_HUMAN	89 kDa	0	0	0	23	0	0
339	Splicing factor 3A subunit 2 GN=SF3A2 PE=1 SV=2	SF3A2_HUMAN	49 kDa	0	0	0	7	0	0
340	Splicing factor 3A subunit 3 GN=SF3A3 PE=1 SV=1	SF3A3_HUMAN	59 kDa	0	0	0	15	2	0
341	Splicing factor 3B subunit 1 GN=SF3B1 PE=1 SV=3	SF3B1_HUMAN	146 kDa	0	0	0	43	16	0
342	Splicing factor 3B subunit 2 GN=SF3B2 PE=1 SV=2	SF3B2_HUMAN	100 kDa	0	4	0	25	13	0
343	Splicing factor 3B subunit 3 GN=SF3B3 PE=1 SV=4	SF3B3_HUMAN	136 kDa	0	2	0	42	21	0
344	Splicing factor 3B subunit 5 GN=SF3B5 PE=1 SV=1	SF3B5_HUMAN	10 kDa	0	0	0	6	0	0
345	Splicing factor 45 GN=RBM17 PE=1 SV=1	SPF45_HUMAN	45 kDa	0	0	0	9	0	0
346	Splicing factor U2AF 35 kDa subunit GN=U2AF1 PE=1 SV=3	U2AF1_HUMAN	28 kDa	0	3	0	5	4	0
347	Splicing factor U2AF 65 kDa subunit GN=U2AF2 PE=1 SV=4	U2AF2_HUMAN	54 kDa	0	5	0	8	7	0
348	Squamous cell carcinoma antigen recognized by T-cells 3 GN=SART3 PE=1 SV=1	SART3_HUMAN	110 kDa	0	0	0	0	2	0
349	Staphylococcal nuclease domain-containing protein 1 GN=SND1 PE=1 SV=1	SND1_HUMAN	102 kDa	0	0	0	6	6	0
350	Stress-70 protein, mitochondrial GN=HSPA9 PE=1 SV=2	GRP75_HUMAN	74 kDa	0	16	4	10	10	0
351	SUMO-activating enzyme subunit 1 GN=SAE1 PE=1 SV=1	SAE1_HUMAN	38 kDa	0	2	0	0	0	0
352	Superkiller viralicidic activity 2-like 2 GN=SKIV2L2 PE=1 SV=3	SK2L2_HUMAN	118 kDa	0	0	0	3	0	0
353	Synembryn-A GN=RIC8A PE=1 SV=3	RIC8A_HUMAN	60 kDa	0	0	0	9	17	0

354	Tetratricopeptide repeat protein 26 GN=TTC26 PE=2 SV=1	TTC26_HUMAN	64 kDa	0	0	0	8	0	0
355	Tetratricopeptide repeat protein 30A GN=TTC30A PE=2 SV=3	TT30A_HUMAN	76 kDa	0	0	0	2	0	0
356	TGF-beta-activated kinase 1 and MAP3K7-binding protein 1 GN=TAB1 PE=1 SV=1	TAB1_HUMAN	55 kDa	0	5	0	0	0	0
357	THO complex subunit 3 GN=THOC3 PE=1 SV=1	THOC3_HUMAN	39 kDa	0	4	0	0	0	0
358	THO complex subunit 4 GN=THOC4 PE=1 SV=3	THOC4_HUMAN	27 kDa	0	0	0	7	3	0
359	Thyroid hormone receptor-associated protein 3 GN=THRAP3 PE=1 SV=2	TR150_HUMAN	109 kDa	0	0	0	9	0	0
360	Transcription factor 25 GN=TCF25 PE=1 SV=1	TCF25_HUMAN	77 kDa	0	0	0	2	8	0
361	Transcription factor A, mitochondrial GN=TFAM PE=1 SV=1	TFAM_HUMAN	29 kDa	0	5	0	0	5	0
362	Transcription initiation factor IIE subunit beta GN=GTF2E2 PE=1 SV=1	T2EB_HUMAN	33 kDa	0	0	0	5	0	0
363	Transcription intermediary factor 1-beta GN=TRIM28 PE=1 SV=5	TIF1B_HUMAN	89 kDa	0	7	0	9	4	0
364	Transcriptional activator protein Pur-alpha GN=PURA PE=1 SV=2	PURA_HUMAN	35 kDa	0	7	0	3	5	0
365	Transformer-2 protein homolog beta GN=TRA2B PE=1 SV=1	TRA2B_HUMAN	34 kDa	0	5	0	0	0	0
366	Translation initiation factor eIF-2B subunit beta GN=EIF2B2 PE=1 SV=3	EI2BB_HUMAN	39 kDa	0	0	0	3	5	0
367	Translation initiation factor eIF-2B subunit delta GN=EIF2B4 PE=1 SV=2	EI2BD_HUMAN	58 kDa	0	0	0	11	11	0
368	Translation initiation factor eIF-2B subunit epsilon GN=EIF2B5 PE=1 SV=3	EI2BE_HUMAN	80 kDa	0	0	0	8	6	0
369	Translation initiation factor eIF-2B subunit gamma GN=EIF2B3 PE=1 SV=1	EI2BG_HUMAN	50 kDa	0	0	0	10	12	0
370	Translocon-associated protein subunit delta GN=SSR4 PE=1 SV=1	SSRD_HUMAN	19 kDa	0	0	0	2	4	0
371	Tripeptidyl-peptidase 2 GN=TPP2 PE=1 SV=4	TPP2_HUMAN	138 kDa	0	0	0	54	9	0
372	tRNA (adenine-N(1)-)-methyltransferase non-catalytic subunit TRM6 GN=TRMT6 PE=1 SV=1	TRM6_HUMAN	56 kDa	0	0	0	5	0	0
373	tRNA (cytosine-5-)-methyltransferase NSUN2 GN=NSUN2 PE=1 SV=2	NSUN2_HUMAN	86 kDa	0	8	0	22	8	0
374	Tubulin alpha-1B chain GN=TUBA1B PE=1 SV=1	TBA1B_HUMAN	50 kDa	0	2	4	0	0	0
375	Tubulin alpha-1C chain GN=TUBA1C PE=1 SV=1	TBA1C_HUMAN	50 kDa	0	3	0	3	3	0
376	Tubulin beta-1 chain GN=TUBB1 PE=1 SV=1	TBB1_HUMAN	50 kDa	0	2	0	4	0	0
377	Tubulin beta-4 chain GN=TUBB4 PE=1 SV=2	TBB4_HUMAN	50 kDa	0	0	0	0	2	0
378	Tubulin beta-6 chain GN=TUBB6 PE=1 SV=1	TBB6_HUMAN	50 kDa	0	3	5	4	2	0
379	Tudor domain-containing protein 3 GN=TDRD3 PE=1 SV=1	TDRD3_HUMAN	73 kDa	0	5	0	0	0	0
380	U1 small nuclear ribonucleoprotein 70 kDa GN=SNRNP70 PE=1 SV=2	RU17_HUMAN	52 kDa	0	0	0	5	0	0
381	U2 small nuclear ribonucleoprotein A' GN=SNRPA1 PE=1 SV=2	RU2A_HUMAN	28 kDa	0	0	0	12	10	0
382	U2 small nuclear ribonucleoprotein B" GN=SNRPB2 PE=1 SV=1	RU2B_HUMAN	25 kDa	0	0	0	5	2	0
383	U2-associated protein SR140 GN=SR140 PE=1 SV=2	SR140_HUMAN	118 kDa	0	0	0	15	0	0
384	U4/U6 small nuclear ribonucleoprotein Prp4 GN=PRPF4 PE=1 SV=2	PRP4_HUMAN	58 kDa	0	0	0	3	5	0
385	U4/U6.U5 tri-snRNP-associated protein 1 GN=SART1 PE=1 SV=1	SNUT1_HUMAN	90 kDa	0	0	0	9	0	0
386	U4/U6.U5 tri-snRNP-associated protein 2 GN=USP39 PE=1 SV=2	SNUT2_HUMAN	65 kDa	0	0	0	12	11	0
387	U5 small nuclear ribonucleoprotein 200 kDa helicase GN=SNRNP200 PE=1 SV=2	U520_HUMAN	245 kDa	0	0	0	83	69	0
388	U5 small nuclear ribonucleoprotein 40 kDa protein GN=SNRNP40 PE=1 SV=1	SNR40_HUMAN	39 kDA	0	0	0	5	0	0
389	Ubiquitin carboxyl-terminal hydrolase 10 GN=USP10 PE=1 SV=2	UBP10_HUMAN	87 kDa	0	6	0	6	13	0
390	Ubiquitin-40S ribosomal protein S27a GN=RPS27A PE=1 SV=2	RS27A_HUMAN	18 kDa	0	6	0	8	6	0

391	Uncharacterized protein C20orf4 GN=C20orf4 PE=1 SV=2	CT004_HUMAN	43 kDa	0	0	0	13	5	0
392	Uncharacterized protein C21orf70 GN=C21orf70 PE=1 SV=2	CU070_HUMAN	25 kDa	0	0	0	0	6	0
393	Uncharacterized protein C7orf50 GN=C7orf50 PE=1 SV=1	CG050_HUMAN	22 kDa	0	0	0	6	6	0
394	UPF0027 protein C22orf28 GN=C22orf28 PE=1 SV=1	CV028_HUMAN	55 kDa	0	15	0	8	9	0
395	UPF0568 protein C14orf166 GN=C14orf166 PE=1 SV=1	CN166_HUMAN	28 kDa	0	0	0	5	6	0
396	Vimentin GN=VIM PE=1 SV=4	VIME_HUMAN	54 kDa	0	13	2	0	13	0
397	WD repeat-containing protein 59 GN=WDR59 PE=1 SV=2	WDR59_HUMAN	110 kDa	0	0	0	0	8	0
398	WD repeat-containing protein mio GN=MIOS PE=1 SV=2	MIO_HUMAN	99 kDa	0	0	0	0	19	0
399	WD40 repeat-containing protein SMU1 GN=SMU1 PE=1 SV=2	SMU1_HUMAN	58 kDa	0	0	0	10	8	0
400	WW domain-binding protein 11 GN=WBP11 PE=1 SV=1	WBP11_HUMAN	70 kDa	0	0	0	6	0	0
401	YTH domain family protein 1 GN=YTHDF1 PE=1 SV=1	YTHD1_HUMAN	61 kDa	0	0	0	0	2	0
402	YTH domain family protein 2 GN=YTHDF2 PE=1 SV=2	YTHD2_HUMAN	62 kDa	0	6	0	3	8	0
403	Zinc finger CCCH domain-containing protein 15 GN=ZC3H15 PE=1 SV=1	ZC3HF_HUMAN	49 kDa	0	0	0	8	3	0
404	Zinc finger CCCH-type antiviral protein 1 GN=ZC3HAV1 PE=1 SV=3	ZCCHV_HUMAN	101 kDa	0	0	0	15	11	0
405	Zinc finger CCHC domain-containing protein 3 GN=ZCCHC3 PE=1 SV=1	ZCHC3_HUMAN	44 kDa	0	5	0	3	0	0

Table A-2: GO functional enrichment analysis of 185 human host proteins that co-eluted with DENV1/2 GFP-NS3. The Benjamini-Hochberg procedure was used to calculate the q-value (false discovery rate adjusted p-value) of each enriched GO feature. For each enriched GO feature that is associated with the generated interaction network, the number of proteins in the interaction network listed in that group, as well as the number of total proteins in the Homo sapiens proteome associated with the same GO feature. The table is arranged in order of increasing q-value.

GO feature	q-value	Genes in network	Genes in genome
translational initiation	1.29E-64	53	150
cytosolic ribosome	9.42E-57	42	90
nuclear-transcribed mRNA catabolic process, nonsense-mediated decay	8.12E-55	44	116
RNA catabolic process	4.72E-54	52	215
ribosomal subunit	4.72E-54	44	121
translational termination	1.86E-53	40	89
SRP-dependent cotranslational protein targeting to membrane	2.93E-53	42	107
protein targeting to ER	3.69E-53	42	108
cotranslational protein targeting to membrane	3.69E-53	42	108
establishment of protein localization to endoplasmic reticulum	5.37E-53	42	109
protein localization to endoplasmic reticulum	9.79E-53	43	120
mRNA catabolic process	1.41E-52	49	190
viral gene expression	1.27E-50	39	94
nuclear-transcribed mRNA catabolic process	4.43E-49	46	179
ribosome	5.51E-49	44	155
translational elongation	5.51E-49	39	102
multi-organism metabolic process	1.30E-48	39	104
cytosolic part	6.63E-48	43	151
protein targeting to membrane	1.96E-45	42	157
cellular protein complex disassembly	3.72E-45	40	135
establishment of protein localization to membrane	3.46E-43	47	253
protein localization to membrane	1.46E-42	45	227
protein complex disassembly	2.31E-42	40	156
viral transcription	4.99E-42	40	159
viral life cycle	4.99E-42	40	159
macromolecular complex disassembly	1.45E-41	40	163
single-organism cellular localization	6.32E-39	45	272
single-organism localization	6.32E-39	45	272
structural constituent of ribosome	1.92E-37	32	97
cytosolic small ribosomal subunit	2.40E-37	24	36
protein targeting	1.04E-35	44	299
small ribosomal subunit	4.23E-33	25	55
cytosolic large ribosomal subunit	7.13E-21	18	51
large ribosomal subunit	4.85E-20	19	67
regulation of translation	6.78E-18	23	152
ribonucleoprotein complex biogenesis	3.03E-16	22	158
posttranscriptional regulation of gene expression	2.06E-15	27	298
mRNA processing	9.57E-15	26	288
ribosome biogenesis	3.33E-14	16	78
ncRNA metabolic process	3.31E-13	21	194
RNA splicing	3.31E-13	24	274
mRNA binding	6.76E-13	15	77
RNA splicing, via transesterification reactions with bulged adenosine as nucleophile	1.27E-12	21	208
mRNA splicing, via spliceosome	1.27E-12	21	208
spliceosomal complex	1.55E-12	17	118
RNA splicing, via transesterification reactions	2.16E-12	21	214
translation initiation factor activity	2.57E-12	11	31
ribosomal small subunit biogenesis	5.81E-11	9	20
ribonucleoprotein complex assembly	8.22E-10	14	102
cytoplasmic stress granule	9.84E-10	9	26
ribonucleoprotein complex subunit organization	2.00E-09	14	109
ncRNA processing	2.53E-09	14	111
rRNA processing	3.22E-09	11	56

translation factor activity, nucleic acid binding	3.88E-09	11	57
double-stranded RNA binding	7.55E-09	10	45
rRNA metabolic process	8.19E-09	11	61
ribosome assembly	2.02E-08	7	15
ribonucleoprotein granule	9.49E-08	11	76
RNA 3'-end processing	1.50E-07	12	101
eukaryotic translation initiation factor 3 complex	1.51E-06	6	15
catalytic step 2 spliceosome	2.58E-06	10	80
negative regulation of translation	3.76E-06	9	62
positive regulation of translation	3.86E-06	8	44
ribonucleoprotein complex binding	4.59E-06	8	45
mRNA 3'-end processing	6.19E-06	10	88
ribosome binding	7.18E-06	6	19
single-stranded RNA binding	9.79E-06	7	33
polysome	1.37E-05	6	21
U12-type spliceosomal complex	3.27E-05	6	24
poly-purine tract binding	3.39E-05	5	13
response to unfolded protein	3.42E-05	10	106
ATP catabolic process	4.13E-05	11	137
ribonucleoside monophosphate catabolic process	4.60E-05	11	139
purine nucleoside monophosphate catabolic process	4.60E-05	11	139
purine ribonucleoside monophosphate catabolic process	4.60E-05	11	139
nucleoside monophosphate catabolic process	4.88E-05	11	140
response to topologically incorrect protein	5.78E-05	10	113
helicase activity	6.56E-05	8	64
RNA helicase activity	9.66E-05	6	29
regulation of translational initiation	1.44E-04	7	49
ATP metabolic process	1.55E-04	11	158
ATPase activity	1.97E-04	12	197
RNA-dependent ATPase activity	4.24E-04	5	21
purine nucleoside monophosphate metabolic process	4.53E-04	11	177
purine ribonucleoside monophosphate metabolic process	4.53E-04	11	177
poly(A) binding	4.57E-04	4	10
maturation of SSU-rRNA	4.57E-04	4	10
regulation of mRNA processing	4.76E-04	7	59
ribonucleoside monophosphate metabolic process	5.10E-04	11	180
nucleoside monophosphate metabolic process	7.30E-04	11	187
purine NTP-dependent helicase activity	8.21E-04	6	42
ATP-dependent helicase activity	8.21E-04	6	42
protein folding	1.02E-03	9	124
positive regulation of mRNA catabolic process	2.64E-03	4	15
mitochondrial matrix	2.64E-03	12	257
ATPase activity, coupled	3.15E-03	9	143
regulation of mRNA stability	3.83E-03	5	33
regulation of mRNA catabolic process	4.32E-03	4	17
mitochondrial nucleoid	4.32E-03	5	34
regulation of RNA stability	4.32E-03	5	34
RNA localization	4.45E-03	7	84
nucleic acid transport	4.67E-03	7	85
establishment of RNA localization	4.67E-03	7	85
RNA transport	4.67E-03	7	85
nucleoid	4.76E-03	5	35
negative regulation of RNA splicing	5.12E-03	4	18
ATP-dependent RNA helicase activity	7.91E-03	4	20
positive regulation of mRNA processing	9.61E-03	4	21
regulation of RNA splicing	9.80E-03	6	66
mRNA polyadenylation	1.14E-02	4	22
'de novo' protein folding	1.25E-02	5	43
RNA stabilization	1.34E-02	4	23
mRNA stabilization	1.34E-02	4	23
RNA polyadenylation	1.58E-02	4	24
nucleobase-containing compound transport	1.73E-02	7	106
mitochondrion organization	1.73E-02	10	225
organelle assembly	1.78E-02	10	226

ATP-dependent DNA helicase activity	1.80E-02	4	25
RNA export from nucleus	1.99E-02	6	76
mRNA 3'-UTR binding	2.08E-02	4	26
translation regulator activity	2.40E-02	4	27
nuclear export	2.45E-02	7	113
MHC protein complex binding	2.49E-02	3	11
MHC class II protein complex binding	2.49E-02	3	11
nuclear body	3.92E-02	8	162
negative regulation of mRNA splicing, via spliceosome	5.24E-02	3	14
telomeric DNA binding	5.24E-02	3	14
DNA strand elongation involved in DNA replication	5.67E-02	4	34
RNA phosphodiester bond hydrolysis	6.19E-02	5	62
replication fork	6.25E-02	4	35
positive regulation of mRNA 3'-end processing	6.31E-02	3	15
regulation of mRNA splicing, via spliceosome	6.87E-02	4	36
intrinsic apoptotic signaling pathway	7.42E-02	8	180
regulation of mRNA 3'-end processing	7.42E-02	3	16
negative regulation of mRNA processing	7.42E-02	3	16
DNA strand elongation	7.42E-02	4	37
DNA helicase activity	8.10E-02	4	38
'de novo' posttranslational protein folding	8.10E-02	4	38
DNA-dependent DNA replication	8.43E-02	6	102
mRNA export from nucleus	8.75E-02	5	68
mRNA transport	9.29E-02	5	69

Table A-3: GO functional enrichment analysis of 298 human host proteins that co-eluted with DENV1 GFP-NS5. The Benjamini-Hochberg procedure was used to calculate the q-value (false discovery rate adjusted p-value) of each enriched GO feature. For each enriched GO feature that is associated with the generated interaction network, the number of proteins in the interaction network listed in that group, as well as the number of total proteins in the Homo sapiens proteome associated with the same GO feature. The table is arranged in order of increasing q-value.

GO feature	q-value	Genes in network	Genes in genome
translational initiation	2.35E-45	48	150
RNA splicing, via transesterification reactions	1.85E-41	51	214
RNA splicing, via transesterification reactions with bulged adenosine as nucleophile	4.50E-41	50	208
mRNA splicing, via spliceosome	4.50E-41	50	208
RNA splicing	4.50E-41	55	274
mRNA processing	1.15E-38	54	288
spliceosomal complex	1.40E-37	39	118
ribonucleoprotein complex biogenesis	3.01E-36	42	158
RNA catabolic process	2.84E-30	42	215
nuclear-transcribed mRNA catabolic process, nonsense-mediated decay	4.51E-29	33	116
catalytic step 2 spliceosome	7.93E-29	29	80
mRNA catabolic process	1.18E-27	38	190
cytosolic ribosome	3.70E-27	29	90
SRP-dependent cotranslational protein targeting to membrane	3.81E-26	30	107
protein targeting to ER	4.56E-26	30	108
cotranslational protein targeting to membrane	4.56E-26	30	108
protein localization to endoplasmic reticulum	5.59E-26	31	120
establishment of protein localization to endoplasmic reticulum	5.59E-26	30	109
translational termination	5.63E-26	28	89
ribosomal subunit	6.67E-26	31	121
translational elongation	1.42E-25	29	102
viral gene expression	2.78E-25	28	94
nuclear-transcribed mRNA catabolic process	3.35E-25	35	179
multi-organism metabolic process	6.06E-24	28	104
ribosome	1.09E-23	32	155
protein targeting to membrane	1.61E-23	32	157
cytosolic part	7.40E-23	31	151
ribonucleoprotein complex assembly	7.40E-23	27	102
ribonucleoprotein complex subunit organization	4.93E-22	27	109
ribosome biogenesis	6.40E-22	24	78
cellular protein complex disassembly	6.61E-22	29	135
protein complex disassembly	3.13E-21	30	156
establishment of protein localization to membrane	3.95E-21	36	253
viral transcription	5.15E-21	30	159
viral life cycle	5.15E-21	30	159
macromolecular complex disassembly	1.08E-20	30	163
protein targeting	1.17E-20	38	299
protein localization to membrane	1.18E-20	34	227
translation initiation factor activity	1.81E-20	17	31
structural constituent of ribosome	1.61E-19	24	97
single-organism cellular localization	4.18E-18	34	272
single-organism localization	4.18E-18	34	272
translation factor activity, nucleic acid binding	6.30E-18	19	57
posttranscriptional regulation of gene expression	5.64E-15	32	298
eukaryotic translation initiation factor 3 complex	7.55E-15	11	15
regulation of translation	1.01E-14	24	152
cytosolic large ribosomal subunit	2.00E-14	16	51
small nuclear ribonucleoprotein complex	3.37E-14	14	35
RNA helicase activity	6.81E-14	13	29
large ribosomal subunit	1.07E-13	17	67
ncRNA metabolic process	2.74E-13	25	194
cytosolic small ribosomal subunit	1.98E-12	13	36
rRNA processing	2.44E-12	15	56

ncRNA processing	4.24E-12	19	111
rRNA metabolic process	9.48E-12	15	61
helicase activity	2.02E-11	15	64
mRNA binding	2.16E-11	16	77
small ribosomal subunit	3.93E-11	14	55
ribonucleoprotein complex binding	4.84E-11	13	45
nuclear body	4.49E-10	20	162
spliceosomal complex assembly	8.93E-10	11	34
RNA-dependent ATPase activity	4.45E-09	9	21
ribosome assembly	6.65E-09	8	15
cytoplasmic stress granule	4.27E-08	9	26
negative regulation of translation	6.60E-08	12	62
regulation of translational initiation	6.80E-08	11	49
ATP-dependent RNA helicase activity	1.14E-07	8	20
purine NTP-dependent helicase activity	2.33E-07	10	42
ATP-dependent helicase activity	2.33E-07	10	42
positive regulation of translation	3.76E-07	10	44
regulation of mRNA processing	5.27E-07	11	59
U12-type spliceosomal complex	5.87E-07	8	24
poly(A) binding	8.08E-07	6	10
nuclear transport	1.29E-06	21	281
ATP catabolic process	1.29E-06	15	137
ribonucleoside monophosphate catabolic process	1.52E-06	15	139
purine nucleoside monophosphate catabolic process	1.52E-06	15	139
purine ribonucleoside monophosphate catabolic process	1.52E-06	15	139
nucleoside monophosphate catabolic process	1.64E-06	15	140
regulation of RNA splicing	1.64E-06	11	66
nuclear speck	1.89E-06	11	67
nucleocytoplasmic transport	5.18E-06	20	278
poly-purine tract binding	5.58E-06	6	13
ribonucleoprotein granule	7.17E-06	11	76
ATP metabolic process	8.02E-06	15	158
single-stranded RNA binding	8.19E-06	8	33
regulation of mRNA splicing, via spliceosome	1.69E-05	8	36
ATPase activity	2.43E-05	16	197
purine nucleoside monophosphate metabolic process	3.42E-05	15	177
purine ribonucleoside monophosphate metabolic process	3.42E-05	15	177
ribonucleoside monophosphate metabolic process	4.22E-05	15	180
nucleoside monophosphate metabolic process	6.85E-05	15	187
ATPase activity, coupled	9.91E-05	13	143
double-stranded RNA binding	9.91E-05	8	45
ribosomal small subunit biogenesis	1.00E-04	6	20
spliceosomal snRNP assembly	1.15E-04	7	32
Cajal body	1.84E-04	6	22
mRNA 3'-end processing	2.64E-04	10	88
negative regulation of translational initiation	3.41E-04	5	14
alternative mRNA splicing, via spliceosome	5.22E-04	6	26
RNA 3'-end processing	9.09E-04	10	101
ribosome binding	1.80E-03	5	19
DNA conformation change	1.99E-03	11	135
regulation of mRNA stability	2.20E-03	6	33
methylosome	2.24E-03	4	10
regulation of RNA stability	2.58E-03	6	34
organelle assembly	2.97E-03	14	226
MHC protein complex binding	3.26E-03	4	11
MHC class II protein complex binding	3.26E-03	4	11
preribosome	3.26E-03	4	11
oligodendrocyte development	3.26E-03	4	11
small nucleolar ribonucleoprotein complex	3.26E-03	4	11
regulation of alternative mRNA splicing, via spliceosome	3.54E-03	5	22
RNA stabilization	4.38E-03	5	23
mRNA stabilization	4.38E-03	5	23
maturation of 5.8S rRNA	4.66E-03	4	12
protein folding	4.83E-03	10	124

mRNA 3'-UTR binding	8.03E-03	5	26
translation regulator activity	9.64E-03	5	27
histone modification	1.04E-02	14	256
regulation of DNA-templated transcription, elongation	1.14E-02	5	28
mRNA splice site selection	1.18E-02	4	15
covalent chromatin modification	1.25E-02	14	261
nuclear export	1.26E-02	9	113
nucleolar part	1.83E-02	5	31
regulation of histone modification	2.88E-02	6	53
oligodendrocyte differentiation	3.68E-02	4	20
positive regulation of DNA-templated transcription, elongation	3.68E-02	4	20
NF-kappaB binding	3.68E-02	4	20
exosome (RNase complex)	3.68E-02	4	20
polysome	4.46E-02	4	21
DNA-templated transcription, elongation	4.83E-02	8	108
mRNA polyadenylation	5.30E-02	4	22
RNA localization	5.48E-02	7	84
U1 snRNP	6.23E-02	3	10
regulation of transcription elongation from RNA polymerase II promoter	6.23E-02	3	10
regulation of chromatin organization	6.86E-02	6	63
RNA polyadenylation	7.23E-02	4	24
regulation of cysteine-type endopeptidase activity involved in apoptotic process	8.10E-02	9	147
ATP-dependent DNA helicase activity	8.38E-02	4	25
positive regulation of cysteine-type endopeptidase activity involved in apoptotic process	9.05E-02	7	92
termination of RNA polymerase II transcription	9.68E-02	5	45
mRNA export from nucleus	9.91E-02	6	68

Table A-4: GO functional enrichment analysis of 273 human host proteins that co-eluted with DENV2 GFP-NS5. The Benjamini-Hochberg procedure was used to calculate the q-value (false discovery rate adjusted p-value) of each enriched GO feature. For each enriched GO feature that is associated with the generated interaction network, the number of proteins in the interaction network listed in that group, as well as the number of total proteins in the Homo sapiens proteome associated with the same GO feature. The table is arranged in order of increasing q-value.

GO feature	q-value	Genes in network	Genes in genome
translational initiation	1.21E-39	43	150
RNA splicing, via transesterification reactions with bulged adenosine as nucleophile	2.77E-28	39	208
mRNA splicing, via spliceosome	2.77E-28	39	208
RNA splicing	2.93E-28	43	274
RNA splicing, via transesterification reactions	5.25E-28	39	214
mRNA processing	1.68E-27	43	288
spliceosomal complex	3.07E-24	29	118
translation initiation factor activity	1.93E-22	18	31
RNA catabolic process	3.70E-22	34	215
catalytic step 2 spliceosome	4.14E-22	24	80
ribonucleoprotein complex biogenesis	8.78E-22	30	158
translation factor activity, nucleic acid binding	1.02E-19	20	57
cytosolic ribosome	1.96E-19	23	90
mRNA catabolic process	1.96E-19	30	190
nuclear-transcribed mRNA catabolic process, nonsense-mediated decay	2.33E-19	25	116
SRP-dependent cotranslational protein targeting to membrane	5.32E-19	24	107
protein localization to endoplasmic reticulum	5.32E-19	25	120
protein targeting to ER	5.74E-19	24	108
ribosomal subunit	5.74E-19	25	121
cotranslational protein targeting to membrane	5.74E-19	24	108
establishment of protein localization to endoplasmic reticulum	6.91E-19	24	109
viral gene expression	8.35E-18	22	94
regulation of translation	1.09E-17	26	152
ribosome	1.75E-17	26	155
eukaryotic translation initiation factor 3 complex	2.27E-17	12	15
protein targeting to membrane	2.27E-17	26	157
translational termination	4.32E-17	21	89
ribonucleoprotein complex assembly	4.32E-17	22	102
translational elongation	4.32E-17	22	102
nuclear-transcribed mRNA catabolic process	4.53E-17	27	179
posttranscriptional regulation of gene expression	5.44E-17	33	298
multi-organism metabolic process	6.16E-17	22	104
cytosolic part	9.82E-17	25	151
ribonucleoprotein complex subunit organization	1.72E-16	22	109
establishment of protein localization to membrane	3.56E-16	30	253
viral life cycle	4.41E-15	24	159
protein targeting	4.41E-15	31	299
protein localization to membrane	1.86E-14	27	227
structural constituent of ribosome	7.85E-14	19	97
cellular protein complex disassembly	2.60E-13	21	135
protein complex disassembly	4.25E-13	22	156
macromolecular complex disassembly	1.07E-12	22	163
RNA helicase activity	1.27E-12	12	29
single-organism cellular localization	1.54E-12	27	272
single-organism localization	1.54E-12	27	272
viral transcription	6.68E-12	21	159
ribosome biogenesis	7.79E-12	16	78
ribonucleoprotein complex binding	1.83E-11	13	45
cytosolic large ribosomal subunit	1.08E-10	13	51
helicase activity	1.26E-10	14	64
large ribosomal subunit	2.43E-10	14	67
cytoplasmic stress granule	5.49E-10	10	26
small nuclear ribonucleoprotein complex	5.49E-10	11	35

regulation of translational initiation	1.39E-09	12	49
RNA-dependent ATPase activity	2.20E-09	9	21
nuclear body	8.48E-09	18	162
cytosolic small ribosomal subunit	2.15E-08	10	36
negative regulation of translation	2.56E-08	12	62
ATP-dependent RNA helicase activity	6.25E-08	8	20
small ribosomal subunit	1.06E-07	11	55
purine NTP-dependent helicase activity	1.06E-07	10	42
ATP-dependent helicase activity	1.06E-07	10	42
positive regulation of translation	1.72E-07	10	44
double-stranded RNA binding	2.14E-07	10	45
ribosome assembly	2.16E-07	7	15
ribonucleoprotein granule	2.70E-07	12	76
spliceosomal complex assembly	2.73E-07	9	34
mRNA binding	3.06E-07	12	77
ribosome binding	1.51E-06	7	19
regulation of mRNA processing	3.23E-06	10	59
ATP catabolic process	3.42E-06	14	137
ribonucleoside monophosphate catabolic process	3.95E-06	14	139
purine nucleoside monophosphate catabolic process	3.95E-06	14	139
purine ribonucleoside monophosphate catabolic process	3.95E-06	14	139
nucleoside monophosphate catabolic process	4.28E-06	14	140
ATPase activity, coupled	5.55E-06	14	143
ncRNA metabolic process	6.27E-06	16	194
ATPase activity	7.69E-06	16	197
U12-type spliceosomal complex	8.54E-06	7	24
nuclear speck	1.01E-05	10	67
ATP metabolic process	1.85E-05	14	158
rRNA processing	2.44E-05	9	56
poly(A) binding	3.41E-05	5	10
rRNA metabolic process	5.12E-05	9	61
purine nucleoside monophosphate metabolic process	7.13E-05	14	177
purine ribonucleoside monophosphate metabolic process	7.13E-05	14	177
single-stranded RNA binding	8.55E-05	7	33
ribonucleoside monophosphate metabolic process	8.55E-05	14	180
nucleoside monophosphate metabolic process	1.34E-04	14	187
ncRNA processing	1.37E-04	11	111
nucleocytoplasmic transport	1.47E-04	17	278
poly-purine tract binding	1.52E-04	5	13
nuclear transport	1.67E-04	17	281
negative regulation of translational initiation	2.28E-04	5	14
regulation of DNA-templated transcription, elongation	5.15E-04	6	28
chaperone binding	7.83E-04	6	30
DNA conformation change	8.86E-04	11	135
regulation of RNA splicing	9.63E-04	8	66
mRNA 3'-end processing	1.02E-03	9	88
regulation of mRNA stability	1.35E-03	6	33
ribosomal small subunit biogenesis	1.52E-03	5	20
positive regulation of DNA-templated transcription, elongation	1.52E-03	5	20
regulation of transcription elongation from RNA polymerase II promoter	1.57E-03	4	10
regulation of RNA stability	1.57E-03	6	34
regulation of mRNA splicing, via spliceosome	2.18E-03	6	36
protein folding	2.38E-03	10	124
oligodendrocyte development	2.38E-03	4	11
Cajal body	2.38E-03	5	22
RNA 3'-end processing	2.87E-03	9	101
RNA stabilization	2.92E-03	5	23
mRNA stabilization	2.92E-03	5	23
DNA replication	3.92E-03	13	222
ATP-dependent DNA helicase activity	4.42E-03	5	25
mRNA 3'-UTR binding	5.36E-03	5	26
translation regulator activity	6.44E-03	5	27
response to heat	9.17E-03	5	29

RNA polymerase binding	1.13E-02	4	16
positive regulation of type I interferon production	1.60E-02	7	74
unfolded protein binding	1.66E-02	6	52
mitochondrial nucleoid	1.96E-02	5	34
type I interferon production	2.02E-02	8	103
regulation of type I interferon production	2.02E-02	8	103
nucleoid	2.19E-02	5	35
replication fork	2.19E-02	5	35
oligodendrocyte differentiation	2.67E-02	4	20
NF-kappaB binding	2.67E-02	4	20
DNA helicase activity	3.18E-02	5	38
positive regulation of NF-kappaB transcription factor activity	3.23E-02	8	111
nuclear export	3.63E-02	8	113
mRNA polyadenylation	3.82E-02	4	22
response to temperature stimulus	3.95E-02	5	40
DNA duplex unwinding	4.41E-02	5	41
endodermal cell fate commitment	4.83E-02	3	10
RNA polymerase II core binding	4.83E-02	3	10
gliogenesis	5.07E-02	6	65
RNA polyadenylation	5.18E-02	4	24
DNA geometric change	5.34E-02	5	43
mitochondrial matrix	5.47E-02	12	257
MHC protein complex binding	6.16E-02	3	11
MHC class II protein complex binding	6.16E-02	3	11
basal transcription machinery binding	6.16E-02	3	11
basal RNA polymerase II transcription machinery binding	6.16E-02	3	11
small nucleolar ribonucleoprotein complex	6.16E-02	3	11
termination of RNA polymerase II transcription	6.29E-02	5	45
alternative mRNA splicing, via spliceosome	6.69E-02	4	26
regulation of cysteine-type endopeptidase activity	7.03E-02	9	159
mRNA cleavage factor complex	7.85E-02	3	12
RNA polymerase core enzyme binding	7.85E-02	3	12
positive regulation of cysteine-type endopeptidase activity	8.20E-02	7	100
endodermal cell differentiation	9.96E-02	3	13

Table A-5: GO functional enrichment analysis of 110 human host proteins that are common to DENV1 and 2 NS3 and NS5. The Benjamini-Hochberg procedure was used to calculate the q-value (false discovery rate adjusted p-value) of each enriched GO feature. For each enriched GO feature that is associated with the generated interaction network, the number of proteins in the interaction network listed in that group, as well as the number of total proteins in the Homo sapiens proteome associated with the same GO feature. The table is arranged in order of increasing q-value.

GO feature	q-value	Genes in network	Genes in genome
translational initiation	2.75E-41	35	150
cytosolic ribosome	1.88E-34	27	90
ribosomal subunit	2.99E-34	29	121
protein localization to endoplasmic reticulum	4.17E-31	27	120
ribosome	4.17E-31	29	155
translational termination	4.17E-31	25	89
SRP-dependent cotranslational protein targeting to membrane	7.27E-31	26	107
protein targeting to ER	7.41E-31	26	108
cotranslational protein targeting to membrane	7.41E-31	26	108
establishment of protein localization to endoplasmic reticulum	7.92E-31	26	109
viral gene expression	7.92E-31	25	94
nuclear-transcribed mRNA catabolic process, nonsense-mediated decay	3.75E-30	26	116
cytosolic part	3.75E-30	28	151
RNA catabolic process	3.75E-30	31	215
translational elongation	5.42E-30	25	102
multi-organism metabolic process	8.74E-30	25	104
mRNA catabolic process	2.60E-27	28	190
cellular protein complex disassembly	9.79E-27	25	135
protein targeting to membrane	1.37E-26	26	157
establishment of protein localization to membrane	3.35E-25	29	253
protein complex disassembly	3.93E-25	25	156
nuclear-transcribed mRNA catabolic process	4.25E-25	26	179
viral transcription	5.68E-25	25	159
viral life cycle	5.68E-25	25	159
macromolecular complex disassembly	1.05E-24	25	163
protein localization to membrane	8.03E-24	27	227
single-organism cellular localization	1.04E-21	27	272
single-organism localization	1.04E-21	27	272
protein targeting	1.28E-20	27	299
structural constituent of ribosome	1.82E-20	19	97
cytosolic small ribosomal subunit	2.33E-17	13	36
cytosolic large ribosomal subunit	6.79E-17	14	51
large ribosomal subunit	9.36E-17	15	67
small ribosomal subunit	2.11E-16	14	55
ribonucleoprotein complex biogenesis	2.57E-16	19	158
RNA splicing	3.66E-14	21	274
ribosome biogenesis	4.02E-14	14	78
RNA splicing, via transesterification reactions with bulged adenosine as nucleophile	4.35E-14	19	208
mRNA splicing, via spliceosome	4.35E-14	19	208
RNA splicing, via transesterification reactions	7.24E-14	19	214
spliceosomal complex	5.99E-13	15	118
mRNA processing	1.23E-12	20	288
regulation of translation	2.63E-11	15	152
posttranscriptional regulation of gene expression	2.89E-11	19	298
translation initiation factor activity	1.14E-10	9	31
eukaryotic translation initiation factor 3 complex	1.04E-09	7	15
ribonucleoprotein complex assembly	1.07E-09	12	102
cytoplasmic stress granule	1.40E-09	8	26
catalytic step 2 spliceosome	1.51E-09	11	80
ribonucleoprotein complex subunit organization	2.24E-09	12	109
mRNA binding	2.57E-08	10	77
translation factor activity, nucleic acid binding	3.82E-08	9	57
ribosome assembly	1.13E-07	6	15

ncRNA metabolic process	1.44E-07	13	194
ribonucleoprotein granule	5.16E-07	9	76
ribosomal small subunit biogenesis	8.07E-07	6	20
rRNA processing	8.93E-07	8	56
ncRNA processing	8.93E-07	10	111
rRNA metabolic process	1.77E-06	8	61
U12-type spliceosomal complex	2.53E-06	6	24
helicase activity	2.53E-06	8	64
positive regulation of translation	3.92E-06	7	44
double-stranded RNA binding	4.54E-06	7	45
RNA helicase activity	8.25E-06	6	29
single-stranded RNA binding	1.85E-05	6	33
ATP catabolic process	7.77E-05	9	137
ribonucleoside monophosphate catabolic process	8.41E-05	9	139
purine nucleoside monophosphate catabolic process	8.41E-05	9	139
purine ribonucleoside monophosphate catabolic process	8.41E-05	9	139
nucleoside monophosphate catabolic process	8.81E-05	9	140
poly(A) binding	9.26E-05	4	10
ribonucleoprotein complex binding	1.16E-04	6	45
ATPase activity	1.64E-04	10	197
ATP metabolic process	2.31E-04	9	158
poly-purine tract binding	2.94E-04	4	13
regulation of mRNA stability	5.46E-04	5	33
purine nucleoside monophosphate metabolic process	5.65E-04	9	177
purine ribonucleoside monophosphate metabolic process	5.65E-04	9	177
regulation of RNA stability	6.12E-04	5	34
ribonucleoside monophosphate metabolic process	6.32E-04	9	180
negative regulation of translation	7.09E-04	6	62
nucleoside monophosphate metabolic process	8.44E-04	9	187
ATPase activity, coupled	9.77E-04	8	143
regulation of RNA splicing	9.89E-04	6	66
negative regulation of RNA splicing	1.08E-03	4	18
purine NTP-dependent helicase activity	1.63E-03	5	42
ATP-dependent helicase activity	1.63E-03	5	42
RNA-dependent ATPase activity	2.01E-03	4	21
RNA stabilization	2.89E-03	4	23
mRNA stabilization	2.89E-03	4	23
protein folding	3.42E-03	7	124
ATP-dependent DNA helicase activity	3.99E-03	4	25
unfolded protein binding	4.43E-03	5	52
mRNA 3'-UTR binding	4.59E-03	4	26
translation regulator activity	5.31E-03	4	27
DNA conformation change	5.63E-03	7	135
regulation of mRNA processing	7.89E-03	5	59
MHC protein complex binding	8.20E-03	3	11
MHC class II protein complex binding	8.20E-03	3	11
response to unfolded protein	1.26E-02	6	106
regulation of mRNA splicing, via spliceosome	1.60E-02	4	36
nuclear body	1.69E-02	7	162
negative regulation of mRNA splicing, via spliceosome	1.70E-02	3	14
telomeric DNA binding	1.70E-02	3	14
response to topologically incorrect protein	1.72E-02	6	113
DNA helicase activity	1.89E-02	4	38
DNA duplex unwinding	2.51E-02	4	41
negative regulation of mRNA processing	2.51E-02	3	16
DNA geometric change	3.00E-02	4	43
positive regulation of apoptotic process	3.95E-02	8	250
ribosome binding	4.13E-02	3	19
positive regulation of programmed cell death	4.43E-02	8	255
mRNA 3'-end processing	4.56E-02	5	88
ATP-dependent RNA helicase activity	4.71E-02	3	20
regulation of translational initiation	4.74E-02	4	49
positive regulation of cell death	6.12E-02	8	269
DNA-dependent ATPase activity	7.81E-02	4	56

RNA 3'-end processing	8.26E-02	5	101

Table A-6: GO functional enrichment analysis of 52 human host proteins that are unique to DENV1/2 NS3. The Benjamini-Hochberg procedure was used to calculate the q-value (false discovery rate adjusted p-value) of each enriched GO feature. For each enriched GO feature that is associated with the generated interaction network, the number of proteins in the interaction network listed in that group, as well as the number of total proteins in the Homo sapiens proteome associated with the same GO feature. The table is arranged in order of increasing q-value.

GO feature	q-value	Genes in network	Genes in genome
nuclear-transcribed mRNA catabolic process, nonsense-mediated decay	1.96E-47	31	116
translational termination	3.55E-47	29	89
mRNA catabolic process	1.33E-46	34	190
translational initiation	2.95E-46	32	150
nuclear-transcribed mRNA catabolic process	1.05E-45	33	179
cytosolic ribosome	3.73E-45	28	90
SRP-dependent cotranslational protein targeting to membrane	4.69E-45	29	107
RNA catabolic process	4.69E-45	34	215
protein targeting to ER	5.10E-45	29	108
cotranslational protein targeting to membrane	5.10E-45	29	108
establishment of protein localization to endoplasmic reticulum	6.30E-45	29	109
viral gene expression	7.82E-45	28	94
translational elongation	1.03E-43	28	102
protein localization to endoplasmic reticulum	1.19E-43	29	120
multi-organism metabolic process	1.67E-43	28	104
cellular protein complex disassembly	4.78E-42	29	135
ribosomal subunit	1.83E-41	28	121
protein complex disassembly	4.30E-40	29	156
protein targeting to membrane	4.98E-40	29	157
viral transcription	6.73E-40	29	159
viral life cycle	6.73E-40	29	159
macromolecular complex disassembly	1.41E-39	29	163
protein localization to membrane	7.22E-39	31	227
cytosolic part	1.23E-38	28	151
ribosome	2.63E-38	28	155
establishment of protein localization to membrane	2.20E-37	31	253
single-organism cellular localization	2.14E-36	31	272
single-organism localization	2.14E-36	31	272
protein targeting	2.38E-33	30	299
structural constituent of ribosome	9.25E-32	22	97
cytosolic small ribosomal subunit	1.59E-25	15	36
small ribosomal subunit	3.14E-22	15	55
cytosolic large ribosomal subunit	1.43E-18	13	51
large ribosomal subunit	7.05E-17	13	67
ribosomal small subunit biogenesis	1.32E-12	8	20
ribosome biogenesis	2.14E-12	11	78
rRNA processing	3.25E-12	10	56
ncRNA metabolic process	3.96E-12	14	194
rRNA metabolic process	7.70E-12	10	61
ncRNA processing	1.07E-10	11	111
ribonucleoprotein complex biogenesis	1.95E-10	12	158
maturation of SSU-rRNA	1.50E-05	4	10
polysome	4.05E-04	4	21
regulation of translation	5.64E-04	7	152
RNA 3'-end processing	7.54E-04	6	101
establishment of RNA localization	5.58E-03	5	85
nucleic acid transport	5.58E-03	5	85
RNA transport	5.58E-03	5	85
RNA localization	5.58E-03	5	84
ribosome assembly	7.76E-03	3	15
regulation of translational initiation	1.12E-02	4	49
ribonucleoprotein complex assembly	1.27E-02	5	102
nucleobase-containing compound transport	1.50E-02	5	106
ribonucleoprotein complex subunit organization	1.69E-02	5	109

positive regulation of mRNA processing	2.03E-02	3	21
RNA phosphodiester bond hydrolysis	2.59E-02	4	62
posttranscriptional regulation of gene expression	3.43E-02	7	298
RNA phosphodiester bond hydrolysis, endonucleolytic	5.18E-02	3	29
RNA export from nucleus	5.45E-02	4	76
translation initiation factor activity	6.13E-02	3	31
nucleic acid phosphodiester bond hydrolysis	6.95E-02	5	151
DNA strand elongation involved in DNA replication	7.84E-02	3	34
mRNA 3'-end processing	8.98E-02	4	88
DNA strand elongation	9.78E-02	3	37

Table A-7: GO functional enrichment analysis of 71 human host proteins that are unique to DENV1 NS5. The Benjamini-Hochberg procedure was used to calculate the q-value (false discovery rate adjusted p-value) of each enriched GO feature. For each enriched GO feature that is associated with the generated interaction network, the number of proteins in the interaction network listed in that group, as well as the number of total proteins in the Homo sapiens proteome associated with the same GO feature. The table is arranged in order of increasing q-value.

GO feature	q-value	Genes in network	Genes in genome
ribonucleoprotein complex biogenesis	2.90E-10	14	158
RNA splicing, via transesterification reactions	5.06E-10	15	214
RNA splicing	7.77E-10	16	274
spliceosomal complex	1.17E-09	12	118
mRNA splicing, via spliceosome	2.19E-09	14	208
RNA splicing, via transesterification reactions with bulged adenosine as nucleophile	2.19E-09	14	208
mRNA processing	1.51E-07	14	288
catalytic step 2 spliceosome	7.86E-06	8	80
ribonucleoprotein complex assembly	4.38E-05	8	102
ncRNA metabolic process	4.38E-05	10	194
ribonucleoprotein complex subunit organization	6.72E-05	8	109
ncRNA processing	7.11E-05	8	111
ribosome biogenesis	1.04E-04	7	78
maturation of 5.8S rRNA	2.79E-04	4	12
rRNA processing	2.80E-04	6	56
rRNA metabolic process	4.41E-04	6	61
nucleolar part	1.37E-02	4	31
preribosome	1.63E-02	3	11
small nuclear ribonucleoprotein complex	1.95E-02	4	35
ribosomal large subunit biogenesis	1.95E-02	3	12
COPII vesicle coating	2.20E-02	3	13
vesicle targeting, rough ER to cis-Golgi	2.20E-02	3	13
COPII-coated vesicle budding	2.20E-02	3	13
mRNA splice site selection	3.32E-02	3	15

Table A-8: GO functional enrichment analysis of 41 human host proteins that are unique to DENV2 NS5. The Benjamini-Hochberg procedure was used to calculate the q-value (false discovery rate adjusted p-value) of each enriched GO feature. For each enriched GO feature that is associated with the generated interaction network, the number of proteins in the interaction network listed in that group, as well as the number of total proteins in the Homo sapiens proteome associated with the same GO feature. The table is arranged in order of increasing q-value.

GO feature	q-value	Genes in network	Genes in genome
establishment of organelle localization	2.83E-14	14	136
Golgi transport vesicle coating	2.83E-14	8	13
COPI-coated vesicle budding	2.83E-14	8	13
COPI coating of Golgi vesicle	2.83E-14	8	13
organelle localization	9.32E-14	14	160
vesicle targeting, to, from or within Golgi	9.32E-14	9	26
single-organism membrane budding	9.32E-14	9	26
Golgi vesicle budding	9.32E-14	8	15
establishment of vesicle localization	1.69E-13	12	94
vesicle localization	3.31E-13	12	100
vesicle coating	5.69E-13	9	32
vesicle targeting	9.70E-13	9	34
COPI-coated vesicle membrane	3.94E-12	7	13
COPI vesicle coat	3.94E-12	7	13
retrograde vesicle-mediated transport, Golgi to ER	3.94E-12	8	24
membrane budding	3.94E-12	9	40
COPI-coated vesicle	2.18E-11	7	16
Golgi-associated vesicle membrane	3.70E-11	8	31
vesicle organization	2.96E-10	10	96
membrane coat	8.38E-10	8	45
coated membrane	8.38E-10	8	45
Golgi-associated vesicle	1.39E-09	8	48
vesicle coat	2.77E-09	7	30
coated vesicle membrane	5.56E-07	8	100
Golgi vesicle transport	7.96E-07	9	156
cytoplasmic vesicle membrane	1.37E-06	10	231
vesicle membrane	1.76E-06	10	238
coated vesicle	3.48E-05	8	172
intra-Golgi vesicle-mediated transport	9.25E-05	4	16
Golgi membrane	1.31E-04	9	287
protein N-linked glycosylation via asparagine	2.92E-04	6	96
peptidyl-asparagine modification	3.01E-04	6	97
protein N-linked glycosylation	4.16E-04	6	103
dolichol-linked oligosaccharide biosynthetic process	1.93E-03	4	34
nucleotide-sugar biosynthetic process	6.43E-03	3	15
anterograde synaptic vesicle transport	6.43E-03	3	15
microtubule-based transport	1.16E-02	4	54
cytoskeleton-dependent intracellular transport	1.60E-02	4	59
anterograde axon cargo transport	1.71E-02	3	21
protein glycosylation	1.87E-02	6	208
nucleotide-sugar metabolic process	1.87E-02	3	22
macromolecule glycosylation	1.87E-02	6	209
post-translational protein modification	1.87E-02	6	209
glycosylation	2.20E-02	6	216
axon cargo transport	3.22E-02	3	27
translation initiation factor activity	4.81E-02	3	31
glycoprotein biosynthetic process	5.96E-02	6	262
mitotic nuclear envelope disassembly	7.54E-02	3	37
membrane disassembly	7.54E-02	3	37
nuclear envelope disassembly	7.54E-02	3	37
microtubule-based movement	7.71E-02	4	96
synaptic vesicle transport	7.71E-02	3	38
establishment of synaptic vesicle localization	7.71E-02	3	38
synaptic vesicle localization	9.50E-02	3	41

Table A-9: GO functional enrichment analysis of 9 human host proteins that are common to GFP-NS3 interaction networks of our and Carpp *et al* (Carpp et al., 2014). The Benjamini-Hochberg procedure was used to calculate the q-value (false discovery rate adjusted p-value) of each enriched GO feature. For each enriched GO feature that is associated with the generated interaction network, the number of proteins in the interaction network listed in that group, as well as the number of total proteins in the Homo sapiens proteome associated with the same GO feature. The table is arranged in order of increasing q-value.

GO feature	q-value	Genes in network	Genes in genome
protein folding	1.97E-17	13	124
response to unfolded protein	2.84E-12	10	106
response to topologically incorrect protein	3.66E-12	10	113
protein refolding	6.41E-09	5	10
'de novo' protein folding	1.49E-07	6	43
unfolded protein binding	4.12E-07	6	52
'de novo' posttranslational protein folding	7.09E-06	5	38
microtubule	1.88E-04	6	149
MHC protein complex binding	9.61E-04	3	11
MHC class II protein complex binding	9.61E-04	3	11
double-stranded RNA binding	1.03E-03	4	45
chaperone-mediated protein complex assembly	1.07E-03	3	12
chaperone-mediated protein folding	3.63E-03	3	18
peptidyl-proline modification	1.20E-02	3	27
chaperone binding	1.55E-02	3	30

Table A-10: Human proteins that were identified to co-elute with GFP-NS3 and GFP-NS5 in our study, and were also up- or down-regulated during DENV2 infection in Pando-Robles *et al*'s study (Pando-Robles *et al.*, 2014). GFP and mock are excluded from the table since they were negative.

Identified Proteins (16)	Molecular Weight	GFP D1NS3	GFP D2NS3	GFP D1NS5	GFP D2NS5
Up-regulated (4)					
Aspartyl-tRNA synthetase, cytoplasmic	57 kDa	9	0	3	3
Protein arginine N-methyltransferase 1	42 kDa	7	0	8	2
Putative RNA-binding protein 3	17 kDa	4	0	3	5
Matrin-3	95 kDa	19	0	18	10
Down-regulated (12)					
Nuclease-sensitive element-binding protein 1 (YB-1)	36 kDa	7	0	6	5
Putative pre-mRNA-splicing factor ATP-dependent RNA helicase DHX15	91 kDa	12	0	18	15
Caprin-1	78 kDa	10	0	5	8
Heterogeneous nuclear ribonucleoproteins C1/C2	34 kDa	6	0	5	3
Heat shock 70 kDa protein 1A/1B	70 kDa	14	9	16	14
Heat shock protein HSP 90-beta	83 kDa	3	3	7	4
Interleukin enhancer-binding factor 3	95 kDa	25	0	19	17
Splicing factor 3B subunit 3	136 kDa	2	0	42	21
Tubulin alpha-1C chain	50 kDa	3	0	3	3
Polyadenylate-binding protein	71 kDa	11	0	3	6
Stress-70 protein, mitochondrial	74 kDa	16	4	10	10
Eukaryotic translation initiation factor 2 subunit 1	36 kDa	2	0	11	10

Table A-11: GO functional enrichment analysis of 12 human host proteins that are common to GFP-NS3 interaction networks of our and the down-regulated list of proteins during DENV2 infection in Pando-Robles *et al*'s study (Pando-Robles *et al.*, 2014). The Benjamini-Hochberg procedure was used to calculate the q-value (false discovery rate adjusted p-value) of each enriched GO feature. For each enriched GO feature that is associated with the generated interaction network, the number of proteins in the interaction network listed in that group, as well as the number of total proteins in the Homo sapiens proteome associated with the same GO feature. The table is arranged in order of increasing q-value.

GO feature	q-value	Genes in network	Genes in genome
cytoplasmic stress granule	9.41E-06	5	26
double-stranded RNA binding	5.70E-05	5	45
RNA splicing	5.70E-05	8	274
RNA splicing, via transesterification reactions	9.65E-05	7	214
protein folding	9.65E-05	6	124
RNA splicing, via transesterification reactions with bulged adenosine as nucleophile	9.65E-05	7	208
spliceosomal complex	9.65E-05	6	118
mRNA splicing, via spliceosome	9.65E-05	7	208
ribonucleoprotein granule	2.77E-04	5	76
mRNA processing	5.68E-04	7	288
poly(A) binding	7.82E-04	3	10
MHC protein complex binding	9.09E-04	3	11
MHC class II protein complex binding	9.09E-04	3	11
poly-purine tract binding	1.46E-03	3	13
RNA stabilization	7.83E-03	3	23
mRNA stabilization	7.83E-03	3	23
U12-type spliceosomal complex	8.41E-03	3	24
catalytic step 2 spliceosome	8.45E-03	4	80
translation initiation factor activity	1.66E-02	3	31
single-stranded RNA binding	1.82E-02	3	33
regulation of mRNA stability	1.82E-02	3	33
regulation of RNA stability	1.90E-02	3	34
response to unfolded protein	2.02E-02	4	106
'de novo' posttranslational protein folding	2.39E-02	3	38

Biography

Moon TAY Yue Feng

Born Januray 19, 1986 in Singapore

Education:

2010-2015	Ph.D., Integrated Biology and Medicine Duke-NUS Graduate Medical School and National University of Singapore, Singapore
2006-2009	B.Sc. (1st class Hons), Biological Sciences Nanyang Technological University, Singapore
2003-2006	Diploma with Certificate of Merit, Medical Technology Singapore Polytechnic, Singapore

Publications:

Tay, M. Y., Saw, W. G., Zhao, Y., Chan, K. W., Singh, D., Chong, Y., Forwood, J. K., Ooi, E. E., Gruber, G., Lescar, J., Luo, D. & Vasudevan, S. G. (2014b). The C-terminal 50 amino acid residues of Dengue NS3 protein are important for NS3-NS5 interaction and viral replication. J Biol Chem 290, 2379-2394.

Tay, M. Y., Lee, C. C., Vasudevan, S. G. & Moreland, N. J. (2014a). Identification of dengue-specific human antibody fragments using phage display. Methods Mol Biol 1138, 161-173.

Zhao, Y., Moreland, N. J., Tay, **M. Y.**, Lee, C. C., Swaminathan, K. & Vasudevan, S. G. (2014). Identification and molecular characterization of human antibody fragments specific for dengue NS5 protein. Virus Res 179, 225-230.

Tay, M. Y., Fraser, J. E., Chan, W. K., Moreland, N. J., Rathore, A. P., Wang, C., Vasudevan, S. G. & Jans, D. A. (2013). Nuclear localization of dengue virus (DENV) 1-4 non-structural protein 5; protection against all 4 DENV serotypes by the inhibitor Ivermectin. Antiviral Res 99, 301-306.

Moreland, N. J., **Tay, M. Y.**, Lim, E., Rathore, A. P., Lim, A. P., Hanson, B. J. & Vasudevan, S. G. (2012). Monoclonal antibodies against dengue NS2B and NS3 proteins for the study of protein interactions in the flaviviral replication complex. J Virol Methods 179, 97-103.

Awards and Honors:

Full NUS Research Scholarship covering the studies towards the Ph.D. degree at Duke-NUS Graduate Medical School and National University of Singapore (2010-2015)